UNIVERSITY OF LILLE

Doctorate school **ED SMRE**

University Department **Unité de Catalyse et Chimie du Solide**

Thesis

Defendend by

Guillaume POMALAZA

On the 25 of October 2019

In order to become a **Doctor of the University of Lille**

Academic Field **Molecules and Condensed Matter**

Specialty **Heterogeneous Catalysis**

Conversion of Ethanol to Butadiene on Zinc-Tantalum Catalysts

Thesis supervised by	Franck Dumeignil	Supervisor
	Mickaël Capron	Co-supervisor

Committee members

Referees	Bert Sels	Professor at the Catholic University of Leuven
	Guylène Costentin	Senior researcher at CNRS
Examiners	Carole Lamonier	Professor at the University of Lille
	Pascal Fongarland	Professor at the Claude Bernard University Lyon 1
Supervisor	Franck Dumeignil	Professor at the University of Lille
Co-supervisor	Mickaël Capron	Lecturer at the University of Lille

UNIVERSITE DE LILLE

École doctorale **ED SMRE**

Laboratoire **Unité de Catalyse et Chimie du Solide**

Thèse

Défendue par

Guillaume POMALAZA

Le 25 octobre 2019

En vue de l'obtention du grade de **Docteur de l'Université de Lille**

Discipline **Molécule et matière condensée**

Spécialité **Catalyse hétérogène**

Conversion de l'éthanol en butadiene avec catalyseurs à base de zinc et tantale

Thesis supervised by	Franck Dumeignil	Supervisor
	Mickaël Capron	Co-supervisor

Committee members

Referees	Bert Sels	Professor at the Catholic University of Leuven
	Guylène Costentin	Senior researcher at CNRS
Examiners	Carole Lamonier	Professor at the University of Lille
	Pascal Fongarland	Professor at the Claude Bernard University Lyon 1
Supervisor	Franck Dumeignil	Professor at the University of Lille
Co-supervisor	Mickaël Capron	Lecturer at the University of Lille

Abstract

Butadiene is a crucial commodity primarily used to manufacture synthetic rubber. However, sustainability and supply problems have been projected to afflict current production methods, namely the steam cracking of naphtha. In response, the ethanol-to-butadiene reaction has gathered notable attention for the on-purpose production of butadiene from renewable sources. However, this process suffers from catalytic performance issues, notably low activity, selectivity and productivity.

The aim of this thesis was to develop a catalyst capable of high performance in the ethanol-to-butadiene reaction. Based on a survey of the literature and a screening study, silica-supported Zn-Ta catalysts were found to be well-suited for attaining high butadiene yield in the conversion of ethanol. A comparison of catalysts carriers for the Zn-Ta active phase indicated that mesoporous silica TUD-1 was highly promising for achieving high butadiene productivity and selectivity. The synthesis of Zn-Ta-TUD-1 was optimized using the design of experiments methodology. The effects of the most important preparation parameters on activity and catalysts morphology were identified by a statistical study. Zn-Ta-TUD-1 with a Zn-to-Ta ratio between 1.5-2, with specific surface area larger than 600 $m^2 \cdot g^{-1}$ and an average pore diameter of 10 – 12 nm were found to be the most active catalysts. Characterization of the catalyst using FTIR, UV-Vis-DRS, XPS, XRD and HR-STEM revealed that the active phase consisted of highly dispersed Zn(II) and Ta(V), with the latter under the form of tetrahedral isolated sites and monolayered clusters. FTIR-pyridine, NH_3-TPD and a poison study enabled establishing that the condensation of acetaldehyde takes place on Lewis acid sites. Stability test indicated that the primary deactivation mechanism was the deposition of heavy carbonaceous species in the pores of the catalyst.

Résumé

Le butadiène est important composé, principalement utilisé dans la fabrication du caoutchouc synthétique. Toutefois, le vapocraquage de naphta, sa méthode de production actuelle, ne répond pas à des critères environnementaux durables dû à l'émission importante de gaz à effet de serre et la nature non-renouvelable des ressources fossiles. De plus, l'offre mondiale de butadiène risque de baisser à cause de l'émergence du gaz de schiste comme matière première. Récemment, la conversion catalytique de l'éthanol en butadiène attire plus particulièrement l'attention en tant que méthode de production alternative renouvelable et sélective. Toutefois, ce procédé ne possède pas les performances requises pour son industrialisation : il souffre de faible activité, sélectivité et productivité.

L'objectif de cette thèse était de développer un catalyseur à hautes performances dans la conversion de l'éthanol en butadiène. Suite à une revue de la littérature et un criblage de catalyseurs, une formulation à base de Zn et Ta supporté sur silice fut identifiée comme un matériau capable de hauts rendements en butadiène. Une comparaison entre différent supports catalytiques permit de surcroît d'identifier la silice TUD-1 comme prometteuse pour atteindre haute productivité et sélectivité en butadiène grâce à sa morphologie mésoporeuse. La synthèse de Zn-Ta-TUD-1 fut optimisé grâce à une approche de type « Plan d'Expérience » consistant en un criblage de paramètres de préparations, et en évaluant leur effet sur la morphologie at l'activité du catalyseur à l'aide d'outils statistiques. Le catalyseur Zn-Ta-TUD-1 optimisé fut identifié comme possédant un rapport molaire Zn/Ta entre 1.5 et 2, avec une surface spécifique plus grande que 600 $m^2 \cdot g^{-1}$ et des pores possédant un diamètre moyen de 10 – 12 nm. La caractérisation des catalyseurs par IR-FT, UV-Vis, SPX, DRX et MET révéla que la phase active comprenait Zn(II) et Ta(V) dispersés. Dans le cas du tantale, il s'agissait de sites isolés tétraédriques et d'agrégats en monocouche. La caractérisation de l'acidité de Zn-Ta-TUD-1 à l'aide de sondes basiques indiqua que la condensation de l'acétaldéhyde se déroule lors de la réaction sur des sites acides de Lewis. L'étude de la stabilité suggéra que la principale cause de désactivation consiste en la déposition d'espèces carbonées lourdes dans les pores des catalyseurs.

Acknowledgments

Because the first version of my acknowledgments was tediously long, I have decided to restrict myself to a single page. I hope it adequately conveys, in spite of its brevity, my true feelings.

First, I would like to thank Pr. Bert Sels and Dr. Guylène Costentin for reviewing my work. Their kind words to me, both in writing and at the end of my defense, were soothing to the ears of a student prone to self-doubt such as myself.

I also thank Pr. Pascal Fongardland for attending my defense and giving me sound advice on scientific matter. Pr. Lamonier has my gratitude for presiding my jury, but also for her efforts as head of the Heterogeneous Catalysis department; I greatly appreciated her efforts to accommodate students in their scientific endeavors.

My two “bosses”, Mickaël and Franck, have my most sincere gratitude for the significant influence they have exerted on my academic career. Ever since they sent me to Japan in the spring of 2015 to complete my master’s degree, my life has been shaped by their hand. Of course, their mentoring had a further impact on the person I am today. I was blessed to have two supervisors that not only could guide me in my research, but could also sit down with me and discuss as friends. Their words after my defense will forever be in my heart.

I must also thank my family for all they have done. I certainly could not have done this without the caring support of my mother and father during these 3 years and a half, but also throughout my life. I also thank my grandparents, whose influence has led me where I am today. To my little brother and sister, although distance and your youth may make these efforts of mine seem arcane, I hope nonetheless they will inspire to strive for the best. Please know that I have held you two in my heart always. To Giuliano, I thank you for being there; knowing that there is someone that understands me was very reassuring during some of the hardest times.

Pardis, you made this work possible and a worthwhile pursuit. I cannot thank you or praise you enough, and perhaps this is not the place to do so; I only hope that you know how much you mean to me.

To all my friends and colleagues, in France, Japan and Quebec, I can’t thank you all individually because of my desire to keep this brief. I hope you also know how much I appreciate you all, but I suspect you do not. In reality, even if I sometimes fail to keep in touch or may not show overt affection, I appreciate you all greatly. I enjoy discussing with you, I enjoy your distinct ways of being, I enjoy hearing from you. I truly care. I was blessed to make great friends throughout my life. I also thank everyone who help in some way or another conducting my research, whether it be discussion, experiments or advice. I am truly indebted to you all.

Symbols, acronyms and abbreviations

AcH	Acetaldehyde
APR	Aqueous Phase Reforming
BAS	Brønsted acid site
BE	Binding Energy
1,3-BD, BD	Butadiene
$C_{2=}$	Ethylene
CZA	$Cu/ZnO/Al_2O_3$ catalyst
DEE	Diethyl ether
DOE	Design of experiment
Dp	Average pore diameter
DRIFTS	Diffuse Reflectance Infrared Fourier Transform Spectroscopy
DRS	Diffuse Reflectance Spectroscopy
DSC	Differential Scanning Calorimetry
EDX	Energy Dispersive X-ray spectroscopy
EtOH	Ethanol
FT	Fourier Transform
FTIR	Fourier Transform Infrared spectroscopy
GC-FID	Gas Chromatography with Flame Ionization Detection
GC-MS	Gas Chromatography with Mass Spectrometry detection
HAADF-STEM	High Angle Annular Dark Field STEM
ICP	Inductively Coupled Plasma

KE	Kinetic energy
K-M	Kerkhof-Moulijn
LAS	Lewis acid site
MCF	Mesocelullar foam
MCM	Mobil Crystalline Materials silica
MPVO	Meerwein-Ponndorf-Verley-Oppenauer
MS	Mass Spectrometry
P.	Productivity
S.	Selectivity
SBA	Santa Barbara Amorphous silica
S_{BET}	Specific surface area determined by BET
SCS	Solution Combustion Synthesis
SEM	Scanning Electron Microscopy
SiBEA	Dealuminated zeolite β
SSNMR	Solid-State Nuclear Magnetic Resonance
STEM	Scanning Transmission Electron Microscopy
T	Temperature
t	Time
TEM	Transmission Electron Microscopy
TEM-EDX	TEM coupled with Energy Dispersive X-ray spectroscopy
$TEA/TEAH_3$	Triethanol amine
TEG	Tetraethylene glyclo

TEOS	Tetraethyl Orthosilicate
TGA	Thermogravimetric Analysis
TEAOH	Tetraethyl Ammonium Hydroxide
TOS	Time on stream
TPD	Temperature-Programmed Desorption
TUD	Technische Universiteit Delft
UV-Vis	diffuse reflectance Ultraviolet-Visible spectroscopy
WHSV	Weight Hourly Space Velocity
X.	Conversion
XPS	X-ray Photoelectron Spectroscopy
XRD	X-ray Diffraction
Y.	Yield
ZSM	Zeolite Socony Mobil

Contents

General Introduction

Butadiene is an important petrochemical owing to its use in the manufacturing of synthetic rubber, which is essential to the production of car tires. However, the steam cracking of naphtha, from which butadiene is predominantly obtained, is expected to encounter certain issues. In terms of environmental sustainability, this process generates large amounts of CO_2 that contribute to climate change. Furthermore, the emergence of shale gas as a potential cracking feedstock risks lowering the availability of butadiene due to its higher selectivity towards ethylene. Consequently, there is an interest in developing on-purpose butadiene production methods from renewable sources. One such technology is the catalytic conversion of ethanol to butadiene, or *"Lebedev process"*. However, it suffers from performance issues that must be addressed before competing financially with petroleum-based methods.

The broad aim of this thesis was to improve the Lebedev process and put it to practical use. Research was done in the broader context of an industrial project. Labelled *'Coupled heterogeneous and homogeneous catalysis: Synthesis and transformation of bio-butadiene for the preparation of unsaturated ethers'* or *'H2CAT'*, this project was sponsored by the *Agence Nationale de la Recherche*. The aim was to design a method of producing renewable ethers from biosourced ethanol *via* the Lebedev process and the telomerization of butadiene with polyols using homogeneous catalysis. This task was divided amongst the VAALBIO and CASECO teams of the *Unité de Catalyse et Chimie du Solide* laboratory belonging to the University of Lille, France. Assigned to the VAALBIO group, the work presented in this document was dedicated to designing new and better catalysts for the conversion of ethanol to butadiene, notably in terms of activity, selectivity and productivity. These requirements were achieved by the development of a Zn-Ta catalyst supported on mesoporous silica TUD-1. As will be discussed, this catalyst possessed the adequate morphological characteristics—3-dimensional mesoporous structure—and chemical properties, notably a high concentration of Lewis acid sites.

Chapter 1 is a bibliographic study of the conversion of ethanol to butadiene. It reviews three aspects of the process. First, a context is provided by discussing the historical, environmental and economic aspects of the ethanol-to-butadiene reaction as an industrial process. Second, the review

investigates topics related to the reaction itself, such as the mechanism, the effect of reaction conditions, the primary byproducts and the source of deactivation. Finally, the most important catalytic systems are reviewed. Attention is brought to the source of their activity, the challenges of catalyst design and a comparison of their performances.

Chapter 2 details the experimental methods used in this work, notably the synthesis catalysts, the characterization methods used, and the catalytic tests conducted.

Chapter 3 introduces the high-performing Zn-Ta-TUD-1 by comparing its activity to that of similar catalysts. A preliminary investigation was also performed to identify physical and chemical properties susceptible to be the source of its activity. Chapter 4 elaborates on the synthesis method of Zn-Ta-TUD-1. It was investigated and optimized using the design of experiment approach. Notably, the effect 11 parameters had on the morphological properties and activity of Zn-Ta-TUD-1 was evaluated by a statistical study. The most important parameter, the Zn-to-Ta ratio, was subsequently further optimized using the Response surface methodology. Chapter 5 focused on the characterization of optimized Zn-Ta-TUD-1 and its activity. First, the structural properties of the catalyst were investigated This was followed with the characterization of surface acidity, which was correlated to catalytic activity. The deactivation mechanism was also studied.

Chapter 6 concludes this work by summarizing the results obtained and an outlook on the research could follow. In the appendix can be found an internal report detailing the results of an initial screening study and the first review that has now been published. It should be noted that chapter 3, 4 and 5 are written in article form, as they have been already published or are to be submitted as soon as possible.

Chapter 1 Bibliographic Review

1.1. Introduction

Biorefineries convert renewable resources to chemicals and fuels.[1–4] The carbon content of biomass makes it an interesting substitute for fossil-based feedstocks on which the petrochemical industry currently relies.[5] A more sustainable economy could potentially be achieved by replacing petrorefineries with biorefineries. However, the low return on investment of bio-based processes hinders their development. The integration of a biorefinery with the production of a single platform molecule from which many value-added chemicals can be derived has been proposed as a strategy to overcome this obstacle.[4] The "*drop-in*" concept is another tactic for improving the financial viability of biomass valorization;[6] platform molecules are used to produce existing fossil-based intermediates, thereby benefiting from preexisting existing value chains and infrastructure. Note that, in that case, direct competition with petro-sourced molecules becomes in turn an issue due to the higher price of the raw material.

Ethanol has been identified as a promising platform molecule.[4,7] Besides its use as vehicle fuel and hydrogen source, ethanol can be catalytically converted to a wide range of value-added chemicals.[7,8] For instance, ethylene and propylene—olefins highly important to the manufacturing of plastics—can be obtained by dehydration of ethanol on solid acid catalysts, a process often compared to the methanol-to-olefin reaction.[9–11] The topic of this review concerns another reaction that generates olefins from ethanol: the catalytic conversion of ethanol to butadiene (Scheme 1.1). The latter is also a crucial commodity, as it is the main feedstock for the production of synthetic rubber, a key good to the automotive industry.[12,13]

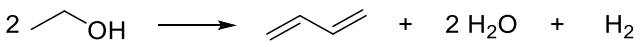

Scheme 1.1 Global equation of conversion of ethanol to butadiene

Two ethanol-to-butadiene processes following the same mechanism exist: the Lebedev (or one-step) process consists in direct conversion of gaseous ethanol to butadiene over multifunctional catalysts;[14] the Ostromislensky (or two-step) process divides the conversion in two reactors—a first one for partial dehydrogenation of ethanol to acetaldehyde and a subsequent one for the conversion of the as-obtained ethanol-acetaldehyde mixtures to butadiene.[15] The aim of this first step is to feed the second reactor with ethanol-acetaldehyde mixtures. In practice, most authors have preferred substituting it by simply co-feeding acetaldehyde with ethanol in a single reactor dedicated to

butadiene formation. After all, ethanol dehydrogenation is easier to optimize for outputting the desired ethanol-acetaldehyde ratio.[16,17] Consequently, references to the two-step or the Ostromislensky process are to be understood as the conversion of acetaldehyde-ethanol mixtures.

Interestingly, the Lebedev and Ostromislensky processes were important sources of butadiene from the 1930s to 1970s, before being supplanted by petroleum-based routes.[15,18,19] However, environmental and economic concerns have spurred a recent interest in this reaction, both in industry and academia.[20] Much effort has been dedicated to improving catalytic performances with the ultimate aim of turning the Lebedev or Ostromislensky processes into technologies capable of competing financially with current butadiene production methods.[15,20] However, achieving this goal has been hindered by the complexity of the reaction, which is only partly understood, and the collectively uncoordinated approach used to study the activity of catalysts. A myriad of catalytic systems has been studied under various conditions with different methods in either of the two processes. Consequently, a wide range of sometimes contradictory observations have been made at the expense of a comprehensive understanding of the reaction, as well as the relationship between the properties of catalysts and their activity. Without this knowledge, the rational design of better performing catalysts is hindered.

This bibliographic part aims at detailing the recent advances in the understanding of the reaction and in the design of improved catalytic systems. A brief summary of the rich historical and economic context of the ethanol-to-butadiene reaction will also be provided. In addition, we hope to build on previous reviews[15,18–21] by discussing topics not yet reviewed, such as the deactivation mechanism.

1.2. Historical & Economic Context

1.2.1 Brief History

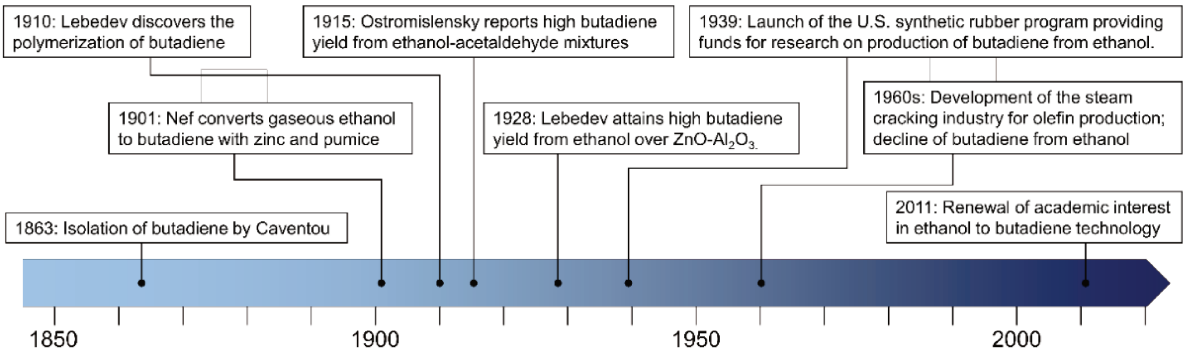

Figure 1.1 Timeline of key events in the development of the butadiene from ethanol process.

Butadiene was first isolated from the pyrolysis of acetylene and ethylene by Caventou in 1863. Its structure was elucidated in 1895 by Ciamician and Magnaghi.[13] Interest in butadiene began in 1910 when Lebedev found it could be converted to rubberlike polymers one year after the discovery of isoprene.[12,13,22,23]

During the Second Industrial Revolution (1870–1914), the vulcanization of natural rubber was the sole means of producing the elastomers used to manufacture the tires demanded by the ongoing industrialization.[22–25] As a result, synthetic rubber greatly interested countries that lacked colonial empires spanning into tropical zones, the only geographic regions where the rubber plant *Hevea Brasiliensis* actually grows.

Although Armstrong and Miller detected butadiene among the products of petroleum cracking in 1886,[13] ethanol (ethanol) remained the main feedstock of butadiene production for the early decades of polybutadiene rubber manufacturing. In 1901, Nef first reported the conversion of gaseous ethanol to butadiene using zinc and pumice.[26,27] Two years later, Ipatiev detected traces of butadiene after passing ethanol on powdered aluminum at high temperatures.[27] In 1915, Orstromislensky reported obtaining practical yields of butadiene by co-feeding ethanol with acetaldehyde on alumina-clay mixtures.[28] Finally, Lebedev reached appreciable butadiene production from pure ethanol on $ZnO\text{-}Al_2O_3$ catalysts, first reported in the 1928.[27] Both catalytic reactions became large-scale industrial processes. In the United-States, the Union Carbide and Carbon Chemical Corporation commercialized a process akin to that developed by Ostromislensky.

In the Soviet Union, Lebedev's work was industrialized so that by the eve of the Second World War, 62% of the 50,000 tons of synthetic rubber were derived from ethanol.[27]

The First World War demonstrated the importance of rubber to modern warfare when shortages forced the Central Powers to use inferior rubberlike material derived from thermal polymerization of isoprene for the production of tires.[23] The Interwar Period saw a further mechanization of war, but also of logistics: armies now relied on fleets of lorries to supply fuel and other goods. The Second World War became a conflict in which natural and industrial resources were crucial. When the dazzling expansion of the Japanese Empire into Southeast Asia drew the United States into the War, it also deprived the allies of their rubber plantations in British Malaya and Dutch Indonesia.[29] Consequently, a special American war committee concluded that—of all strategic goods crucial to Ally victory—rubber shortages posed the most immediate threat, more than steel, aluminum or gasoline. In response, the U.S. invested heavily in an emergency synthetic rubber research.[23,30–35]

In 1939, the American government launched a synthetic rubber program in partnership with industry and academe with the aim of expanding the U.S. synthetic rubber industry.[23,35,36] It also sponsored research on the catalytic conversion of ethanol to butadiene to meet the demand for monomer.[30,37] In this context, scientists at the Carbide and Carbon Chemicals Corporation and the Mellon Institute conducted seminal works on the reaction, including high-throughput catalyst screening,[37,38] process optimization[30,32] and mechanistic studies.[39,40] Soon, the U.S. government was able to commission three plants with a combined yearly production capacity of 220,000 tons of butadiene from ethanol.[27] By the end of the War, the Allies dwarfed the Axis in every strategic resource reserves, including butadiene and synthetic rubber.

With the advent of the inexpensive butadiene from petroleum cracking following the Second World War, the ethanol route fell into obsolescence. Industrially, very few plants remain in operation and only in countries where specific economic situation makes them profitable.[15]

Scientific interest declined simultaneously: only a few papers on the subject were published from the 1960s to the 2000s.[20] However, recent years have seen a renewed interest in the ethanol-to-butadiene reaction due to economic and environmental factors, which Weckhuysen *et al.* described as a renaissance of the subject. Although a subjective choice, we find that the 2011 publication by Jones *et al.*[41] is an ideal starting point for this renaissance, which has been marked by new insight into the reaction mechanism and more productive catalysts, as discussed below.

1.2.2. Butadiene Today

1.2.2.1. Butadiene Demand

Today, butadiene is crucial to the world economy. Due to its conjugated double bonds, this highly reactive molecule is involved in numerous chemical processes. Butadiene finds use in Diels-Alder, dimerization and oligomerization, hydrogenation and oxidation reactions.[12,13] Still, polymerization remains the main industrial process of butadiene; nearly 85% of the 11 million metric tons produced in 2015 were consumed as monomers. Synthetic elastomers, most notably styrene-butadiene rubber (SBR) and polybutadiene rubber (PBR), represent the largest share of butadiene derivatives. Other important products include acrylonitrile-butadiene-styrene resins (ABS). As depicted in Figure 1.2, butadiene-derived polymers have a variety of uses, from sealants to computer parts and clothing—a more complete list can be found in the review of White.[42] However, the fabrication of tires remains the most important downstream use of butadiene. Including tires, a typical medium size automobile contains 16.7 kg and 6.5 kg of SBR and PBR, respectively. As car manufacturing consumes around 70% of synthetic rubber, the automotive industry is considered the principal economic driver of the butadiene market.

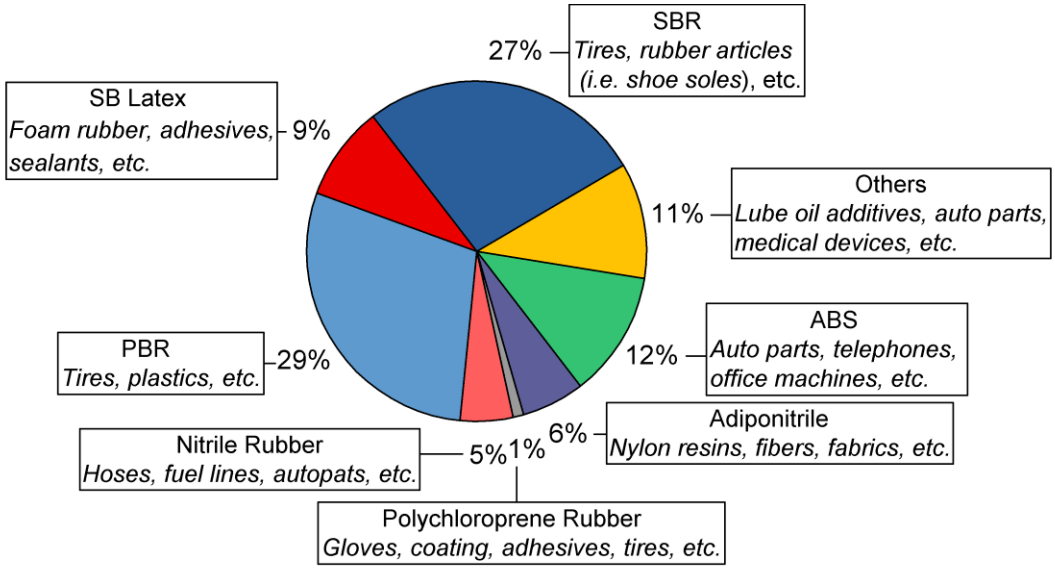

Figure 1.2 Butadiene demand and its end uses in 2015.[42,43]

Valued at around 30–40 billion USD, the global butadiene market is predicted to gradually increase in the coming years. While stagnating in the West, Asian countries are expected drive this growth, owing to the rising appetite for automobiles of their burgeoning middle classes. Dargay *et*

al. forecasted that personal car ownership would reach 2 billion units in 2030, twice the ownership of 2010.[44] China alone could reach 330 million cars and match the projected ownership of the US by that date.[45] A paradigm shift in tire manufacturing technology withstanding, butadiene production must to keep pace with the increasing global vehicle stock, an issue with which current processes may be ill-equipped for.

1.2.2.2. Current Butadiene Production

Nowadays, butadiene is primarily derived from ethylene production *via* steam cracking of naphtha, a C_{6-11} petroleum distillate. The process is a highly endothermic pyrolysis conducted in the presence of steam.[12,13] A vaporized hydrocarbon feed is heated to more than 1073 K at low pressure in a pyrolysis chamber. Under these conditions, carbon-carbon and carbon-hydrogen bonds can break down, resulting in a mixture of olefins, aromatics, tar and gases. Cracking lasts less than one second to prevent product degradation through secondary reactions. The addition of steam reduces the partial pressure of hydrocarbons, inhibiting the problematic formation of coke. After cooling, these products are fractionated into different cuts: C_1, C_2, C_3, C_4, *etc.* Due to the shared boiling range, simple distillation cannot extract butadiene from the C_4 fraction. Refineries generally address this issue by using extractive distillation, which operates using selective organic solvents to decrease the volatility of target compounds, thereby enabling their separation by distillation. The purity of butadiene is important because polymerization catalysts cannot operate properly in the presence of impurities.[13,46] Modern plants use *N*-methylpyrrolidone or dimethylformamide, and reach butadiene recovery rates are of 99 – 100%. Other C_4 species include butane, *n*-butenes and armful acetylenes. The C_4 products' distribution depends on the cracking conditions and the nature of the raw material. Generally, heavier hydrocarbons such as naphtha generate more butadiene. However, the main economic incentive of steam cracking remains the production of ethylene which is the most important olefin in the world. Consequently, crackers may seek to maximize ethylene output at the expense of butadiene and other byproducts by using lighter raw material. Figure 1.3 illustrates the influence of the feedstock on the production ratio between butadiene and ethylene: lighter hydrocarbons generate significantly less butadiene for the same amount of ethylene. [13]

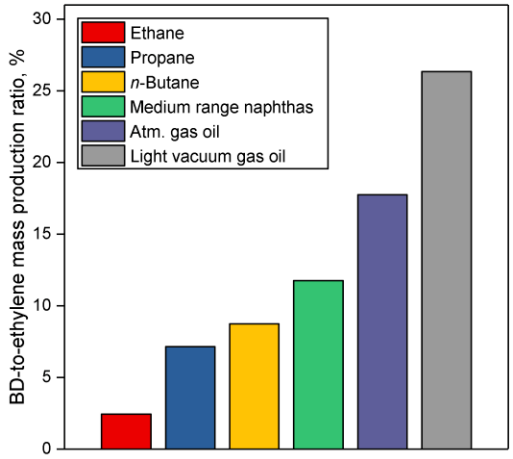

Figure 1.3 Mass production ratio between butadiene and ethylene in steam crackers according to the feed used.[13]

Due to its ties with ethylene production, recent trends in the petrochemical industry threaten the supply of butadiene. Ethylene-producing steam cracking plants are moving toward lighter feedstocks, yielding less butadiene for the same amount of ethylene.[43,47–49] Most notably, the emergence of inexpensive butane from shale gas as cracking feedstock has led to a decrease in the production of butadiene in North America[48,49] As Figure 1.4 illustrates, North American steam crackers are projected to generate less butadiene.[50] European crackers are also switching from naphtha to liquefied petroleum gas, further reducing global butadiene production.[43] China—the world's primary supplier of naphtha-derived butadiene—is commercializing the coal-to-olefin process: by converting coal to methanol *via* syngas, this technology can synthesize ethylene through the well-established methanol-to-olefin reaction.[43,47,51] However, these plants do not generate butadiene. If this these trends continue, butadiene shortages and the ensuing price increase can be expected.[48] Filling the gap caused by the issues resulting from production may require new technologies capable of producing butadiene on purpose.[48]

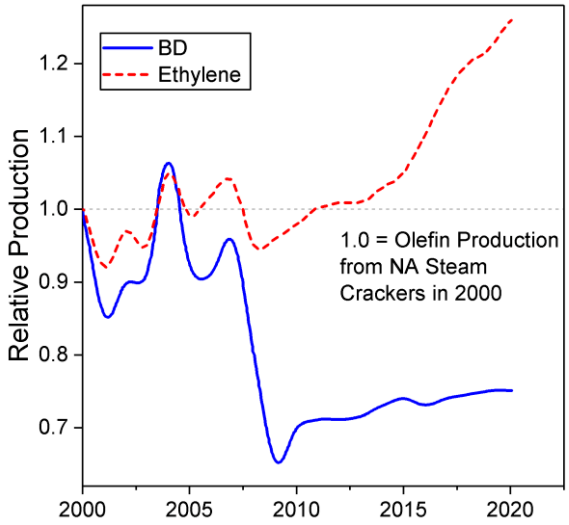

Figure 1.4 Projected figures for the yield of ethylene and butadiene from North American steam crackers relative to 2000 production levels.[50]

In addition, current butadiene production is unsustainable. Due to the highly endothermic pyrolysis step, steam cracking the most energy-consuming process used by chemical industry.[52] Because of its prevalence, the process generates yearly 180–200 million tons of CO_2, which is the most significant long-lived greenhouse gas (GHG).[52–54] Therefore, the naphtha cracking route to butadiene contributes significantly to climate change. With the adoption of the historic global climate accord, nations have agreed limit global warming to below 2 °C by reducing their GHG emissions.[55] Achieving this goal requires emissions to be cut by 40–70% by 2050. However, lowering the CO_2 production of an industrial process is highly complex.[53] Optimizing naphtha cracking using state-of-the-art technologies would reduce CO_2 emissions by 30% at best, according to the open literature.[52,54] Ultimately, considering that petroleum reserves are finite, it is unlikely that current butadiene production methods will ever be environmentally sustainable.

In summary, butadiene is predominantly obtained by the steam cracking of naphtha, which is primarily used to produce ethylene. However, the emergence of lighter alternative feedstocks threatens the supply of butadiene by favoring ethylene yield at expense of the former. As a result, meeting the butadiene demand, which is expected to grow with the increase of car ownership, may not be achieved with current technologies. Furthermore, steam cracking emits large quantities of CO_2, which is harmful to the environment. This situation is a good opportunity to develop and implement a sustainable and on-purpose process to produce butadiene.[1,15,48,56]

1.2.3. Alternative Butadiene Production Method

1.2.3.1. Dehydrogenation of C_4 hydrocarbons

The one-step catalytic dehydrogenation of n-butane, the Catadiene© process, already contributes to a small proportion of the global butadiene output.[13,57] However, its high endothermicity, rapid deactivation and relatively low yields currently restrict this process to limited economic circumstances.[13] With the rise of butane-rich Liquefied Petroleum Gas (LPG) extraction,[48] this option may become increasingly lucrative. Already, plans are being made to build units utilizing the similar Catofin process to convert propane to propylene, which suffers from similar supply issues.[47,58–60]

Oxidative dehydrogenation of butene, *i.e.*, the Oxo-D-type process, offers an additional route to butadiene.[13,60] The oxidation step significantly favors the reaction, resulting in butadiene yields comparatively higher than with the Catadiene process.[13] Furthermore, the formation of steam reduces coking. However, butanes are detrimental to this process, instead forming undesirable by products.[13] Consequently, it cannot directly operate from a C_4 fraction without prior purification. In any case, butanes are predominantly obtained from the steam cracking of naphtha,[57] defeating the purpose of detaching butadiene production from ethylene. Integrating oxidative dehydrogenation with a Catofin process producing propylene and butenes from LPG may be a practical way to obtain butadiene from hydrocarbon feedstocks other than naphtha. Nevertheless, their reliance on finite fossil resources does not address the sustainability issues of butadiene production.

1.2.3.2. Sustainable Butadiene

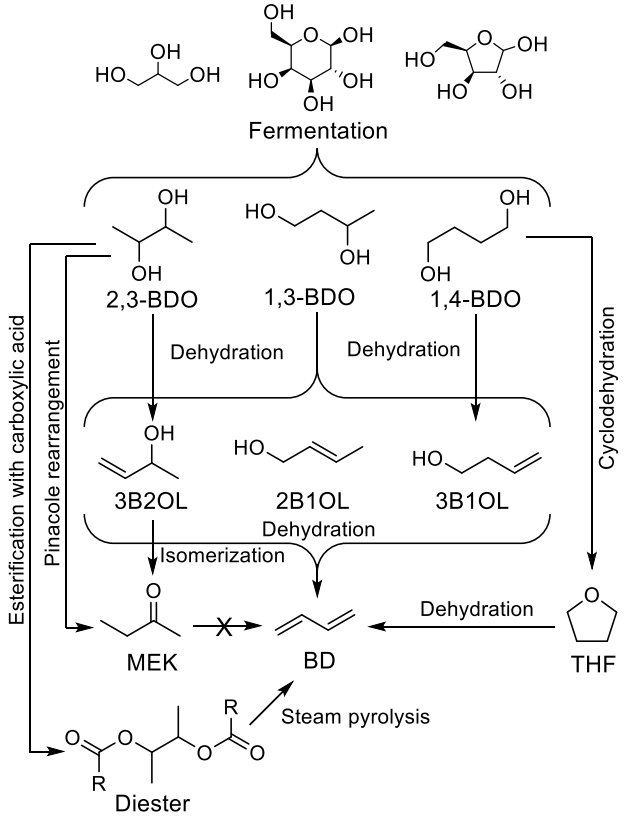

Figure 1.5 Main pathways from sugars to butadiene *via* butanediols.[15,61]

In recent years, new technologies have been developed to produce butadiene from renewable resources. In 2015, Genomatica, in collaboration with Braskem, announced the lab scale conversion of sugars to butadiene with bioengineered microorganisms.[62] More recently, Genomatica with Versalis favored a different approach to renewable butadiene: the conversion of butanediol (BDO), further identifying butanediol as the best suited precursor for this process.[63] Butanediol isomers can be produced from sugar fermentation[64–67], from industrial waste or from biomass-sourced syngas.[68,69] These can be subsequently converted to butadiene by the double dehydrogenation of the alcohol groups. In their review, Sato *et al*. highlighted how the butadiene yield depends on the type of BDO and catalyst used, as well as the reaction conditions.[61] Generally, BDO dehydrogenation reactions generate significant amounts of the corresponding butenols, formed by partial dehydrogenation of the substrates, but their recovery and further dehydration can ensure a high butadiene yield.[61]

BDO is well suited to be a precursor of butadiene: high selectivity towards butadiene are achieved at temperatures below 573 K using acid metal oxides, *i.e.*, Al_2O_3, ZrO_2, TiO_2, Al_2O_3-SiO_2, and liquid *3*-buten-*1*-ol (3B1OL) is easily recycled so that 90% yield are possible.[61,70] Our group reported how a 60% butadiene yield could be obtained at 473 K using Al-SBA-15 catalysts, demonstrating the ease with which BDO undergoes conversion.[71]

1,4-BDO has the advantages of being a crucial commodity traded in the millions of tons *via* the Reppe process[67,72,73] and of notably being an intermediate of the obsolete acetylene-to-butadiene process.[12,13,72–74] Double dehydration of 1,4-BDO generates butadiene, but high selectivity towards tetrahydrofuran (THF) when using acidic and amphoteric oxide catalysts at high temperatures reduces the overall yield.[15,75,76] Further research is needed to improve butadiene selectivity.[61]

In addition to butadiene, 2,3-BDO dehydration produces large amounts of methyl ethyl ketone (MEK) *via* a Pinacole rearrangement.[77–84] Although a potentially desirable product, MEK cannot be further converted to butadiene. As a result, butadiene production maximization necessitates specific catalytic systems and appropriate reaction conditions, namely high temperature. For instance, using a Sc_2O_3/Al_2O_3 double-bed, Sato *et al.* reached 94% selectivity towards butadiene.[84] However, it was the only rare-earth oxide screened out of 17 not to predominantly yield MEK, highlighting the unfavourability of butadiene formation. It should be noted that MEK synthesis using a new process in which 2,3-BDO is esterified with a carboxylic acid, where butadiene is obtained from the steam pyrolysis of the resulting ester.[85]

Many technologies are being developed for producing sustainable butadiene. Most advances have focused on the catalytic conversion of butadenediols, obtainable from the fermentation of bio-derived feedstocks (Figure 1.5). Selectivity issues have hindered butadiene productivity, but these are being addressed by recent breakthroughs. However, butanediol production levels remain too low to significantly replace current production methods.[1]

1.2.4. Ethanol-sourced butadiene

1.2.4.1. Ethanol production

The numerous advantages of ethanol make it a potential feedstock for sustainable on-purpose production of butadiene. Contrarily to other ascendant renewable feedstocks, ethanol is already an important global commodity.[4] Due to government incentives to promote biofuels, global ethanol supply is already at the industrial scale. It ranges in the 100s of billions of liters annually and is projected to grow in the coming years (Figure 1.6).[56,86] Predominantly obtained from the fermentation of agricultural biomass, it can also be produced sustainably and safely under the right conditions.[87] Although well-established, research on ethanol production carries on, providing further improvements and insights.[87] Currently, starch and sugar crops account for about 60% and 40% of ethanol, respectively.[88,89] Corn in the USA and sugar cane in Brazil are the principal raw materials of two largest suppliers of ethanol. But ethanol is not without issues: certain crops require more energy and water to cultivate, others compete for farmland with food. Ethics aside, these factors influence the commerciality and environmental impact of any process utilizing ethanol as feedstock.[87]

More specific to the practical production of butadiene from ethanol is the question of water content. Biomass-derived ethanol must be purified of water before being used in combustion engine,[88,89] which increases its cost, notably because of the ethanol-water azeotrope (95.5 wt.% ethanol). However, ethanol-to-butadiene processes can operate in presence of water, albeit not without changes to catalytic performances compared to anhydrous ethanol.[90] Nevertheless, under optimized conditions, it would be beneficial both in financially and environmentally to use water-containing ethanol as feedstock for producing butadiene as it would it would not require the more expensive drying steps.

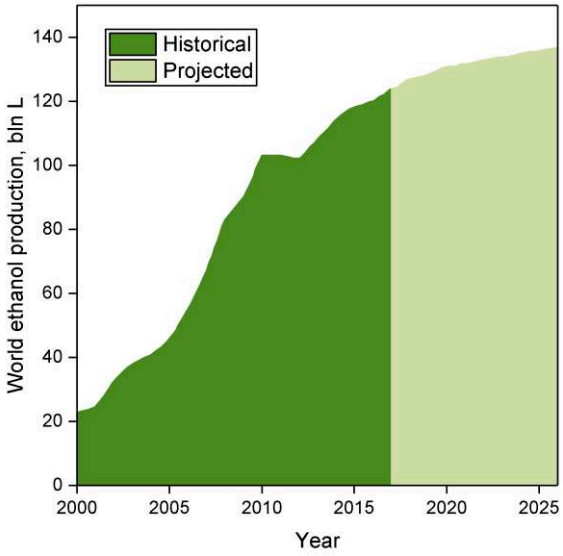

Figure 1.6 Historical and projected ethanol production.[86]

1.2.4.2. The Economics of Ethanol Conversion to Butadiene

New routes to butadiene must compete economically with the fossil-based production methods. Cavani *et al.* performed a life-cycle analysis which was extended to include economic considerations.[56] Performances aside, two factors dominated economic sustainability: low ethanol and high butadiene prices. Because each region uses different crops for fermentation, ethanol prices depend on the location of the production site. The US and Brazil were better suited to host ethanol-to-butadiene processes due to the affordability and availability of ethanol. A European plant would be disadvantaged by costlier raw materials and utilities. Butadiene production from ethanol in China was also dismissed as uncompetitive, despite the expected growth of Asia's BD market, because of high local ethanol prices. Due to a greater ethanol need and the investment required by the additional reactor for acetaldehyde production, the Ostromislensky process was judged as less likely to be financially sustainable.

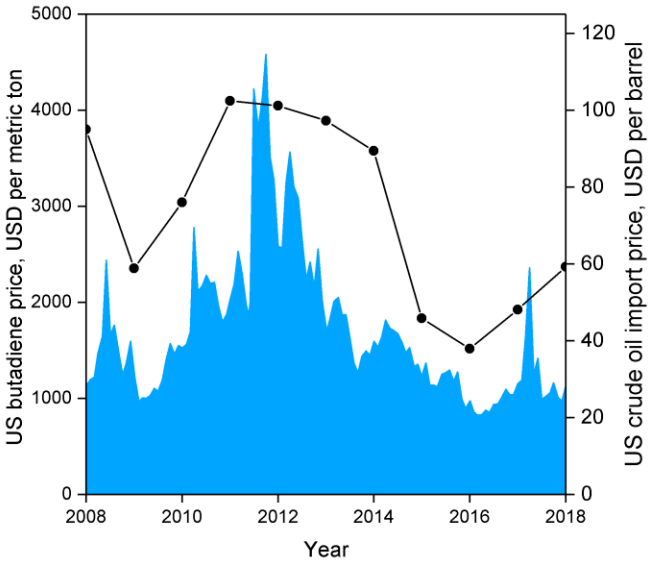

Figure 1.7 Historical American butadiene price in USD per metric ton from Intratec Solutions LLC (www.intratec.us)[91] versus historical crude oil import prices.[92]

Techno-economic analyses of Brazilian and American scenarios have provided further insight into the profitability of ethanol-to-butadiene processes.[93,94] Using 2012 prices, Burla *et al.*[93] determined a US-based plant employing the two-step process to be a highly promising venture. However, butadiene prices, which are partly influenced by that of oil, peaked in 2012 and have fluctuated significantly in the last 10 years (Figure 1.7). Considering the average price of butadiene between 2008 and 2018, the scenario described by Burla *et al.* was not profitable. Similarly, using a 5-year price average (2007 - 2011), Farzad *et al.*[94] found a Brazil-located plant employing the two-step process to have a 0% chance at profitability. Nevertheless, it found that integrating the butadiene production plant to the ethanol production process increased profitability by reducing infrastructure. It should be noted that both simulations were conducted using reaction parameters dating back to the 1950s; recent catalytic systems boast superior performances, albeit at the laboratory scale. To the best of our knowledge, no techno-economic analysis of the Lebedev process has been performed, ostensibly due to the lack of kinetic data. Incidentally, Michelin, in partnership with French energy enterprises, announced in 2013 the launch of a project for the development of a bio-sourced Lebedev process for the purpose of developing renewable synthetic rubber.[95] Accurately assessing the economic viability of ethanol-based butadiene would necessitate the modelling the reaction kinetics of modern catalytic systems. Whereas the price of ethanol and butadiene are subject to complexity of our modern economy, scholars have pointed out that

improving the catalytic performances of the process would enhance the viability of ethanol-to-butadiene process.[15,96]

1.2.4.3. Environmental Impact of Ethanol-to-Butadiene Processes

Assuming the use of first-generation ethanol production, Cavani et al. broadly compared the environmental impact of the Lebedev and Ostromislensky processes with naphtha-derived butadiene.[56] Because of the larger amount of resources involved, the two-step process was less sustainable than the one-step process, and in two scenarios, more damaging to the environment than naphtha cracking. Contributing factors were the transportation and transformation of biomass. As with profitability, sustainability depends on the geographic location as a result of the different crops in use. Sugar cane ethanol from Brazil was found to be more suitable compared ethanol produced in Europe and the US. The environmental burden of the Lebedev process was inferior to naphtha cracking, chiefly due to the reduction in fossil fuel depletion. With regards to climate change, only in Brazil did the Lebedev process comparatively reduce GHG emissions. Additionally, both the one- and two-step processes introduced other issues relating to crop culture: comparatively higher water consumption, eco-toxicity and food competition. Farzad *et al.*[94] simulated a process integrating a Brazilian sugar cane mill with on-site ethanol production and conversion to butadiene via the two-step process. The reduction of transport needs and the omission of ethanol purification beyond distillation prior to the ethanol-to-butadiene process both reduced energy needs. The combustion of butadiene and ethanol production residues also enabled energy self-sufficiency, further reducing GHG emissions. Overall, the integrated process presented significantly less harm to the environment, including human toxicity, ecotoxicity and climate change, than naphtha-derived butadiene. By situating a simulated ethanol-to-butadiene plant in existing American petrochemical facilities, Shylesh et al. argue that CO2 sequestration can be increased through hydrogen exports, thereby offsetting the use of natural gas in petroleum refineries.[97] However, this strategy could not outweigh the significant amounts of GHG emitted by corn grain-based ethanol; only by using Brazilian ethanol, imported through the port of Houston, and corn stub-derived ethanol was the process found to combat climate change. Under the right circumstances, ethanol-to-butadiene processes have a great potential for producing sustainable butadiene. While geographic location largely influences the amount of harm to the environment, several strategies can leverage to further improve the sustainability of the process.

1.3. The Ethanol-to-Butadiene Reaction

1.3.1. Toussaint-Kagan Pathway

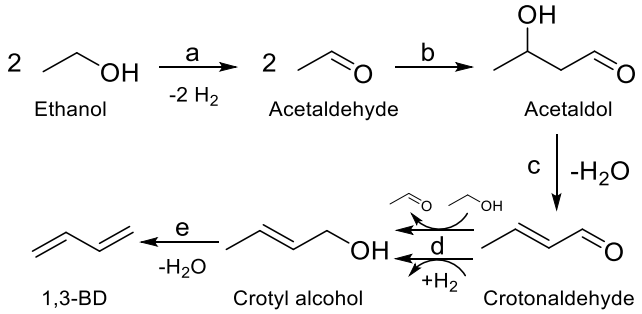

Scheme 1.2 The generally accepted pathway from ethanol to butadiene in the Lebedev and Ostromislensky processes.

Fully elucidating the mechanism of a reaction enables rational design of catalysts with tailored performances,[98] but also assists in kinetic modelling, which is important for process design.[99] Although alternatives have been proposed,[1,100,101] the Lebedev and Ostromislensky processes are now generally recognized to follow the same pathway (Scheme 1.2).[102–104] It consists of five steps: dehydrogenation of ethanol to acetaldehyde (Scheme 1.2 (a)); aldol condensation or aldolization of acetaldehyde to *3*-hydroxybutanal, commonly known as acetaldol (Scheme 1.2 (b)); dehydration of acetaldol to crotonaldehyde (Scheme 1.2 (c)); reduction of crotonaldehyde to crotyl alcohol (Scheme 1.2 (d)); dehydration of crotyl alcohol to butadiene (Scheme 1.2 (e)).

However, the consensus remains limited to the overall pathway: the molecular-level mechanism leading to butadiene remains under debate. Part of the issue can be attributed to the relative difficulty of observing intermediate species at the surface of heterogeneous catalysts.[105] Our current understanding of the reaction mechanism comes predominantly from fragmentary evidence gathered over the span of several decades by different research teams. Consequently, attempts at elucidating the mechanism have relied on various techniques, which have led to some discrepancies. This situation is further aggravated using diverse catalytic systems and reactions, possibly leading to different yet valid mechanisms. In our opinion, not enough evidence has been gathered to conclude whether the generally accepted pathway follows a single mechanism or is dependent on the experimental conditions. Often denominated the Toussaint[19,32,39,103] or

Kagan[18,106–108] pathway or mechanism, we will refer to the pathway illustrated in Scheme 1.2 as the Toussaint-Kagan mechanism to highlight the pioneering work of both teams.

1.3.1.1. Ethanol Dehydrogenation

The Lebedev process begins with the non-oxidative dehydrogenation of ethanol, forming acetaldehyde and hydrogen (Scheme 1.2 (a)). In an Ostromislensky-type process, it takes place in a separate reactor so that the butadiene-producing reactor operates with an ethanol-acetaldehyde feed. This step is important because it generates acetaldehyde which participates in the formation of butadiene.

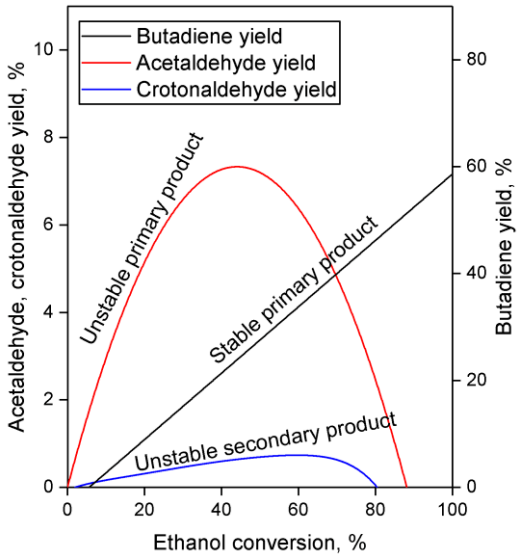

Figure 1.8 Typical Wojciechowski plots of the Lebedev process.[109,110]

Ostromislensky first proposed acetaldehyde to be a key intermediate, as evidenced by the design of his process.[28] By applying Wojciechowski's criteria,[111,112] which involves plotting product yield as a function of reactant conversion and conceiving a kinetic interpretation of the resulting curve, Ivanova *et al.*[109] and Villanueva Perales *et al.*[110] determined that acetaldehyde was a primary product of ethanol conversion that was involved in subsequent reaction steps leading to butadiene (Figure 1.8). Isotopic tracer experiments co-feeding ethanol with deuterated and ^{14}C-labelled acetaldehyde demonstrated the reversibility of the ethanol dehydrogenation[113] and confirmed that acetaldehyde participated in the formation of butadiene.[41,107]

Much insight on the mechanism of ethanol dehydrogenation in the context of the Lebedev process has been acquired using recent temperature-programmed surface reaction (TPSR) studies.

By coupling this technique with *in situ* direct reflectance infrared spectroscopy and mass spectrometry, Taifan *et al*. identified ethoxy species formed by the dissociation of ethanol on the surface of MgO-SiO_2 and correlated their disappearance at increased temperature with the emergence of acetaldehyde.[114] Similar observations were made on pure MgO.[100,115] It has been proposed that during the Lebedev process, ethanol dehydrogenation proceeds *via* surface ethoxide intermediates.[100,114,115] On metal oxides with acid-base pairs, the literature suggests acetaldehyde is formed by a sequential mechanism that begins with the dissociation of ethanol into a surface ethoxy intermediate followed by the E2 or E1cb-elimination of a proton (Figure 1.9 (a)).[103,116–119] According to Sykes *et al*, acetaldehyde formation occurs similarly on defective Cu,[120] suggesting this mechanism is not limited to metal oxides. Surface ethoxy species were also detected on other transition metal oxide catalysts during IR-TPSR experiments with ethanol.[121–123] However, the possibly these species were intermediates for the dehydration of ethanol[124] cannot be ignored.

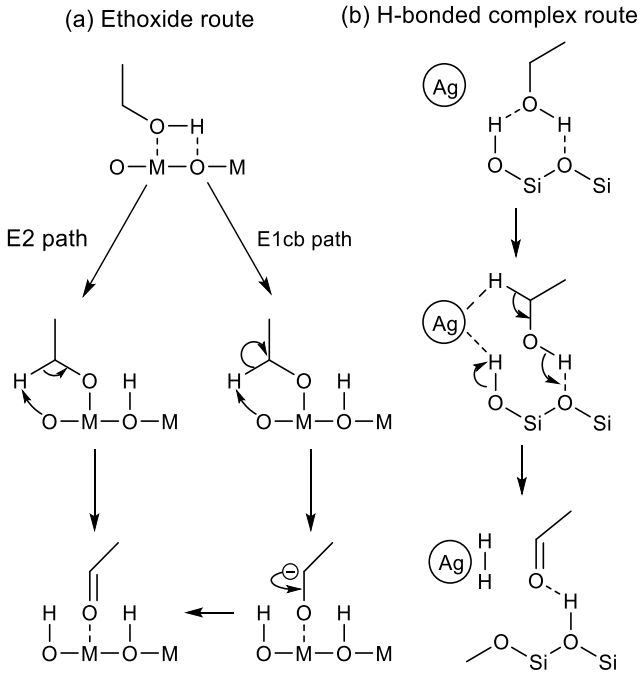

Figure 1.9 Proposed mechanisms for the dehydrogenation of ethanol to acetaldehyde *via* (a) an ethoxide intermediate[116] or (b) an H-bonded complex.[118]

Ivanova *et al*. did not detect surface ethoxy species during the dehydrogenation of ethanol on SiO_2-supported silver using *in situ* IR spectroscopy.[118] The authors explain this discrepancy by a weak interaction between the substrate and the catalyst carrier. Instead of ethoxy intermediates, density functional theory (DFT) calculations and spectroscopic evidence suggested that ethanol

forms a H-bonded complex with silanol groups prior to a simultaneous proton abstraction by metallic silver nanoparticles that forms hydrogen and acetaldehyde

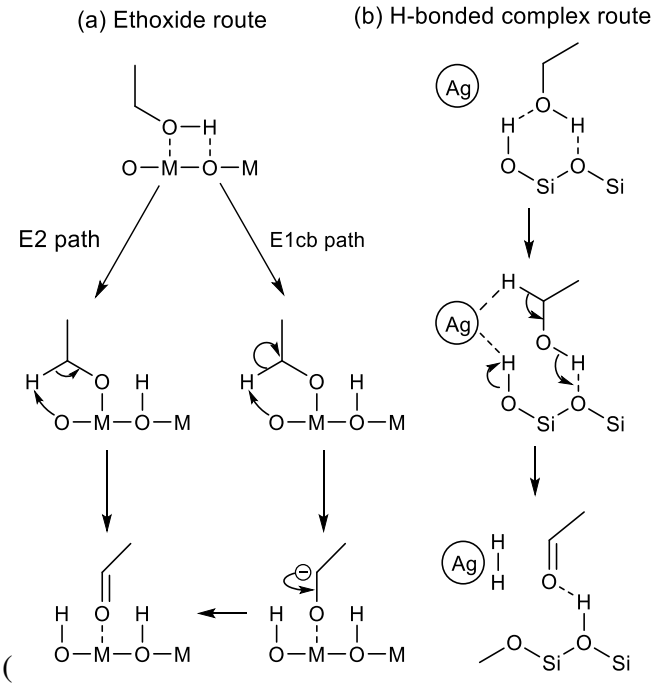

(Figure 1.9(b)).[125] Additionally, kinetic isotope effect (KIE) studies with various ethanol isotopomers on $Ag/ZrO_2/SiO_2$ indicated that both the Cα-H bond cleavage and proton abstraction occur simultaneously during the Lebedev process, disproving the involvement of surface ethoxy species.[102]

Ethanol dehydrogenation to acetaldehyde and hydrogen is well-established as the first step of the Lebedev process according to the Toussaint-Kagan pathway. Studies of the surface intermediates suggested that the reaction mechanism depends on the type of catalyst. Over metal oxides on metallic copper, a sequential mechanism involving the dissociation of ethanol to ethoxy species and the subsequent elimination of a proton to form acetaldehyde has been proposed. On silica-supported silver, the reaction has instead been proposed to proceed *via* the simultaneous proton abstraction of an H-bonded complex formed between ethanol and surface silanol groups. However, it should be noted that in the broad context of light alcohol dehydrogenation, other mechanisms have been proposed.[126] Further studies should seek to confirm the nature of surface intermediates on the various catalysts active in the Lebedev process.

1.3.1.2. Aldol Condensation of Acetaldehyde

Synthesizing butadiene from C_2 compounds necessarily involves the formation of new C–C bonds. Although the aldol condensation/aldolization of acetaldehyde to crotonaldehyde (Scheme 1.2 (b)) is now recognized as the bond-forming reaction, this topic has been the subject of much debate.[1,15,100] A summarized by Quattlebaum *et al.*[39] the involvement of crotonaldehyde was proposed following the observation that: (1) crotonaldehyde readily forms when passing acetaldehyde over Ostromislensky active catalysts; (2) crotonaldehyde is not present in significant amounts when converting ethanol-acetaldehyde mixtures over the same catalyst; (3) crotonaldehyde converts to butadiene when co-fed with ethanol under the same conditions.[39,40]

A glaring issue with this theory has been the repeated absence of acetaldol, the immediate product of acetaldehyde coupling, in the output stream of catalytic tests. Several authors attributed the absence of acetaldol to its rapid dehydration to crotonaldehyde, which subsequently reacted with ethanol.[103,109,113,127] Nonetheless, Corson *et al.* failed to observe any improvement in the yield of butadiene when co-feeding ethanol with acetaldol on a commercial Ta/SiO_2 catalyst, concluding instead that the latter reverted to acetaldehyde.[8,40] Cavani *et al*. confirmed this reversibility of acetaldol when testing the substrate over MgO catalysts.[100] However, Taifan *et al*. argued that the reverse reaction of acetaldol was promoted by the absence of ethanol to react with crotonaldehyde, shifting the equilibrium towards acetaldehyde.[128] Cavani *et al*. further suggested that crotonaldehyde may instead be a byproduct of ethanol conversion to butadiene, not an intermediate.

Recent publications have provided more evidence for the intermittent presence of acetaldol during the conversion of ethanol to butadiene. For instance, Zhang *et al.* studied the Lebedev process using the pulse reaction technique,[129] which is more adequate than continuous flow heterogeneous catalytic reactions for observing intermediates.[130] Using mass-spectrometry to monitor the products formed, ethanol pulsed over $MgO\text{-}SiO_2$, indicated the sequential formation of acetaldehyde, acetaldol, crotonaldehyde and butadiene. Surprisingly, crotyl alcohol, another key intermediate discussed further below, was undetected, possibly because of its rapid dehydration. Furthermore, Taifan *et al*. observed with DRIFTS a band at 1273 cm^{-1} previously assigned to acetaldol when reacting ethanol over $MgO\text{-}SiO_2$ during TPSR experiments.[114] It should be noted that the authors recognized the conditions used were not optimized for the observation of acetaldol.

Whether or not the elusive acetaldol plays a role in the ethanol-to-butadiene, the validity of the aldol condensation pathway is also dependent on the involvement of crotonaldehyde. New publications now suggest crotonaldehyde to be a key intermediate. Zhang *et al.* found butadiene to be kinetically subsequent to crotonaldehyde in their pulse study of the reaction on $MgO\text{-}SiO_2$.[129] TPSR experiments with EtOH on $MgO\text{-}SiO_2$,[114] Ag/ZrO_2[121] and ZnY/SiBEA[122] demonstrated the appearance of IR bands associated with crotonaldehyde when increasing the temperature, further coinciding with the detection of butadiene in the gas phase by mass spectrometry in the latter case.[131] Hermans *et al*. conducted complex modulated co-feeding experiments monitored operando DRIFTS-MS.[104] The mechanistic implication of their observation was that acetaldehyde formed crotonaldehyde, which was consumed by ethanol to form butadiene, but would accumulate when switching the feed of ethanol off and the surface species were depleted. Furthermore, a surface intermediate formed only in the presence of crotonaldehyde and ethanol was detected, and was proposed to play an important role in the formation of butadiene. Ivanova *et al*.[109] and Villanueva Perales *et al*.[110] further found crotonaldehyde to be a secondary stproduct of the Lebedev process using Wojciechowski's criteria (Figure 1.8), suggesting that: (1) crotonaldehyde is formed from a primary product, *e.g.*, acetaldehyde; (2) crotonaldehyde is consumed during the reaction.

Although most authors now recognize that the conversion of ethanol to butadiene comprises the aldol condensation of acetaldehyde, there remains disagreements concerning the molecular-level mechanism of this reaction step. In its simplest form, the prevalent rationalization involves the enolization of an acetaldehyde molecule on acid-base pair sites; the resulting activated intermediate reacts with a neighboring acetaldehyde molecule to create a new C–C bond. Dehydration to crotonaldehyde is assumed to occur readily upon formation of the adol. However, different molecular-level mechanisms have been proposed to take place depending on the type of catalyst used.

On predominantly basic oxides, *i.e.*, earth-alkaline oxides such as MgO and CaO, the strong basic sites of acid-base pairs are believed to fully abstract the α-proton of acetaldehyde, resulting in an enolate that is stabilized by the Lewis acid moiety of the acid-base pair. Because the *d* orbital of pre-transition metal oxides is not accessible, the role of their Lewis acidic cations is limited to stabilizing *via* electrostatic interactions the electron-rich carbonyl group of both the enolate and the second acetaldehyde molecule. Once in proximity, the β-carbon of the enolate reacts with the α-carbon of the acetaldehyde molecule to form the new C–C bond. Acetaldol is finally formed by the

back-transfer of a proton from the surface of the catalyst. Figure 1.10 (b) depicts the sequential steps involved in this mechanism. In agreement with this mechanism, Taifan *et al.* reported observing surface enolates during the TPSR experiments with ethanol and acetaldehyde on MgO-SiO_2 using DRIFTS.[114]

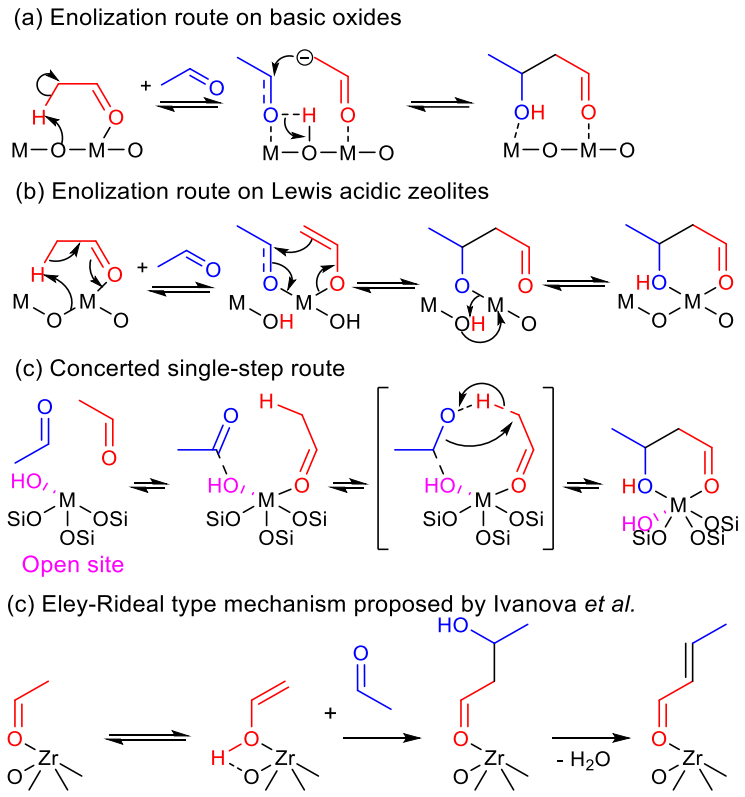

Figure 1.10 Proposed mechanisms for the aldolization of acetaldehyde taking place during the conversion of ethanol to butadiene.

Over transition metal oxides possessing strong Lewis acid characteristics, the metal cation is believed to polarize the carbonyl group of the first acetaldehyde molecule, acidifying the α-proton.[132] Oxygen from the catalyst framework acts as a base and abstract the proton, resulting in cleavage of Si–O–M bonds in the case of silica-supported catalysts.[133] Contrarily to pre-transition metal oxides, the partially filled *d* orbital of transition metal oxides is accessible for bonding. It can form an enolate or enol intermediates coordinated on cation sites depending on the type of metal used (Figure 1.10 (b)).[133] The metal center can accommodate a second acetaldehyde molecule, which is followed by a similar C–C bond and proton back-transfer previously described for basic oxides. The unstable presence of surface enolates was observed by Li *et al*. using DRIFTS on Zn-Y/SiBEA catalysts during TPSR experiments following the adsorption of ethanol and acetaldehyde.

However, Ivanova *et al.* recently proposed an alternative mechanism in which the coupling of both acetaldehyde molecules on transition metal cations does not involve the formation of an enolate intermediate, proceeding instead *via* a single-step concerted mechanism (Figure 1.10 (c)).[133] This theory comes from the failure to observe the *in situ* formation of enolates with IR spectroscopy during the condensation of acetaldehyde on Zr-BEA and Ti-BEA. Hydrogen–deuterium exchange activity studies with heavy water further suggested that the catalysts did not stabilize enolate species, as evidenced by to the low degree of deuterium incorporation in acetaldehyde. In the case of Zr-BEA, DFT calculations indicated that the two acetaldehyde molecules preferably formed an H-bonded complex stabilized by the metal cation and OH group of so-called Lewis open sites—isolated atoms in the tetrahedral positions of a zeolite structure connected to three −O−Si linkages and one OH group.[134] C–C coupling would occur in a single concerted step involving an α-proton transfer from one aldehyde molecule to the carbonyl group of the second. Having failed to observe enolate species with in situ IR spectroscopy during the two-step process, Hermans *et al*. advocated a similar one-step mechanism for the same condensation reaction over Ta-BEA.[104] However, rather than an adsorption on the metal sites, the authors suggest that acetaldehyde reacts on OH groups—either coordinated to Ta(V) or from neighboring silanol groups.

Ivanova *et al.* later revisited the aldol condensation mechanism by combining kinetic measurements, steady-state isotopic transient Kinetic Analysis (SSITKA) and deuterium-tracing techniques for the conversion of ethanol to butadiene over $Ag/ZrO_2/SiO_2$. Since a kinetic effect was observed with β-deuterated ethanol, the authors dismissed the direct aldol condensation pathway previously proposed (Figure 1.10 (c)), which would have otherwise involved the α-proton of acetaldehyde (the β-proton of ethanol), in favor of a stepwise mechanism involving enolization. Furthermore, the rapid growth and decay of labeled and unlabeled butadiene response curves following the switch from isotopic-labelled to unlabeled feed during SSTIKA experiments suggested the coupling reaction occurred between an acetaldehyde molecule strongly adsorbed on the catalyst surface and an acetaldehyde molecule in the gas phase. Consequently, a new mechanism combining both observations was proposed for the aldolization of acetaldehyde: it proceeds *via* a stepwise mechanism involving enolization, followed by C–C bond formation between the enolate intermediate and a gas phase acetaldehyde molecule, *e.g.*, an Eley-Rideal mechanism (Figure 1.10 (d)). This proposal differs from most mechanistic interpretation of

acetaldehyde coupling in the context of the ethanol-to-butadiene reaction[103,104,114,122,128] or the closely related Guerbet coupling[117,135], which assumes a Langmuir-Hinshelwood type reaction, although Eley-Rideal mechanisms were proposed for the condensation of other short-chain aldehydes.[136,137]

While the formation of crotonaldehyde *via* the aldol condensation of acetaldehyde is generally accepted as a key-step of the Toussaint-Kagan pathway from ethanol to butadiene, our understanding of the molecular-level phenomena takin place remains limited. Several mechanisms have been proposed, but the direct observation of surface intermediates and their correlation to activity has been limited, ostensibly due to their high instability.[114,122] Clarifying these issues would be benefit catalyst design—are open Lewis acid sites necessary for the one-step aldol condensation?—and kinetic modelling by identifying intermediate steps and answering whether an Eley-Rideal or Langmuir-Hinshelwood type reaction is involved. However, DFT calculations have also shown the favorability of different mechanisms to depend on the nature of the catalytic systems used.[103,133,138–140] This may limit the validity of observations made to the system under study.

1.3.1.3. Crotonaldehyde Conversion to Butadiene

Obtaining butadiene from a crotonaldehyde feed on catalysts for the Ostromislensky process has only proceeded when co-feeding ethanol.[39,40] This observation highlights the importance of ethanol to reaction beyond its role as source of acetaldehyde. It also explains why the Ostromislensky process requires ethanol-acetaldehyde mixtures to operate. Early mechanistic theories considered the direct catalytic deoxygenation of crotonaldehyde to butadiene with ethanol as hydrogen source to be the reaction step.[39] Having noted that: (1) crotonaldehyde was reduced to crotyl alcohol under H_2 and (2) crotyl alcohol readily dehydrated to butadiene under typical reaction conditions, Kagan *et al.* proposed that crotonaldehyde was first reduced to crotyl alcohol, which dehydrated to form butadiene.[15,27,108] Although sometimes absent from the output stream of reactors during catalytic testing due to its rapid dehydration, the participation of crotyl alcohol is now generally recognized and supported by several experimental observations. For instance, ethanol conversion over magnesia at very short contact time enable the detection of crotyl alcohol and identified it as a kinetic precursor to butadiene.[100] DRIFTS-monitored TPSR of experiments with crotyl alcohol adsorbed on the surface of MgO-SiO_2 physisorbed and chemisorbed species, with the disappearance of the latter coinciding with the detection of vapor-phase butadiene.[114] The MS-

monitored operando modulated co-feeding experiments for the Lebedev and Ostromislensky processes further provided insight on this reaction step.[104,122] As the signal patterns of crotyl alcohol and butadiene behaved similarly upon feed switching, *i.e.*, from ethanol-acetaldehyde to pure acetaldehyde, the authors concluded that both shared the same precursor, *e.g.*, crotonaldehyde. The detection of deuterated crotyl alcohol when reacting labelled ethanol with crotonaldehyde, and its replacement by unlabeled crotyl alcohol upon switching to a non-isotopic feed further confirmed both crotyl alcohol to be the intermediate between crotonaldehyde and butadiene, but also that ethanol was involved in its formation.

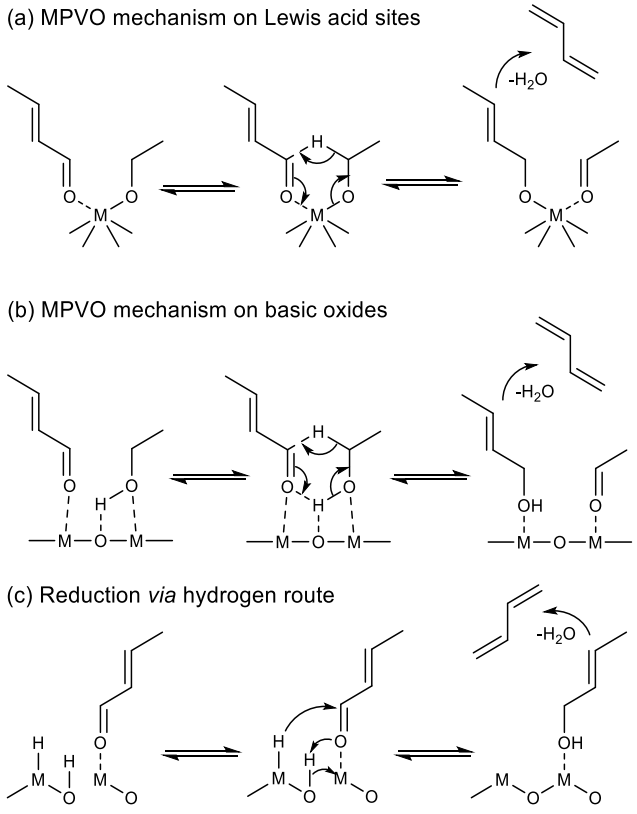

Figure 1.11 Mechanisms of crotonaldehyde reduction to crotyl alcohol and its dehydration to butadiene on different catalysts.[102,119,141]

How crotonaldehyde is reduced to crotyl alcohol has raised further questions. Undoubtedly, ethanol enables the conversion of crotonaldehyde to butadiene, but so does hydrogen,[142] propanol,[40,143] which yields C_3 and C_5 byproducts, or even crotyl alcohol itself.[40] Therefore, its role has been the subject of debate. Some scholars have argued that ethanol is the reducing agent (Figure 1.11 (a) and (b)),[102–104,140,143] others that it acts as an *in situ* source of surface hydrogen species responsible reducing the carboxyl group of crotyl alcohol (Figure 1.11 (c)),[144] or both.[122] Old[142,145]

and new[15,19] thermodynamic studies have shown the reduction of crotyl alcohol with hydrogen to be less favorable than that with ethanol. As a result, publications often disregard the role of hydrogen,[103] focusing instead on crotonaldehyde reduction with ethanol, which Niiyama *et al*. proposed to proceed *via* an intermolecular transfer involving acid-base sites.[15,143] This reaction is believed to follow a Meerwin-Pondorf-Verley reduction mechanism, also referred to as a Meerwin-Pondorf-Verley-Oppenauer (MPVO) reaction to account for the oxidation of ethanol to acetaldehyde.

The MPVO reaction mechanism consists in the stabilization of ethanol and crotonaldehyde on Lewis acid sites—the same site for transition metals such as Zr[102] and Ta[104] (Figure 1.11 (a)) and neighboring sites on pre-transition metal oxides[119] (Figure 1.11 (b))—followed by the formation of a six-membered transition state; the reaction then proceeds by a hydride transfer from the alcohol to the carbonyl group, which forms acetaldehyde and crotyl alcohol. Relatively few studies have focused on studying this mechanism in the context of the in the context of the ethanol-to-butadiene reaction. Ivanova *et al*. observed a reactivity trend typical of Langmuir-Hinshelwood type mechanisms when changing the partial pressure of ethanol co-fed with crotonaldehyde to form butadiene over $Ag/ZrO_2/SiO_2$.[102] More interestingly, their catalytic tests with ethanol deuterated in the α-carbon position resulted in the formation of $CD_2–CH=CD–CH_2$, a butadiene isotopomers that is only obtainable by the D-shift taking place with this six-membered transition state.[102] MPVO reactions between other carbonyl and reductive alcohols on heterogeneous catalysts substantiate the validity of this mechanism in the conversion of crotonaldehyde to crotyl alcohol.[146–148]

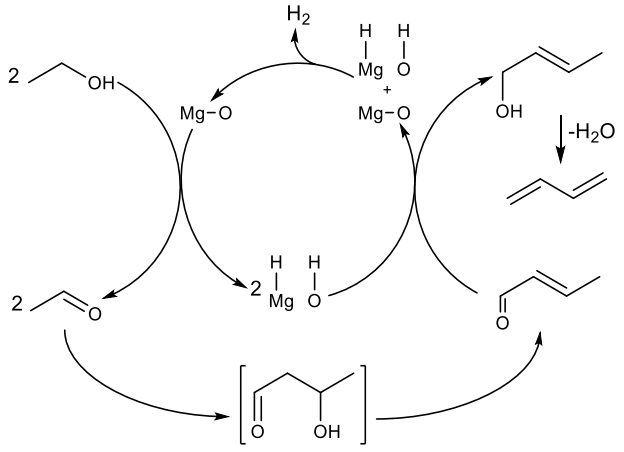

Figure 1.12 The ethanol-to-butadiene pathway on MgO considering dissociated hydrogen as the reductive agent in the conversion of crotonaldehyde, as proposed by Baba *et al*.[144,149,150]

Recently, Baba *et al*. reiterated that ethanol is not the sole reducing agent of crotonaldehyde in the ethanol-to-butadiene reaction. This claims stems from the fact that the reaction can proceed on MgO,[100,144,149] but not CaO, despite both being alkali-earth metal oxides with basic properties. According to the authors, contrarily to MgO, CaO cannot perform the heterolytic dissociation of hydrogen. Therefore, the hydride and hydroxide species formed at the surface of MgO were attributed a role to explain the discrepant activity of the two oxides. Baba *et al*. suggested that chemisorbed hydrogen could reduce crotonaldehyde to crotyl alcohol during the conversion of ethanol to butadiene (Figure 1.12). Incidentally, ZrO_2,[151] Ag^{+}[152] and ZnO,[153,154] well-established components of ethanol-to-butadiene catalysts, can also promote the heterolytic dissociation of hydrogen. Bhattacharyya and Ganguly compared the yield of H_2 and acetaldehyde following the conversion of ethanol-crotonaldehyde mixtures on $ZnO\text{-}Al_2O_3$ to investigate the reduction step.[142] According to these authors, the relative excess of acetaldehyde compared to hydrogen suggests that crotonaldehyde reduction by ethanol preferably takes place. However, the opposite conclusion—that the observed lower quantity of H_2 demonstrates its consumption in the reduction step—may also be drawn from the same results. Clarifying the degree of participation of dissociated hydrogen in the conversion of ethanol to butadiene is crucial for proper kinetic modelling which would consist on rate laws depending on the concentration of reactants involved. Accurately predicting the output of hydrogen is also crucial considering that selling it has been considered a strategy for reducing the environmental impact of the Lebedev process.[97]

Dehydration of crotyl alcohol to butadiene and water (Figure 1.11) has long been known to occur readily on catalysts active for the Ostromislensky process.[40,108] Recently, Villanueva Perales *et al.* confirmed it also occurred on catalysts for the Lebedev process.[110] Studies found the dehydration of crotyl alcohol to be highly favored thermodynamically.[15,19,142,145] Consequently, this reaction step has not attracted significant attention: it is assumed to readily take place during the conversion to butadiene upon crotyl alcohol formation.

1.3.1.4. All-inclusive Toussaint-Kagan mechanism proposals

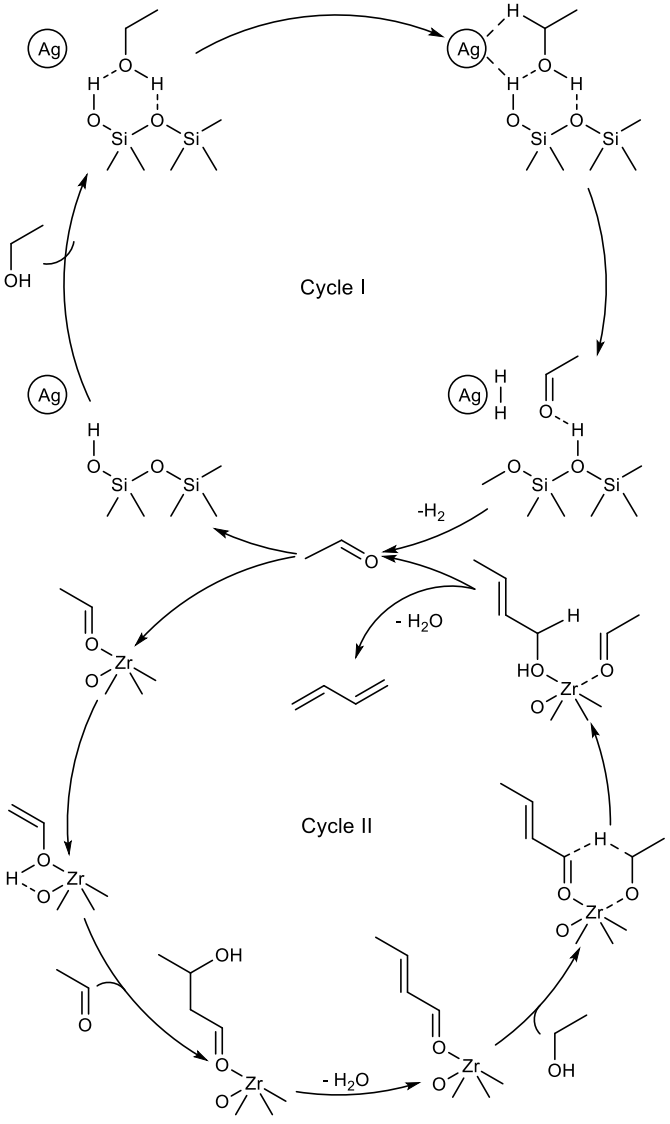

Figure 1.13 Dual cycle molecular-level mechanism for the ethanol-to-butadiene reaction proposed by Ivanova *et al.*[102]

In 2017, Ivanova *et al*. presented the first fully-fledged molecular-level mechanism of the ethanol-to-butadiene reaction. Their proposal stems from results obtained with kinetic measurements, SSITKA and deuterium tracing techniques performed using $Ag/ZrO_2/SiO_2$. The authors interpret the reaction as two distinct catalytic cycles (Figure 1.13): cycle I, the dehydrogenation of ethanol, and cycle II, the condensation-reduction-dehydration pathway of acetaldehyde to butadiene; two distinct active sites were considered. Cycle II essentially described the reactions taking place during the Ostromislensky process on catalysts lacking dehydrogenating

properties. At present, the mechanistic interpretation of Ivanova *et al*. is the most detailed in the literature. Hermans *et al*. further elaborated on the catalytic cycle II with Ta-BEA, namely by distinguishing two activated surface intermediates for the aldol condensation and MPVO reaction steps.[104] Li *et al*. proposed a similar reaction mechanism over a bifunctional Zn-Y/SiBEA catalyst, albeit in the form of a single cycle containing both active sites.[122] The authors chose to represent crotonaldehyde reduction with dissociated hydrogen rather than ethanol, but recognized both pathways may take place. Comprehensive mechanistic elucidations of the mechanism on MgO and ZrO_2 were also performed using DFT calculations by Taifan *et al*.[103] and Yu *et al*.[140] However, the mechanisms proposed in the literature disagree on certain aspects, notably at the molecular level. We have highlighted some points of contention that could be addressed in future works:

- Verifying whether the choice of catalyst causes significant mechanistic differences at the molecular level, and whether these differences are relevant to catalyst design and kinetic modelling. At present, the evidence gathered suggests this to be the case;
- Verifying the involvement of surface intermediates, such as ethoxy species for the dehydrogenation of ethanol, and enolate species for the aldolization of acetaldehyde;
- Clarifying the mechanism forming crotonaldehyde from acetaldehyde. Notably whether it involves a direct coupling reaction,[133] or a step-wise coupling with enolate intermediates, and whether the latter follows an Eley-Rideal[102] or Langmuir-Hinshelwood mechanism;[155]
- Measuring the contribution of hydrogen and ethanol to the reduction of crotonaldehyde to crotyl alcohol. Is the participation of hydrogen dismissible?

1.3.2. Alternative Pathways to Butadiene

More than variants of the Toussaint-Kagan pathways, alternative pathways with different reaction steps have been considered for the conversion of ethanol to butadiene. The main point of divergence with the common only accepted pathway concerns the formation of the C – C bond. Unfortunately, only a few scholars have taken account of these alternative mechanisms in their own study of the mechanism. Consequently, it is difficult to assess their validity; they may co-exist as complementary pathways to butadiene, may be wrong, but also may be the main pathway under specific conditions.

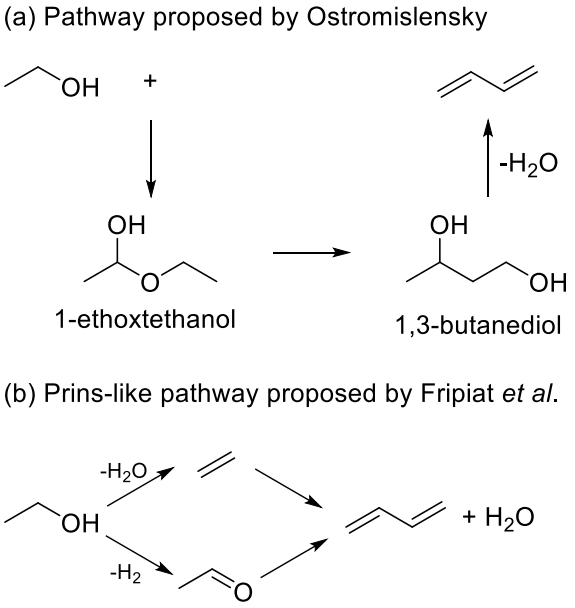

Figure 1.14 Ethanol-to-Butadiene Pathways proposed by (a) Ostromislensky and Balandin; (b) Fripiat et al.[15,19]

Ostromislensky[28] and Balandin[156] proposed that ethanol reacted with acetaldehyde to form *1*-ethoxyethanol. The latter would undergo a hemiacetal rearrangement to form butanediol, which would dehydrate to form butadiene. Quattlebaum *et al*. later dismissed this mechanism, arguing that the rearrangement reaction did not have experimental support.[39] Furthermore, butanediol yielded significantly less butadiene than ethanol-acetaldehyde mixtures when reacted on a Ta_2O_5/SiO_2 catalyst active in the Ostromislensky process.[40] Recently, Taifan *et al*. studied the viability of this pathway on MgO using DFT calculations.[103] They found the thermodynamic stability of *1*-ethoxyethanol to prevent further reaction *via* a hemiacetal rearrangement.

Fripiat *et al*. studied the ethanol-to-butadiene reaction on silver-exchanged aluminated sepiolite.[101] In plotting product selectivity version ethanol conversion, the authors found a linear relation between ethylene and butadiene yield. On this basis, they argued ethylene reacted with acetaldehyde *via* a Prins-like mechanism to form butadiene. Thermodynamic equilibrium calculations of the proposed mechanism found it to be favorable, albeit slightly less than the Toussait-Kagan mechanism.[19] However, these calculations omitted the formation of the intermediate *3*-buten-*2*-ol, the expected product of a Prins reaction between acetaldehyde and ethylene. Our own calculations, made using the Aspen Plus® software with mixtures of pure components (*vide infra*), indicated that the intermediate product formation step is highly

endergonic. Although they also proposed a Prins-like mechanism, Natta and Rigamonti reject it after the addition of 20% ethylene to the reactant feed failed to improve butadiene yield. Taifan *et al.*[103] and Yu *et al.*[140] investigated the Prins-like mechanism in their DFT calculations on the conversion of ethanol, finding the new C–C bond to have a higher energy barrier than the aldol condensation on MgO and ZrO_2 respectively. Taifan *et al.* added that aldolization pathway must be kinetically favored, as the Prins-like mechanism was more exergonic, suggesting that the latter occur under specific conditions.

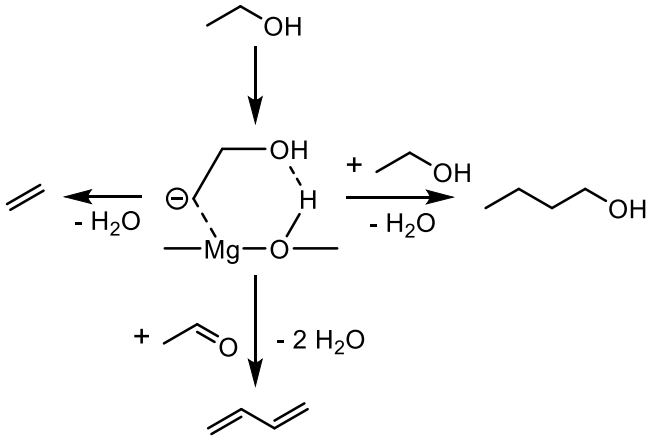

Figure 1.15 Pathway to butadiene, ethylene and butanol proposed by Cavani *et al.*[100]

Instead of acetaldehyde self-coupling, Cavani et al. proposed that new C–C bonds stemmed from the reaction between C2-oxygenated species and a surface carbanion formed from ethanol.[100] The authors reached this conclusion after studying the reactivity of ethanol over basic oxides, *e.g.*, MgO and MgO-containing catalysts. Certain observations were considered incompatible with the Toussaint-Kagan pathway. Catalytic tests performed at very short contact showed crotonaldehyde kinetically consecutive to crotyl alcohol, which was recognized as the precursor to butadiene. Furthermore, Cavani et al. questioned the role of acetaldol, the presumed transient intermediate of the aldol coupling of acetaldehyde to crotonaldehyde. Alone or co-fed with ethanol, the compound failed to produce butadiene on MgO. In FTIR-TPSR experiments using MgO with pre-adsorbed ethanol, peaks assigned to crotyl alcohol also emerged at lower temperature than those attributed to crotonaldehyde. Consequently, the aldolization step of the Toussaint-Kagan pathway was rejected on the grounds that C4 alcohols appeared to kinetically precede their alleged precursor. Instead, the authors proposed that a surface carbanion formed by the methyl deprotonation of ethanol participated in a coupling reaction. DFT and spectroscopic studies served as the basis for

this argumentation. In the aforementioned FTIR-TPSR experiments, the increase of a band at v = 1143 cm-1 above 573 K coinciding with formation crotyl alcohol, but distinct to it was observed, suggesting a relationship between the two species. This unidentified signal matched with one IR band of a C2 carbanion on MgO simulated by DFT calculations, to which it was tentatively assigned. However, the experimental results lacked the other peaks of the simulated IR spectra, a discrepancy that admittedly remained unclear.

With DFT calculations, a pathway involving the reaction between the theorized surface C2 carbanion and acetaldehyde was found to rival the Toussaint-Kagan pathway energy-wise (Figure 1.15). First, ethanol underwent proton abstraction from its β-carbon to form the carbanion, which was stabilized by the catalyst surface. This intermediate could then follow three different pathways. Its hydroxyl group may react with the previously dissociated proton to form water and ethylene. It may also attack the oxygen-bound carbon atom a neighboring adsorbed ethanol or acetaldehyde molecule. In the first case, butanol and water were produced. With acetaldehyde, the reaction generated water and either crotyl alcohol or *3*-buten-*1*-ol. These alkenols were proposed to dehydrate into butadiene. Cavani et al. further made similar observations on MgO-SiO2, a more conventional catalyst for the Lebedev process than pure MgO.[157] The carbanion mechanism was thus suggested to take place on MgO-containing catalysts, explaining the presence of ethylene, butanol and butadiene amongst the products. So far, no other scholars have corroborated some key observations made by the authors. DFT calculations made by Taifan et al. found the carbanion to be unstable on MgO, preferably forming ethylene rather than following the pathway leading to butadiene.[103] Furthermore, Taifan *et al.* did not report the IR bands attributed to the carbanion specie over MgO-SiO_2.[114] Admittedly, Cavani et al. noted that Mg:Si ratio of 15 was necessary to observe it distinctively, whereas the catalyst used by Taifan et al. had a ratio of 1. It may be the case that this pathway occurs preferably on specific catalysts, such as pure MgO and MgO-SiO_2 with high magnesia content.

Alternative pathways should be considered when studying the ethanol-to-butadiene reaction. Although the Toussaint-Kagan pathway is now generally accepted, the possibility that these different pathways may occur in the conversion of ethanol remains to be disproved. Notably, the Prins-like mechanism proposed by Fripiat *et al*. was shown to be thermodynamically favorable with DFT calculations. In addition, the observations suggesting the involvement of carbanion on MgO should be investigated further.

1.3.3. Thermodynamic considerations

Several thermodynamic studies of the Toussaint-Kagan pathway and the Prins-like mechanism for the conversion of ethanol to butadiene have been performed. Natta and Rigamontti first calculated the Gibbs free energy change of potential reaction steps at 673–703 K, concluding that what we now refer to as Toussaint-Kagan pathway mast the most likely route to butadiene.[145] Bhattacharyya and Ganguly, although neglecting the reduction of crotonaldehyde step by combining it with the subsequent dehydration of crotyl alcohol, found it to be more endergonic with hydrogen rather than ethanol as reductive agent.[142] Recently, Weckhuysen *et al*. performed thermodynamic calculations with HSC7 software package, confirming the favorability of the ethanol-induced reduction pathway at 673 K. Their results further indicate the reaction becomes favorable above 420 K. The authors also determined the conversion of ethanol to butadiene to be endothermic by 102 – 109 $kJ.mol^{-1}$ from 473 to 773 K. In their review of the ethanol-to-butadiene reaction, Sels *et al*. reported the most comprehensive thermodynamic study of the reaction, which was performed with the Aspen Plus® software using pure compounds in their gaseous states for simulating the various reaction steps at different temperatures. We performed thermodynamic simulations of our own using the same approach as Sels *et al*. with the Aspen Plus® software to further investigate the investigate the theoretical influence of pressure on the feasibility of the reaction. Since our results coincide mostly with those of Sels *et al*., we consider this section complimentary to their work and refer the reader to their article for further details.

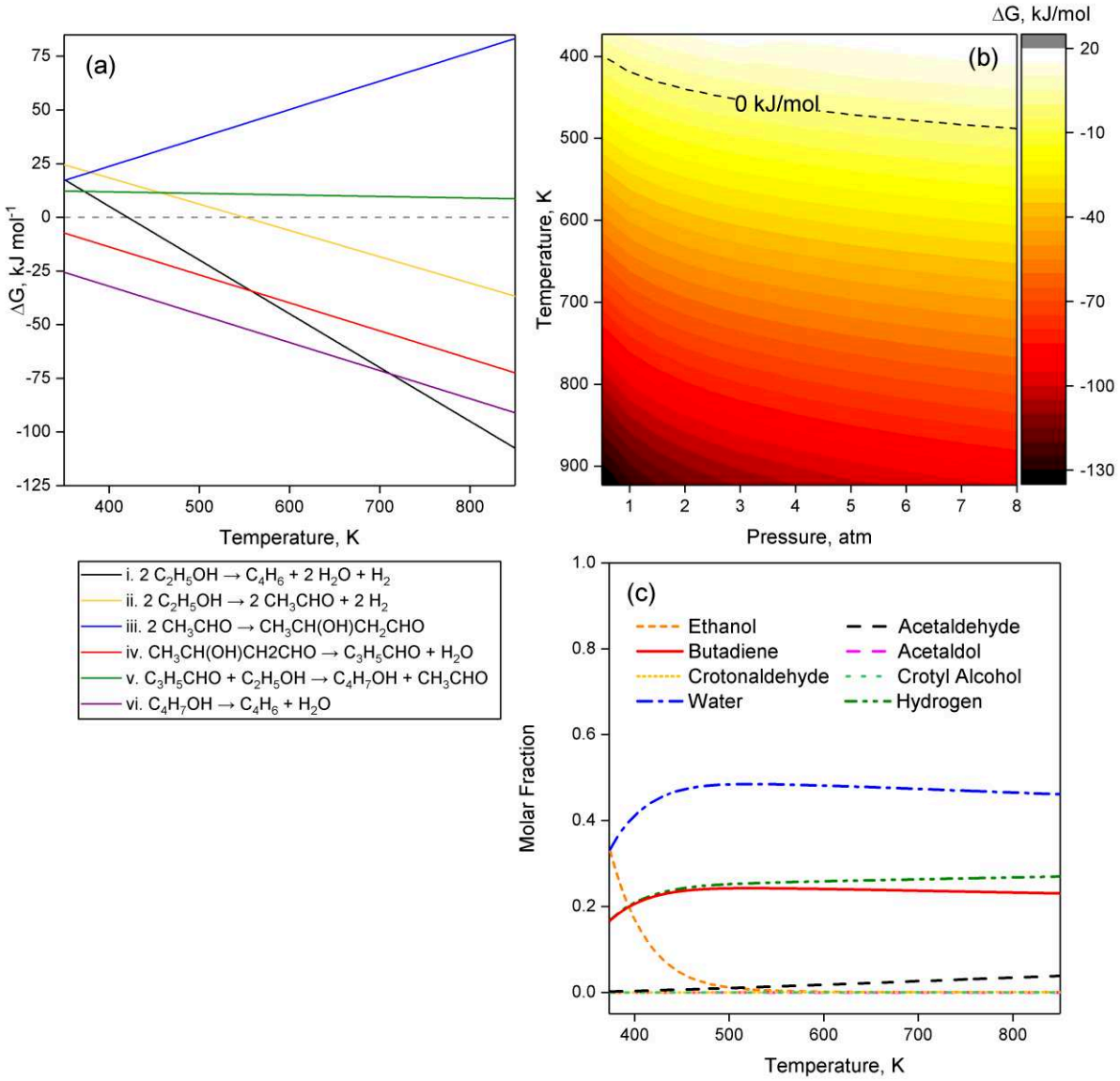

Figure 1.16 Thermodynamic modelling of the ethanol-to-butadiene conversion considering the Toussaint-Kagan mechanism. Calculations were performed using the Aspen Plus® software for mixtures of pure components at given temperatures and pressures. (a) Ellingham-type plot of Gibbs free energy change of the reaction steps in the Toussaint-Kagan pathway at 1 atm. (b) Gibbs free energy change of the overall reaction at different pressures. (c) Molar composition at equilibrium for the overall reaction at different temperatures and atmospheric pressure.

As depicted in Figure 1.16 (a) step i), ethanol conversion to butadiene becomes thermodynamically favorable beyond 418-420 K.[15,19] However, ethanol dehydrogenation to acetaldehyde (Figure 1.16 (a), step ii) only becomes exergonic at higher temperature: 550 K according to our calculations and 585 K according to Sels et al.15 Acetaldol formation from acetaldehyde (Figure 1.16 (a), step iii) is the least thermodynamically favored step of the Toussaint-

Kagan mechanism.[15] At 1 atm, it is always endergonic and becomes increasingly so at greater temperature. In contrast, thermodynamics favor acetaldol dehydration to crotonaldehyde significantly (Figure 1.16 (a), step iv), substantiating the claims of its rapid disappearance and absence from the output of catalytic tests. Contrarily to Weckuysen *et al*. the Aspen® simulation showed the MPVO reaction between crotonaldehyde and ethanol (Figure 1.16 (a), step v) to have comparatively low, but steady ΔG values over the entire temperature range studied.[19] Sels *et al*. also found this step to be endergonic, but with a Gibbs free energy change almost close to zero. Although thermodynamically favored overall, the Toussaint-Kagan pathway possesses a single highly endergonic step: the acetaldehyde condensation to acetaldol.[15,19] According to gas-phase thermodynamic calculations for the pure components, all other steps have either lower ΔG values or are highly exergonic. Figure 1.16 (b) illustrates the influence of pressure on the Gibbs free energy change of the overall reaction: it becomes exergonic at 400 K temperature when reducing the pressure to 0.5 atm.

According to Sels *et al*., the direct conversion of ethanol to butadiene at equilibrium was complete above 400 K.[15] However, modelling the equilibrium composition of the reaction including every reaction intermediate showed a slight decrease in butadiene above 613 K due to unconverted acetaldehyde and crotonaldehyde. Our calculations confirm this assessment (Figure 1.16 (c)). According to this thermodynamic model, the maximum butadiene yield at a typical temperature of 673 K is 90%. At 1 atm, Sels *et al*. further found that the individual reactions steps were limited by the thermodynamic equilibrium and could not reach full conversion, except for ethanol dehydrogenation above 800 K and crotyl alcohol dehydration at every temperature tested. The authors concluded their thermodynamic study by stating that the preferable reaction temperature lied between 602 K and 703 K. Furthermore, within this temperature yield, butadiene yield and selectivity were determined by reaction kinetics, highlighting the importance of the catalyst choice.

1.3.4. Kinetics & Reaction Conditions

1.3.4.1. Kinetic modelling

Understanding the relationship between reaction conditions and the activity of a catalytic process is crucial for its application.[99] With kinetic modelling, it comes possible to predict the reaction rate according to temperature, pressure and the composition of reactants. Catalytic testing is required to procure rates of reaction needed for conceiving a kinetic model. This task which is facilitated by an understanding the reaction mechanism, which can be used to simplify the model. However, there exists a trade-off between the accuracy and complexity of kinetic models. Few authors have sought to model the kinetics of the ethanol-to-butadiene, ostensibly due to the intricacy of its mechanism—most have instead established empirical relations between reaction conditions and catalytic activity.

To the best of our knowledge, only Tretyakov *et al*. have proposed a kinetic model of the Lebedev process.[158,159] Interestingly, the authors used hydrogen peroxide to initiate the reaction and reduce deactivation from coke formation. Their study was performed using a ZnO-Al_2O_3 catalyst prepared using aluminum nitrate and doped K_2O. Three distinct active sites were proposed: two sites responsible for the formation of butadiene (A and B) and all intermediates involved, and a third site involved in the formation of oxygenated byproducts such as diethyl ether and butanal (C). The reaction network used was based on the Toussaint-Kagan pathway (Table 1.1 (2,3)), but considered hydrogen to be the only reducing agent in obtaining butadiene from acetaldehyde. Surprisingly, it also incorporated the Prins-like mechanism (Table 1.1 (3)), *e.g.*, the coupling of acetaldehyde with ethylene to form butadiene, but also the dimerization of ethylene to *1*-butene along with its dehydrogenation to butadiene (Table 1.1 (7)),. Although the latter reaction is feasible,[12,13] Sels *et al*. have shown it to be thermodynamically unfavored due to the stability of *1*-butene.[15] The corresponding set of rate expression (Table 1.1) were used to solve the mass balance of an integral reactor and fit the model. The kinetic parameters obtained showed the butadiene formation from aldol condensation (Table 1.1 (5)) to have the lowest activation energy barrier. Other notable features of this kinetic model are: the apparent zero order of the butadiene formation steps, the competition between the adsorption of acetaldehyde and butanal on the main active site, and the Eley-Rideal mechanism of ethylene dimerization. Unfortunately, no statistical information was provided to assess the validity of the model. This problem is exacerbated by the absence of

units for the equilibrium constants used and some kinetic parameters. However, it remains the only formal kinetic on the Lebedev process, which may assist further research on the subject.

Table 1.1 Reaction network and rate expressions used in the kinetic model of the ethanol-to-butadiene reaction on ZnO-Al_2O_3 with H_2O_2 designed by Tretyakov et al.[158,159]

No.	Reaction scheme	Rate expression of the limiting step, s^{-1}	Rate parameters, s^{-1}
1	$C_2H_5OH \rightarrow C_2H_4 + H_2O$	$r_1 = \frac{k_1 \cdot X_{C_2H_5OH}}{1 + K_A \cdot X_{CH_3CHO}}$	$k_1 = 4.86 \pm 1.2 \cdot 10^{16} \cdot e^{\frac{-210600 \pm 2100}{R \cdot T}}$
2	$C_2H_5OH \rightarrow CH_3CHO + H_2$	$r_2 = \frac{k_3 \cdot X_{C_2H_5OH}}{1 + K_B \cdot X_{CH_3CHO} \cdot X_{C_4H_8O}^{-1}}$	$k_2 = 2.30 \pm 0.7 \cdot 10^{3} \cdot e^{\frac{-19050 \pm 190}{R \cdot T}}$
3	$CH_3CHO + C_2H_4 \rightarrow C_4H_6 + H_2O$	$r_3 = \frac{k_5 \cdot X_{C_2H_4}}{1 + K_B \cdot X_{CH_3CHO} \cdot X_{C_4H_8O}^{-1}}$	$k_1 = 1.26 \pm 0.3 \cdot 10^{2} \cdot e^{\frac{-13650 \pm 136}{R \cdot T}}$
4	$CH_3CHO + C_2H_4 \rightarrow C_4H_8O$	$r_4 = \frac{k_8}{1 + K_C \cdot X_{CH_3CHO}}$	$k_1 = 2.29 \pm 0.7 \cdot 10^{2} \cdot e^{\frac{-13070 \pm 130}{R \cdot T}}$
5	$2\ CH_3CHO + H_2 \rightarrow C_4H_6 + 2\ H_2O$	$r_5 = \frac{k_{12}}{1 + K_B \cdot X_{CH_3CHO} \cdot X_{C_4H_8O}^{-1}}$	$k_1 = 3.76 \pm 1.0 \cdot 10^{3} \cdot e^{\frac{-6890 \pm 70}{R \cdot T}}$
6	$2\ C_2H_4 \rightarrow C_4H_8$	$r_6 = \frac{k_{13} \cdot X_{C_2H_4}^2}{1 + K_A \cdot X_{CH_3CHO}}$	$k_1 = 3.06 \pm 1.3 \cdot 10^{2} \cdot e^{\frac{-10650 \pm 120}{R \cdot T}}$
7	$C_4H_8 \rightarrow C_4H_6 + H_2$	$r_6 = \frac{k_{15} \cdot X_{C_4H_8}}{1 + K_A \cdot X_{CH_3CHO}}$	$k_1 = 2.90 \pm 1.0 \cdot 10^{38} \cdot e^{\frac{-497500 \pm 4900}{R \cdot T}}$

NB: X_i refers to the output molar fraction of compound *I*, K_n is the equilibrium adsorption constant for active sites A, B or C, 500, 100, 550, respectively.

1.3.4.2. Effects of Ethanol Flow Rate and Temperature

In lieu of formal kinetic modelling, statistical modelling has been used to assess the effect of reaction conditions on catalytic performances. Pinto *et al.*[160] and Villanueva Perales *et al.*[90] each developed empirical mathematical models to predict the activity of K_2O-ZrO_2-ZnO/MgO-SiO_2 and hemimorphite-HfO_2/SiO_2 catalysts, respectively, in the Lebedev process as a function of temperature and ethanol flow rate. The effect of water, which Villanueva Perales *et al.* studied, will be discussed later. Both models were constructed by fitting polynomial equations to experimental results, choosing selectivity, yield, molar fraction or productivity as responses. Although the accuracy of empirical models is limited to the range of operation conditions studied, the activity trends observed are comparable to results obtained by other scholars in their studies of the ethanol-to-butadiene reaction. Consequently, it is ideal for visualizing the general impact of operation conditions.

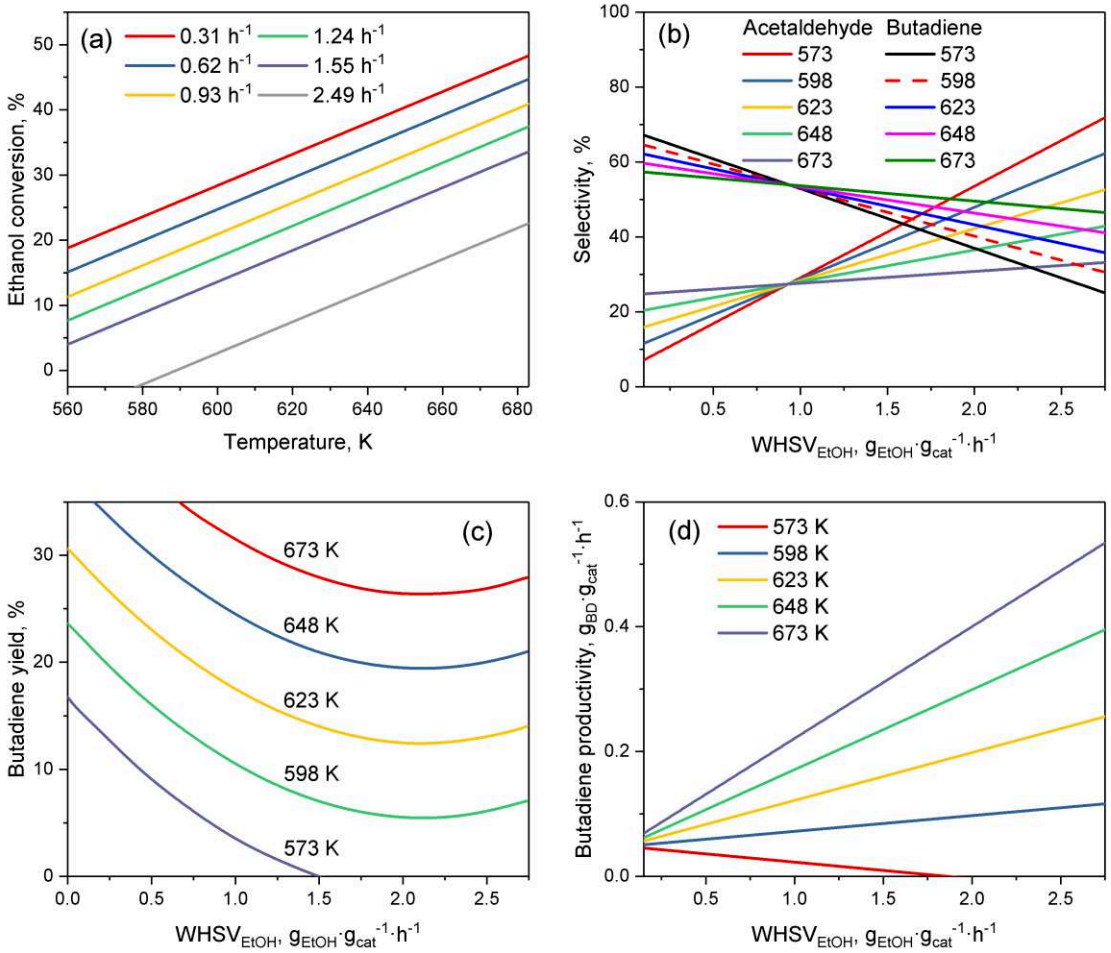

Figure 1.17 Empirical model by Pinto *et al.* predicting the effect of temperature and ethanol flow rate on selected performance metrics: (a) ethanol conversion; (b) acetaldehyde and butadiene selectivity; (c) butadiene yield.[160]

As depicted in Figure 1.17 (a), temperature showed a positive effect on ethanol conversion, whereas $WHSV_{EtOH}$ displayed a negative influence. Although similar results were found on other catalysts system,[110,161] the linear relationship between conversion and temperature depicted was not observed.[110,162,163] Ethanol-acetaldehyde mixtures also displayed comparable conversion trends.[164] Due to the endergonic nature of the reaction, a temperature increase is expectedly beneficial to conversion. However, Bhattacharyya and Avashti noted a decrease in ethanol conversion between 673 and 723 K on ZnO-Al_2O_3,[165] which may be explained by the thermodynamic unfavourability of the aldol condensation at higher temperatures.

Figure 1.17 (b) depicts the change in selectivity occurring when tuning the operation conditions. When increasing ethanol flow, selectivity towards butadiene decreased in favor of acetaldehyde,

but also of other byproducts (not shown). In the Lebedev process, the accumulation of acetaldehyde with reduced contact time is often observed, leading many authors to conclude that aldol condensation is the rate-limiting step.[32,39,109,163] Product selectivity was also highly dependent on temperature. Increasing it had the opposite effect, favoring butadiene selectivity meaningfully. Different results were obtained on other catalytic systems: on Cu-Ta/SiBEA, higher temperature (> 573 K) significantly reduced butadiene selectivity to the benefit of ethylene;[162] on Au/MgO-SiO_2, butadiene selectivity increased, before falling when temperature rose above 573 K.[97] Interestingly, butadiene selectivity was almost unaffected by temperature on MgO-SiO_2 when conversion was maintained at 40% by adjusting the ethanol flow rate, whereas byproduct selectivity changed significantly.[144] Explaining the discrepancies reported is difficult, due to the drastically different catalysts and reactor set-ups used. However, it is noteworthy that the product selectivity does not have a clear relationship with temperature.

Butadiene yield (Figure 1.17 (c)), important for the practical application of the reaction, was favored in a non-linear fashion by high temperatures and low ethanol flow rate, which are also beneficial to conversion.[142,157,162,163,165] Increasing $WHSV_{EtOH}$ suppressed butadiene yield non-linearly, in agreement with observations made on other catalytic systems.[110] This is highly relevant due to the fact that high ethanol flow rate is required for attaining the high butadiene productivity needed to meet industrial standards.[96] Although the model of Pinto *et al*. indicated a linear relationship between productivity and $WHSV_{EtOH}$ (Figure 1.17 (c)), it is unlikely that its validity extends beyond the range of studied reaction conditions due to reducing effect of the latter. For instance, Kyriienko *et al*. found the suppression of butadiene yield to be compensated by increased ethanol flow rate, resulting in an overall lower productivity on Cu-Ta/SiBEA.[162]

The relationship between activity and temperature or $WHSV_{EtOH}$ appears to vary greatly depending on the catalytic system used. The empirical model established by Pinto *et al*. could only be considered valid for the specific operation conditions studied. Generally, reducing the ethanol flow rate during the Lebedev process improved catalytic butadiene selectivity and yield. However, the resulting lower butadiene productivity is not very interesting for industrial application. High $WHSV_{EtOH}$ increases productivity, but only to some extent, as it suppressed butadiene formation, possibly due to diffusion limitations. In the range found ideal by Sels *et al*.[15] (602 – 703 K), increasing the temperature improves ethanol conversion. However, the unclear relationship

between butadiene selectivity, temperature and the catalytic system used means that the benefits to butadiene yield are not straightforward.

Pinto *et al*. also performed a microkinetic analysis of the ethanol-to-butadiene reaction on $MgO\text{-}SiO_2$ which highlighted this phenomenon.[166] The authors established that experimental fluctuations of the molar fraction of distinct species in the output stream of their catalytic tests were not independent of one another. Local microkinetic information was extracted from the covariance matrix of experimental fluctuations. A negative correlation coefficient between the molar fraction of two given product signaled a fluctuation in opposite direction, indicative of a reactant-product relationship. Contrarily, a positive correlation coefficient could either be interpreted a co-reactant or co-product relationship, or a reactant-product connection with no bearing on the reaction rate. Pinto *et al.* reported in change in mechanism with increasing temperature on the basis of a change in correlation coefficient. At 723 K, the reactant-product relationship between ethanol and acetaldehyde becomes unclear; incidentally, a reactant-product relationship between butadiene and acetaldehyde emerges when at lower temperatures there was none. Pinto *et al*. interpret these observations as a change in the reaction kinetics. Between 573 K and 673 K, the rate –determining step was the aldol condensation. At 723 K, the availability of acetaldehyde became kinetically relevant, *e.g.*, its formation by ethanol dehydrogenation determined the reaction rate. Interestingly, the correlation coefficient of H_2 remained positive, indicating that it was not involved in the reduction of crotonaldehyde.

1.3.4.3. Effects of the Ethanol-Acetaldehyde Ratio on the Two-Step Process

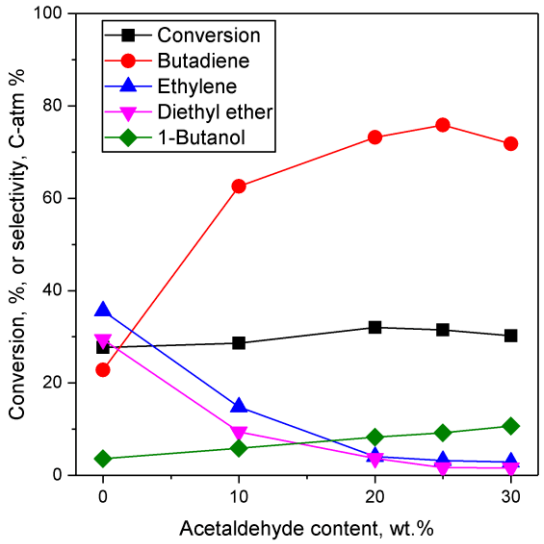

Figure 1.18 Effect of acetaldehyde content in the ethanol-acetaldehyde mixture used for Ostromislensky process on MgO-SiO_2.[164]

In the Ostromislensky process, the molar ratio of ethanol to acetaldehyde in the reactant feed is a crucial reaction parameter, usually ranging between 2 and 4,[16,20,167] and between 0.7[17] and 9[164] in extreme cases. Although catalysts for the Ostromislensky process generally lack a dehydrogenation function, the best ethanol-acetaldehyde ratios reported are most often above 1, indicating that the reaction regenerates acetaldehyde by the MPVO reaction. Several scholars have sought to improve their process by tuning the ethanol-acetaldehyde ratio, such as Tan *et al*. who studied the influence of this reaction parameter when using MgO-SiO_2 catalysts (Figure 1.18).[17,40,164,167] However, there is no recognized optimal value. This phenomenon is ostensibly due to the different properties of each catalytic system and the reaction conditions used.[17,164] Consequently, the ethanol-acetaldehyde ratio adds another dimension to the reaction conditions that must be optimized to maximize butadiene formation. To the best of our knowledge, no modelling of this parameter has been reported.

1.3.4.4. Effects of the Water in the Feed

As previously mentioned, using water-containing ethanol would be economically and environmentally beneficial. In this regard, the influence of co-feeding water with ethanol or ethanol-acetaldehyde mixtures is a crucial reaction parameter for the practical application of the ethanol-to-butadiene reaction what degree of water, if any, must be removed. Furthermore, since

water is generated *in situ*, processes designed to recycle unconverted ethanol would inevitably operate with water in the feed due to their azeotrope, unless incorporating additional purification steps.[90] Unfortunately, the effect of water is an understudied subject, most researchers preferring to use anhydrous ethanol when performing catalytic tests.

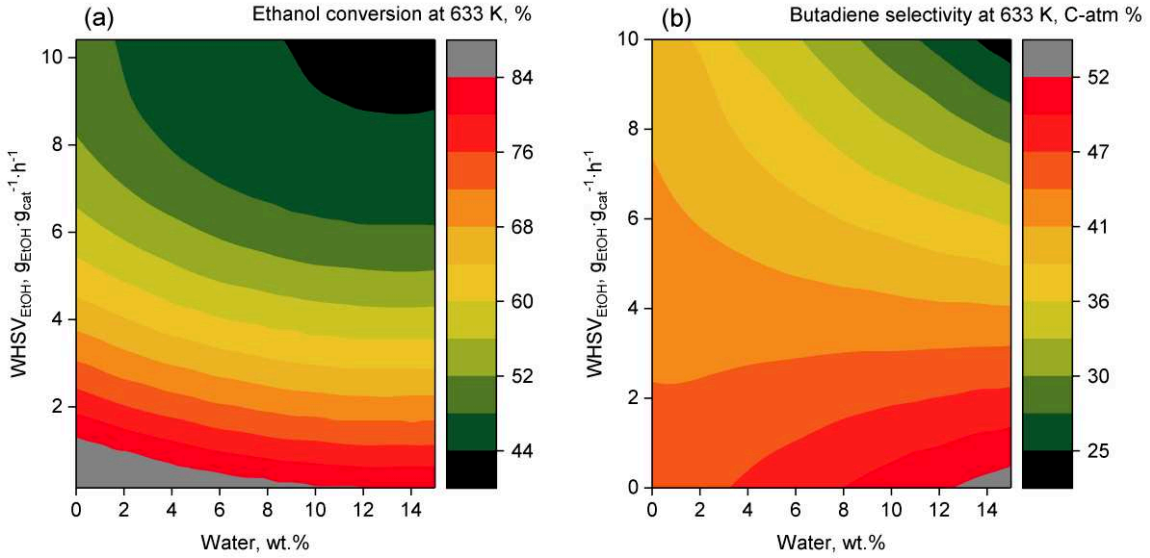

Figure 1.19 Empirical model for the effect of water content in the Lebedev process over hemimorphite-HfO_2/SiO_2[90]

Recent studies have provided insight on the subject, but some discrepancies remained to be answered. In the Lebedev process, three major effects have been observed. First, co-feeding water suppresses ethanol conversion.[90,157,165] Villanueva Perales *et al.*, who modeled the impact of water, ethanol flow rate and temperature on the reaction, found that increasing the water content of the feed progressively reduced conversion (Figure 1.19 (a)).[90] Second, product selectivity was altered by the presence of water, generally reducing butadiene selectivity in favor of ethylene and acetaldehyde,[90,157] although this effect also depended on the other reaction conditions (Figure 1.19 (b)). Third, water decreased the rate of catalytic deactivation.[90,157,165] The poisoning effect was attributed to the adsorption of water molecules on active sites, notably the Lewis acid sites responsible for acetaldehyde condensation. This also explained the reduced deactivation observed, as the condensation of aldehydes into heavier carbonaceous species has been identified as a source of catalyst poisoning.[110,131,168] IR spectroscopy identified the *in situ* formation of Brønsted acid sites upon addition of water, which are known to catalyze the dehydration of ethanol, explaining the increased ethylene selectivity.[90,157] Ultimately, process design and economic analysis will

decide whether an optimal water content, where the drawbacks of using water-containing ethanol for the Lebedev process, mainly the loss of butadiene yield and the increase of byproduct, are outweighed by the economic benefits of reduced separation cost, as well as the increased catalyst lifespan.

In the case of the Ostromislensky process, the suppression heavy carbon species formation by co-feeding water was also observed.[164,168] Although ethanol-acetaldehyde conversion was slightly reduced, Jiang *et al*. and Tan *et al.* have found butadiene selectivity over ZnO-ZrO_2 and MgO-SiO_2 to be mostly unaffected by the addition of up to 50 wt.% of water to the feed.[164,168] Whether this contrast in activity with the Lebedev process is owed to the difference in reaction conditions or is inherent to the Ostromislensky process remains to be answered. For instance, Toussaint *et al*. found 10 wt.% water to decrease the rate of butadiene formation on Ta_2O_5/SiO_2, while also reporting an enhance catalyst lifetime.[32]

1.3.5. Catalyst deactivation

Sels *et al*. identified catalytic stability to be a factor in the ethanol-to-butadiene route's ability to compete with existing fossil-based technologies.[15] Despite this, research has focused on strategies to improve stability, rather than on understanding deactivation itself, which is a field of study on its own.[169,170] Carbon species formed during ethanol conversion to butadiene are generally recognized to result in catalyst decay.[131,142,168] But details on the exact nature and mechanism of deactivation are lacking. Deactivation is reported in almost every instance of catalytic testing. The time-scale of deactivation can be in the matter of hours, comparable to the ethanol-to-propylene process with ZSM-5, another pathway to renewable olefins,[171–173] or extend to the hundreds of hours depending to the reaction conditions. Most published catalytic reactions did not go beyond 10 – 20 hours on stream, with the longest instances of stability testing lasting 143 hours[174] and 175 hours.[32]

Numerous factors influence the observed catalyst decay. Like selectivity, deactivation rates vary greatly depending on the catalyst. The choice of metal demonstrably affects stability of materials in otherwise identical catalytic tests.[175–177] In turn, the resulting chemical surface properties correlate with the ability of a sample to resist deactivation: strong acidic and basic sites are believed to accelerate carbonaceous compound formation.[163,178] Catalyst support and its morphology unambiguously influences the speed of catalytic decay.[41,163,174,179] Toussaint *et al*.

reported that lower temperature reduces deactivation.[32,39] They also noted that the ethanol-acetaldehyde ratio is a factor the stability of catalysts in the Ostromislensky process.

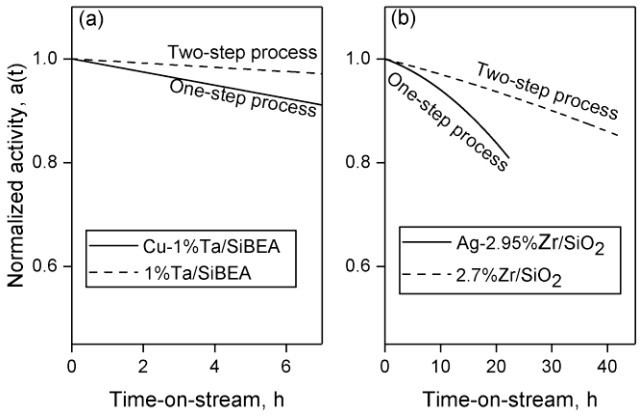

Figure 1.20 Stability comparison between two similar catalytic systems in the one and two-step processes. (a) Cu-1%Ta/SiBEA (T = 598 K, $WHSV_{EtOH}$ = 0.5 h^{-1});[162] 1%Ta/SiBEA (T = 598 K, $WHSV_{EtOH}$ = 0.792 h^{-1}, EtOH:AcH = 3.2).[175] (b) Ag-2.95%Zr/SiO_2 (T = 598 K, $WHSV_{EtOH}$ = 0.23 h^{-1});[180] 2.7%Zr/SiO_2 (T = 673 K, $WHSV_{EtOH}$ = 1.5 h^{-1}, EtOH:AcH = 1.16-1.60).[17] Normalized activity was defined as the specific activity at any time-on-stream divided by the initial activity obtained by extrapolation to TOS = 0 h.[169]

Based on a review of literature, Corson *et al*. stated that the Ostromislensky process suffers from slower decay than the Lebedev process.[37] However, the disparity may be owed to the different nature of catalysts employed at the time, *e.g.*, Ta_2O_5/SiO_2 compared with $ZnO\text{-}Al_2O_3$ in the two and one-step processes respectively. Many recent two-step processes show remarkable stability albeit at relatively low $WHSV_{EtOH}$,[17,168,174,175] possibly a contributing factor. An accurate comparison would require catalytic testing using similar materials and conditions. In one such instance, the normalized activity of Ta/SiBEA in the two-step process remained slightly more stable than that of Cu-Ta/SiBEA in converting pure ethanol (Figure 1.20, (a)).[162,175] When comparing deactivation rates on silica-supported zirconia at a longer time-on-stream, the Ostromislensky process again showed a superior stability (Figure 1.20 (b)).[17,180] However, the different reaction conditions makes this comparison less conclusive. So far, the conclusion of Corson *et al*. appears correct.

Deactivation during alcohol catalytic conversions generally takes place *via* two mechanisms[181–183]: (i) active site poisoning by carbonaceous molecules and/or (ii) pore obstruction or blockage by large species. In the first case, adsorbed molecules sterically prevent the access of reactants to the

active sites.[169] In the second case, pore obstruction decreases reactant mass transfer rates by reducing accessibility to pore network; complete blockage may also occur, further hindering access to active sites.[169] The contribution of each mechanism to deactivation depends on several factors,[169] such reaction conditions, *i.e.*, temperature and contact time, the nature of reactants and the catalytic system.

In the ethanol-to-butadiene reaction, pore blockage by carbonaceous species has been speculated as a significant deactivation mechanism. Notably, mesoporous catalyst carriers with larger pores have remained relatively more stable, suggesting pore size played a role in deactivation.[17,41,106,174] BET analysis of deactivated catalysts also demonstrated the loss of pore volume, pore size and specific surface.[168] The fact that the calcination under air has repeatedly be used to regenerate spent catalysts[17,162,184] is a strong indicator that such morphological changes are owed to the deposition of organic species and not framework collapse. A feature of the blockage mechanism is the accumulation of large amounts of heavy carbonaceous molecules.[169] Thermogravimetric analysis (TGA) of different mesoporous catalysts showed significant accumulation of such species, identifiable by high-temperature weight loss.[17,168,174] For instance, Chae *et al*. reported nearly 25 wt.% heavy carbon content in spent Ta/SBA-100 catalyst after a TOS of 40 h.[174] Large carbonaceous species are formed by the polymerization of lighter hydrocarbons, which can take place on catalytic sites active for condensation reactions. In their study of deactivation on ZnO doped ZrO_2-SiO_2,[168] Jiang *et al*. characterized the surface of spent catalysts using X-ray Photoemission Spectroscopy (XPS). They found a large proportion of the C 1s signal to be attributable to graphitized carbon. Consequently, Jiang *et al*. argue that pore blockage by large polymerized aromatic species contributes to deactivation. As noted in section 1.3.4.4. co-feeding water consistently suppressed the formation of carbon species and extended catalyst lifetime, ostensibly due to the inhibition of its activity in condensation reactions.[90] Interestingly, this suppression effect shifted the nature of retained carbonaceous species from heavy carbon to lighter carbon molecules.[168]

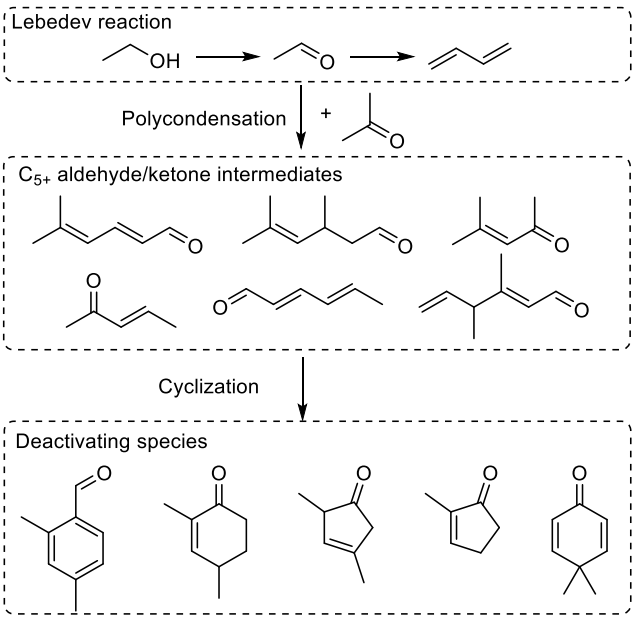

Figure 1.21 Deactivation mechanism on ZnY/SiBEA proposed by Li *et al.*[131] The list of intermediate and deactivating species is not exhaustive.

Li *et al*. investigated the deactivation mechanism during the Lebedev process on a microporous Zn-Y/SiBEA catalyst.[131] Contrarily to mesoporous materials, the TGA of spent catalysts revealed more light carbonaceous species and fewer heavy compounds—the coking rate was lower than with other catalytic system.[168,174] In addition, organic extracts from HF-dissolved samples contained no polycyclic aromatics indicative of large polymerized coke, but many carbonyl-possessing unsaturated five or six-membered rings. *In situ* DRIFTS and UV-vis corroborated the presence of these compounds, but also the formation of C_{5+} carbonyl molecules. Accordingly, Li *et al*. proposed that, rather than pore blockage, deactivation on zeolite-based catalyst results from the gradual coverage of Zn and Y sites by the deposition of large unsaturated cyclic compounds. Aldolization of acetaldehyde and acetone formed C_{5+} carbonyl intermediates, which were also observed on Zr-contraining materials,[109,179] subsequently undergoing cyclization, resulting in the deactivating species (Figure 1.21). At present, it is difficult to judge whether the alternative deactivation mechanism reported by Li *et al.* can be attributed to the chemical or morphological properties of the catalyst, or different reaction conditions. Incidentally, Villanueva Perales *et al.* similarly found the deposition of oxygenated aromatic species on active sites to be a source of deactivation for the Lebedev process on hemimorphite-HfO_2/SiO_2, suggesting this mechanism is not limited to microporous catalysts.[110]

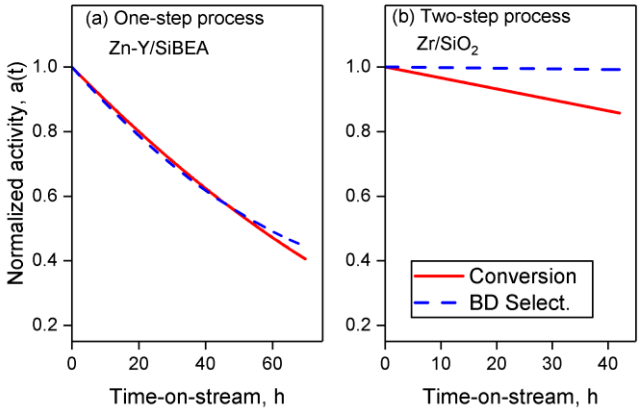

Figure 1.22 Effect of time-on-stream on conversion and selectivity for catalysts in the one and two-step process. (a) ZnY/SiBEA (T = 673 K, $WHSV_{EtOH}$ = 1.0 h^{-1}).[131] (b) Zr/SiO_2 (T = 673 K, $WHSV_{EtOH}$ = 1.5 h^{-1}).[17]

In the Lebedev process, both conversion and selectivity towards butadiene tend to decrease with time-on-stream, which also results in greater acetaldehyde selectivity (Figure 1.22 (a)).[106,122,185] Contrarily, during the Ostromislensky process, although ethanol conversion also declines, butadiene selectivity is generally unaffected (Figure 1.22 (b)).[17,168,174,175] A possible explanation for this discrepancy may be the selective poisoning of active sites. If sites responsible for the aldol condensation also form the heavier carbonaceous species ostensibly responsible for deactivation, they are more likely to be blocked by carbon depositions. On multi-functional catalysts for the Lebedev process, this phenomenon could lead to an excess of dehydrogenating sites, explaining the greater acetaldehyde selectivity observed. In the Ostromislensky process, catalysts generally lack a dehydrogenating function. As a result, poisoning would proceed uniformly by only targeting the sites responsible for condensation, resulting in a lesser impact on selectivity.

Deactivation processes unrelated to carbon deposition have also been proposed for specific catalytic systems. For instance, Taifan *et al.*, who studied the Lebedev process on CuO and ZnO-modified $MgO\text{-}SiO_2$, distinguished two deactivation mechanisms depending on the choice of promoter. Using *operando* X-ray analysis, the authors observed the disappearance of Cu–O bonds and the emergence of Cu–Cu pairs at 673 K after several hours on stream, whereas zinc bonds were resilient under the same operating conditions. They proposed that deactivation on $Cu/MgO\text{-}SiO_2$ resulted in part from Cu reduction and sintering. Carbon deposition was judged more likely on the

ZnO-containing catalyst. Perales Villanueva *et al*. tested a HfO_2/SiO_2 catalyst modified with the zinc silicate hemimorphite in the Lebedev process.[110] XPS analysis indicated that the Zn(II) was reduced in the spent catalyst. The authors proposed that part of the deactivation could be attributed to this phenomenon, as the Zn(II) sites of hemimorphite were considered the sites responsible for ethanol dehydrogenation. Ostensibly, this phenomenon is reserved to hemimorphite, has other scholars analyzing the Zn 2p peak of ZnO-containing catalysts observed to change to the oxidation state of Zn.[131]

Understanding and preventing catalyst deactivation during the conversion of ethanol to butadiene has progressed in recent years. Pore blockage appears to be the predominant deactivation mechanism at high coking rate, whereas active site poisoning by bulky oxygenated species has been reported at low coking rate on a zeolite catalyst.[131] What catalyst properties or reaction conditions favor one mechanism over the other is not yet understood. Due to the repeated observation of bulky oxygenated carbonaceous species,[109,110,131] both mechanisms are possibly initiated by the condensation of carboxylic species on Lewis acid sites. It is unlikely that the olefin condensation mechanism leading to the formation of deactivating polyaromatic coke that takes place in other ethanol-to-olefin reactions[186] occurs in the conversion of ethanol to butadiene. Indeed, catalysts active in the Lebedev and Ostromislensky processes predominantly possess Lewis acidity,[128,162,164] whereas the condensation of olefin produced by the dehydration of ethanol has been found to preferably take place on Brønsted acid sites.[187–189] Incidentally, the co-feeding of water, which has been found to poison Lewis acid sites, but also to generate new Brønsted acid sites,[110,157] alleviated the formation of heavy coke species and extend catalyst lifetime. Consequently, one approach to consider for reducing the reduce catalyst deactivation is the passivation of acid sites to prevent the over-condensation of carboxylic intermediates. As discussed below, alkali-doping in one strategy to achieve this. Deactivation mechanisms unrelated to carbon formation should be considered, as Taifan *et al.* observed that particle sintering can take place during the reaction[190] and Villanueva *et al*. found metal oxide active sites to be reduced *in situ*,[110] both hindering catalytic activity. However, such mechanisms appear to be limited to specific catalytic systems and should therefore be dealt with on a case-by-case basis.

1.3.6. Byproducts

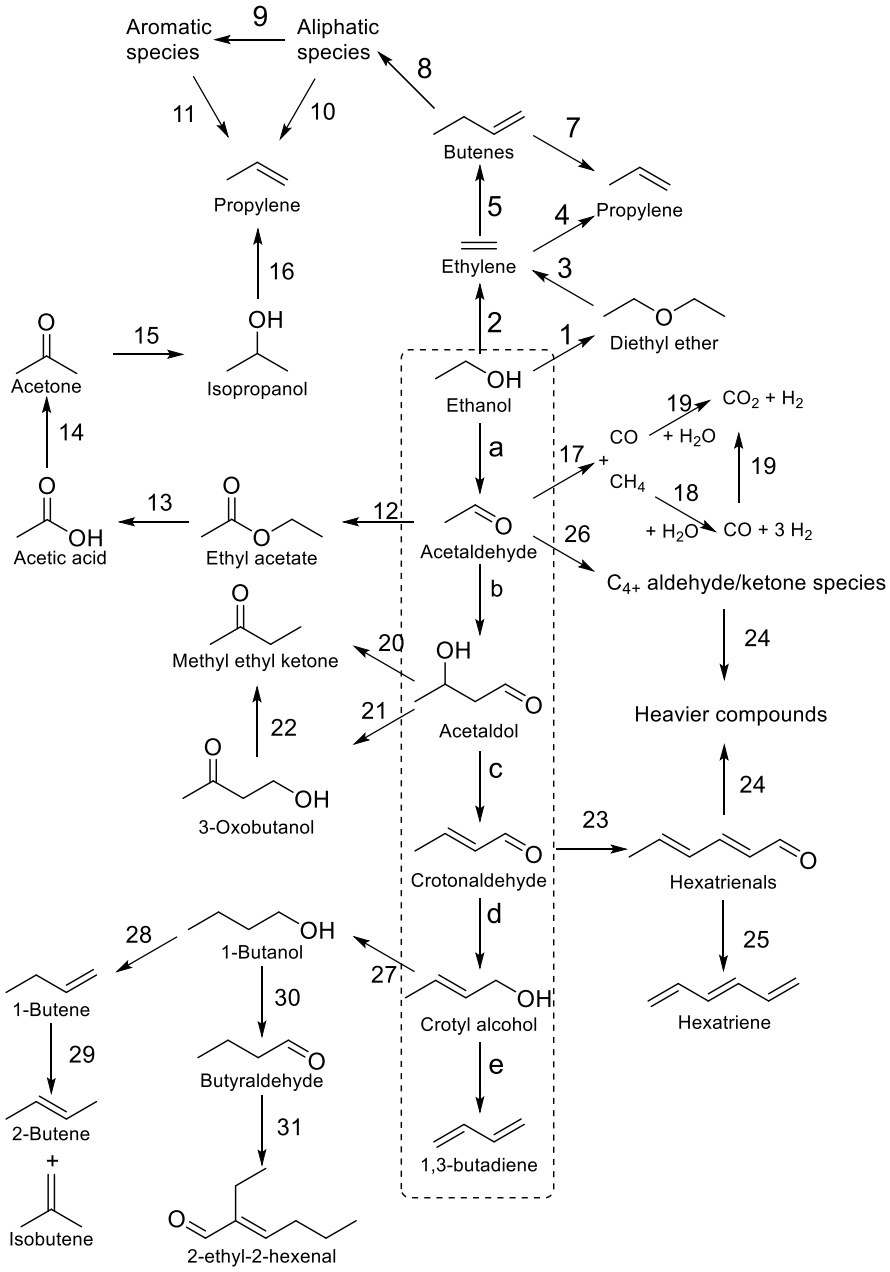

Figure 1.23 Main byproducts pathway taking place during the ethanol-to-butadiene reaction.

Ethanol conversion to butadiene generates many byproducts. Their presence increases separation costs, reducing the ability of an ethanol-to-butadiene process to compete with petroleum-based routes. Consequently, suppressing the formation of undesired compounds coincides with the aim of improving butadiene selectivity. Doing so requires an understanding of

byproduct formation. butadiene itself does not convert to other compounds, as evidenced by its stability under catalytic test conditions.[110] Side-reactions occurring along the pathway to the final product cause the emergence of such undesired species. However, their amount and nature depend on the reaction conditions and the catalytic system employed. We review in this section the theorized or demonstrated routes to the many undesired compounds formed during butadiene production regardless of reaction parameters. Figure 1.23 illustrates the reaction network of main byproducts.

Ethylene and diethyl ether are the principal undesired byproducts of butadiene synthesis. Both species result from the dehydration of ethanol, potentially taking place on acidic[191] or basic sites.[100] Diethyl ether forms from an intermolecular dehydration of two ethanol molecules (Figure 1.23 (1)). Ethylene may result from the direct intramolecular dehydration of ethanol (Figure 1.23 (2)), but from also a subsequent conversion of diethyl ether (Figure 1.23 (3)), alternatively described as a dehydration[191] or cracking[192] reaction. The triangular scheme describes the parallel series of reactions ostensibly happening. The reaction conditions and the nature of the catalyst dictate which route dominates the production of ethylene.[193–195] Generally, the diethyl ether pathway to ethylene takes place at lower temperature (*i.e.*, below 543 K),[195] whereas the direct dehydration route predominates at higher temperatures. With the kinetic curves obtained with a Zn and Hf-containing catalytic tests at 633 K—a temperature more typical of the Lebedev process—Villanueva Perales *et al*. concluded that ethylene was a primary stable product, not a secondary one derived from diethyl ether.[110] Compared to acetaldehyde, ethylene is thermodynamically the favored product of ethanol conversion.[15] Furthermore, DFT calculations on MgO showed the direct dehydration of ethanol possessed a lower energy barrier than its dehydrogenation.[103] Consequently, ethylene formation is in direct competition with the ethanol-to-butadiene pathway. High ethylene yields plagues the process so much so that catalyst design strategies have been adopted to specifically limit ethanol dehydration, namely the use of alkaline dopants to suppress the responsible acid sites.[176,196,197]

Ethylene is also an intermediate of various ethanol-to-hydrocarbon reactions. Propylene can be formed from the reaction between surface carbene species and ethylene (Figure 1.23 (4)), from the cracking of bigger aliphatic species Figure 1.23 (7) and (10)), or *via* the hydrocarbon pool mechanism involving aromatic intermediates (Figure 1.23 (11)). The dimerization of ethylene

(Figure 1.23 (5)) can also lead to the formation of larger aliphatic species (Figure 1.23 (8)) and their cyclisation to aromatics (Figure 1.23 (9)).

Numerous lesser byproducts may form during the subsequent steps of the ethanol-to-butadiene reaction. Besides condensing to crotonaldehyde, the highly active acetaldehyde may undergo the Lewis acid-driven Tischenko reaction to yield ethyl acetate (Figure 1.23 (12)).[15,109,110,114,179] Hydrolysis of ethyl acetate forms acetic acid (Figure 1.23 (13)), which produces acetone through decarboxylation (Figure 1.23 (14)).[15,109,110,179] Propylene can ultimately be obtained by the reduction of acetone to isopropanol (Figure 1.23 (15)) and its subsequent dehydration (Figure 1.23 (16)).[109,110,179] Ethanol reforming,[198–200] which involves acetaldehyde decarbonylation (Figure 1.23 (17)), steam reforming of methane (Figure 1.23 (18)) and the water-gas shift of carbon monoxide to carbon dioxide (Figure 1.23 (19)), may explain the traces of these compounds often detected amongst the products distribution.[96,144,163] Methyl ethyl ketone formation[39] can be explained by various mechanism: the rearrangement of deoxygenated acetaldol (Figure 1.23 (20))[15,201] or the dehydration of *3*-oxobutanol formed *via* the intramolecular H transfer of acetaldol (Figure 1.23 (21) and (22)).[201] Other possibilities include the dehydration of butanediol (not shown) or crotyl alcohol isomerization (not shown).[15]

Many scholars identified crotonaldehyde as a precursor to heavier,[109,110,179] potentially poisoning,[131] compounds. It may undergo aldol coupling with other carboxyl-containing molecules, such as acetaldehyde and acetone to form larger C_{6+} compounds. For instance, cross-coupling between acetaldehyde and crotonaldehyde lead to hexadienal (Figure 1.23 (23)), which may convert to hexatriene (Figure 1.23 (25)) or couple with aldehydes into heavier compounds (Figure 1.23 (24)). Besides crotonaldehyde, a host of aldehyde and ketones molecules may form from the aldol condensation of acetaldehyde. Li *et al*. argue the cyclization of such heavy compounds initiates the coking process responsible for catalytic deactivation (Figure 1.23 (26)).[131]

The Guerbet reaction, believed to follow a pathway akin to that of the ethanol-to-butadiene reaction, likely forms the majority of C_4 byproducts. *1*-butanol, ostensibly obtained from hydrogenation of crotonaldehyde via crotyl (Figure 1.23 (27)),[117,135,202] can undergo dehydration to 1-butene (Figure 1.23 (28))which subsequently isomerizes to *iso*butene and *2*-butene (Figure 1.23 (29)).[15,109,110,179] C_4 olefins are problematic since their separation, required to achieve high-purity butadiene is an expensive process.[12,13] The small presence of butyraldehyde[144,203] may be owed to

the dehydrogenation of 1-butanol (Figure 1.23 (30))[110] or the partial hydrogenation of crotonaldehyde (not show).[201,204] Self-coupling of butyraldehyde may also lead to bulky oxygenated carbonaceous compounds (Figure 1.23 (31)).[110]

The high reactivity of oxygenated hydrocarbons and olefins cause the ethanol-to-butadiene reaction to generate several unwanted species. Reaction intermediates such as acetaldehyde may be recycled, but these byproducts impede the economic viability of the ethanol-to-butadiene reaction. Catalyst design should aim to suppress their formation, notably that of ethylene, which forms in large amounts, and butenes, due to their difficult separation from butadiene.

1.4. Catalytic Systems

Many catalysts have been tested and reported in the literature since research first began on the conversion of ethanol to butadiene. Notably, screening studies by Corson *et al.*[34] and Bhattacharyya *et al*.[165,205] have generated over 600 different materials. This section reviews the two predominant catalytic systems: (i) group 4 and 5 transition metals and (ii) magnesia-silica mixed oxides. These two categories have been the subject of several studies, affording precious hindsight on their activity and the different methods used to prepare them. In addition, rare-earth metal oxides catalysts, a recent topic of interest is discussed. Furthermore, the use of alkali and alkaline-earth dopants, a design strategy used to tune the chemical properties of any catalytic system is addressed.

Other catalytic systems, notably mixed oxides of other transition metals, have not been the subject of recent investigation. As a result, there is a comparative lack of characterization using modern techniques available. The reader is referred to previous reviews, which have addressed the omitted catalytic systems in depth.[15,19,27]

1.4.1. Group 4 and 5 Transition Metals

Catalysts containing transition metals belonging to groups 4 and 5 of the periodic table have shown remarkable activity in converting ethanol to butadiene. Initially reported in the 1940s by scientists from the Carbide and Carbon Chemicals Corporation,[32,39,206] these catalytic systems have been carefully studied throughout the years. As detailed in the original patent, silicates of zirconium, tantalum or niobium oxide were first used to convert ethanol-acetaldehyde mixtures into butadiene due to their condensation ability.[206] Furthermore, the wartime screening of over 500 catalysts by Corson *et al*. found silica-supported titanium and hafnium oxide capable of high butadiene yield in

the Ostromislensky process.[31,37,203] It also that established that dehydrogenation promoters, *i.e.*, MgO or CuO, could be incorporated to make these catalysts active in the Lebedev process. As vanadium oxide performed poorly,[37] research then and now has generally concerned Zr, Nb, Hf and Ta—Ti has mostly been ignored, ostensibly due to its lower activity. Since scholars have argued that these metals share a similar catalytic activity in the ethanol-to-butadiene reaction,[104,127] this section will discuss them as closely related catalytic systems, despite Zr and Ta clearly being the most studied of all group 4 and 5 transition metals. Section 4.1.1. discusses the origin of their catalytic activity; section 4.1.2. elaborates on the design of these catalyst systems, highlighting the important parameters of concern from preparing catalysts active in the one and two-step processes by providing examples from the literature; section 4.1.3. features notable instances of materials with high catalytic active.

1.4.1.1. Acidity and Activity

Due to the their high activity in the Ostromislensky process,[37,175,207] but poor performances in the Lebedev process when lacking dehydrogenation promoters,[174,175] Zr, Nb, Hf and Ta oxides have long been assumed to catalyze the aldol condensation and MPVO steps of the ethanol-to-butadiene reaction.[203] Through spectroscopic studies of these reactions steps, Ivanova *et al*. evidenced that the Lewis acid character of Zr(IV) was the source of catalytic activity.[208,209] As Nb, Hf and Ta-containing catalysts also display Lewis acidity[210–213] and show comparable activity in various organic reactions,[214] it is generally assumed that the involvement of Lewis acid sites is valid for all four transition metals.[104,110,127,207]

Solid Lewis acids consisting of transition and post-transition metal oxides, often supported on zeolites and other silicates, have emerged as adaptable catalysts for organic chemistry due to their capacity to activate and convert oxygen-containing molecules.[214] For metal sites incorporated within a silica framework or in bulk metal oxides, Lewis acidity, *e.g.*, the ability to accept electron pairs, is owed to their partial positive charge resulting from the formation of covalent bonds with adjacent oxygen atoms, which become Lewis bases.[214] Due to their partial positive charge, metal sites can stabilize oxygenated organic molecules *via* electrostatic interaction or activate them by accepting electrons from their electron-rich groups. With their basic character, neighboring oxygens are also available for reacting with organic molecules. These acid-base pairs can work in

tandem to catalyze a variety organic reactions, notably the aldol condensation[132] and MPVO reaction.[155,215]

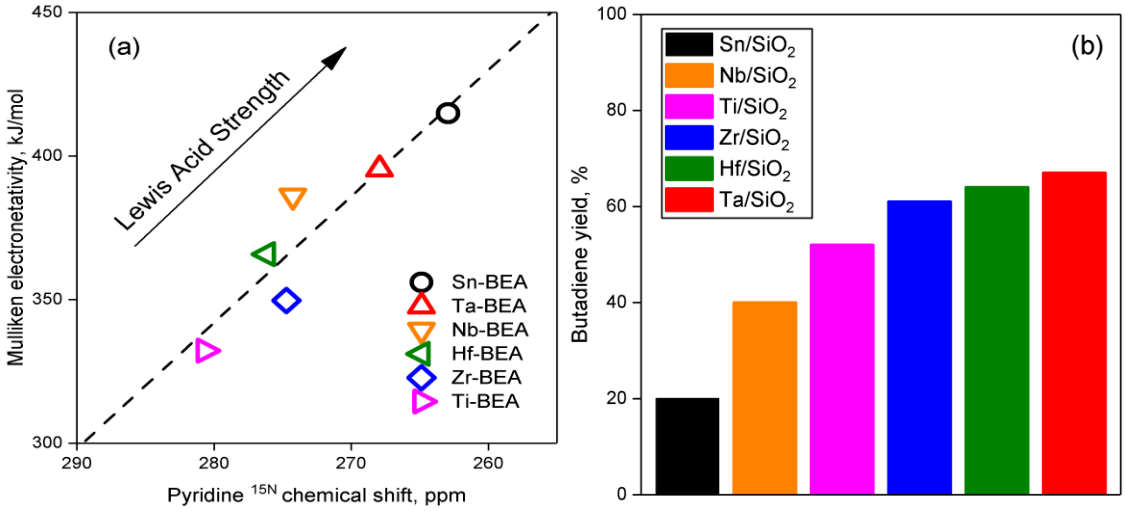

Figure 1.24 (a) Experimental Mulliken electronegativity versus pyridine ^{15}N magic angle spinning nuclear magnetic resonance chemical shift.[216] (b) Butadiene yield obtained in the two-step process obtained at 573-623 K, $LHSV_{EtOH}$ of 0.4 h^{-1}, 2.75 ethanol-acetaldehyde ratio.[34]

In the Zr, Nb, Hf and Ta catalysts for the ethanol-to-butadiene reaction, the relationship between catalytic activity and the properties of these Lewis acid sites is not fully understood, in part due to the difficulty of defining and quantifying Lewis acidity.[217] For instance, Corson *et al.* observed a trend with regards to the activity of silica-supported metal oxides in the Ostromislensky process that is generally valid: Sn < Nb < Ti < Zr ≈ Hf < Ta (Table 1.2, entries 1 to 6).[37,127,175,207] However, when compared to their Lewis acid strength when incorporated inside a zeolite, as determined by Román-Leshkov using Mulliken electronegativities and pyridine adsorption energies as descriptors (Figure 1.24 (a)),[216] there appears to be little correlation with activity, as expressed by butadiene yield (Figure 1.24 (b)).[37] Admittedly, the difference in preparation method may explain this discrepancy. However, even for other organic reactions, there is generally only a loose correlation between Lewis acid strength and activity;[214] the electronic properties of metal sites were also found to play a significant role.[217] How these factors impact the activity of group 4 and 5 transition metals in the ethanol-to-butadiene reaction remains to be elucidated.

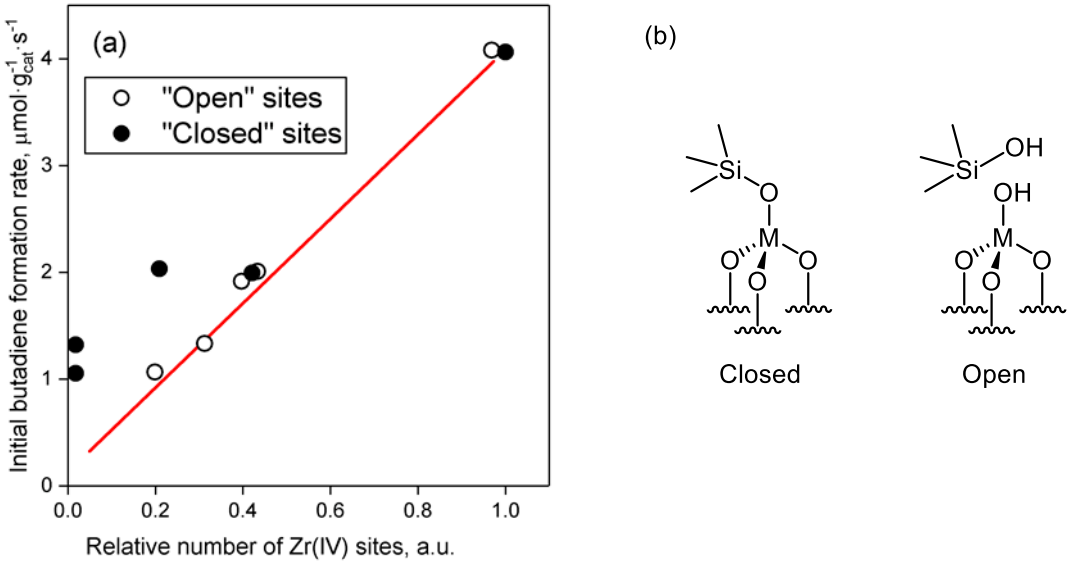

Figure 1.25 (a) Correlation between the relative number of open and closed Lewis sites determined by FTIR spectroscopy of adsorbed CO and the initial rates of butadiene formation on Ag/Zr-BEA.[134] (b) Closed and open Lewis acis sites.

Another important structural property of silicate-supported catalysts related to activity was identified by Ivanova *et al.* In their study of Ag/Zr-BEA, the authors found a direct correlation between the relative amount of tetrahedral Zr(IV) "open" Lewis acid sites present in the zeolite matrix and the initial rate of butadiene formation (Figure 1.25 (a)).[134,218,219] As Figure 1.25 (b) illustrates, metals incorporated into a silicate carrier can be fully coordinated with the silica framework, *e.g.*, "closed" sites, or have "open" sites due to the hydrolysis of Si–O–M bonds. Ivanova *et al.* argued that these configurations influence the reactivity of a metal site: "open" sites are known to require less energy to adopt the geometric distortion required by transition state of a reaction mechanism; the metal hydroxide and its adjacent silanol group may also participate in the reaction.[134,214,220] Accordingly, "open" Lewis metal sites are believed to be more active in the aldol condensation of acetaldehyde, the rate-limiting step on supported metal oxides of periodic group 4 and 5, due to their acid strength and steric accessibility.[102,104,134,175] Tetrahedral Lewis acid sites were also detected ZrO_2, ZrO_2/SiO_2 and ZrO_2/MCM-41 using FTIR with CO adsorption, but were found less active in the MPVO reaction.[209] Tetrahedral hafnium, niobium and tantalum oxides sites are also know to form when dispersed on catalysts carriers, but can adopt different structure when in bulk.[221–226]

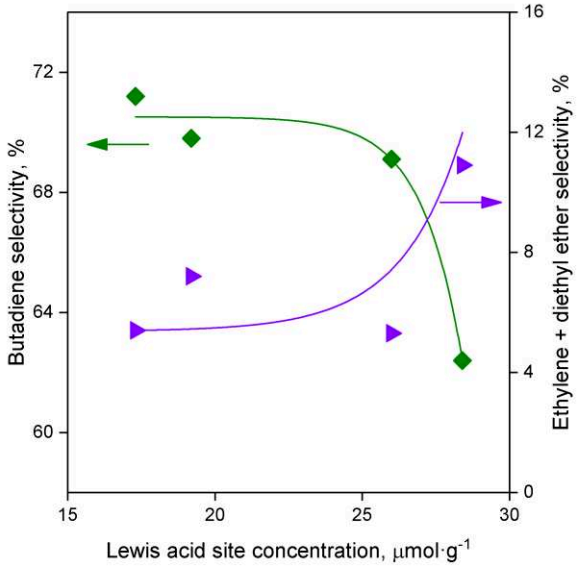

Figure 1.26 Evolution of selectivity in the Lebedev process on $Ag/ZrO_2/SiO_2$ versus the concentration of Lewis sites determined by FTIR of pyridine.[180] T = 598 K, $WHSV_{EtOH}$ = 0.45 h^{-1}.

Linear correlations between the acidity and catalytic activity with different catalysts were observed by other scholars: Kyriienko *et al.* reported a correlation between the relative concentration of Lewis acid sites in Zr-MTW catalysts determined by the FTIR spectroscopy of adsorbed CD_3CN and butadiene productivity;[227] the present authors reported a direct correlation between the number of acid sites probed in Zn-Ta catalysts by NH_3 and the selectivity towards butadiene.[106] Contrarily, Dagle *et al.*, who quantified the Lewis acid sites of $Ag/ZrO_2/SiO_2$ catalysts with the FTIR spectroscopy of pyridine, found that excessive Lewis acid site concentration caused by modifying the ZrO_2 loading lowered both butadiene selectivity and productivity in favor of ethanol dehydration products (Figure 1.26).[180] The authors argued that a small number of acid sites was preferable to avoid site reactions. Nevertheless, a scientific explanation as to why excessive Lewis acid site concentration favors undesirable reactions has yet to be provided.

Spectroscopic studies of supported Zr, Nb, Hf and Ta showed that the most active materials predominantly possess Lewis acid sites, but also small amounts of Brønsted acid sites.[127,162,207,219] The latter may be so weak that they risk being undetected with pyridine or $CDCN_3$, requiring the use of alternative probes, such as the strong organic base *2,6*-di-*tert*-butylpyridine or CO.[110,162] Brønsted acidity undermines selectivity towards butadiene by catalyzing the dehydration of ethanol. It should be noted that due to the Lewis acid-base pair nature of these metal oxides, basic properties

can also be detected,[223,228,229] although amphoteric suggest catalysts highly active in the conversion of ethanol to butadiene are primarily acidic.[106,175,208]

On the basis of observations made with Zr by Ivanova *et al*.,[134,208,209,219] catalysts containing group 4 and 5 metals possesses the Lewis acid characteristics required to catalyze the aldol condensation of acetaldehyde to crotonaldehyde and its subsequent conversion to butadiene *via* an MPVO reaction (reaction mechanisms are detailed in sections 1.3.1.2. and 1.3.1.3.).[104,110,127,162,207] Nonetheless, there exists a complex relationship between the properties of Lewis acid sites and their activity in the conversion of ethanol to butadiene. An explanation for the trend observed when comparing the performances of silica-supported group 4 and 5 transition metals in the Ostromislensky process has yet to be found, as no correlation was found with intrinsic acid strength, one possibility being the difference in electronic properties of each metal. Direct correlations between the number of Lewis acid sites and butadiene formation rate have been reported,[106,134,162,219] however excessive Lewis acid site concentration appears to be detrimental by favoring side reactions.[180] Furthermore, not all Lewis acid sites perform equally: Ivanova *et al*. identified the ideal active site as "*open*" isolated metal atoms in tetrahedral positions of the zeolite crystalline structure due to their enhanced steric accessibility and greater acid strength.[134] Other Lewis acid sites are believed to be comparatively less active.[209]

1.4.1.2. Catalyst design and activity

Supported metal oxides are the predominant types of catalysts containing Zr, Nb, Hf or Ta. Designing materials highly active in the conversion of ethanol to butadiene has generally involved the following considerations: (i) the choice of metal; (ii) the metal loading method; (iii) the choice of catalyst carrier and (iv) the choice of dopant if used in the Lebedev process. Comparison between the performances of the various catalysts discussed in this section and those found in the literature is discussed below are summarized in Table 1.2 and Table 1.3. The reader is also invited to consult them for details on the reaction conditions used in each test.

Choice of Metal

As highlighted in section 1.4.1.1. there appears to be a hierarchy in the catalytic activity of group 4 and 5 metal tested in the Ostromislensky process under when in the form of silica-supported metal oxides : Nb < Ti < Zr ≈ Hf < Ta (Table 1.2, entries 1 to 6).[34] Due to their relatively poor

performances, Nb and Ti are seldom used.[109,207] Instead, research has predominantly focused on Zr and Ta. Hf was found slightly superior to Zr as it lowered selectivity towards dehydration products while maintaining a similar activity; this observation attributed to the softer nature of Hf according to the hard-soft acid-base theory.[127] We believe all three metals are suitable for preparing highly active catalysts for the conversion of ethanol to butadiene. Likely, the availability of raw material and price will be an important factor in choosing the right active phase.

Rarely, two group 4 and 5 metals are combined in a single supported catalyst. Corson *et al.* tested Ta_2O_5 and ZrO_2 on silica, which was highly active in the two-step process, reaching a butadiene yield of 64%, but showed no obvious advantage over using each metal oxide alone other than their price difference (Table 1.2, entry 7).[34] Cadran and Chaumonnot reported a synergetic effect between tantalum and niobium oxide supported on silica.[230] The combination of both metals improved butadiene productivity and selectivity in the Ostromislensky process and Lebedev process when doped with zinc oxide when compared to summed performances of monometallic catalysts with equivalent metal content (Table 1.2, entry 8 and 9).

Metal Loading Methods

Generally, the group 4 and 5 metal loading of highly active supported catalysts has ranged between 0.1 and 10 wt.% preferably between 0.5 and 5 wt.% on a mass basis.[15,20] Generally, activity does not proportionally scale with metal loading. For instance, Kyriienko *et al*. observed that increasing from 0.7 – 1.0 wt.% to 2.0 – 3.0 wt.% the content of Nb and Ta in zeolite catalysts did not proportionally increase butadiene yield in the Orstromislensky process, instead resulting in moderate improvements to selectivity (Table 1.2, entries 10 to 13).[175,207] This phenomenon was attributed to the formation of less-active extra-framework metal oxide particles by sintering, which was evidenced by solid UV-vis spectroscopy. Furthermore, the Inversely, Ivanova *et al.* found that low Zr content in Zr-BEA catalysts prepared by hydrothermal synthesis favored the formation of "open" Lewis acid sites.[134] Metal content can be considered to affect the morphological and chemical properties of a catalyst and should therefore be adjusted to favor the dispersion the active phase for enhanced catalytic activity.

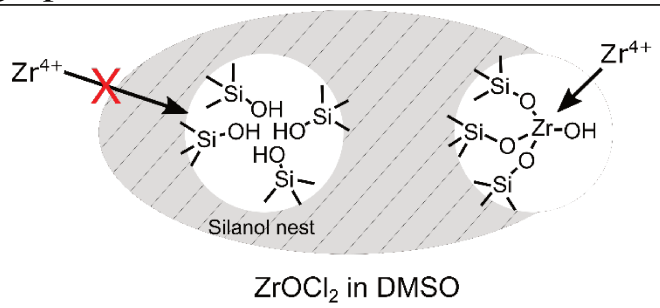

Figure 1.27 Schematic representation of Zr grafting to generate "open" Zr(IV) sites by treatment of dealumianted *β* zeolite with $ZrOCl_2$ in DMSO.[219]

Various means of metal incorporation have been used to prepare catalysts with highly dispersed active phases. Wet and dry impregnation can be found extensively in the literature concerning the ethanol-to-butadiene.[34,109,110,127,162,175,219,231,232] Several parameters influence the properties of the final material: the type and amount of precursor, solvent and carrier, but also experimental conditions such as pH, temperature and contact time, etc.[233] For instance, De Vos *et al*. noted that using $ZrCl_4$ instead of $Zr(NO)_3$ in the impregnation slurry improved the stability and butadiene selectivity of a Cu-Zr-Zn/SiO_2 catalyst (Table 1.3, entries 1 and 2).[127] Ivanova *et al.* developed an impregnation method to induce the formation of monoatomic "open" metal sites at higher metal loadings in their Ag/Zr/SiBEA catalyst.[219] By impregnating dealuminated commercial β zeolite with $ZrOCl_2$ in DMSO rather than in alcohol, they prevented the formation of "closed" Lewis acid sites. The authors explain that Zr cations in DMSO—either through diffusion limitations, steric hindrance of the nested silanol groups or due to energetically unfavorable formation of $Zr(OSi)_4$—grafted onto the terminal silanol groups formed by the dealumination process, but not on silanol nests within carrier, thereby exclusively forming "open" Zr(IV) sites Figure 1.27. A catalyst with 3.5 wt.% of Zr and a high concentration of "open" Lewis acid sites was achieved, resulting in a high butadiene formation rate and butadiene selectivity of ~60% (Table 1.3, entry 7). Unfortunately, the dealumination of commercial zeolite could not remove all traces of Brønsted acidity, which caused a high selectivity towards dehydration products. Introduction of metal precursors in the synthesis gel of aluminum-free *β* zeolite enabled the synthesis of solid Lewis acids without the need for post-synthesis modifications.[234] However, the necessity of a hydrofluoric medium and long preparation time may discourage this approach.

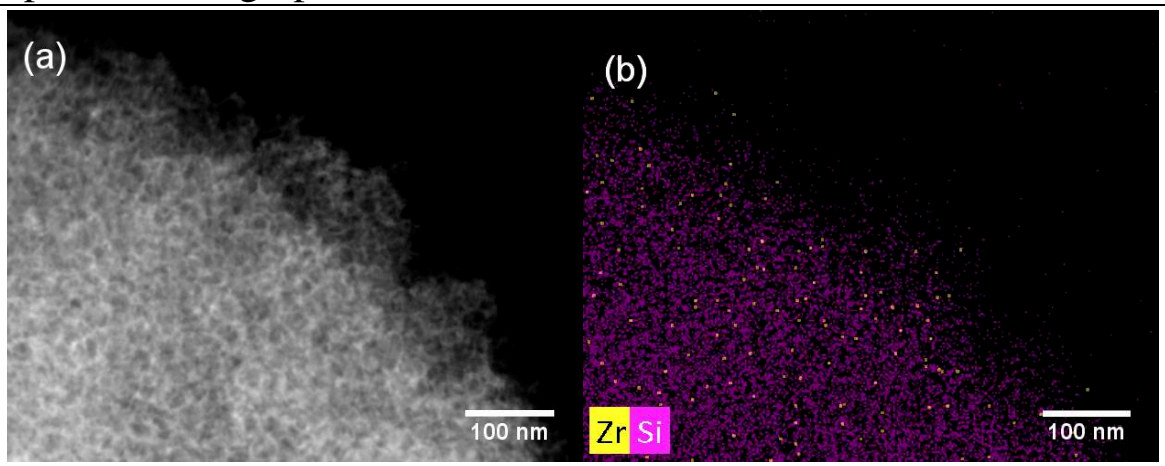

Figure 1.28 (a) HAADF-STEM of Zr/MCF (b) EDX mapping of Zr/MCF showing the high degree of dispersion obtained by urea hydrolysis precipitation.17

Lee *et al*. reported a highly active Zr catalyst on a mesocellular siliceous foam (MCF). [17] The authors used the urea hydrolysis method, which consists of a controlled precipitation that avoid concentration gradients of precipitants in the solution, to achieve a high degree of dispersion, as evidenced by SfigureTEM images depicted in Figure 1.28. Accordingly, the Zr/MCF catalyst performed exceptionally in the Ostromislensky process, reaching butadiene selectivity of 73% and unprecedented butadiene productivity (Table 1.2, entry 15). Foam-like mesoporous silica was also used by the present authors as carrier for a highly active Zn-Ta catalyst for the Lebedev process.[106] Using the TUD-1 methodology with tetraethylene glycol as both chelating and structuring agent, metal incorporation was included during the sol-gel step of the silica synthesis. The Zn-Ta-TUD-1 catalysts achieved a butadiene selectivity of 63% in spite of a high ethanol flow rate (8 h^{-1}) resulting in the highest butadiene productivity reported for the Lebedev process (Table 1.3, entry 14), which was attributed to the morphological properties of the catalyst and the high dispersion of the active phase. Sol-gel synthesis was used by Zhang *et al.* to synthesize ZrO_2-SiO_2 catalyst with highly dispersed ZrO_2 that achieved remarkable butadiene selectivity in the Ostromislensky process. Importantly, the concentration and strength of predominantly Lewis acid sites could be tuned by adjusting the metal loading, as evidenced by NH_3-TPD and pyridine-FTIR. 2 wt.% of ZrO_2 leading to a moderate amount of relatively weak acid sites was found ideal to maximize butadiene formation (Table 1.2, entry 16).

Choice of Catalyst Carrier

Three broad types of supports have been used to prepare such catalysts for the ethanol-to-butadiene reaction: microporous and mesoporous molecular sieves, and amorphous silica. These materials predominantly differ in their morphology, *i.e.*, pore size, porous volume and specific surface, with repercussion on the activity of the end-material. The structure of microporous molecular sieves causes steric hindrance, which may result in a potentially beneficial shape selectivity of the products.[235] By providing confinement effects, small pores may enhance the stability of reaction transition states of a reaction, thus improving catalytic activity.[236] However, the size similarity between micropore diameter and reacting molecules may restrict molecular transportation, resulting in intraparticule diffusion limitations curtailing catalytic activity.[237] Mesoporous carriers generally lack the benefits of confinement and shape selectivity but are less prone to mass transfer issues. Due to their porosity, both types of materials usually possess large specific surface area, increasing the active phase accessible to reactants per volume of catalyst and facilitating the dispersion of metal oxide phases during the preparation process.[233] In fact, Pinto *et al.* reported a direct correlation between the specific surface of K/ZnO-ZrO_2/MgO-SiO_2 catalysts and their butadiene yield (Table 1.8 entry 3), highlighting the importance of this parameter.[197] Compared to other oxide carriers, *i.e.*, ZrO_2, Al_2O_3 or TiO_2, the relative inertness of amorphous silica can be advantageous—it is simple and convenient catalyst support. Corson *et al.* tested a variety of metal oxide supports in the one and two-step processes, finding SiO_2 to be a more suitable carrier for highly active Ta_2O_5, HfO_2 and ZrO_2.[34]

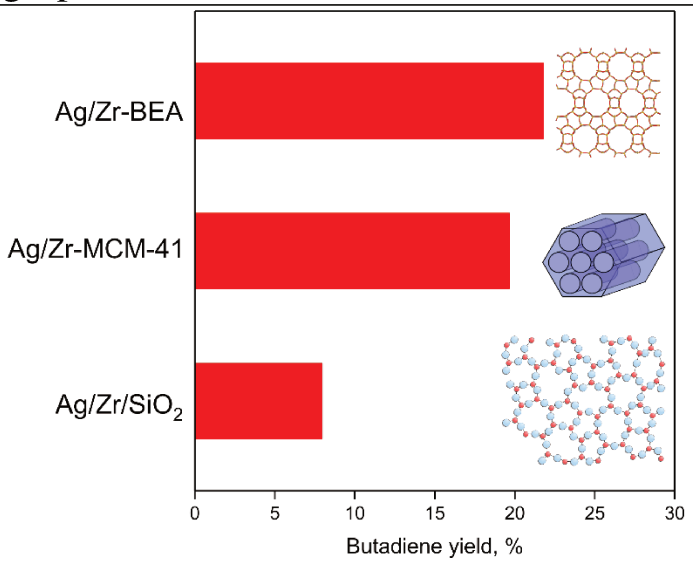

Figure 1.29 Effect of silicate carrier on the butadiene yield of Ag-Zr catalyst in the Lebedev process.[179] T = 593 K, $WHSV_{EtOH}$ = 0.32, TOS = 3 h.

Ivanova *et al*. compared the activity of all three categories of support in the Lebedev process with equimolar Ag and Zr as active phase; *β* zeolite (BEA), MCM-41 and commercial silica were respectively used for the three types of carrier. The authors found performances to scale with the content of Lewis acid sites, highlighting the influence of the chosen support on the chemical properties of the catalyst. As illustrated in Figure 1.29 the activity trend is as follows: $Ag/ZrO_2/SiO_2$ < Ag/Zr-MCM-41 < Ag/Zr-BEA (Table 1.3, entries 8 to 10). The authors argued that only the microporous material generated an ideal tetrahedral Zn(IV) isolated site. As a result, subsequent efforts by the team have focused on *β* zeolite. The latter has been extensively used to create highly active, hydrophobic, single-site Lewis acids *via* the incorporation of transition metals. This hydrophobic nature enhances the hydrothermal stability of the material. As a result, catalysts are less susceptible to framework collapse and deactivation by the effect of steam produced *via* the dehydration of alcohol groups in the ethanol-to-butadiene reaction.[238] At low group 4 and 5 metal loading, mononuclear Lewis acids can be generated in *β* zeolite catalysts by impregnation. Consequently, many excellent catalysts capable of butadiene selectivity greater than 60% in the one and two-step process have been reported with Ta and Zr in the literature.

In its aluminosilicate form, unmodified *β* zeolite performs poorly in the one and two-step processes due to its strong Brønsted acid sites which favor dehydration reactions.[16,41] Fortunately, aluminum-free synthesis of *β* zeolite[239,240] or post-synthesis removal of aluminum,[212,241,242] which

generates also generates new mesopores, are easily accomplished. Palkovits *et al*. observed that zeolite catalysts used in the Ostromislensky process benefited from a hierarchical micro-meso porous structure with an increase in ethanol conversion. The introduction of mesopores into a microporous zeolite is an established strategy to address diffusion limitations.[237] Two instances of successful designs of hierarchical catalyst for the Lebedev process have been reported. Zhang *et al.* synthesized a hierarchical catalyst by impregnating alumina-free MFI zeolite nanosheets with Zn and Hf.[243] The microporosity-mesoporosity provided by the three-dimensionally intergrown zeolite nanosheets increased butadiene yield from 27.3 % to 40.8 % when compared to a similar Zn/Hf-MFI catalyst prepared with microporous MFI zeolite (Table 1.3, entries 16 and 17). These results coincided with an increase in the concentration of Lewis acid sites. Kyriienko *et al*. prepared a hierarchical copper-doped Zr-MTW zeolite as catalyst for the Lebedev process.[227] It was found that the nature and concentration of fluoride-containing mineralizing agents used during synthesis influenced the morphological characteristics, acid-base properties and catalytic activity in the Lebedev process. Better catalytic performances were obtained with HF and Si:F ratio of 4, affording a butadiene selectivity of 68% and ethanol conversion of 81% (Table 1.3, entry 22).

Although Ivanova *et al*. first found microporous β zeolite to outperform mesoporous MCM-41, Zr and Ta-containing mesoporous catalysts have since demonstrated exceptional activity in the one and two-step processes. The present authors conducted a similar study comparing the activity of Zn-Ta catalysts supported on TUD-1 mesoporous silica, dealuminated β zeolite and amorphous silica.[106] Contrarily to Ivanova *et al.* mesoporous silica-supported samples outperformed Zn-Ta/SiBEA, suggesting that microporous materials are not necessarily the best suited carriers. In another comparison of catalyst carrier influence on the performances of Zn-Y, Li *et al*. agreed with Ivanova *et al.* that dealuminated zeolites were superior to MCM-41 and commercial silica.[184] A possible explanation could be that MCM-41, with its two-dimensional pore structure, was unsuited for the ethanol-to-butadiene reaction, which was found to benefit from three-dimensional mesoporous structure.[17] At present, concluding whether one carrier morphology is superior to the other is difficult considering that these studies were conducted under different reaction condition with distinct catalytic systems.

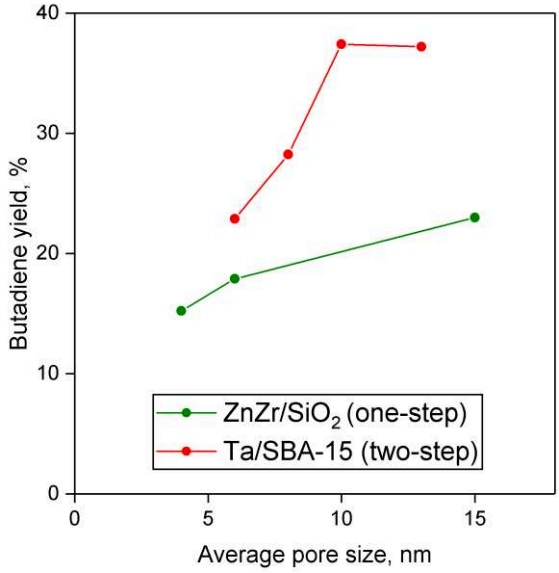

Figure 1.30 Effect of pore size on the butadiene yield during the one and two-step process over mesoporous catalysts.[41,174]

The IUPAC defines mesoporous materials as solids possessing pores with diameters between 2 and 50 nm.[244] A wide range of mesoporous silicates exist, many of which have been tested as catalyst carriers in the ethanol-to-butadiene reaction. Although ostensibly lacking the morphology required to induce confinement effect or size selectivity, several scholars highlight the influence of mesopore size on catalytic activity. Using a Zn-Zr active phase supported on mesoporous silica for the Lebedev process, Jones *et al*. observed a progressive improvement in catalytic performances by increasing the average pore diameter from 4 nm to 15 nm (Figure 1.30). Although ethanol conversion was not significantly affected, butadiene selectivity rose by 20%, resulting in an increase of 8% in butadiene yield. Similarly, Lee *et al*. reported a 15% improvement in butadiene yield during the Ostromislensky process over ordered mesoporous Ta/SBA-15 (Table 1.2, entries 17 and 18) after increasing the average pore diameter from 6 nm to 13 nm (Figure 1.30).[174] The authors attributed this phenomenon to a better active site accessibility of the reactants and products, noting that pore and crystal size were more important than the shape of the ordered silica. Additionally, Zr and Ta-containing mesoporous catalysts displayed notable catalytic activity and stability at industrially relevant conditions, namely a high hourly space velocity, for both types of ethanol-to-butadiene processes. Li *et al*. partly attribute such performances to the three-dimensional pore structure enabling greater reactant accessibility and improved mass transfer within the pore channels, thereby preventing coke formation and pore blockage. One downside of mesoporous

silica support is the relatively poorer hydrothermal stability,[245] which may be an issue for post-synthesis modifications involving water. For instance, Mg-containing MCM-41 collapsed after aqueous impregnation introduction of the oxide phase, rendering active sites inaccessible, resulting in poor catalytic performances.[163] Thicker pore walls and more micropores can increase the hydrothermal stability of mesoporous silicates.[245]

Dehydrogenation Promoters

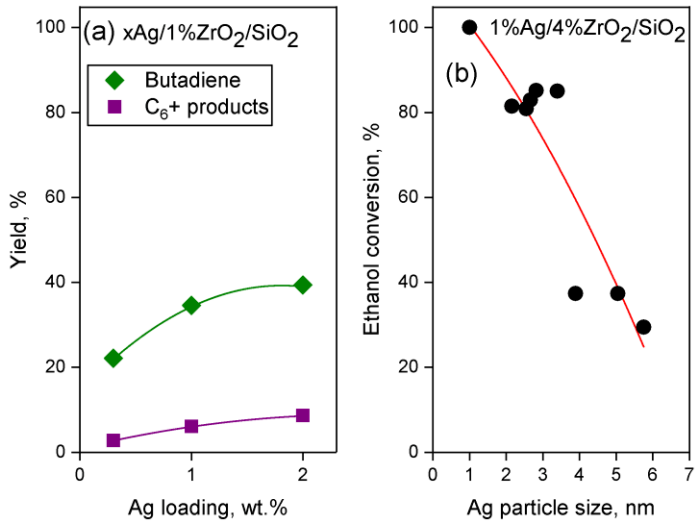

Figure 1.1.31(a) Effect of Ag loading on the performances of $Ag/ZrO_2/SiO_2$ in the Lebedev process. T = 593 K, $WHSV_{EtOH}$ = 0.31 h^{-1}.[109] (b) Effect of particle size on the activityof $Ag/ZrO_2/SiO_2$ in the Lebedev process at equimolar metal loading. T = 598 K, $WHSV_{EtOH}$ = 0.45 h^{-1}.[180]

Supported group Zr, Nb, Hf and Ta catalysts are inadequate to perform in the Lebedev process due to their poor ability to dehydrogenate ethanol to acetaldehyde. The addition of metals or metal oxides with dehydrogenation capabilities has been used to address this limitation. The use of promoter adds Ivanova *et al*. demonstrated that the performances of Ag-modified ZrO_2/SiO_2 could be improved by increasing the promoter content from 0.3 wt.% and 2 wt.% (Table 1.3 entry 10 and Figure 1.1.31 (a)). However, more than 1 wt.% of Ag reduced catalytic stability over time on stream—a sign that promoter loading also affected the properties and activity of catalysts for the Lebedev process. This phenomenon was attributed to an excessive of aldehyde, as evidenced by the increase in C_6+ compounds, which formed deactivation carbonaceous species. Dagle *et al*. also found that the activity of Lebedev catalysts depended on promoter dispersion (Figure 1.1.32 (b)). With equimolar amounts of Ag-modified ZrO_2 dispersed on various silicates, the authors established a correlation between Ag nanoparticle size and ethanol and ethanol conversion, with 1

nm being the preferred diameter to enhance ethanol conversion (Table 1.3 entry 17). However, butadiene selectivity was not directly affected by Ag particle size, suggesting the predominant feature of the catalyst remained Zr(IV) sites. In general, alcohol dehydrogenation with metals such as Au and Ag benefit from nanosized particles.[126]

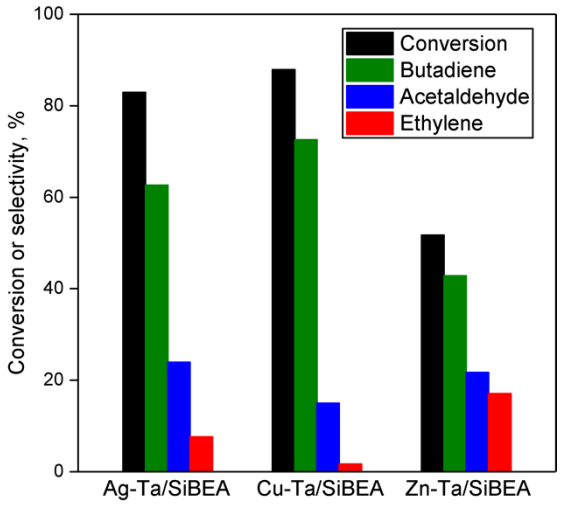

Figure 1.1.32 Influence of dehydrogenation promoters on the catalytic performances of Ta/SiBEA.[162] T = 598 K, $WHVS_{EtOH}$ = 0.5 h^{-1}.

The type of promoter used is another crucial aspect of catalyst design when preparing group 4 and 5 materials active in the Lebedev process. Larina *et al*. compared the performances of Ta-SiBEA catalyst modified with different metal dopants.[162] Impregnating these catalysts with Ag, Cu or Zn ion solutions modified their acid-based properties, resulting in a change in catalytic performances. Studied by the FTIR of chemical probes, the promoters generated new Lewis acid sites, weak Brønsted acid sites and weak basic sites. Of the three resulting catalysts, performances followed the trend: Zn-Ta/SiBEA < Ag-Ta/SiBEA < Cu-Ta/SiBEA, with the latter being one of the most selective catalysts in the literature (Table 1.3, entries 19 to 21). This hierarchy reflected some observations made for each promoters dispersed on pure silica for the dehydrogenation of ethanol: Cu/SiO_2 had previously been found to be more selectivity towards acetaldehyde and more sTable 1.than Ag/SiO_2,[16] whereas Zn/SiO_2, although active, was reported to produce significant amounts of ethylene along with acetaldehyde.[232] However, this promoter hierarchy is not valid for every catalytic system. For instance, Ivanova *et al.*, who compared 0.3 wt.% of Ag, Cu, and Ni as promoters for ZrO_2/SiO_2, found Ag to be the superior dopant, whereas Ni gave very poor performances (Table 1.3, entries 11 to 13).[109] This suggests that the performance enhancement of

dehydrogenation promoters also depends on the properties of the unmodified material. Both Ag and Cu can enable high butadiene formation under the right conditions. The same can be said of zinc, which has successfully been combined with group 4 and 5 transition metals to prepare catalysts highly active in the Lebedev process.[106,110,127]

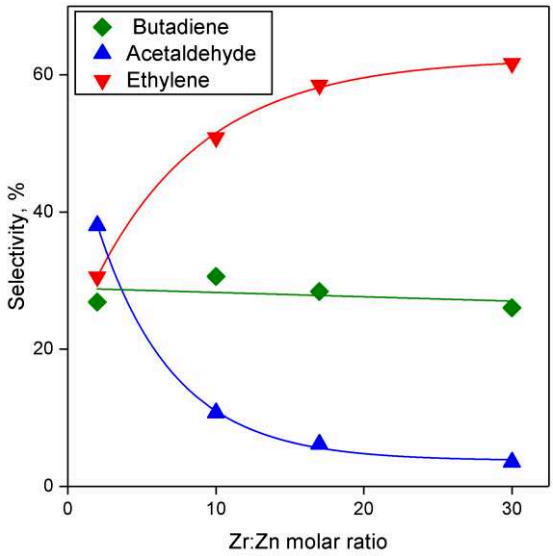

Figure 1.1.33 Effect of Zn content in $ZnZrO_x$ on the selectivity of the Lebedev process.[196] T = 623 K, $WHSV_{EtOH}$ = 0.789 h^{-1}.

The zinc silicate hemimorphite is one such promoter: it was used by De Vos *et al.*[127] and Villanueva Perales *et al.*[90,110] to make HfO_2/SiO_2 a highly active, selective and stable in the Lebedev process, performing better than Cu-containing catalysts (Table 1.3, entries 3, 4, 22 and 23). The authors noted that the addition of hemimorphite, in addition to increasing the ethanol dehydrogenation activity, passivated Brønsted acid sites, reducing selectivity towards dehydration products and improving stability. Baylon *et al.* reported a similar effect with $ZnO\text{-}ZrO_2$ mixed metal oxide. As illustrated in Figure 1.1.33, increasing the Zr:Zn ratio suppressed the stronger acid sites of ZrO_2, reducing selectivity towards dehydration products (Table 1.3 entry 24).[196] Even if dehydrogenation activity was not required, Zhang *et al.* used ZnO to suppress ethylene formation on a $ZrO_2\text{-}SiO_2$ catalyst in the Ostromislensky process (Table 1.3, entry 19); it decreased the number of acid sites without reducing their strength.[246] The addition of ZnO or hemimorphite, which are known to be amphoteric materials, have also shown to introduce new Lewis acid sites in catalysts.[110,127,232,247] Some authors have attributed the higher selectivity towards dehydration

products comparatively to Ag or Cu to these acid properties.[162,232] Others have found Zn(II) to contribute to the condensation activity in ethanol-to-butadiene due to their Lewis acid properties.[122]

Although Ag was ultimately found to be the best performing promoter of their study, Dagle *et al.* achieved high butadiene yield when using iridium to enhance the dehydrogenation abilities of ZrO_2/SiO_2 (Table 1.3, entry 18). Interestingly, when compared to Ag, Ir suppressed ethylene formation, but generated significantly more butenes. From an industrial standpoint, is it unlikely that Ir will be used due to its restrictive cost compared to silver and the fact that undesired C_4 compounds drive up the cost of butadiene purification.

Cu and Zn were simultaneously added to HfO_2/SiO_2 and ZrO_2/SiO_2 to prepared catalysts highly active and selective towards butadiene in the Lebedev process (Table 1.3 entries 1 to 3).[41,127] With both group 4 metals, the mixed dehydrogenation promoters resulted in in higher butadiene selectivity compared to their separate use. It is difficult to judge whether this improvement resulted from a synergy between Cu and Zn or simply the increased availability of active sites for ethanol dehydrogenation. Interestingly, Jones *et al.* noticed the deactivation of $1\%Cu/1.5\%Zr/0.5\%Zn/SiO_2$ compared to $1.5\%Zr/0.5\%Zn/SiO_2$, whereas De Vos *et al.* observed the contrary; $1\%Cu/3.0\%Hf/0.5\%Zn/SiO_2$ was significantly more stable than $3.0\%Hf/0.5\%Zn/SiO_2$. $Cu/ZnO/Al_2O_3$ (CZA), a catalyst active in the steam reforming of short-chain alcohols was combined with tetragonal ZrO_2 to prepare a new material active in the Lebedev process (Table 1.3, entry 27). CZA suppressed ethanol dehydration and greatly increased selectivity towards butadiene.[121]

Many other transition and noble metals were tested as dehydrogenation promoters but failed to give satisfactory performances in the Lebedev process. When introduced to ZrO_2 over SiO_2, 1 wt.% of Co, Mn and Ce were each unable to achieve butadiene selectivity greater than 29%, instead favoring ethanol dehydration products.[41] Despite being capable of non-oxidative dehydrogenation of light alcohols,[126] Pt gave remarkably poor performances when added to ZrO_2/SiO_2, yielding less than 2% butadiene in favor of methane, CO and CO_2 due to steam reaforming.[180] As previously mentioned, $0.3\%Ni/4\%ZrO_2/SiO_2$ was not very active with a butadiene yield below 8%.[109] Ostensibly, these metals and metal oxides are not active enough in the non-oxidative dehydrogenation of ethanol to acetaldehyde to enable the Lebedev process.

Catalysts consisting of metal oxides belonging to group 4 and 5 elements (Zr, Nb, Hf and Ta) are active in the Ostromislensky process and can perform in the Lebedev process by introducing metal or metal oxide promoters with dehydrogenation capabilities. The majority of these catalytic systems has consisted of silicate-supported materials, although mixed metal oxides have also been reported. Their condensation ability, which has been correlated with Lewis acid sites, is the key characteristic for achieving good catalytic performances, as the aldol condensation of acetaldehyde to crotonaldehyde is recognized to be the rate limiting step.

A primary concern of catalyst design has been to obtain isolated Lewis acid sites, which have been identified as most active and selective in the aldol condensation.[134] Impregnation of a support with metal precursor salts appear to be the predominant method of choice. However, it is susceptible to particle sintering during the synthesis process, which may result in large oxide particles with inferior catalytic activity. Consequently, a variety of synthesis methods have been employed to achieve highly dispersed active phases. In most cases, metal loading was shown to be an important parameter, often necessitating to be optimized in order to obtain the ideal acid characteristics that lead to good performances.

Besides the metal introduction method, the catalyst carrier was highly influential on catalytic performances. Al-free zeolites, mesoporous silicates and amorphous silica are generally used to dispersed metal oxides belong to group for 4 and 5 of the periodic table. Several authors have reported enhanced activity and selectivity by tuning the morphological properties of catalyst carriers, notably with the introduction of mesopores, which are believed to reduce mass transfer limitations.[41,106,174,177] Lee *et al.* suggested preparing catalysts possessing: (i) a highly dispersed active phase and (ii) a three-dimensional pore structure. A high surface area was also shown to improve catalytic performances.[197] However, other scholars have instead found that microporous zeolite supports afforded better catalysts than their mesoporous equivalents.[184,234] Some instances have shown that hierarchical materials possessing both micro and mesoporous morphologies were also very active in the ethanol-to-butadiene reaction.[227,243]

Zr, Nb, Hf and Ta catalysts can become active in the Lebedev process by introducing metal or metal oxide promoters with dehydrogenation capabilities. So far, Ag, Cu and Zn have been used to prepare catalysts demonstrating remarkable performances. However, their usage adds new dimensions to catalyst design that must be taken in consideration. Not only are the promoter effects

dependent on their nature and properties, but these dopants can also affect the properties of the unmodified catalyst, notably by altering their acid characteristics.[162,180] Consequently, preparing highly active and selective materials for the Lebedev process requires tuning both the condensation component provided by group 4 and 5 transition metals and the dehydrogenation component, but also to consider interactions between the two.

1.4.1.3. Catalytic Performance Data

Table 1.2 and Table 1.3 list the catalysts consisting of group 4 and 5 transition metals discussed in section 4.1.2. and their performances in the one and two-step processes, respectively. Accurate comparison between the catalysts is impossible due to the different reaction conditions used, namely temperature, contact time and conversion (Table 1.2 and Table 1.3), but also reactant concentration (not show).[110,248] In absence of such data, butadiene productivity and selectivity are useful metrics for comparison, as the former is an important to the industrialization of the ethanol-to-butadiene reaction,[96] and the latter is necessary to reduce separation costs. To some extent, high acetaldehyde selectivity can be considered beneficial, as it can be recycled into the reactant stream,[197] whereas ethylene selectivity should be kept as low as possible.

In the Lebedev process, the most productive catalyst consisted of Zn-Ta supported on mesoporous silica (Table 1.3, entry 14).[106] A productivity of 2.45 $g_{BD} \cdot g_{cat}^{-1} \cdot h^{-1}$ was achieved by maintaining relatively high ethanol conversion and selectivity towards butadiene despite an elevated ethanol flow. This was attributed to the three-dimensional mesopore structure, high specific surface area and high acid site concentration. A similar conclusion was reached for explaining the highest productivity obtained in the Ostromislensky (1.4 $g_{BD} \cdot g_{cat}^{-1} \cdot h^{-1}$) process with Zr supported on meso-cellular foam (Table 1.2, entry 15).[17] The best selectivity reported was achieved on Ta/SiBEA for both the Ostromislensky process and the Lebedev process, with copper being the dehydrogenation promoter (Table 1.2, entry 14 and Table 1.3, entry 20).[162,175] This high activity was attributed to the formation of "open" Lewis Ta(V) sites in the tetrahedral position of the dealuminated zeolite framework.[212] As discussed in section 3.5, catalyst deactivation is one issue that plagues the ethanol-to-butadiene reaction. Few studies have investigated this phenomenon in group 4 and 5 transition metal catalysts. Yet, the primary cause of deactivation has been attributed to coke deposition.[110,168,174] According to Lee *et al.*, three-dimensional pore structures help to reduce coking by facilizing mass transport within the catalyst.[17] Although direct

evidence remains to be found, it should be noted that the two most productive mesoporous catalysts exhibited remarkable resistance to deactivation.[17,106]

Table 1.2 Reviewed group 4 and 5 transition metal catalysts for the Ostromislensky process.

Entry	Catalyst	E:A	WHSV	TOS	T	X	BD S.	C2=	BD Y.	P_{BD}	Ref
			h^{-1}	h	K	%	%	%	%		
1	1.2%Ta_2O_5/SiO_2[a]	2.75	0.3	8	623	-	-	-	69	-	[34]
2	2.8%ZrO_2/SiO_2[a]	2.75	0.3	8	573	-	-	-	64	-	[34]
3	2%HfO_2/SiO_2[a]	2.75	0.3	8	573	-	-	-	64	-	[34]
4	1%TiO_2/SiO_2[a]	2.75	0.3	8	623	-	-	-	52	-	[34]
5	1%Nb_2O_5/SiO_2[a]	2.75	0.3	8	623	-	-	-	39	-	[34]
6	2%SnO_2/SiO_2[a]	2.75	0.3	8	673	-	-	-	20	-	[34]
7	1.7%Ta_2O_5/1.8%Zr/SiO_2[a]	2.75	0.3	48	623	-	-	-	64	-	[34]
8	0.5%Ta-0.5%Nb/SiO_2[b]	2.6	9.5	-	623	25	71	-	18	1.02	[249]
9	0.5%Ta/SiO_2 + 0.5%Nb/SiO_2[b]	2.6	4.4	-	623	25	61	-	15	0.36	[249]
10	0.7%Nb/SiBEA	2.7	0.8	4	623	43	55	36	24	0.11	[207]
11	2%Nb/SiBEA	2.7	0.8	4	623	26	53	30	14	0.06	[207]
12	1%Ta/SiBEA	3.2	0.8	4	623	45	78	14	36	0.17	[175]
13	3%Ta/SiBEA	3.2	0.8	4	623	59	73	21	43	0.20	[175]
14	3%Ta/SiBEA	2.2	0.8	4	598	31	90	0	28	0.13	[175]
15	2.7%Zr/MCF	1.38	3.7	1	673	95	70	6	67	1.4	[17]
16	2%ZrO_2-SiO_2	3.5	1.8	3	593	45	70	16	32	0.33	[167]
17	2%Ta/SBA-15	2.5	2.1	10	623	31	73	9	23	0.28	[174]
18	2%Ta/SBA-15	2.5	2.1	10	623	47	79	5	37	0.46	[174]
19	0.5%ZnO-ZrO_2-SiO_2	3.5	1.8	10	593	37	84	5	31	0.32	[246]

a: LHSV = 0.4. *b*: Pressure = 1.5 atm. X, S., Y. and P. are conversion, selectivity, yield and productivity. BD and $C_{2=}$ are butadiene and ethylene, respectively. Productivity is expressed in terms of $g_{BD} \cdot g_{cat}^{-1} \cdot h^{-1}$. Active phases are expressed in terms of wt.%.

Table 1.3 Reviewed group 4 and 5 transition metal catalysts for the Lebedev process.

Entry	Catalyst	WHSV	TOS	T	X	BD S.	AcH S.	$C_{2=}$ S.	BD Y.	P_{BD}[g]	Ref.
		h^{-1}	H	K	%	%	%	%	%		
1	1%Cu-1%Zr-0.5Zn%/SiO_2[a]	0.21	0.5	633	98	61	6	16	60	0.07	127
2	1%Cu-1%Zr-0.5Zn%/SiO_2[b]	0.21	0.5	633	96	65	8	10	63	0.08	127
3	1%Cu-3%-Hf0.5-%Zn/SiO_2	0.21	0.5	633	99	72	3	6	71	0.09	127
4	3%Hf-9.3%Zn/SiO_2	0.64	0.5	633	99	70	5	10	69	0.26	127
5	10%Zn-1%Ta-0.25%Nb/SiO_2[c]	0.7	-	648	55	64	-	-	35	0.18	230
6	5%Zn-1%Ta/SiO_2 + 5%Zn-0.25%Nb/SiO_2[c]	0.8	-	648	55	59	-	-	32	0.14	230
7	1%Ag-3.5%Zr/SiBEA	1.2 - 15	3	593	15	59	-	10	9	0.58	219
8	1%Ag/Zr-BEA[d]	0.32	3	593	31	66	-	5	20	0.04	234
9	1%/Zr-MCM-41[d]	0.32	3	593	30	66	-	7	20	0.04	234
10	1%Ag-ZrO_2/SiO_2[d]	0.32	3	593	12	67	-	3	8	0.01	234
11	0.3%Ag-4%ZrO_2/ SiO_2	0.3	5	593	30	74	-	3	22	0.04	109
12	0.3%Cu-4%ZrO_2/ SiO_2	0.3	5	593	27	74	-	3	20	0.03	109
13	0.3%Ni-4%ZrO_2/ SiO_2	0.3	5	593	10	68	-	6	7	0.01	109
14	6.1%Zn-3.4%Ta-TUD-1	8	3	673	82	63	27	9	52	2.45	106
15	4%Ag-4%ZrO_2/SiO_2[e]	0.45	-	598	91	67	7	11	61	0.16	180
16	1.5%Zn-8.9%Hf/MFI-NS[f]	0.47	3	693	67	53	0	15	36	0.10	243
17	1.5%-Zn-8.9%Hf/MFI-M[f]	0.47	3	693	64	43	1	11	27	0.08	243
18	1%Ir-4%ZrO_2SiO_2[e]	0.35	-	598	85	63	9	2	54	0.11	180
19	1%Ag-1%Ta/SiBEA	0.5	3.5	598	83	63	24	8	52	0.15	162
20	1%Cu-1%Ta/SiBEA	0.5	3.5	598	88	73	15	2	64	0.19	162
21	1%Zn-1%Ta/SiBEA	0.5	3.5	598	52	43	22	17	22	0.06	162
22	2%Cu/2%Zr-MTW	0.5	-	648	81	68	8	18[g]	55	0.06	227
23	1%Cu-1.5%-Zr0.5%Zn/SiO_2	-	3	648	45	67	5	21	30	-	41
24	3%Hf-9.3%Zn/SiO_2	1.12	-	633	87	43	7	4	38	0.25	110
25	3%Hf-9.3%Zn/SiO_2	11.2	-	633	50	29	43	2	15	0.96	110
26	ZnZrOx[h]	0.8	-	623	98	26	51	11	26	0.06	196
27	02.5CZA + ZrO_2[i]	-	6	673	76	54	12	16	42	0.73	121

a: Prepared with $Zr(NO_3)_2$. *b*: Prepared with $Zr(NO_3)_2$. *c:* Pressure was 1.4 atm. *d:* Si-Zr ratio = 200. *e:* SiO_2 was Davasil 636.*f:* NS = nanosheet, M = microporous *g:* Includes diethyl ether selectivity. *h:* Zr-Zn ratio = 10. *i:* CZA refers to $Cu/ZnO/Al_2O_3$; tetragonal ZrO_2 was used. WHSV: weighted hourly space velocity of ethanol. BD, AcH, $C_{2=}$ are butadiene, acetaldehyde and ethylene, respectively. X, S., Y. and P. are conversion, selectivity, yield and productivity, respectively. Productivity is expressed in terms of $g_{BD} \cdot g_{cat}^{-1} \cdot h^{-1}$. Active phases are expressed in terms of wt.%.

1.4.2. Magnesia-Silica Catalysts

Catalysts consisting of mixed magnesia and silica can perform the one-step conversion of ethanol to butadiene without the need for dehydrogenation promoters. This catalytic system dates back at least to 1944,[250] but some scholars[251] suggested MgO and SiO_2 to be the components of an undisclosed catalyst in Lebedev's earlier patents on the one-step process.[252,253] MgO-SiO_2 has since become one of the most studied catalytic systems. Research predominantly focuses on elucidating the relationship between properties of MgO-SiO_2 and its catalytic activity—a prerequisite of rational catalyst design. Section 1.4.2.1. reviews the literature on the structure-activity relationship of MgO-SiO_2 catalysts; section 1.4.2.2. discusses the synthesis methods and parameters; section 4.2.3. presents examples of MgO-SiO_2 catalysts with remarkable performances.

1.4.2.1. Acidity, Basicity & Activity

At present, the relationship between the reactivity of MgO-SiO_2 and its properties is not fully understood. Scholars agree that combining magnesia and silica produces materials with acidic and basic properties that enable the conversion of ethanol; a subtle balance between these properties is believed to be crucial for maximizing butadiene synthesis.[254] Still, only a limited consensus exists regarding the exact nature of these active sites, or what role each play in the reaction. Notably, the contribution of silica to the catalytic activity of MgO-SiO_2 is a contested topic. Disagreements appear to result from conflicting experimental observations reported the literature. Likely, the diversity of methods to prepare and study MgO-SiO_2 catalysts, but also the limits of analytic techniques often employed, are partly responsible for these discrepancies. The wide variety of characterization and preparation methods used has made comparison between different materials described in the literature difficult.

Kvisle *et al*. observed that active MgO-SiO_2 possess structural defects in the magnesia phase and magnesium silicate domains, but did not establish a direct correlation with them and catalytic activity.[255] Defects in magnesia are known to possess specific chemical properties and are often catalytically active sites.[229] The authors questioned whether silica, through the mixing process, merely induced catalytically active defects in MgO, or whether it was an essential component needed for the formation of catalytically active Mg–O–Si interactions. Generally, pure MgO predominantly converts ethanol to *1*-butanol *via* the Guerbet reaction.[100,135,256] However, Baba *et al*. reported that MgO, when subjected to hydrothermal treatment, became highly selective towards

butadiene.[144,149] This suggests that silica is not an essential component of the catalytic system and MgO structural defects, which are formed by the hydrothermal treatment, are the active sites of the ethanol-to-butadiene reaction. However, the two answers to the question above are not mutually exclusive: silica mixing may simultaneously induce defects in MgO, but also generate active magnesium silicates. In fact, the latter have often been associated with superior catalytic activity. As a result, SiO_2 and magnesium silicates, though not a prerequisite for enabling the activity of MgO in the Lebedev process, should not be dismissed when discussing this catalytic system.

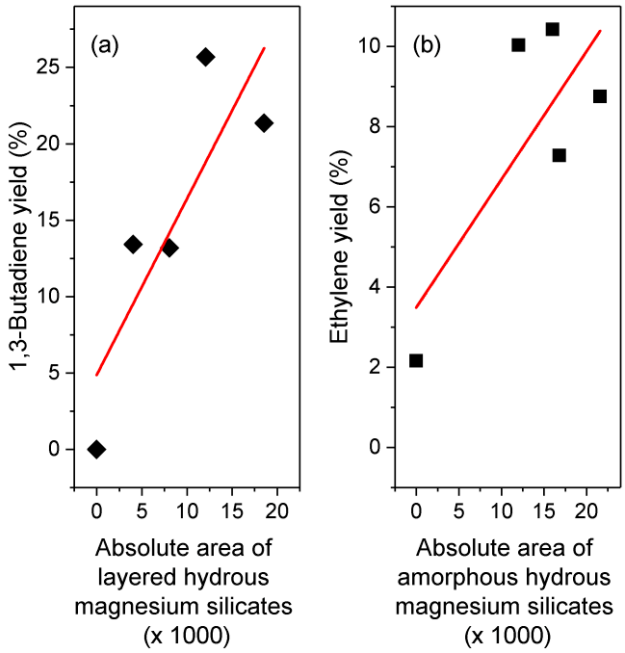

Figure 1.1.34 (a) Butadiene and (b) ethylene yield versus absolute area detected for layered hydrous magnesium silicates and amorphous hydrous magnesium silicates, respectively, according to Weckhuysen *et al.*[257]

Weckhuysen *et al*. studied the influence that three groups of magnesium silicates—anhydrous crystalline magnesium silicates, amorphous hydrous magnesium silicates and layered hydrous crystalline magnesium silicates—had on the catalytic activity of MgO-SiO_2.[257] By relatively quantifying each group within various MgO-SiO_2 samples using ^{1}H-^{29}Si CP/MAS-NMR, the authors were able to correlated specific structures with catalytic activity. Butadiene yield directly correlated with the relative of amount layered hydrous magnesium silicates, *i.e.*, talc, stevensite, lizardite (Figure 1.1.34, (a)). Incidentally, Zn-modified talc has proved to be one of the most active catalysts in the conversion of ethanol to butadiene, and pure talc was highly found highly active in the aldol condensation of acetaldehyde.[144,149] Weckhuysen *et al*. further established a correlation

between ethylene yield and the relative amount of amorphous hydrous magnesium silicate phase (Figure 1.1.34, (b)). Contrarily, Tan *et al*. attributed the high activity of their MgO-SiO_2 catalyst in the Ostromislensky process to the presence of amorphous magnesium silicates, which XPS analysis confirmed to have a low binding energy, possibly related to their disordered configuration.[164] In other instances, scholars have noted the negative effect of anhydrous magnesium silicate fosterite (Mg_2SiO_2) sometimes detected in MgO-SiO_2 catalysts, the presence of which coincided with greater selectivity towards dehydration products. Forsterite formation occurred when using high calcination temperature during prepration[164,258] or using the sol-gel method with low Mg to Si ratio.[157] Unfortunately, the chemical properties and catalytic activity of these magnesium silicates have not been properly evaluated.[257] As a result, their role in the ethanol-to-butadiene reaction has yet to be confirmed.

Weckhuysen *et al*. determined through a Hammett indicator study that well-performing MgO-SiO_2 catalysts were predominantly basic.[178] Nevertheless, these catalysts also possessed significant amounts of acid sites, as evidenced by IR spectroscopy with chemical probes. Consequently, MgO-SiO_2 can be considered and amphoteric catalyst. Identifying nature of these sites and their role has been an important research topic.

Catalyst poisoning studies with propionic acid demonstrated that weaker basic sites were active for the dehydrogenation of ethanol, whereas stronger basic sites catalyzed the aldol condensation and MPVO reactions.[97,128] Temperature-programmed and spectroscopic studies with probe molecules confirmed the presence of weak, medium and strong basic sites on MgO-SiO_2.[97,128,163,259] These studies, including *in situ* DRIFT spectroscopy, further identified surface Mg–OH groups as the weak basic sites responsible for ethanol dehydrogenation, as evidenced by their consumption during the reaction.[128]

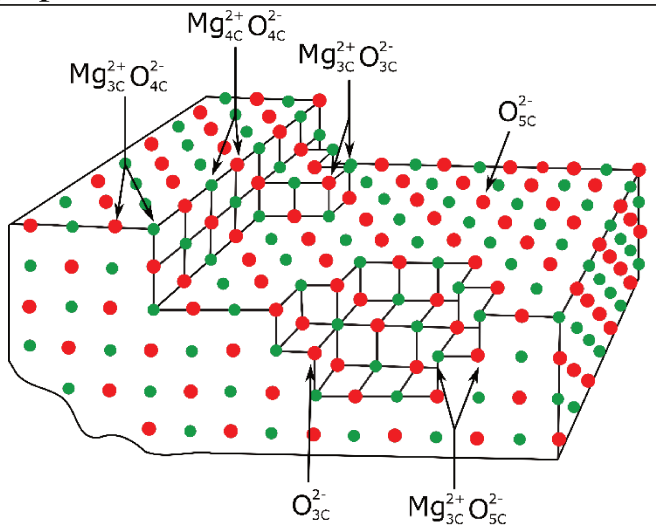

Figure 1.1.35 Model of structural defects on the surface of MgO.[260]

The stronger basic sites responsible the aldol condensation and MVPO reaction are believed to belong to Lewis acid-base pairs.[97,128,163] In basic metal oxides, such sites are well-known for operating in tandem to promote alcohol coupling, aldolization and MPVO reactions.[119,261] In Mg–O ion pairs, Mg^{2+} and O^{2-} exhibit Lewis acidic and basic characters, respectively. The strength of each moiety increases the lower their coordination number is, owing to electron deficiency and lowered stability respectively.[262] Consequently, pairs with varying degrees of coordination ($Mg_{3C}^{2+}O_{4C}^{2-}$, $Mg_{3C}^{2+}O_{3C}^{2-}$ and $Mg_{4C}^{2+}O_{4C}^{2-}$, see Figure 1.1.35) have been proposed as active sites and found to be active in the ethanol-to-butadiene reaction through DFT computational studies.[100,103,138,263] Acid-base pairs with vicinal Si^{4+} ions have also been suggested as active sites.[259] Sels *et al.* argued that the stronger basic sites, ostensibly tricoordinated oxygen anions found in corner defects, rapidly deactivated under the poisoning effect of polycondensation products formed by their larger strength.[163,208] Many authors have noted that excessive basicity, both in terms of site quantity and strength, correlated with poorer catalytic performances.[163,164,178] Consequently, acid-base pairs of moderate basic strength are believed to participate in the aldol condensation and MPVO reactions.[97,163] DFT computational calculations further confirmed that $Mg_{3C}^{2+}O_{4C}^{2}$, as opposed to tricoordinated oxygen anions O_{3C}^{2-}, was the most active site for the condensation step.[138]

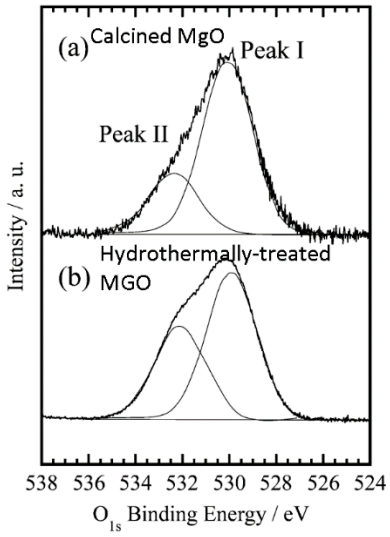

Figure 1.36 X-ray photoelectron spectra of O 1s for (a) calcined MgO and (b) hydrothermally-treated MgO, according to Baba *et al*.[144]

Interestingly, the XPS spectra of O 1s for hydrothermally treated MgO prepared by Baba *et al*. showed the presence of a noticeable shoulder peak at 532.1 eV which was less pronounced in calcined MgO (Figure 1.36).[144] The higher binding energy indicated that the oxygen atoms contributing to this peak were comparatively weaker basic sites.[229] The authors suggested these sites participated in the formation of butadiene, as only the hydrothermally treated MgO showed significant butadiene formation rate. This conclusion agrees with the aforementioned theory that reducing the basic strength of MgO is beneficial to its performances in the Lebedev process. Although Taifan *et al.* assigned this peak to uncoordinated oxygen anions,[128] the literature suggests it could belong to the oxygen in Mg(OH)[264–266] or $MgCO_3$.[267]

Generally, introducing Si into MgO generates new acid sites.[178] However, the contribution of surface acidity to the catalytic activity of MgO-SiO_2 in the ethanol-to-butadiene reaction is not fully understood. Correlating the nature of acid sites (Brønsted or Lewis) or their strength to any specific reaction step has proven difficult, in part due to the limitations of spectroscopic techniques used to characterize the surface acidity of MgO-SiO_2.

In theory, the Lewis acid moiety of Mg–O acid-base pairs is limited to electrostatic interactions with electron-rich intermediate species such as alkoxides, carbonyls and alcohols.[262] Unlike its transition metal counterparts, the d orbital of Mg cations is not accessible for bonding. However, its partial positive charge can stabilize the electron-rich function of transition state species in

organic reactions catalyzed by the vicinal basic oxygen anion. According to DFT calculations, this ability—which increases with Lewis acid strength—is believed to play a crucial role in the ethanol-to-butadiene reaction.[138] Acid-base pairs are active in aldol condensation[119,261] and MPVO reactions,[268] but also in alcohol dehydration.[116] The $Mg_{3C}^{2+}O_{4C}^{2-}$ pair was shown to be active in each catalytic step of the Lebedev mechanism by a DFT study.[103]

In practice, the relationship between acid sites and activity is not obvious. Most scholars agree that the acid sites of MgO-SiO_2 are responsible for the dehydration of acetaldol and crotyl alcohol, but also of ethanol. However, the dehydration of ethanol and C_4 alcohols are believed to occur on different sites. NH_3 poisoning experiments of MgO-SiO_2 in the one-step process revealed that weak acid sites dehydrated ethanol to ethylene and strong acid sites participated in the formation of butadiene.[128] The authors proposed that the latter were responsible for the dehydration of acetaldol and crotyl alcohol as NH_3 poisoning irreversibly suppressed the butadiene formation rate. Contrarily, acid quantification techniques with NH_3 showed that MgO-SiO_2 catalysts with excessive numbers of strong acid sites generated more dehydration products—an observation which led the authors to conclude that weak and medium strength acid sites were instead responsible for the dehydration of C_4 alcohols which are necessary to the formation of butadiene. Additionally, MgO-SiO_2 possessing forsterite phases showed possessed stronger acidity and higher selectivity towards dehydration products.[259] The possibility that mildly acidic silanol group on the silica phase—too weak to be probed by pyridine—are responsible for the dehydration of crotyl alcohol, a reaction thermodynamically favorable, was also proposed.[15]

Having observed with IR spectroscopy that Brønsted acid formed after co-adsorbing water and pyridine on the surface of MgO-SiO_2, Cavani *et al*. proposed a different role for Lewis acid sites. The authors suggested that Mg–O–Si Lewis acid sites become Brønsted acid sites in the presence of water which forms by the dehydration of ethanol.[157] These sites would possess the right acid strength for dehydrating the alkenol intermediates of the ethanol-to-butadiene reaction due to the influence of neighboring Si groups. Such phenomena may result in acid properties characterized *ex situ* that do not reflect the those of MgO-SiO_2 as the ethanol-to-butadiene reaction takes place. Contrarily, Taifan *et al*., using *in situ* DRIFT spectroscopy with pyridine to assess the surface acidity of spent catalyst, did not observe new Brønsted acid sites,[128] suggesting that the chemical properties of different MgO-SiO_2 are not influenced by water in the same fashion.

The conflicting theories regarding the role of acid sites may also partly be explained by experimental limitations. For instance, several research teams have observed an absence of Brønsted acid sites on the surface of MgO-SiO_2 when using pyridine as a chemical probe with IR spectroscopy.[19,163,164,269] On this basis, several many authors described highly active catalysts as possessing the right balance of Lewis acid sites and basic sites. However, Taifan *et al.* recently identified Brønsted acid sites on the surface of wet-kneaded MgO-SiO_2 from the deconvoluted DRIFT spectra of chemisorbed ammonia.[128] According to the authors, the bulkiness of pyridine presumably prevented it from reaching isolated, less-accessible Brønsted acid sites of unspecified strength. Consequently, theories regarding the participation of acid site in the Lebedev process may have been formulated with an inaccurate assessment of the acidic character of MgO-SiO_2 catalysts.

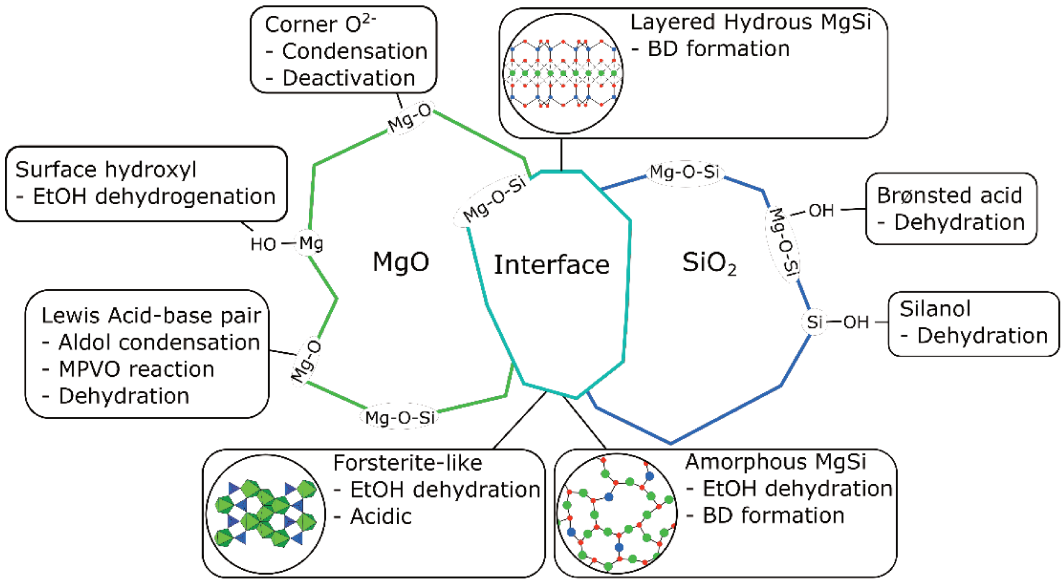

Figure 1.37 Visual representation of the different active sites on MgO-SiO_2 catalysts theorized to participate in the ethanol-to-butadiene reaction.

The role of MgO-SiO_2 surface acidity in the ethanol-to-butadiene reaction has not yet been fully understood. Ostensibly, Lewis acid sites—found on highly active catalysts—participate as part of the acid-base pair catalyzed condensation and MPVO reactions. Their *in situ* transformation into Brønsted acid sites active in the dehydration of alkenol intermediates requires further investigation. Of unspecified nature, weak acid sites dehydrated ethanol. The role of stronger acid sites in the different alcohol dehydration reactions remains under debate. In comparison, scholars generally agree on the contribution of basic sites: weak basic sites, likely hydroxyl groups on the surface of MgO, dehydrogenate ethanol; Mg-O pairs of medium-strength basic sites enable aldol

condensation and MPVO reaction; strongly basic tri-coordinated oxygen anions deactivate quickly due to their poisoning by condensation products. How these chemical properties related to the structural properties of MgO-SiO_2, notably of the different magnesium silicates, is another topic of research that requires further investigation. Figure 1.37 summarizes the active sites on MgO-SiO_2 evidenced or theorized to participate in the Lebedev process.

1.4.2.2. Catalyst preparation

Despite uncertainty concerning the exact nature and role of active sites, there is a consensus that maximizing the catalytic performances of MgO-SiO_2 catalysts requires a balance between the acidic and basic properties. Many authors agree with the recommendation of Weckhuysen *et al.*: small amounts of strong basic sites in the proximity of intermediate amounts of moderate strength acid sites is the optimal balance for maximizing butadiene yield and suppressing byproduct formation.[164,178,259] In light of the findings described above, the presence of weak basic sites Mg-OH may be added to this recommendation. Men *et al*. provided an experimental value for the ideal acid-base balance based on the results of TPD quantification techniques using NH_3 and CO_2 with various MgO-SiO_2 catalysts.[185] A surface total basicity/total acidity between 0.24-0.3 with an optimal strong acidity/total acidity between 0.46-0.5—small amounts of strong acid sites—maximized butadiene yield. However, Weckhuysen *et al*. demonstrated that CO_2 did not probe all the basic sites of MgO-SiO_2.[178] Consequently, despite the insight provided, the approach of Men *et al*. remains only approximate.

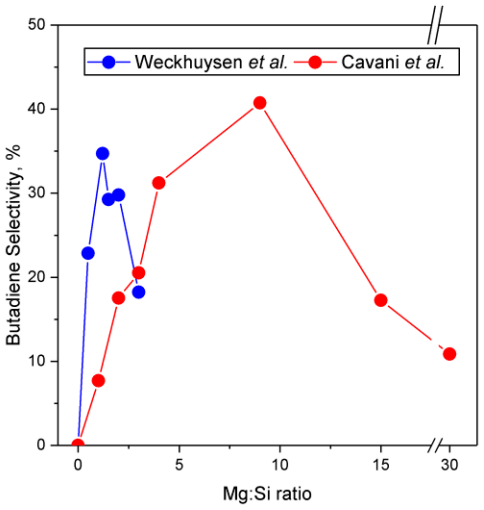

Figure 1.38 Influence of the Mg:Si ratio on the selectivity of MgO-SiO_2 prepared by wet-kneading (blue)[257] and the sol-gel technique (red).[157]

In practice, optimizing the acidic and basic properties of MgO-SiO_2 to maximize butadiene formation often proceeds by tuning the Mg-to-Si ratio. Since MgO is a strong basic oxide and the introduction of Si generally produces new acid sites, the Mg-to-Si ratio loosely reflects the basic-to-acid site ratio. However, the properties and activity of MgO-SiO_2 catalysts also depend on the level of interaction between each phase, which depends on the synthesis method used. As several preparation techniques are available to prepare MgO-SiO_2 materials, different optimal Mg-to-Si ratios have been reported.[143,157,255,257] Consequently, the Mg-to-Si ratio is a parameter better suited for comparing catalysts prepared by the same method. Figure 1.38 illustrates how butadiene selectivity can be improved by tuning the Mg-to-Si ratio and how the optimized value can differ significantly as a result of the synthesis method.[157,257]

Several procedures are used to prepare MgO-SiO_2 materials. Wet-kneading—the process of combining two or more solid precursor materials (mechanically or magnetically) in a liquid medium[257]—is a very common method for preparing MgO-SiO_2 catalyst in the ethanol-to-butadiene reaction; with water as a solvent, it has produced the most active catalyst of its kind[185] and a majority of studies used wet-kneaded samples.[96,114,257,269–272,128,129,178,185,232,251,254,255] The high butadiene yield provided by wet-kneaded MgO-SiO_2 has been attributed to the controlled mixing it provides. TEM and EDX-STEM have indicated that wet-kneaded materials exist in two bulk phases—crystalline MgO sheets and amorphous SiO_2 particles—with limited contact with one another.[255,257] LEIS revealed that MgO and SiO_2 are only intimately mixed at the surface of the two bulk oxide phases.[128] Weckhuysen *et al.* explained that, during the preparation, water dissolved MgO into Mg(OH), which provides alkali conditions that dissolve further silica; each ions are free to redeposit on the surface of the two oxides due to the use of water.[257] Wet-kneading conditions are known to influence the properties and activity of MgO-SiO_2.[251,254] Notably, the choice oxide precursor is important for achieving high activity. Weckhuysen *et al*. found that using nanosized Mg(OH) enhanced the degree of mixing between both phases, resulting in better performances.[257] Men *et al*. prepared the most productive MgO-SiO_2 catalyst (Mg-to-Si = 1.86) by using magnesium acetate, which resulted in a hierarchical flower-like MgO phase.[185] Similarly, the MgO precursor possessed a large surface area, making it suitable to maximize the interaction between the two oxide phases.

Other synthesis methods include: co-precipitation,[160,166,178,197,254] the sol-gel technique,[259] incipient wetness impregnation,[16,164,177,271] dry-milling[163,255] and mechanochemical mixing.[269] Co-

precipitated metal oxides resulted in excessive phase mixing, more Mg–O–Si linkages were detected compared to wet-kneaded MgO-SiO_2. These materials also possessed high amounts of acid sites and strong basic sites, resulting in poor butadiene selectivity. Catalysts prepared by the sol-gel method were highly sensitive to the Mg-to-Si ratio used.[259] At ratio below 9, forsterite and silica domains formed, giving rise to high ethylene selectivity. Optimal activity was achieved with a Mg-to-Si ratio of 15 (Figure 1.38), which resulted in highly dispersed Mg–O–Si linkages within a predominant magnesia phase. Impregnation of silica with ethanol-dissolved Mg precursors showed Mg–O–Si linkages can be obtained in absence of water, forming amorphous magnesium silicates in addition to crystalline MgO and silica phases.[164] With balanced acid-base properties, this MgO-SiO_2 catalyst proved highly active in the Ostromislensky process. Generally, dry-milling proved inferior to wet-kneading due to the lesser degree of mixing generated.[255] Mechanochemical mixing—heating during a dry-milling process—provided the energy to generate chemical interaction between magnesia and silica, resulting in a material comparable to wet-kneaded MgO-SiO_2 in terms of activity.[269]

Hydrothermal treatment was shown to turn calcined MgO highly active in the ethanol-to-butadiene reaction. The origin of this enhancement is unclear, but the treatment induced changes in the morphological and surface chemical properties of this oxide.[144,273] Kovařík *et al*. discovered that post-synthesis hydrothermal treatment of MgO-SiO_2 led to an increase both in its surface area and pore volume, improving activity and butadiene selectivity.[274] Men *et al*. prepared their highly active MgO-SiO_2 by wet-kneading hydrothermally synthesized MgO with silica; its catalytic performances were attributed in part to the morphological properties of the magnesia phase, which consisted in hierarchical flow-like inter-grown nanosheets.[185] Hydrothermal treatment was also suggested as an alternative regeneration procedure for deactivated catalyst.[274]

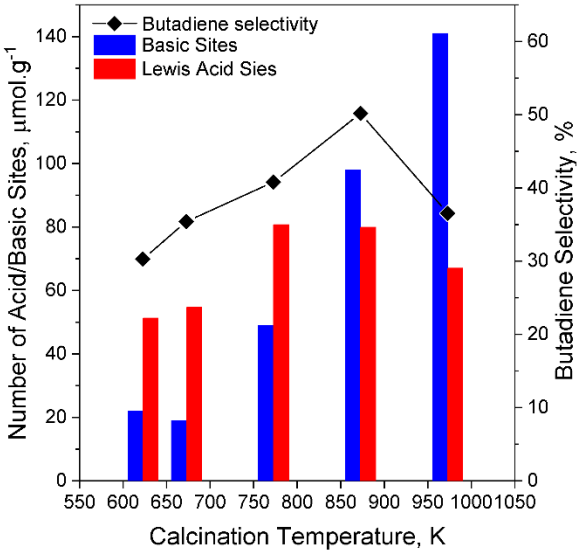

Figure 1.39 Effect of calcination temperature on the acid and basic properties of MgO-SiO_2 catalysts versus butadiene selectivity in the Ostromislensky process.[164]

Calcination conditions affect the chemical and structural properties of MgO-SiO_2 catalysts. Generating new basic sites on MgO requires the removal of deactivating surface contaminants—notably acidic CO_2—which generally proceeds by heating.[229] Furthermore, thermal processing provides the energy to create new bonds between the magnesia and silica phases forming new crystalline magnesium silicates.[164,275] Consequently, calcination conditions can influence the activity of MgO-SiO_2 catalysts by modifying their acid-base and structural properties. Zhu *et al.* studied the relationship between the calcination temperature under air of MgO-SiO_2 and its chemical properties;[164] their results are summarized in Figure 1.39. As illustrated, the ratio between the number of Lewis acid sites and basic sites was significantly affected by the calcination conditions. Calcination between 773 and 873 K generated a balanced number of Lewis acid and basic sites, resulting in higher butadiene selectivity. However, higher temperature generated too many basic sites, favoring undesirable side reactions. Weckhuysen *et al.* also found the thermal treatment conditions to influence the properties of CuO/MgO-SiO_2, including the nature of the atmosphere, noting that stagnant air was preferable to an N_2 atmosphere.[254]

Table 1.4 Effect of metallic promoters on the selectivity of $MgO\text{-}SiO_2$ at 25% conversion of ethanol studied by Shylesh *et al.*

Catalyst	Selectivity at 25% conversion, %					
	Butadiene	Acetaldehyde	Ethylene	Butenes	Butanol	Methane
$Au/MgO\text{-}SiO_2$	61	30	5	3	1	-
$Ag/MgO\text{-}SiO_2$	54	43	2	1	-	-
$Cu/MgO\text{-}SiO_2$	37	55	2	1	5	-
$Pd/MgO\text{-}SiO_2$	2	12	1	-	-	85

Conditions: T = 523 K, $WHSV_{EtOH}$ = 1.1 h^{-1}

Over bare $MgO\text{-}SiO_2$ catalysts, temperature-programmed surface reactions, catalytic tests, DFT calculations and poisoning studies suggest that the conversion of ethanol to acetaldehyde limits the reaction.[103,114,128,143,163,254] Consequently, several dehydrogenation promoters have successfully been used to improve catalytic performances. Taifan *et al.*[190] and Weckhuysen *et al.*[254,270] studied the promoting role of copper. It was found to increase butadiene yield due to its dehydrogenation abilities improving acetaldehyde formation rate, but also by poisoning acid sites, ostensibly suppressing undesired side-reactions. However, contrarily to bare $MgO\text{-}SiO_2$, Cu-modified samples deactivated faster. Both the sintering of metallic copper particle and blockage by coke have been proposed as deactivation mechanisms. Ag, Au and Pd have also been used to promote the activity of $MgO\text{-}SiO_2$.[97,161,163] Transition and noble metal nanoparticles, well established for promoting alcohol dehydrogenation reactions, are believed to provide redox properties to the catalytic system. Shylesh *et al.* investigated the potential of all three elements and copper: the catalytic test results are listed in Table 1.4.[97] A clear hierarchy can be seen in terms of selectivity at iso-conversion: Au > Ag > Cu >> Pd, but its origin has yet to be determined. Several parameters can influence the nonoxidative dehydrogenation ability of noble and transition metals, such as particle size, pretreatment conditions and metal-support interactions. These factors may also explain why Kyriienko *et al.* observed a different hierarchy for the promoters of their zeolite-supported tantalum catalyst for the conversion of ethanol to butadiene.[162] Sels *et al.* used Ag to enhance the activity of dry-milled $MgO\text{-}SiO_2$.[163] The introduction of Ag by aqueous impregnation improved acetaldehyde formation and generated new Lewis attributable to silver cations, Additionally, water itself increase the mixing between the oxide by dissolving Mg cation. Laosiripojna *et al.* reported a $Cu\text{-}Ag/MgO\text{-}SiO_2$ catalyst with high activity and stability compared to catalysts with monometallic promoters, a phenomenon which was a attributed to a synergism between Cu and Ag.[161]

Zinc oxide and zirconium oxide dispersed on MgO-SiO_2 were also used to enhance its catalytic performances. Zinc oxide contributed to the dehydrogenation reactivity of MgO-SiO_2. Zn-modified MgO-SiO_2 was found to yield more butadiene and acetaldehyde, but also to be more stable than a Cu-modified equivalent, possibly due to the lesser reducibility of Zn(II).[190] Both Zn and Zr oxides introduced new Lewis acid sites believed to promote the aldol condensation reaction (see section 4.1), but also to increase the rate of ethanol dehydration.[232,272] As a result, another dimension is added to catalyst design: the ZnO-ZrO_2 must also be balanced to maximize ethanol conversion to butadiene.[197] One may consider that the contribution of zinc and zirconium goes beyond that of a promoter. In fact, Kyriienko *et al*. found ZnO-ZrO_2/SiO_2 to be more active than its ZnO-ZrO_2/MgO-SiO_2.[272]

1.4.2.3. Examples of MgO-SiO_2 catalysts and performance data

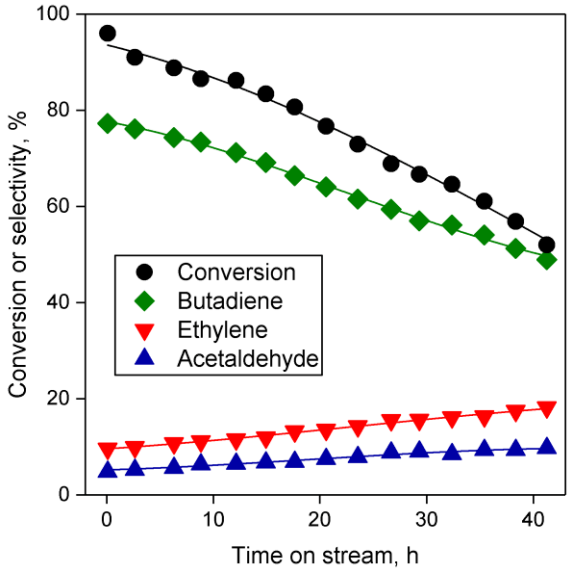

Figure 1.40 Stability test of highly active hierarchical MgO-SiO_2 catalyst prepard using Magnesium acetate and polyvinylpyrrolidone.[185] T = 723 K, $WHSV_{EtOH}$ = 4.1 h^1.

Men *et al*. reported the most productive MgO-SiO_2 catalyst in the literature: at high $WHSV_{EtOH}$ of 4.1 h^{-1} and a temperature of 723 K, it exhibited an initial conversion of 95% with a butadiene selectivity of 77%, resulting in a productivity of 1.76 $g_{BD}g_{cat}^{-1}h^{-1}$.[185] These performances were attributed to the morphological and chemical properties of the catalyst resulting from the synthesis method used. The authors prepared MgO using an ethylene glycol mediated self-assembly reported by Cui *et al*.[276] Magnesium acetate and polyvinylpyrrolidone—a structure-directing polymer—are dissolved in ethylene glycol and hydrothermally-treated in a Teflon-lined autoclave before

calcination of the MgO precursors at 773 K. This procedure afforded flower-like hierarchical oxide with larger surface area and pore size than commercial MgO. It was combined with SiO_2 by a wet-kneading process. The acidic and basic properties were optimized by tuning the Mg-to-Si ratio between 1 and 19, which also affected the textural properties of the mixed oxides; butadiene selectivity ranged between 50 and 80%. Ultimately, the authors obtained an optimal ratio of 1.87, arguing that it provided the material with the right balance of acid and basic sites, notably by limiting the number of strong acid sites. They also attributed the impressive catalytic performances to the high surface area and better access to catalytic sites provided by the hierarchical morphology. A stability test indicated that the catalyst deactivated slowly over a period of 42 hours: ethanol conversion and butadiene selectivity decreased from 95% and 77% to 51% and 49%, respectively (Figure 1.40). The authors attributed the loss of activity to gradual covering of active sites by coke deposition.

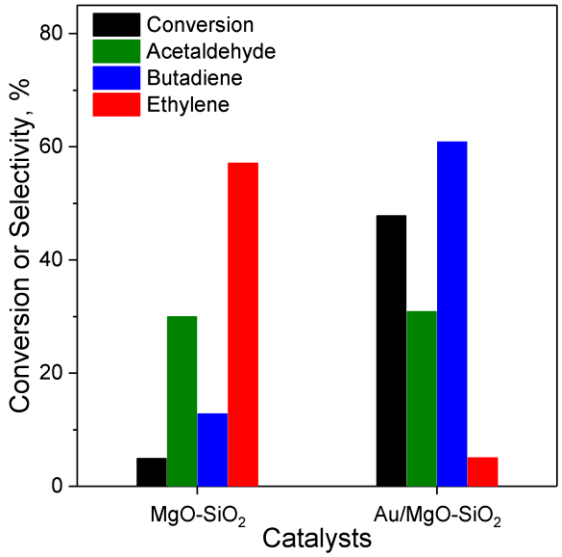

Figure 1.41 Effect of 3 wt.% Au on the performance of MgO-SiO_2. T = 573 K, $WHSV_{EtOH}$ = 1.1 h^{-1}.

As previously mentioned, Shylesh *et al*. used metallic dopants to enhance the catalytic activity of MgO-SiO_2.[97] Their work illustrates the beneficial effects of promoters. Prepared by incipient wetness impregnation of commercial silica using a magnesium nitrate solution, the bare initial catalyst with an Mg-to-Si ratio of 2.6 performed poorly. With an ethanol conversion below 10% at 573 K and a $WHSV_{EtOH}$ of 4.1, it mainly yielded ethylene. Au was added using the deposition-precipitation method with urea, well-known for introducing highly dispersed nanoparticles. As

illustrated in Figure 1.41, ethanol conversion underwent a seven-fold increase. As illustrated in Figure 1.41, the addition of Au further suppressed ethylene selectivity, increasing selectivity towards butadiene to near 60%. The authors attributed the performance enhancement observed to the redox properties provided by Au which are necessary to catalyze the dehydrogenation of ethanol. Characterization further indicated a close, but limited mixing of the magnesia and silica phase, a property that Weckhuysen *et al*. had associated with superior activity. The contribution of deposition-precipitation method to the catalytic activity was not explored. It may be possible that a basic pH combined with the mixing required replicated conditions akin to that of wet-kneading, further enhancing the textural and chemical properties of the catalyst. The work of Shylesh *et al*. illustrates how post-synthesis modifications can drastically improve the catalytic performances of $MgO\text{-}SiO_2$.

Weckhuysen *et al*. correlated butadiene yield with the relative quantity of layered hydrous magnesium silicates.[257] Baba *et al*. studied the catalytic activity of talc, a layered hydrous magnesium silicate, in the ethanol-to-butadiene reaction.[144,149,273] Pure synthetic talc produced very little butadiene from ethanol but showed >75% selectivity towards dehydration products at 38.8% conversion. The addition of zinc oxide to the hydrothermal synthesis process produced talc catalysts with Zn(II) substituted within the layered structure and highly selective towards butadiene. By tuning the Zn concentration, it reached 51.8% at a $WHSV_{EtOH}$ of 8.4 h^{-1} and a temperature of 673 K, amounting to a productivity one 1.1 $g_{BD}g_{cat}h^{-1}$—one of the highest in the literature. Catalytic tests with acetaldehyde alone demonstrated Zn suppressed ethanol dehydration, but also crotonaldehyde formation, indicating that pure talc was more active in the aldol condensation. Experimental and computational studies were conducted to explain the promoter effect of Zn. XPS revealed that the growing incorporation of Zn increased the binding energy of the O 1s level, indicating a progressive lowering of the basic character of talc. These results support the theory that limiting the among of strong basic sites is beneficial to butadiene yield, but also indicate that strong basic sites are more active in the aldol condensation. The promoter effect of Zn was attributed to its contribution to ethanol dehydrogenation. Based on DFT calculations and the hard-soft acid-base theory, the authors argued that Zn cations, acting as softer Lewis acid-base pair, favored dehydrogenation compared to purely Mg-containing catalysts. Zinc also increased the lifetime of the catalyst. Pure talc deactivated after 1 hour due to severe coking, whereas ethanol decreased by around half over a period of 15 hours with Zn-talc. However, selectivity towards

acetaldehyde progressively increased at the expense of butadiene, indicating that the stronger basic sites responsible for aldol condensation were progressively poisoned.

MgO-SiO_2 has proved to be one of the best catalytic system for the Lebedev process. Table 1.5 provides the performance detail of many catalysts directly or indirectly addressed in this section. Again, accurately comparing the different materials reported in the literature is hindering by the different reaction conditions employed. Nonetheless, from an industrial standpoint, it is worth highlighting that high butadiene selectivity, low selectivity towards dehydration products and high butadiene productivity were achieved, despite the challenges associated with MgO-SiO_2 catalysts design.

Table 1.5 Performances in the Lebedev process of reviewed MgO-SiO_2 catalysts and others found in the literature.

Entry	Catalyst	Mg:Si	WHSV	TOS	T	X	BD S.	AcOH S.	$C_{2=}$ S.	BD Y.	P_{BD}	Ref
			h^{-1}	h	K	%	%	%	%	%		
1	MgO-SiO_2[a]	1.86	4.1	-	723	95	77	2	13	73	1.76	[185]
2	3%Au/ MgO-SiO_2	2.6	1.1	3.3	573	45	60	28	7	27	0.14	[97]
3	Zn-Talc	-	8.4	7	673	42	52	22	8	22	1.06	[144]
4	MgO-SiO_2[b]	1	0.275	4	748	93	41	-	-	38	0.06	[277]
5	MgO-SiO_2[c]	1	1	-	673	41	57	5	34	24	0.14	[269]
6	1%Ag/MgO-SiO_2	2	1.2	3.3	753	84	50	6	10	42	0.29	[163]
7	1%CuO/MgO-SiO_2	1	1.1	0.5	698	74	48	7	5	38	0.25	[254]
8	6.3%Zr-1.4%Zn/MgO-SiO_2	3	0.62	3	648	40	36	8	32	30	0.13	[197]
9	4%ZnO/ MgO-SiO_2	1	1	3	648	56	62	22	10	35	0.20	[232]
10	2.5%Cu-2.5%Ag/ MgO-SiO_2	2	-	-	573	64	72	15	9	46	-	[161]
11	0.5%Ag/ MgO-SiO_2[d]	1	0.2	6	598	85	76	6	3	64	0.02	[278]
12	MgO-SiO2	0.63	0.03	11	623	53	30	10	53	16	0.003	[255]

a : Wet-kneading with hierarchical MgO; *b* : Wet-kneading with nano-sized MgO; *c* : Mechano-chemical synthesis; *d* : Hydrogen was co-fed. WHSV: weighted hourly space velocity of ethanol. X: ethanol conversion. BD, AcH, $C_{2=}$ are butadiene, acetaldehyde and ethylene, respectively. S., Y. and P. are selectivity, yield and productivity, respectively. Productivity is expressed in terms of $g_{BD} \cdot g_{cat}^{-1} \cdot h^{-1}$. Active phases are expressed in terms of wt.%.

Part of the issue can be attributed to unknowns regarding the identity of active sites. For instance, the extent to which SiO_2 is necessary to the formation of the active phase has yet to be identified.[255] Nevertheless, it is understood that a balance between acidic and basic properties is required to maximize catalytic activity. The prevalent theory on catalyst design suggests that weak and medium basic sites found on the MgO phase are required to catalyze the ethanol dehydrogenation and aldol condensation, respectively, with strong basic sites being detrimental to activity. However, the role of acid sites remains under debate: although moderate numbers of Lewis acid sites have been correlated with superior activity, there is no consensus on their identity. Identifying their ideal acid strength and the influence of neighboring Si atoms requires further investigation. Finally, the role of different magnesium silicate formed by the mixing of MgO and SiO_2 must be clarified.[257]

Even with the knowledge of the active phase, achieving the ideal balance of acidic and basic properties would be challenging. No systematic understanding of the numerous synthesis parameters susceptible to affect the acid-base character of MgO-SiO_2 (Mg-to-Si ratio, calcination temperature, mixing of the oxide phases, solvents, etc.) has been formulated. An overview of the best performing catalysts suggests that a limited mixing at the interface of MgO and SiO_2 phases, resulting in layered hydrous amorphous silicate, is preferable. Ostensibly, the MgO phase remains available to provide the weak and medium basic sites, while the new magnesium silicate possesses a suitable Lewis acidity, thereby providing the material with complementary actives requires. Excessive mixing between the two oxides leads to amorphous magnesium silicates responsible for ethanol dehydration.

The most successful preparation method appears to be wet-kneading MgO and SiO_2 precursors with morphological properties (nanosized, hierarchical) intended to maximize the limited interaction between them. The optimal Mg-to-Si ratio has varied depending on the synthesis method used. Contrarily, the ideal calcination temperature was found to vary between 773 K and 873 K.[164]

Because the rate limiting step of the ethanol-to-butadiene conversion MgO-SiO_2 is believed to be the formation of acetaldehyde, catalytic activity can be further improved by introducing transition and noble metals active in the dehydrogenation of ethanol. According to the results of Shylesh *et al*. Au is the most promising promoter for MgO-SiO_2.[97]

As illustrated in Figure 1.40, MgO-SiO_2 is susceptible to deactivation, ostensibly by coke deposition believed to be formed by strong basic sites. Yet, few studies have addressed the improvement of catalytic stability, or even the regeneration of spent catalyst.[274] It may be worth investigating the deactivation mechanism of MgO-SiO_2.

1.4.3. Rare Earth Elements

Rare earth metal oxides have found numerous uses in heterogeneous catalysis.[279,280] Recently, some authors have investigated the potential application of rare earth elements as catalysts for the conversion of ethanol to butadiene. Li *et al*. studied the activity of various rare earth (Y, La, Ce, Pr, Nd) oxide catalysts supported on dealuminated zeolite. Although zeolite-supported monometallic catalysts primarily dehydrated ethanol to ethylene and diethyl ether, Y, La and Ce were found capable of converting acetaldehyde to crotonaldehyde, indicating their condensation ability. By

combining these elements with metal oxides capable of ethanol dehydrogenation, catalysts highly active in the ethanol-to-butadiene reaction were recently reported in the literature. However, due to their novelty, these catalytic systems have not been investigated as other catalytic systems detailed in section 4.1. and 4.2. Consequently, the understanding of their activity is limited.

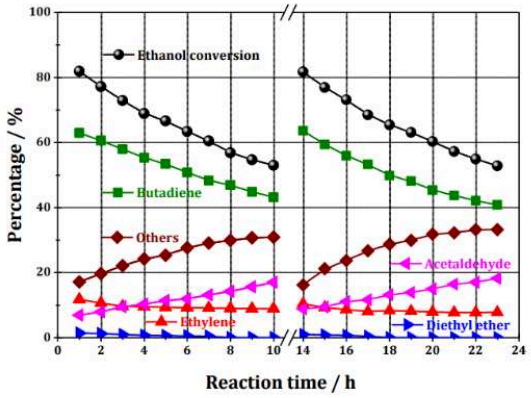

Figure 1.42 Stability and regenration test of 2%Zn-8%Y/SiBEA. T = 673 K, $WHSV_{EtOH}$ = 7.9 h^{-1}.

Owing to the work of Li *et al*., yttrium-containing catalysts have been the most studied of all rare earth-based ones for the ethanol-to-butadiene reaction.[122,184] Supported on dealuminated β zeolite, Y lead primarily to ethanol dehydration products. Promotion with copper marginally increased butadiene yield, yet diethyl ether and other carbonaceous species remained the principal products. Significant activity was obtained by combining Zn and Y. Li *et al.* tuned the Zn-to-Y ratio, ultimately obtaining 2%-Zn8%Y/SiBEA as the most active catalyst. Butadiene selectivity as high as 81% was reported. This catalyst achieved an exceptional productivity of 2.33 $g_{BD}g_{cat}^{-1}.h^{-1}$ at 673 K and a $WHSV_{EtOH}$ of 7.9 h^{-1}, making it one of the best for the Lebedev process found in the in the literature. The authors attributed these remarkable performances to a synergic effect between both Zn(II) and Y(III), which was enhanced by their proximity within the zeolite pores. Owing to the confinement effect of zeolites, Zn-Y clusters were suggested to form within the zeolite cages, as evidenced by the fact MCM-41-supported Zn-Y did not perform as well. Furthermore, XPS analysis found a stronger interaction between Zn(II) and Y(III) unique to the zeolite supported catalyst. The deactivation of 2%Zn8%Y/BEA was discussed in section 3.5. Li *et al*. determined that pore blockage did not play a significant role in the loss of activity.[131] Rather, cyclic unsaturated aldehydes and ketones gradually cover the Zn and Y sites of the catalyst. At conditions enabling high productivity, butadiene yield dropped by half in the first 10 hours of catalyst testing, which is

more severe than other highly productive catalysts recently reported (Figure 1.42).[106,185] Nevertheless, ZnY/SiBEA recovered its high productivity activity after calcination under air.

Li *et al*. have proposed a model of activity and deactivation of their 2%Zn-8%Y/SiBEA catalyst.[122] Since Zn/SiBEA produced acetaldehyde from ethanol, but also some butadiene, the authors argued Zn(II) primarily provided the catalyst with redox properties active in the dehydrogenation reaction. Since each component taken as a stand-alone catalytic system were found by MAS-NMR coupled with NH_3 and acetone-2-^{13}C adsorption experiments to introduce Lewis acidity into SiBEA, the authors argued that both metals contributed to the condensation activity, although Y(III) as found to be more active. Li *et al*. concluded that synergistic effect between Zn(II) and Y(III), but also the proximity of the two phases, enable the high selectivity observed, as it increased the chance of the intermediates reaction with each other on these sites during the aldol condensation.

Larina *et al*. mixed lanthanum oxide, which the literature identifies silica-supported La_2O_3 as a multifunctional catalyst,[281] with silica, zirconia and zinc oxide to prepare a catalyst highly active in the Lebedev process.[231] The preparation process combined incipient wetness impregnation and wet-kneading; several samples with different compositions were synthesized to study the role of each component in catalytic tests at 748 K and $WHSV_{EtOH}$ of 1 h^{-1}. La_2O_3-SiO_2 proved poorly active, yielding primarily dehydration products. The addition of zinc oxide successfully suppressed ethanol dehydration—a phenomenon observed in many catalytic systems for ethanol-to-butadiene reaction.[127,196,246] Still, butadiene yield remained below 20%. Only with the addition of ZrO_2, could a yield of 52.5% be achieved, marked by a sharp consumption of acetaldehyde compared to other samples. Ultimately, the best catalyst was 2%ZnO-7%La_2O_3-1%ZrO_2-SiO_2, which reached butadiene yield reached 60.2% at 743 K. The authors suggested that a synergy between each component explained the catalytic performances of the mixed catalyst. ZnO promoted ethanol dehydrogenation, whereas both ZrO_2 and La_2O_3 catalyzed the aldol condensation and MPVO reactions. In fact, La_2O_3 been shown to be active in aldol condensation[184,282] and MPVO reactions.[283] The condensation activity La_2O_3 can be attributed to its basic propertie, confirmed by Larina *et al.* with pyrrole-FTIR, but also well-known to the literature on La_2O_3.[281] Potential active sites are La-O acid base pairs and isolated O^{2-}.

Zhao *et al.* reported a Zn-Ce catalyst encapsulated within mesoporous SBA-15 active in the Lebedev process.[284] 10%Zn-5%Ce/SBA-15 catalysts were prepared using the solid-state grinding method to mix SBA-15 samples with metal precursors. By mixing the as-prepared SBA-15 sample containing the organic templates, a higher degree of active phase dispersion was obtained. This dispersion increased the concentration of Lewis acid sites compared to calcined SBA-15, which resulted in higher ethanol conversion and butadiene selectivity in the Lebedev process. At 648 K and a $WHSV_{EtOH}$ of 1.62 h^{-1}, butadiene reached 36 after 5 hours on stream. These performances were ostensibly attributed to a better condensation activity provided by the greater number of Lewis acid sites.

Development of rare earth catalysts for the ethanol-to-butadiene reaction is a recent subject. Characterization studies together with the literature available for other organic reactions suggest parallels may be drawn with other catalytic systems, as Y, La and Ce oxides possess chemical properties comparable to those of the previously discussed systems: basic sites and Lewis acid-base pairs. Correlating these properties with specific catalytic activity remains to be fully elucidated before proceeding to rational design. As demonstrated by Li *et al.*[184] rare earth metal oxides are active in the aldol condensation and MPVO reaction, implying that dehydrogenation promoters must be introduced to make them active in the Lebedev process. So far, Zn has been the preferred promoter, which some authors have suggested in synergy with Y.[184] The performances of the most active catalysts reviewed are listed in Table 1.6

Table 1.6 Reviewed rare earth catalysts active in the Lebedev process.

Entry	Catalyst	WHSV	TOS	T	X	BD S.	AcOH S.	$C_{2=}$ S.	BD Y.	P_{BD}	Ref.
		h^{-1}	h	K	%	%	%	%	%		
1	2%Zn-8%Y/SiBEA	7.9	1	673	82	63	7	2	52	2.33	[184]
2	2%ZnO-7%La_2O_3-1%ZrO_2-SiO_2	2	-	673	100	60	-	-	60	0.71	[231]
3	10%Zn-5%Ce/SBA-15	1.62	5	648	79	45	22	22	36	0.339	[285]

WHSV: weighted hourly space velocity of ethanol. X: ethanol conversion. BD, AcH, $C_{2=}$ are butadiene, acetaldehyde and ethylene, respectively. S., Y. and P. are selectivity, yield and productivity, respectively. Productivity is expressed in terms of $g_{BD} \cdot g_{cat}^{-1} \cdot h^{-1}$. Active phases are expressed in terms of wt.%.

1.4. Alkali & Alkaline Earth Dopants

The balance of acidic and basic properties influences the activity of catalysts in the ethanol-to-butadiene reaction. A simple, but efficient strategy has been to modulate them with alkali and alkaline-earth dopants,[16,121,176,196,197,243,286,287] an approach employed when dealing with solid acids.[288,289] The main benefit is the suppression of ethanol dehydration, sometimes at the expense of overall activity.[16,197] Although successfully put in practice, the fundamental aspects of this approach are not fully understood and no established method for using these dopants has been formulated.

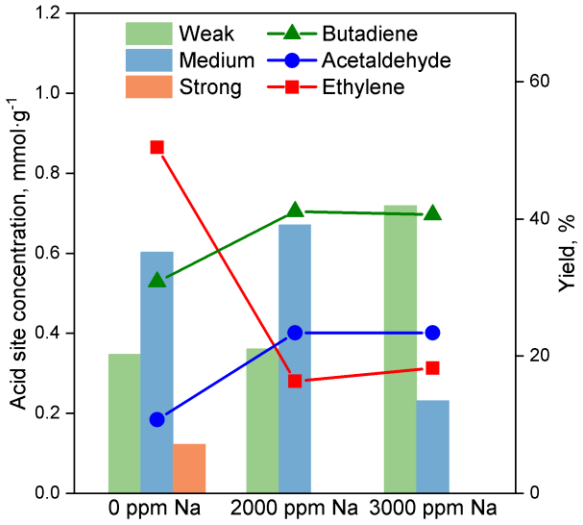

Figure 1.43 Product yield for the Lebedev process and the concentration of weak, meadium and stron acid sites on $ZnZrO_x$(Zr:Zn = 10) versus the concentration of Na dopant.[196]

The suppression of side reactions is attributed to the modulation of acid sites resulting from their interaction with alkali and alkaline-earth cations, which can be introduced into catalysts *via* impregnation.[16,121,176,196,197,243,286,287] In theory, these cation undergo proton-exchange with Brønsted acid sites, thereby deactivating them. The suppression of ethylene and diethyl ether formation is attributed to this poisoning effect, as Brønsted acid sites are known dehydration active sites. In practice, alkali and alkaline-earth cations have been shown to weaken or poison acid sites, but also to act as Lewis acid sites themselves, owing to their positive charge.[290,291] The influence of alkali and alkaline-earth dopants depends on both the nature of their nature and the amount added to the parent material. Sun *et al*. demonstrated that the principal effect of Na doping was to weaken

the acid strength of a $ZnO\text{-}ZrO_2$ catalyst without significantly lowering the total number of sites (Figure 1.43).[196] As a result, acetaldehyde and butadiene formation became favored over ethanol dehydration (Table 1.5, entries 1 and 2). However, the enhancement of butadiene yield plateaued when as the acid strength decreased. Similarly, Da Ros *et al.* progressively increasing the amount of Na from 0 to 2 wt.% on $ZnO\text{-}ZrO_2/MgO\text{-}SiO_2$ lowered butadiene yield (Table 1.8, entry 3).[197] These results suggest that, although these dopants can alleviate unwanted side-reaction by tuning the acid properties of a catalyst through the poisoning, a minimum of acid sites with moderate strength are required to enable to conversion of ethanol to butadiene.

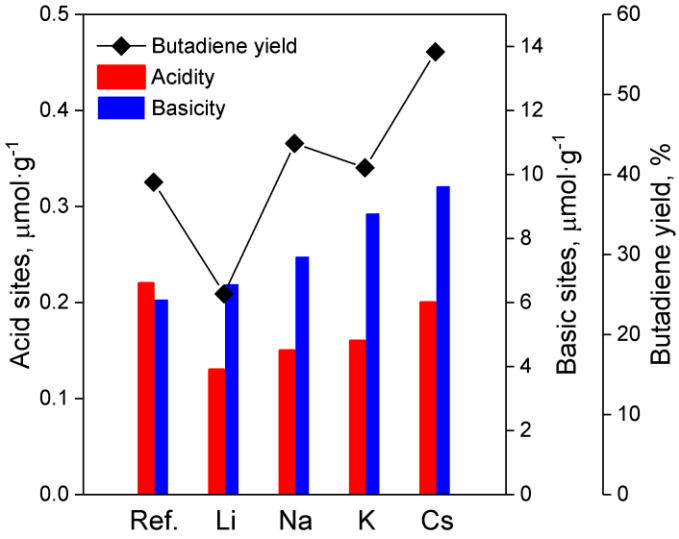

Figure 1.44 Influence of alkali and alkaline-earth dopants on the acid-base concentration of référence $1\%ZnO\text{-}5\%ZrO_2/SiO_2$ versus butadiene yield.[176]

Beyond their role as dehydration suppressors, Patil *et al.*[176] have proposed that alkali and alkaline-earth oxide could also contribute to butadiene production since they are known to possess basic properties,[229] After all, the basic alkaline-earth metal oxide MgO is active in the ethanol-to-butadiene reaction (section 4.2.). In comparing the performance enhancement of various promoters (Li, Na, K, Cs), the authors found that—although every dopant increased the number of basic site and suppressed ethylene selectivity—only Cs increased butadiene yield compared to the $ZnO\text{-}ZrO_2$ reference material (Figure 1.44). Notably, this promoter effect was verified at equimolar amounts of alkali and alkaline-earth dopants. The authors argued that Cs alone possessed the basic strength necessary to promote the aldol condensation step, thereby increasing the butadiene yield (Table 1.5, entry 3).

However, Palkovits *et al*. possibly contradicted this conclusion. Catalytic tests of alkali and alkaline-earth (Cs, K, Ca, Mg) doped β zeolite during the Ostromislensky process indicated that Cs/BEA did not catalyze the aldol condensation, reaching only 5% conversion; only magnesium-doped samples showed significant activity. This suggests magnesium oxide is better suited for providing the condensation activity required the ethanol-to-butadiene reaction.[144,149]

The only instance of an alkaline-earth oxide other than MgO being used as the catalyst component providing condensation activity was reported by La-Salvia *et al.*[287] The authors used barium oxide to promote the condensation of acetaldehyde on the acidic mesoporous aluminosilicate Al-MCM-41, with chromium oxide being used a dopant for ethanol dehydrogenation. With barium oxide and the aluminosilicate alone, ethylene was the predominant specie, indicating that the alkaline-earth oxide did not perform adequately in the dehydrogenation of ethanol. Only by adding chromium oxide and barium oxide could selectivity towards butadiene attain a maximum of 28% (Table 1.7, entry 5). Compared to other doped catalysts review in this section, ethylene selectivity remained very high, a phenomenon ostensibly due to Bronsted acid formed by the presence of Al cations within the silicate framework.

Table 1.7 Effect of morphological properties and the nature of alkali and alkaline-earth dopants on the performances of Zn-Hf catalysts supported on MFI zeolites.[243] T = 593 K, $WHSV$ = 0.47 h^{-1}, TOS = 3 h.

Catalyst	Conversion	Selectivity		
		Butadiene	Acetaldehyde	Ethylene
1.5%Zn-8.9%Hf/MFI(M)	63.6	43.0	1.1	11.1
1.5%Zn8.9%Hf/MFI (NS)	76.2	53.3	0	14.6
1.7%Li-1.5%-Zn8.9%Hf/MFI (M)	21.3	36.4	10.3	3.8
1.7%Li-1.5%Zn8.9%Hf/MFI (NS)	64.6	73.0	0	5.3
1.7%Na-1.5%Zn-8.9%Hf/ (NS)	54.2	45.2	3.2	2.3
1.7%K-1.5%Zn-8.9%Hf/MFI (NS)	35.6	32.1	5.6	1.2

NS = nanosheets. M = microporous.

Zhang *et al*. recently demonstrated how the morphology of a catalyst plays a significant role on the promoter effect of alkali and alkaline-earth cations.[243] Two zinc-hafnium oxide catalysts were compared: one supported on microporous MFI zeolite, another on nanosheets of the same molecular sieve. As listed in Table 1.7, the latter performed better, ostensibly due to the hierarchical morphology of the carrier. Interestingly, introducing of 1.5 wt.% Li led to very different changes in activity depending on the support. In the microporous material, the alkali cation reduced ethanol conversion by two-thirds, also suppressing butadiene selectivity. Contrarily, adding Li to the nanosheet-supported catalyst significantly enhanced butadiene selectivity while lowering ethylene

formation at minimal loss in ethanol conversion. The reason for the discrepancy is unclear, but it demonstrated that the properties of catalyst support influenced the dopant effect of alkali and alkaline-earth dopants. Furthermore, the authors compared the promoter effect of other cations (Na, K), concluding that Li was a better dopant (Table 1.7).

Post-synthesis introduction of alkali and alkaline-earth cations in various catalytic system—mixed oxides, supported metal oxides, zeolites—suppresses side-reactions, most notably ethanol dehydration. Generally, this is accompanied with a decrease in ethanol conversion. Alkali and alkaline-earth modifications also influence acetaldehyde and butadiene selectivity. The extent to which the catalytic performances are modified depends on the type and amount of dopant, as well as the nature of the catalytic system. Various studies indicated that these oxides lower the strength and/or number of acid sites. Generally, an excess of dopant results in a clear decrease in butadiene yield to the benefit of acetaldehyde yield, a phenomenon attributed to the poisoning of acid sites required to form butadiene. It is still unclear whether alkali and alkali-earth oxides also promote condensation activity *via* their basic properties, as discrepant results have published.[16,176]

Table 1.8 lists the performances of notable instances in which alkali and alkaline-earth dopants were used to enhance the catalytic activity of a parent material. Judging from the studies reviewed, it is difficult to conclude whether one dopant is inherently superior in their ability to enhance catalytic performances, a problem exacerbated by the different conditions used. For instance, Ohishi *et al.* reported one of the best catalytic performances by adding Na_2O to $MgO\text{-}SiO_2$ (Table 1.8, entry 7). However, many authors have pointed out that product distribution was recorded at very short time on stream, thereby ignoring any contribution from deactivation.[15,19] Nevertheless, alkali and alkaline-earth doping offer a facile approach to modifying the crucial acid-base properties of a given catalytic system. And as Da Ros *et al*. pointed out, the loss of butadiene yield sometimes observed can be compensated by the reduction of undesired byproducts considering that acetaldehyde can be recycled to take part in a two-step process.[197]

Table 1.8 Notable catalytic systems using alkali and alkaline-earth dopants to enhance activity in the Lebedev process.

Entry	Catalyst	WHSV	TOS	T	X	BD S.	AchOH S.	$C_{2=}$ S.	BD Y.	PBD	Ref.
		h^{-1}	h	K	%	%	%	%	%		
1	2000 ppm Na/ZnZrOx[a]	6.2	-	623	54	26	37	28	14	0.49	[196]
2	2000 ppm Na/ZnZrOx[a]	0.2	-	623	97	47	11	47	46	0.06	[196]
3	1.2%K-1.5%Zr-0.5%Zn/MgO-SiO_2	0.62	3	648	26	55	17	12	27	0.12	[197]
4	0.5%Cs_2O-17%ZnO-5%ZrO_2/SiO_2	1	-	673	98	56	16	15	55	0.32	[176]
5	1.4% Cr-16% Ba/Al-MCM-41	0.07	10	723	90	28	-	-	25	0.01	[287]
6	1.7%Li-1.5%Zn8.9%Hf/MFI (NS)	0.47	3	593	65	73	0	5	47	0.13	[243]
7	0.1%Na_2O/MgO-SiO_2	0.18	0.17	623	100	87	-	-	87	0.09	[286]

a: Zr:Zn ratio = 10.

1.5. Conclusion

After decades of being considered an obsolete technology, ethanol conversion to butadiene has begun to gather attention again. The primary cause of interest is the necessity of finding alternatives to the steam cracking of naphtha, which suffers from sustainability and supply issues. Under the right circumstances, notably geographical location and the type of biomass feedstock, butadiene from bio-ethanol is more sustainable than fossil-based routes. Financially, ethanol-to-butadiene processes cannot yet compete with current production methods, in part due to low petroleum cost, but also due to insufficient catalyst performances.

In the last 8 years, significant progress has been made in gaining insight into several aspects of the ethanol-to-butadiene reaction, namely its mechanism and the design of materials exhibiting optimal catalytic activity. The mechanism of the ethanol-to-butadiene is known to be complicated, partly because several of the intermediate species believed to be involved are seldom detected. Nevertheless, recent development owing to the use of techniques such as infrared spectroscopy, isotope tracing experiments and DFT studies have provided new evidence. The general pathway formulated by various authors more than fifty years ago has now come to be recognized as valid: ethanol first dehydrogenates to acetaldehyde, which condensates to crotonaldehyde; the latter reacts with another ethanol molecule to form crotyl alcohol and acetaldehyde *via* an MPVO reaction; crotyl alcohol dehydrates to butadiene.

At a molecular level, there remains differences amongst the conclusions of the various team, particularly concerning the aldol condensation mechanism, which may consist of an Eley-Rideal or Langmuir-Hinshelwood-type mechanism. These discrepancies are not inconsequential, as

kinetic modelling greatly benefits from our understanding of the reaction. Incidentally, the ethanol-to-butadiene reaction lacks adequate kinetic studies that can be used in process simulations. Consequently, studies on the viability of this technology often rely on industrial data—only for the Ostromislensky process—obtained after the Second World War with catalysts that have now be outclassed by recent findings. Another topic important to the implementation of ethanol-to-butadiene processes is the deactivation mechanism. The major cause of deactivation on almost all catalytic systems has been identified that the deposition of coke, with calcination under air a viable method of catalyst regeneration. However, some studies have found alternative sources of deactivation, such as the poisoning by active sites by bulky oxygenated species that are not coke, the reduction of metal oxide active phases and particle sintering.

A wide variety of catalysts have been reported throughout the years. Two primary categories of catalytic systems have been reviewed: group 4 and 5 transition metals, and $MgO\text{-}SiO_2$. In the first case, catalytic activity has been attributed to the Lewis acid characteristics of these metals when in their oxide form, generally supported over silicates. Lewis acid sites are known to catalyze the aldol condensation, making Ta, Hf and Zr catalysts some of the most active found in the literature. Maximizing the condensation ability of these catalysts by achieving monoatomic dispersion, preferably in the form of tetrahedral “open” sites within the framework of silicate carriers. To this end, several metal dispersion methods and catalysts carrier have been investigated, with exceptional performances obtained using mesoporous silica supports. The Lebedev process requires the addition of dehydrogenation promoters, with Ag, Cu and Zn being most successful. Recent research has found rare-earth metal oxides to also be active in the ethanol-to-butadiene reaction. Notably, zeolite-supported yttrium oxide catalysts have shown remarkable performances when combined with zinc oxide. Ostensibly, the Lewis acid properties of Y plays a role similar to Ta, Hf, Zr and Nb catalysts, that is to say to provide the material with condensation abilities.

$MgO\text{-}SiO_2$ catalysts are inherently active in the Lebedev process and have also shown remarkable performances. The main issue regarding this catalytic system concerns the uncertainty regarding the nature of the active sites. Weak and medium-strength basic sites on the MgO phase have been shown to enable the dehydrogenation of ethanol and the aldol condensation. However, the role and character of the acid sites formed by the mixing between MgO and SiO_2 remains under debate. To maximize the activity of $MgO\text{-}SiO_2$ catalysts, a subtle balance between the acid and base properties must be attained. However, the effect many synthesis parameters have on this

balance make the design of catalysts challenging. Activity can be further improved by the use of dehydrogenation promoters, as the formation of acetaldehyde has been identified as the rate-limiting step on $MgO\text{-}SiO_2$.

Modifying catalysts with alkali and alkaline-earth ions was shown to be a practical strategy to tune the acid-base properties of catalysts. These can poison stronger acid sites associated with undesired side-reactions, enhancing selectivity towards butadiene. To some extent, alkali and alkaline-earth ions can also introduce basic site, although the remains to be clear evidence that these new sites significantly participate in the reaction.

Although much insights have been acquired in recent years, there remains room for improving our understanding of the ethanol-to-butadiene reaction. A full elucidation of the molecular-level mechanism has been proposed, but its validity on different catalysts remains to be confirmed. Ostensibly, the subtle differences between the conclusions reached by various research groups could be explained by the different properties of each active phases. With such elucidation, kinetic modelling and accurate process simulation will be facilitated. Such modelling should include the effect of co-feeding water, and deactivation. Improving the reactivity of catalysts—all systems included—will require further investigation of the structure-activity relationship, but also the development of synthesis methods better suited to generate the most desirable active sites.

1.6. References

(1) Cavani, F.; Albonetti, S.; Basile, F.; Gandini, A. *Chemicals and Fuels from Bio-Based Building Blocks*; John Wiley & Sons, 2016.

(2) Dumeignil, F.; Capron, M.; Katryniok, B.; Wojcieszak, R.; Löfberg, A.; Girardon, J. S.; Desset, S.; Araque-Marin, M.; Jalowiecki-Duhamel, L.; Paul, S. Biomass-Derived Platform Molecules Upgrading through Catalytic Processes: Yielding Chemicals and Fuels. *J. Japan Pet. Inst.* **2015**, *58* (5), 257–273.

(3) Cherubini, F. The Biorefinery Concept: Using Biomass Instead of Oil for Producing Energy and Chemicals. *Energy Convers. Manag.* **2010**, *51* (7), 1412–1421.

(4) Bozell, J. J.; Petersen, G. R. Technology Development for the Production of Biobased Products from Biorefinery Carbohydrates—the US Department of Energy's "Top 10" Revisited. *Green Chem.* **2010**, *12* (4), 539.

(5) Climent, M. J.; Corma, A.; Iborra, S. Conversion of Biomass Platform Molecules into Fuel Additives and Liquid Hydrocarbon Fuels. *Green Chem.* **2014**, *16* (2), 516–547.

(6) Vennestrøm, P. N. R.; Osmundsen, C. M.; Christensen, C. H.; Taarning, E. Beyond

Petrochemicals: The Renewable Chemicals Industry. *Angew. Chemie - Int. Ed.* **2011**, *50* (45), 10502–10509.

(7) Sun, J.; Wang, Y. Recent Advances in Catalytic Conversion of Ethanol to Chemicals. *ACS Catal.* **2014**, *4* (4), 1078–1090.

(8) Chieregato, A.; Ochoa, J. V.; Cavani, F. Olefins from Biomass. In *Chemicals and Fuels from Bio-Based Building Blocks*; Wiley-VCH Verlag GmbH & Co. KGaA: Weinheim, Germany, 2016; pp 1–32.

(9) Mohsenzadeh, A.; Zamani, A.; Taherzadeh, M. J. Bioethylene Production from Ethanol: A Review and Techno-Economical Evaluation. *ChemBioEng Rev.* **2017**, *4* (2), 75–91.

(10) Furumoto, Y.; Harada, Y.; Tsunoji, N.; Takahashi, A.; Fujitani, T.; Ide, Y.; Sadakane, M.; Sano, T. Effect of Acidity of ZSM-5 Zeolite on Conversion of Ethanol to Propylene. *Appl. Catal. A Gen.* **2011**, *399* (1–2), 262–267.

(11) Iwamoto, M. Selective Catalytic Conversion of Bio-Ethanol to Propene: A Review of Catalysts and Reaction Pathways. *Catal. Today* **2015**, *242* (PB), 243–248.

(12) Sun, H. N.; Wristers, J. P. Butadiene. In *Kirk-Othmer Encyclopedia of Chemical Technology*; John Wiley & Sons, Inc.: Hoboken, NJ, USA, 2002; Vol. 4.

(13) Dahlmann, M.; Grub, J.; Löser, E. Butadiene. In *Ullmann's Encyclopedia of Industrial Chemistry*; Wiley-VCH Verlag GmbH & Co. KGaA: Weinheim, Germany, 2011; Vol. 100 C, pp 1–24.

(14) Lebedev, S. V. Lebedev Process. In *Comprehensive Organic Name Reactions and Reagents*; John Wiley & Sons, Inc.: Hoboken, NJ, USA, 2010; p FR665917.

(15) Makshina, E. V; Dusselier, M.; Janssens, W.; Degrève, J.; Jacobs, P. A.; Sels, B. F. Review of Old Chemistry and New Catalytic Advances in the On-Purpose Synthesis of Butadiene. *Chem. Soc. Rev.* **2014**, *43*, 7917–7953.

(16) Klein, A.; Keisers, K.; Palkovits, R. Formation of 1,3-Butadiene from Ethanol in a Two-Step Process Using Modified Zeolite-β Catalysts. *Appl. Catal. A Gen.* **2016**, *514*, 192–202.

(17) Cheong, J. L.; Shao, Y.; Tan, S. J. R.; Li, X.; Zhang, Y.; Lee, S. S. Highly Active and Selective Zr/MCF Catalyst for Production of 1,3-Butadiene from Ethanol in a Dual Fixed Bed Reactor System. *ACS Sustain. Chem. Eng.* **2016**, *4* (9), 4887–4894.

(18) Ezinkwo, G. O.; Tretyakov, V. P.; Aliyu, A.; Ilolov, A. M. Fundamental Issues of Catalytic Conversion of Bio-Ethanol into Butadiene. *ChemBioEng Rev.* **2014**, *1* (5), 194–203.

(19) Angelici, C.; Weckhuysen, B. M.; Bruijnincx, P. C. A. Chemocatalytic Conversion of Ethanol into Butadiene and Other Bulk Chemicals. *ChemSusChem* **2013**, *6* (9), 1595–1614.

(20) Pomalaza, G.; Capron, M.; Ordomsky, V.; Dumeignil, F. Recent Breakthroughs in the Conversion of Ethanol to Butadiene. *Catalysts* **2016**, *6* (12), 203.

(21) Jones, M. Catalytic Transformation of Ethanol into 1,3-Butadiene. *Chem. Cent. J.* **2014**, *8* (1), 53.

(22) Threadingham, D.; Obrecht, W.; Wieder, W.; Wachholz, G.; Engehausen, R. Rubber, 3.

Synthetic Rubbers, Introduction and Overview. *Ullmann's Encycl. Ind. Chem.* **2011**, 597–622.

(23) Morton, M. History of Synthetic Rubber. *J. Macromol. Sci. Part A - Chem.* **1981**, *15* (7), 1289–1302.

(24) Whitby, G. S.; Katz, M. Synthetic Rubber. *Ind. Eng. Chem.* **1933**, *25* (11), 1204–1211.

(25) Greve, H.-H. Rubber, 2. Natural. In *Ullmann's Encyclopedia of Industrial Chemistry*; Wiley-VCH Verlag GmbH & Co. KGaA: Weinheim, Germany, 2000; Vol. 9, pp 245–260.

(26) Nef, J. U. Dissociationsvorgänge Bei Den Einatomigen Alkoholen, Aethern Und Salzen. *Justus Liebig's Ann. der Chemie* **1901**, *318* (2–3), 137–230.

(27) Egloff, G.; Hulla, G. Conversion of Oxygen Derivatives of Hydrocarbons into Butadiene. *Chem. Rev.* **1945**, *36* (1), 63–141.

(28) Ostromislenskiy, J. Production of Butadiene. *J. Russ. Phys. Chem. Soc.* **1915**, No. 47, 1472–1506.

(29) Toland, J. *The Rising Sun: The Decline and Fall of the Japanese Empire, 1936-1945*; Modern Library, 2014.

(30) Kampmeyer, P. M.; Stahly, E. E. BUTADIENE FROM ETHYL ALCOHOL Improved Production Processes. *Ind. Eng. Chem.* **1949**, *41* (3), 550–555.

(31) Corson, B. B.; Stahly, E. E.; Jones, H. E.; Bishop, H. D. Butadiene from Ethyl Alcohol. *Ind. Eng. Chem.* **1949**, *41* (5), 1012–1017.

(32) Toussaint, W. J.; Dunn, J. T.; Jackson, D. R. Production of Butadiene from Alcohol. *Ind. Eng. Chem.* **1947**, *39* (2), 120–125.

(33) Wendt, P. The Control of Rubber in World War II. *South. Econ. J.* **1947**, *13* (3), 203.

(34) Corson, B. B.; Jones, H. E.; Welling, C. E.; Hinckley, J. A.; Stahly, E. E. Butadiene from Ethyl Alcohol. Catalysis in the One-and Two-Stop Processes. *Ind. Eng. Chem.* **1950**, *42* (2), 359–373.

(35) U.S. Synthetic Rubber Program - National Historic Chemical Landmark - American Chemical Society https://www.acs.org/content/acs/en/education/whatischemistry/landmarks/syntheticrubber.html (accessed Jul 12, 2019).

(36) Tuttle, W. M. The Birth of an Industry: The Synthetic Rubber "Mess" in World War II. *Technol. Cult.* **2006**, *22* (1), 35.

(37) Corson, B.; Jones, H.; Welling, C.; Hinckley, J.; Stahly, E. Butadiene from Ethyl Alcohol. Catalysis in the One-and Two-Stop Processes. *Ind. Eng. Chem.* **1950**, *42* (2), 359–373.

(38) Whitlock, M. H.; Haddad, G. J.; Stahly, E. E. System for Rapid Evaluation of Catalysts for Production of Butadiene from Ethanol. *Anal. Chem.* **1947**, *19* (10), 767–770.

(39) Quattlebaum, W. M.; Toussaint, W. J.; Dunn, J. T. Deoxygenation of Certain Aldehydes and Ketones: Preparation of Butadiene and Styrene. *J. Am. Chem. Soc.* **1947**, *1491* (1915), 593–599.

(40) Jones, H. E.; Stahly, E. E.; Corson, B. B. Butadiene from Ethanol. Reaction Mechanism. *J.*

Am. Chem. Soc. **1949**, *71* (5), 1822–1828.

(41) Jones, M.; Keir, C.; Iulio, C.; Robertson, R.; Williams, C.; Apperley, D. Investigations into the Conversion of Ethanol into 1,3-Butadiene. *Catal. Sci. Technol.* **2011**, *1* (2), 267.

(42) White, W. C. Butadiene Production Process Overview. *Chem. Biol. Interact.* **2007**, *166* (1–3), 10–14.

(43) Plotkin, J. S. The Continuing Quest for Butadiene. American Chemical Society 2016.

(44) Dargay, J.; Gately, D.; Sommer, M. Vehicle Ownership and Income Growth, Worldwide: 1960-2030. *Energy J.* **2007**, *28* (4), 143–170.

(45) Huo, H.; Wang, M.; Johnson, L.; He, D. Projection of Chinese Motor Vehicle Growth, Oil Demand, and CO $_2$ Emissions Through 2050. *Transp. Res. Rec. J. Transp. Res. Board* **2007**, *2038*, 69–77.

(46) Ouhadi, T.; Abdou-Sabet, S.; Wussow, H.-G.; Ryan, L. M.; Plummer, L.; Baumann, F. E.; Lohmar, J.; Vermeire, H. F.; Malet, F. L. G. Thermoplastic Elastomers. In *Ullmann's Encyclopedia of Industrial Chemistry*; Wiley-VCH Verlag GmbH & Co. KGaA: Weinheim, Germany, 2014; pp 1–41.

(47) Amghizar, I.; Vandewalle, L. A.; Van Geem, K. M.; Marin, G. B. New Trends in Olefin Production. *Engineering* **2017**, *3* (2), 171–178.

(48) Bruijnincx, P. C. A.; Weckhuysen, B. M. Shale Gas Revolution: An Opportunity for the Production of Biobased Chemicals? *Angew. Chemie - Int. Ed.* **2013**, *52* (46), 11980–11987.

(49) Derosa, S. E.; Allen, D. T. Impact of Natural Gas and Natural Gas Liquids Supplies on the United States Chemical Manufacturing Industry: Production Cost Effects and Identification of Bottleneck Intermediates. *ACS Sustain. Chem. Eng.* **2015**, *3* (3), 451–459.

(50) Yoshimoto, H. Global Petrochemicals Business and Role of Trading Houses. In *PETROCHEMICAL CONCLAVE 2013*; Gurgaon, 2013.

(51) Tian, P.; Wei, Y.; Ye, M.; Liu, Z. Methanol to Olefins (MTO): From Fundamentals to Commercialization. *ACS Catal.* **2015**, *5* (3), 1922–1938.

(52) Ren, T.; Patel, M. K.; Blok, K. Steam Cracking and Methane to Olefins: Energy Use, CO2emissions and Production Costs. *Energy* **2008**, *33* (5), 817–833.

(53) Gielen, D. J.; Moriguchi, Y.; Yagita, H. CO2emission Reduction for Japanese Petrochemicals. *J. Clean. Prod.* **2002**, *10* (6), 589–604.

(54) Ren, T.; Patel, M.; Blok, K. Olefins from Conventional and Heavy Feedstocks: Energy Use in Steam Cracking and Alternative Processes. *Energy* **2006**, *31* (4), 425–451.

(55) Tollefson, J.; Weiss, K. R. Nations Approve Historic Global Climate Accord. *Nature* **2015**, *528* (7582), 315–316.

(56) Cespi, D.; Passarini, F.; Vassura, I.; Cavani, F. Butadiene from Biomass, a Life Cycle Perspective to Address Sustainability in the Chemical Industry. *Green Chem.* **2016**, *18* (6), 1625–1638.

(57) Bhasin, M. M.; McCain, J. H.; Vora, B. V.; Imai, T.; Pujadó, P. R. Dehydrogenation and

Oxydehydrogenation of Paraffins to Olefins. *Appl. Catal. A Gen.* **2001**, *221* (1–2), 397–419.

(58) Stallwood, Y. McDermott Awarded PDH (Propane Dehydrogenation) Technology Contract in Europe by INEOS. **2018**, No. April, 1–2.

(59) Jing, F.; Katryniok, B.; Araque, M.; Wojcieszak, R.; Capron, M.; Paul, S.; Daturi, M.; Clacens, J.-M.; De Campo, F.; Liebens, A.; et al. Direct Dehydration of 1,3-Butanediol into Butadiene over Aluminosilicate Catalysts. *Catal. Sci. Technol.* **2016**, *6* (15), 5830–5840.

(60) Al-Douri, A.; Sengupta, D.; El-Halwagi, M. M. Shale Gas Monetization – A Review of Downstream Processing to Chemicals and Fuels. *J. Nat. Gas Sci. Eng.* **2017**, *45*, 436–455.

(61) Duan, H.; Yamada, Y.; Sato, S. Future Prospect of the Production of 1,3-Butadiene from Butanediols. *Chem. Lett.* **2016**, *45* (9), 1036–1047.

(62) Genomatica and Braskem Confirm Direct, Single-Step Biological Production of Butadiene https://www.genomatica.com/wp-content/uploads/2017/01/genomatica-and-braskem-confirm-direct-biological-production-of-butadiene.pdf (accessed Mar 6, 2019).

(63) Versalis and Genomatica produce bio-rubber with bio-butadiene from sugars https://www.eni.com/en_IT/media/2016/02/versalis-and-genomatica-produce-bio-rubber-with-bio-butadiene-from-sugars (accessed Mar 6, 2019).

(64) Kataoka, N.; Vangnai, A. S.; Tajima, T.; Nakashimada, Y.; Kato, J. Improvement of (R)-1,3-Butanediol Production by Engineered Escherichia Coli. *J. Biosci. Bioeng.* **2013**, *115* (5), 475–480.

(65) Yim, H.; Haselbeck, R.; Niu, W.; Pujol-Baxley, C.; Burgard, A.; Boldt, J.; Khandurina, J.; Trawick, J. D.; Osterhout, R. E.; Stephen, R.; et al. Metabolic Engineering of Escherichia Coli for Direct Production of 1,4-Butanediol. *Nat. Chem. Biol.* **2011**, *7* (7), 445–452.

(66) Ji, X. J.; Huang, H.; Ouyang, P. K. Microbial 2,3-Butanediol Production: A State-of-the-Art Review. *Biotechnol. Adv.* **2011**, *29* (3), 351–364.

(67) Plotkin, J. S. The Many Lives of BDO https://www.acs.org/content/acs/en/pressroom/cutting-edge-chemistry/the-many-lives-of-bdo.html (accessed Mar 6, 2019).

(68) Köpke, M.; Mihalcea, C.; Liew, F. M.; Tizard, J. H.; Ali, M. S.; Conolly, J. J.; Al-Sinawi, B.; Simpson, S. D. 2,3-Butanediol Production by Acetogenic Bacteria, an Alternative Route to Chemical Synthesis, Using Industrial Waste Gas. *Appl. Environ. Microbiol.* **2011**, *77* (15), 5467–5475.

(69) Daniell, J.; Köpke, M.; Simpson, S. D. *Commercial Biomass Syngas Fermentation*; 2012; Vol. 5.

(70) Ichikawa, N.; Sato, S.; Takahashi, R.; Sodesawa, T. Catalytic Reaction of 1,3-Butanediol over Solid Acids. *J. Mol. Catal. A Chem.* **2006**, *256* (1–2), 106–112.

(71) Jing, F.; Katryniok, B.; Paul, S.; Fang, L.; Liebens, A.; Shen, M.; Hu, B.; Dumeignil, F.; Pera-Titus, M. Al-Doped SBA-15 Catalysts for Low-Temperature Dehydration of 1,3-Butanediol into Butadiene. *ChemCatChem* **2017**, *9* (2), 258–262.

(72) Hort, E. V.; Taylor, P. Acetylene-Derived Chemicals. In *Kirk-Othmer Encyclopedia of Chemical Technology*; John Wiley & Sons, Inc.: Hoboken, NJ, USA, 2003; Vol. 1.

(73) Gannon, R. E.; Manyik, R. M.; Dietz, C. M.; Sargent, H. B.; Thribolet, R. O.; Schaffer, R. P. Acetylene. In *Kirk-Othmer Encyclopedia of Chemical Technology*; John Wiley & Sons, Inc.: Hoboken, NJ, USA, 2003; Vol. 1.

(74) Travis, A. S.; Center, E. UNINTENDED TECHNOLOGY TRANSFER: ACETYLENE CHEMISTRY IN THE UNITED STATES. *Bull. Hist. Chem* **2007**, *32* (1), 27.

(75) Sato, S.; Takahashi, R.; Sodesawa, T.; Yamamoto, N. Dehydration of 1,4-Butanediol into 3-Buten-1-Ol Catalyzed by Ceria. *Catal. Commun.* **2004**, *5* (8), 397–400.

(76) Sato, S.; Takahashi, R.; Sodesawa, T.; Honda, N. Dehydration of Diols Catalyzed by CeO2. *J. Mol. Catal. A Chem.* **2004**, *221* (1–2), 177–183.

(77) Duan, H.; Sun, D.; Yamada, Y.; Sato, S. Dehydration of 2,3-Butanediol into 3-Buten-2-Ol Catalyzed by ZrO2. *Catal. Commun.* **2014**, *48* (3), 1–4.

(78) Tsukamoto, D.; Sakami, S.; Ito, M.; Yamada, K.; Ito, M.; Yonehara, T. Production of Bio-Based 1,3-Butadiene by Highly Selective Dehydration of 2, 3-Butanediol over SiO2-Supported Cesium Dihydrogen Phosphate Catalyst. *Chem. Lett.* **2016**, *45*, 831–833.

(79) Zhang, L.; Singh, R. K.; D, S.; Guo, Z.; Li, J.; Chen, F.; He, Y.; Guan, X.; Kang, Y. C.; Lee, J.-K. *Artificial Synthetic Pathway for Acetoin, 2,3-Butanediol, and 2-Butanol Production from Ethanol Using Cell Free Multi-Enzyme Catalysis*; 2017.

(80) Zhang, W.; Yu, D.; Ji, X.; Huang, H. Efficient Dehydration of Bio-Based 2,3-Butanediol to Butanone over Boric Acid Modified HZSM-5 Zeolites. *Green Chem.* **2012**, *14* (12), 3441.

(81) Kim, W.; Shin, W.; Lee, K. J.; Song, H.; Kim, H. S.; Seung, D.; Filimonov, I. N. 2,3-Butanediol Dehydration Catalyzed by Silica-Supported Sodium Phosphates. *Appl. Catal. A Gen.* **2016**, *511*, 156–167.

(82) Song, D. Kinetic Model Development for Dehydration of 2,3-Butanediol to 1,3-Butadiene and Methyl Ethyl Ketone over an Amorphous Calcium Phosphate Catalyst. *Ind. Eng. Chem. Res.* **2016**, *55* (45), 11664–11671.

(83) Igarashi, A.; Ichikawa, N.; Sato, S.; Takahashi, R.; Sodesawa, T. Dehydration of Butanediols over CeO2 Catalysts with Different Particle Sizes. *Appl. Catal. A Gen.* **2006**, *300* (1), 50–57.

(84) Duan, H.; Yamada, Y.; Sato, S. Efficient Production of 1,3-Butadiene in the Catalytic Dehydration of 2,3-Butanediol. *Appl. Catal. A Gen.* **2015**, *491*, 163–169.

(85) Jacquin, M.; Pacheco, N.; Fauvarque-nuytten, C. Conversion of Butanediol into Butadiene, with Scrubbing Using Diesters. Google Patents May 30, 2019.

(86) *OECD-FAO Agricultural Outlook 2017-2026*; OECD-FAO Agricultural Outlook; OECD, 2017.

(87) Baeyens, J.; Kang, Q.; Appels, L.; Dewil, R.; Lv, Y.; Tan, T. Challenges and Opportunities in Improving the Production of Bio-Ethanol. *Prog. Energy Combust. Sci.* **2015**, *47*, 60–88.

(88) Logsdon, J. E. Ethanol. In *Kirk-Othmer Encyclopedia of Chemical Technology*; John

Wiley & Sons, Inc.: Hoboken, NJ, USA, 2004.

(89) Kosaric, N.; Duvnjak, Z.; Farkas, A.; Sahm, H.; Bringer-Meyer, S.; Goebel, O.; Mayer, D. Ethanol. In *Ullmann's Encyclopedia of Industrial Chemistry*; Wiley-VCH Verlag GmbH & Co. KGaA: Weinheim, Germany, 2011; pp 1–72.

(90) Cabello González, G. M.; Concepción, P.; Villanueva Perales, A. L.; Martínez, A.; Campoy, M.; Vidal-Barrero, F. Ethanol Conversion into 1,3-Butadiene over a Mixed Hf-Zn Catalyst: Effect of Reaction Conditions and Water Content in Ethanol. *Fuel Process. Technol.* **2019**, *193* (April), 263–272.

(91) https://www.intratec.us/ https://www.intratec.us/ (accessed Feb 1, 2018).

(92) OECD (2019), Crude oil import prices (indicator).

(93) Burla, J.; Fehnel, R.; Louie, P.; Terpeluk, P. *Two-Step Production of 1,3-Butadiene from Ethanol*; 2012.

(94) Farzad, S.; Mandegari, M. A.; Görgens, J. F. Integrated Techno-Economic and Environmental Analysis of Butadiene Production from Biomass. *Bioresour. Technol.* **2017**, *239*, 37–48.

(95) Tire Business Staff. Michelin in Bio-Butadiene Partnership. *Tire Business*. 2013.

(96) Makshina, E. V.; Janssens, W.; Sels, B. F.; Jacobs, P. A. Catalytic Study of the Conversion of Ethanol into 1,3-Butadiene. *Catal. Today* **2012**, *198* (1), 338–344.

(97) Shylesh, S.; Gokhale, A. A.; Scown, C. D.; Kim, D.; Ho, C. R.; Bell, A. T. From Sugars to Wheels: The Conversion of Ethanol to 1,3-Butadiene over Metal-Promoted Magnesia-Silicate Catalysts. *ChemSusChem* **2016**, *9* (12), 1462–1472.

(98) Van Speybroeck, V.; De Wispelaere, K.; Van der Mynsbrugge, J.; Vandichel, M.; Hemelsoet, K.; Waroquier, M. First Principle Chemical Kinetics in Zeolites: The Methanol-to-Olefin Process as a Case Study. *Chem. Soc. Rev.* **2014**, *43* (21), 7326–7357.

(99) Kapteijn, F.; Berger, R. J.; Moulijn, J. A. Macrokinetics and Transport Processes. *Handb. Heterog. Catal.* **2008**, *1*, 1693–1714.

(100) Chieregato, A.; Velasquez Ochoa, J.; Bandinelli, C.; Fornasari, G.; Cavani, F.; Mella, M. On the Chemistry of Ethanol on Basic Oxides: Revising Mechanisms and Intermediates in the Lebedev and Guerbet Reactions. *ChemSusChem* **2015**, *8* (2), 377–388.

(101) Gruver, V.; Sun, A.; Fripiat, J. J. Catalytic Properties of Aluminated Sepiolite in Ethanol Conversion. *Catal. Letters* **1995**, *34* (3–4), 359–364.

(102) Sushkevich, V. L.; Ivanova, I. I. Mechanistic Study of Ethanol Conversion into Butadiene over Silver Promoted Zirconia Catalysts. *Appl. Catal. B Environ.* **2017**, *215*, 36–49.

(103) Taifan, W. E.; Bučko, T.; Baltrusaitis, J. Catalytic Conversion of Ethanol to 1,3-Butadiene on MgO: A Comprehensive Mechanism Elucidation Using DFT Calculations. *J. Catal.* **2017**, *346*, 78–91.

(104) Müller, P.; Burt, S. P.; Love, A. M.; McDermott, W. P.; Wolf, P.; Hermans, I. Mechanistic Study on the Lewis Acid Catalyzed Synthesis of 1,3-Butadiene over Ta-BEA Using Modulated Operando DRIFTS-MS. *ACS Catal.* **2016**, *6* (10), 6823–6832.

(105) Santilli, D. S.; Gates, B. C. Hydrocarbon Reaction Mechanisms. In *Handbook of Heterogeneous Catalysis*; Wiley-VCH Verlag GmbH & Co. KGaA: Weinheim, Germany, 2008; pp 1624–1637.

(106) Pomalaza, G.; Vofo, G.; Capron, M.; Dumeignil, F. ZnTa-TUD-1 as an Easily Prepared, Highly Efficient Catalyst for the Selective Conversion of Ethanol to 1,3-Butadiene. *Green Chem.* **2018**, *20* (14), 3203–3209.

(107) Kolmogorov, A. N.; Tikhomirov, V. M.; Vinogradova, O. M.; Keier, N. P.; Roginskii, S. Z. An Investigation of the Mechanism Underlying the Production of Divinyl According to SV Lebedev with the Use of Radioactive Carbon. In *Dokl. Akad. Nauk SSSR*; 1957; Vol. 112, pp 1075–1078.

(108) Kagan, M. Y., Lyubarskii, G. D., Podurovskaya, O. M. Hydrocarbons. *Izv. Akad. Nauk SSSR, Ser. Khim. Nauk* **1947**, 173–181.

(109) Sushkevich, V. L.; Ivanova, I. I.; Ordomsky, V. V.; Taarning, E. Design of a Metal-Promoted Oxide Catalyst for the Selective Synthesis of Butadiene from Ethanol. *ChemSusChem* **2014**, 2527–2536.

(110) Cabello González, G. M.; Murciano, R.; Villanueva Perales, A. L.; Martínez, A.; Vidal-Barrero, F.; Campoy, M.; González, G. M. C.; Murciano, R.; Perales, A. L. V.; Martínez, A.; et al. Ethanol Conversion into 1,3-Butadiene over a Mixed Hf-Zn Catalyst: A Study of the Reaction Pathway and Catalyst Deactivation. *Appl. Catal. A Gen.* **2019**, *570* (July 2018), 96–106.

(111) Miller, J. H.; Bui, L.; Bhan, A. Pathways, Mechanisms, and Kinetics: A Strategy to Examine Byproduct Selectivity in Partial Oxidation Catalytic Transformations on Reducible Oxides. *React. Chem. Eng.* **2019**, *4* (5), 784–805.

(112) Pachousky, R. a.; Best, D. a.; Wojciechowski, B. W. Applications of the Time-on-Stream Theory of Catalyst Decay. *Ind. Eng. Chem. Process Des. Dev.* **1973**, *12* (3), 254–261.

(113) Lewandowski, M.; Babu, G. S.; Vezzoli, M.; Jones, M. D.; Owen, R. E.; Mattia, D.; Plucinski, P.; Mikolajska, E.; Ochenduszko, A.; Apperley, D. C. Investigations into the Conversion of Ethanol to 1,3-Butadiene Using MgO:SiO2 Supported Catalysts. *Catal. Commun.* **2014**, *49*, 25–28.

(114) Taifan, W.; Yan, G. X.; Baltrusaitis, J. Surface Chemistry of MgO/SiO2 Catalysts during the Ethanol Catalytic Conversion to 1,3-Butadiene: In Situ DRIFTS and DFT Study. *Catal. Sci. Technol.* **2017**.

(115) Takezawa, N.; Hanamaki, C.; Kobayashi, H. The Mechanism of Dehydrogenation of Ethanol on Magnesium Oxide. *J. Catal.* **1975**, *38* (1–3), 101–109.

(116) Díez, V. K.; Apesteguía, C. R.; Di Cosimo, J. I. Acid-Base Properties and Active Site Requirements for Elimination Reactions on Alkali-Promoted MgO Catalysts. *Catal. Today* **2000**, *63* (1), 53–62.

(117) Ho, C. R.; Shylesh, S.; Bell, A. T. Mechanism and Kinetics of Ethanol Coupling to Butanol over Hydroxyapatite. *ACS Catal.* **2016**, *6* (2), 939–948.

(118) Sushkevich, V. L.; Ivanova, I. I.; Taarning, E. Mechanistic Study of Ethanol Dehydrogenation over Silica-Supported Silver. *ChemCatChem* **2013**, *5* (8), 2367–2373.

(119) Di Cosimo, J. I.; Díez, V. K.; Xu, M.; Iglesia, E.; Apesteguía, C. R. Structure and Surface and Catalytic Properties of Mg-Al Basic Oxides. *J. Catal.* **1998**, *178* (2), 499–510.

(120) Wang, Z. T.; Xu, Y.; El-Soda, M.; Lucci, F. R.; Madix, R. J.; Friend, C. M.; Sykes, E. C. H. Surface Structure Dependence of the Dry Dehydrogenation of Alcohols on Cu(111) and Cu(110). *J. Phys. Chem. C* **2017**, *121* (23), 12800–12806.

(121) Chagas, L. H.; Matheus, C. R. V.; Zonetti, P. C.; Appel, L. G. Butadiene from Ethanol Employing Doped T-ZrO2. *Mol. Catal.* **2018**, *458* (August 2017), 272–279.

(122) Yan, T.; Dai, W.; Wu, G.; Lang, S.; Hunger, M.; Guan, N.; Li, L. Mechanistic Insights into One-Step Catalytic Conversion of Ethanol to Butadiene over Bifunctional Zn–Y/Beta Zeolite. *ACS Catal.* **2018**, *8* (iv), 2760–2773.

(123) Müller, P.; Wang, S.-C.; Burt, S. P.; Hermans, I. Influence of Metal Doping on the Lewis Acid Catalyzed Production of Butadiene from Ethanol Studied by Using Modulated Operando Diffuse Reflectance Infrared Fourier Transform Spectroscopy and Mass Spectrometry. *ChemCatChem* **2017**, *9* (18), 3572–3582.

(124) Kondo, J. N.; Ito, K.; Yoda, E.; Wakabayashi, F.; Domen, K. An Ethoxy Intermediate in Ethanol Dehydration on Brønsted Acid Sites in Zeolite. *J. Phys. Chem. B* **2005**, *109* (21), 10969–10972.

(125) Natal-Santiago, M. A.; Dumesic, J. A. Microcalorimetric, FTIR, and DFT Studies of the Adsorption of Methanol, Ethanol, and 2,2,2-Trifluoroethanol on Silica. *J. Catal.* **1998**, *175* (2), 252–268.

(126) Shimizu, K. I.; Sugino, K.; Sawabe, K.; Satsuma, A. Oxidant-Free Dehydrogenation of Alcohols Heterogeneously Catalyzed by Cooperation of Silver Clusters and Acid-Base Sites on Alumina. *Chem. - A Eur. J.* **2009**, *15* (10), 2341–2351.

(127) De Baerdemaeker, T.; Feyen, M.; Müller, U.; Yilmaz, B.; Xiao, F. S.; Zhang, W.; Yokoi, T.; Bao, X.; Gies, H.; De Vos, D. E. Bimetallic Zn and Hf on Silica Catalysts for the Conversion of Ethanol to 1,3-Butadiene. *ACS Catal.* **2015**, *5* (6), 3393–3397.

(128) Taifan, W. E.; Baltrusaitis, J. In Situ Spectroscopic Insights on the Molecular Structure of the MgO/SiO 2 Catalytic Active Sites during Ethanol Conversion to 1,3-Butadiene. *J. Phys. Chem. C* **2018**, *122* (36), 20894–20906.

(129) Gao, M.; Liu, Z.; Zhang, M.; Tong, L. Study on the Mechanism of Butadiene Formation from Ethanol. *Catal. Letters* **2014**, *144* (12), 2071–2079.

(130) Hattori, T.; Murakami, Y. Study on the Pulse Reaction Technique I. Theoretical Study. *J. Catal.* **1968**, *10* (2), 114–122.

(131) Yan, T.; Yang, L.; Dai, W.; Wang, C.; Wu, G.; Guan, N.; Hunger, M.; Li, L. On the Deactivation Mechanism of Zeolite Catalyst in Ethanol to Butadiene Conversion. *J. Catal.* **2018**, *367*, 7–15.

(132) Lewis, J. D.; Van De Vyver, S.; Román-Leshkov, Y. Acid-Base Pairs in Lewis Acidic Zeolites Promote Direct Aldol Reactions by Soft Enolization. *Angew. Chemie - Int. Ed.* **2015**, *54* (34), 9835–9838.

(133) Palagin, D.; Sushkevich, V. L.; Ivanova, I. I. C-C Coupling Catalyzed by Zeolites: Is Enolization the Only Possible Pathway for Aldol Condensation? *J. Phys. Chem. C* **2016**,

120 (41), 23566–23575.

(134) Sushkevich, V. L.; Palagin, D.; Ivanova, I. I. With Open Arms: Open Sites of ZrBEA Zeolite Facilitate Selective Synthesis of Butadiene from Ethanol. *ACS Catal.* **2015**, *5* (8), 4833–4836.

(135) Young, Z. D.; Hanspal, S.; Davis, R. J. Aldol Condensation of Acetaldehyde over Titania, Hydroxyapatite, and Magnesia. *ACS Catal.* **2016**, *6* (5), 3193–3202.

(136) Hernández-Giménez, A. M.; Ruiz-Martínez, J.; Puértolas, B.; Pérez-Ramírez, J.; Bruijnincx, P. C. A.; Weckhuysen, B. M. Operando Spectroscopy of the Gas-Phase Aldol Condensation of Propanal over Solid Base Catalysts. *Top. Catal.* **2017**, *60* (19–20), 1522–1536.

(137) Puértolas, B.; Keller, T. C.; Mitchell, S.; Pérez-Ramírez, J. Deoxygenation of Bio-Oil over Solid Base Catalysts: From Model to Realistic Feeds. *Appl. Catal. B Environ.* **2016**, *184*, 77–86.

(138) Fan, D.; Dong, X.; Yu, Y.; Zhang, M. A DFT Study on Aldol Condensation Reaction on MgO in the Process of Ethanol to 1,3-Butadiene: Understanding the Structure-Activity Relationship. *Phys. Chem. Chem. Phys.* **2017**, *19*, 25671–25682.

(139) Dong, X.; Lu, J.; Yu, Y.; Zhang, M. A DFT Study on Zr-SBA-15 Catalyzed Conversion of Ethanol to 1,3-Butadiene. *Phys. Chem. Chem. Phys.* **2018**, *20* (18), 12970–12978.

(140) Zhang, M.; Zhuang, J.; Yu, Y. Applied Surface Science A DFT Study on ZrO 2 Surface in the Process of Ethanol to 1 , 3-Butadiene : A Comprehensive Mechanism Elucidation. **2018**, *458* (July), 1026–1034.

(141) Tamura, M.; Tokonami, K.; Nakagawa, Y.; Tomishige, K. Selective Hydrogenation of Crotonaldehyde to Crotyl Alcohol over Metal Oxide Modified Ir Catalysts and Mechanistic Insight. *ACS Catal.* **2016**, *6* (6), 3600–3609.

(142) Bhattacharyya, S. K.; Sanyal, S. k. Kinetic Study on the Mechanism of the Catalytic Conversion of Ethanol to Butadiene. *J. Catal.* **1967**, *7* (2), 152–158.

(143) Niiyama, H.; Morii, S.; Echigoya, E. Butadiene Formation from Ethanol over Silica-Magnesia Catalysts. *Bull. Chem. Soc. Jpn.* **1972**, *45* (3), 655–659.

(144) Hayashi, Y.; Akiyama, S.; Miyaji, A.; Sekiguchi, Y.; Sakamoto, Y.; Shiga, A.; Koyama, T.; Motokura, K.; Baba, T. Experimental and Computational Studies of the Roles of MgO and Zn in Talc for the Selective Formation of 1,3-Butadiene in the Conversion of Ethanol. *Phys. Chem. Chem. Phys.* **2016**, *18* (36), 25191–25209.

(145) Natta, G.; Rigamonti, R. Sintesi Del Butadiene Da Alcool Etilico. Considerazioni Termodinamiche e Comportamento Specifico Dei Catalizzatori. *Chim. Ind.* 1947, pp 195–200.

(146) Corma, A.; Domine, M. E.; Valencia, S. Water-Resistant Solid Lewis Acid Catalysts: Meerwein-Ponndorf-Verley and Oppenauer Reactions Catalyzed by Tin-Beta Zeolite. *J. Catal.* **2003**, *215* (2), 294–304.

(147) Plessers, E.; Fu, G.; Tan, C.; De Vos, D.; Roeffaers, M. Zr-Based MOF-808 as Meerwein–Ponndorf–Verley Reduction Catalyst for Challenging Carbonyl Compounds. *Catalysts* **2016**, *6* (7), 104.

(148) Jiménez-Sanchidrián, C.; Ruiz, J. R. Tin-Containing Hydrotalcite-like Compounds as Catalysts for the Meerwein-Ponndorf-Verley Reaction. *Appl. Catal. A Gen.* **2014**, *469*, 367–372.

(149) Miyaji, A.; Hiza, M.; Sekiguchi, Y.; Akiyama, S.; Shiga, A.; Baba, T.; Paper, R. Catalysis by MgO and the Role of Zn^{2+} in Talc Catalysts for the Selective Production of 1,3-Butadiene from Ethanol. *J. Japan Pet. Inst.* **2018**, *61* (3), 171–181.

(150) Akiyama, S.; Miyaji, A.; Hayashi, Y.; Hiza, M.; Sekiguchi, Y.; Koyama, T. ru; Shiga, A.; Baba, T. Selective Conversion of Ethanol to 1,3-Butadiene Using Germanium Talc as Catalyst. *J. Catal.* **2018**, *359*, 184–197.

(151) Centers, B.; Property, A. 3 Acid and Base Centers: Structure and Acid-Base Property. In *Studies in Surface Science and Catalysis*; 1989; Vol. 51, pp 27–213.

(152) Ono, Y.; Baba, T. Unique Properties of Silver Cations in Solid-Acid Catalysis by Zeolites and Heteropolyacids. *Phys. Chem. Chem. Phys.* **2015**, *17* (24), 15637–15654.

(153) Kiss, J.; Witt, A.; Meyer, B.; Marx, D. Methanol Synthesis on ZnO (000 1̄). I. Hydrogen Coverage, Charge State of Oxygen Vacancies, and Chemical Reactivity. *J. Chem. Phys.* **2009**, *130* (18).

(154) Aleksandrov, H. A.; Vayssilov, G. N.; Rösch, N. Heterolytic Dissociation and Recombination of H2 over Zn,H-ZSM-5 Zeolites-A Density Functional Model Study. *J. Mol. Catal. A Chem.* **2006**, *256* (1–2), 149–155.

(155) Boronat, M.; Corma, A.; Renz, M. Mechanism of the Meerwein - Ponndorf - Verley - Oppenauer (MPVO) Redox Equilibrium on Sn- and Zr - Beta Zeolite Catalysts. *J. Phys. Chem. B* **2006**, *110* (42), 21168–21174.

(156) Balandin, A. A. No Title. *Zh. Fiz. Khim.* **1935**, *6*, 357.

(157) Velasquez Ochoa, J.; Bandinelli, C.; Vozniuk, O.; Chieregato, A.; Malmusi, A.; Recchi, C.; Cavani, F. An Analysis of the Chemical, Physical and Reactivity Features of MgO-SiO2 Catalysts for Butadiene Synthesis with the Lebedev Process. *Green Chem.* **2015**.

(158) Ezinkwo, G. O.; Tretjakov, V. F.; Talyshinky, R. M.; Ilolov, A. M.; Mutombo, T. A. Creation of a Continuous Process for Bio-Ethanol to Butadiene Conversion via the Use of a Process Initiator. *Catal. Commun.* **2014**, *43*, 207–212.

(159) Tret'yakov, V. F.; Talyshinskii, R. M.; Ilolov, A. M.; Maksimov, A. L.; Khadzhiev, S. N. Initiated Conversion of Ethanol to Divinyl by the Lebedev Reaction. *Pet. Chem.* **2014**, *54* (3), 195–206.

(160) Da Ros, S.; Jones, M. D.; Mattia, D.; Schwaab, M.; Noronha, F. B.; Pinto, J. C. Modelling the Effects of Reaction Temperature and Flow Rate on the Conversion of Ethanol to 1,3-Butadiene. *Appl. Catal. A Gen.* **2017**, *530*, 37–47.

(161) Tripathi, A.; Faungnawakij, K.; Laobuthee, A.; Assabumrungrat, S.; Laosiripojna, N. Catalytic Activity of Bimetallic Cu-Ag/MgO-SiO2 toward the Conversion of Ethanol to 1,3-Butadiene. *Int. J. Chem. React. Eng.* **2016**, *14* (5), 945–954.

(162) Kyriienko, P. I.; Larina, O. V.; Soloviev, S. O.; Orlyk, S. M.; Calers, C.; Dzwigaj, S. Ethanol Conversion into 1,3-Butadiene by the Lebedev Method over MTaSiBEA Zeolites (M = Ag, Cu, Zn). *ACS Sustain. Chem. Eng.* **2017**, *5* (3), 2075–2083.

(163) Janssens, W.; Makshina, E. V.; Vanelderen, P.; De Clippel, F.; Houthoofd, K.; Kerkhofs, S.; Martens, J. A.; Jacobs, P. A.; Sels, B. F. Ternary Ag/MgO-SiO2 Catalysts for the Conversion of Ethanol into Butadiene. *ChemSusChem* **2015**, *8* (6), 994–1008.

(164) Zhu, Q.; Wang, B.; Tan, T. Conversion of Ethanol and Acetaldehyde to Butadiene over MgO–SiO $_2$ Catalysts: Effect of Reaction Parameters and Interaction between MgO and SiO $_2$ on Catalytic Performance. *ACS Sustain. Chem. Eng.* **2017**, *5* (1), 722–733.

(165) Bhattacharyya, S. K.; Avasthi, B. N. One-Step Catalytic Conversion of Ethanol to Butadiene in a Fluidized Bed. *Ind. Eng. Chem. Process Des. Dev.* **1963**, *2* (1), 45–51.

(166) Da Ros, S.; Jones, M. D.; Mattia, D.; Schwaab, M.; Barbosa-Coutinho, E.; Rabelo-Neto, R. C.; Bellot Noronha, F.; Carlos Pinto, J. Microkinetic Analysis of Ethanol to 1,3-Butadiene Reactions over MgO-SiO2 Catalysts Based on Characterization of Experimental Fluctuations. *Chem. Eng. J.* **2016**, *308*, 988–1000.

(167) Han, Z.; Li, X.; Zhang, M.; Liu, Z.; Gao, M. Sol–Gel Synthesis of ZrO 2 –SiO 2 Catalysts for the Transformation of Bioethanol and Acetaldehyde into 1,3-Butadiene. *RSC Adv.* **2015**, *5* (126), 103982–103988.

(168) Zhang, M.; Tan, X.; Zhang, T.; Han, Z.; Jiang, H. The Deactivation of a ZnO Doped ZrO 2 –SiO 2 Catalyst in the Conversion of Ethanol/Acetaldehyde to 1,3-Butadiene. *RSC Adv.* **2018**, *8* (59), 34069–34077.

(169) Bartholomew, C. H. Mechanisms of Catalyst Deactivation. *Appl. Catal. A Gen.* **2001**, *212* (1–2), 17–60.

(170) Moulijn, J. A.; van Diepen, A. E.; Kapteijn, F. Deactivation and Regeneration. In *Handbook of Heterogeneous Catalysis*; Wiley-VCH Verlag GmbH & Co. KGaA: Weinheim, Germany, 2008.

(171) MacHado, N. R. C. F.; Calsavara, V.; Astrath, N. G. C.; Matsuda, C. K.; Paesano, A.; Baesso, M. L. Obtaining Hydrocarbons from Ethanol over Iron-Modified ZSM-5 Zeolites. *Fuel* **2005**, *84* (16), 2064–2070.

(172) Johansson, R.; Hruby, S. L.; Rass-Hansen, J.; Christensen, C. H. The Hydrocarbon Pool in Ethanol-to-Gasoline over HZSM-5 Catalysts. *Catal. Letters* **2009**, *127* (1–2), 1–6.

(173) Van der Borght, K.; Batchu, R.; Galvita, V. V.; Alexopoulos, K.; Reyniers, M. F.; Thybaut, J. W.; Marin, G. B. Insights into the Reaction Mechanism of Ethanol Conversion into Hydrocarbons on H-ZSM-5. *Angew. Chemie - Int. Ed.* **2016**, *55* (41), 12817–12821.

(174) Kim, T. W.; Kim, J. W.; Kim, S. Y.; Chae, H. J.; Kim, J. R.; Jeong, S. Y.; Kim, C. U. Butadiene Production from Bioethanol and Acetaldehyde over Tantalum Oxide-Supported Spherical Silica Catalysts for Circulating Fluidized Bed. *Chem. Eng. J.* **2014**, *278*, 217–223.

(175) Kyriienko, P. I.; Larina, O. V.; Soloviev, S. O.; Orlyk, S. M.; Dzwigaj, S. High Selectivity of TaSiBEA Zeolite Catalysts in 1,3-Butadiene Production from Ethanol and Acetaldehyde Mixture. *CATCOM* **2016**, *77*, 123–126.

(176) Patil, P. T.; Liu, D.; Liu, Y.; Chang, J.; Borgna, A. Improving 1,3-Butadiene Yield by Cs Promotion in Ethanol Conversion. *Appl. Catal. A Gen.* **2017**, *543* (January), 67–74.

(177) Klein, A.; Palkovits, R. Influence of Structural Parameters on the Conversion of Ethanol

into 1,3-Butadiene Using Mesoporous Zeolites. *Catal. Commun.* **2016**, *91*, 72–75.

(178) Angelici, C.; Velthoen, M. E. Z.; Weckhuysen, B. M.; Bruijnincx, P. C. A. Influence of Acid–Base Properties on the Lebedev Ethanol-to-Butadiene Process Catalyzed by SiO2–MgO Materials. *Catal. Sci. Technol.* **2015**, *5* (5), 2869–2879.

(179) Sushkevich, V. L.; Ivanova, I. I.; Taarning, E. Ethanol Conversion into Butadiene over Zr-Containing Molecular Sieves Doped with Silver. *Green Chem.* **2015**, *17* (4), 2552–2559.

(180) Dagle, V. L.; Flake, M. D.; Lemmon, T. L.; Lopez, J. S.; Kovarik, L.; Dagle, R. A. Effect of the SiO 2 Support on the Catalytic Performance of Ag/ZrO 2 /SiO 2 Catalysts for the Single-Bed Production of Butadiene from Ethanol. *Appl. Catal. B Environ.* **2018**, *236* (May), 576–587.

(181) Chen, D.; Moljord, K.; Fuglerud, T.; Holmen, A. The Effect of Crystal Size of SAPO-34 on the Selectivity and Deactivation of the MTO Reaction. *Microporous Mesoporous Mater.* **1999**, *29* (1–2), 191–203.

(182) Janssens, T. V. W. A New Approach to the Modeling of Deactivation in the Conversion of Methanol on Zeolite Catalysts. *J. Catal.* **2009**, *264* (2), 130–137.

(183) Müller, S.; Liu, Y.; Vishnuvarthan, M.; Sun, X.; Van Veen, A. C.; Haller, G. L.; Sanchez-Sanchez, M.; Lercher, J. A. Coke Formation and Deactivation Pathways on H-ZSM-5 in the Conversion of Methanol to Olefins. *J. Catal.* **2015**, *325*, 48–59.

(184) Dai, W.; Zhang, S.; Yu, Z.; Yan, T.; Wu, G.; Guan, N.; Li, L. Zeolite Structural Confinement Effects Enhance One-Pot Catalytic Conversion of Ethanol to Butadiene. *ACS Catal.* **2017**, *7* (5), 3703–3706.

(185) Huang, X.; Men, Y.; Wang, J.; An, W.; Wang, Y. Highly Active and Selective Binary MgO–SiO 2 Catalysts for the Production of 1,3-Butadiene from Ethanol. *Catal. Sci. Technol.* **2017**, *7* (1), 168–180.

(186) Qian, Q.; Ruiz-martínez, J.; Mokhtar, M.; Asiri, A. M.; Al-thabaiti, S. A.; Basahel, S. N.; Weckhuysen, B. M. Single-Catalyst Particle Spectroscopy of Alcohol-to-Olefins Conversions : Comparison between SAPO-34 and SSZ-13. *Catal. Today* **2014**, *226*, 14–24.

(187) Ferreira Madeira, F.; Ben Tayeb, K.; Pinard, L.; Vezin, H.; Maury, S.; Cadran, N. Ethanol Transformation into Hydrocarbons on ZSM-5 Zeolites: Influence of Si/Al Ratio on Catalytic Performances and Deactivation Rate. Study of the Radical Species Role. *Appl. Catal. A Gen.* **2012**, *443–444*, 171–180.

(188) Madeira, F. F.; Gnep, N. S.; Magnoux, P.; Maury, S.; Cadran, N. Ethanol Transformation over HFAU , HBEA and HMFI Zeolites Presenting Similar Brønsted Acidity. **2009**, *367*, 39–46.

(189) Qian, Q.; Ruiz-martínez, J.; Mokhtar, M.; Asiri, A. M.; Al-thabaiti, S. A.; Basahel, S. N.; Weckhuysen, B. M. Single-Catalyst Particle Spectroscopy of Alcohol-to-Olefins Conversions : Comparison between SAPO-34 and SSZ-13. *Catal. Today* **2014**, *226*, 14–24.

(190) Taifan, W. E.; Li, Y.; Baltrus, J. P.; Zhang, L.; Frenkel, A. I.; Baltrusaitis, J. Operando Structure Determination of Cu and Zn on Supported MgO/SiO 2 Catalysts during Ethanol Conversion to 1,3-Butadiene. *ACS Catal.* **2019**, *9* (1), 269–285.

(191) Zhang, M.; Yu, Y. Dehydration of Ethanol to Ethylene. *Ind. Eng. Chem. Res.* **2013**, *52*

(28), 9505–9514.

(192) Phung, T. K.; Busca, G. Diethyl Ether Cracking and Ethanol Dehydration: Acid Catalysis and Reaction Paths. *Chem. Eng. J.* **2015**, *272*, 92–101.

(193) Phillips, C. B.; Datta, R. Production of Ethylene from Hydrous Ethanol on H-ZSM-5 under Mild Conditions. *Ind. Eng. Chem. Res.* **1997**, *36* (11), 4466–4475.

(194) Ouyang, J.; Kong, F.; Su, G.; Hu, Y.; Song, Q. Catalytic Conversion of Bio-Ethanol to Ethylene over La-Modified HZSM-5 Catalysts in a Bioreactor. *Catal. Letters* **2009**, *132* (1–2), 64–74.

(195) Le Van Mao, R.; Nguyen, T. M.; Yao, J. Conversion of Ethanol in Aqueous Solution over ZSM-5 Zeolites. *Appl. Catal.* **1990**, *61* (1), 161–173.

(196) Baylon, R. A. L.; Sun, J.; Wang, Y. Conversion of Ethanol to 1,3-Butadiene over Na Doped ZnxZryOz Mixed Metal Oxides. *Catal. Today* **2014**, *259*, 446–452.

(197) Da Ros, S.; Jones, M. D.; Mattia, D.; Pinto, J. C.; Schwaab, M.; Noronha, F. B.; Kondrat, S. A.; Clarke, T. C.; Taylor, S. H. Ethanol to 1,3-Butadiene Conversion by Using ZrZn-Containing MgO/SiO 2 Systems Prepared by Co-Precipitation and Effect of Catalyst Acidity Modification. *ChemCatChem* **2016**, *8* (14), 2376–2386.

(198) Benito, M.; Sanz, J. L.; Isabel, R.; Padilla, R.; Arjona, R.; Daza, L. Bio-Ethanol Steam Reforming: Insights on the Mechanism for Hydrogen Production. *J. Power Sources* **2005**, *151* (1–2), 11–17.

(199) Mattos, L. V.; Jacobs, G.; Davis, B. H.; Noronha, F. B. Production of Hydrogen from Ethanol: Review of Reaction Mechanism and Catalyst Deactivation. *Chem. Rev.* **2012**, *112* (7), 4094–4123.

(200) Cavallaro, S. Ethanol Steam Reforming on Rh/Al 2 O 3 Catalysts. *Energy & Fuels* **2000**, *14* (6), 1195–1199.

(201) Gines, M. J. L.; Iglesia, E. Bifunctional Condensation Reactions of Alcohols on Basic Oxides Modified by Copper and Potassium. *J. Catal.* **1998**, *176* (1), 155–172.

(202) Kozlowski, J. T.; Davis, R. J. Heterogeneous Catalysts for the Guerbet Coupling of Alcohols. *ACS Catal.* **2013**, *3* (7), 1588–1600.

(203) Jones, H. E.; Stahly, E. E.; Corson, B. B. Butadiene from Ethanol. Reaction Mechanism. *J. Am. Chem. Soc.* **1949**, *71* (5), 1822–1828.

(204) Silvester, L.; Lamonier, J.-F.; Faye, J.; Capron, M.; Vannier, R.-N.; Lamonier, C.; Dubois, J.-L.; Couturier, J.-L.; Calais, C.; Dumeignil, F. Reactivity of Ethanol over Hydroxyapatite-Based Ca-Enriched Catalysts with Various Carbonate Contents. *Catal. Sci. Technol.* **2015**, *5* (5), 2994–3006.

(205) Bhattacharyya, S. K.; Ganguly, N. D. One-Step Catalytic Conversion of Ethanol to Butadiene in the Fixed Bed. I. Single-Oxide Catalysts. *J. Appl. Chem.* **1962**, *12* (3), 97–104.

(206) Toussaint, J.; Charleston, S.; Dunn, T.; War, W.; Toussaint, W. J.; Dunn, J. T. Process for Making Diolefins. US 2,421,361, May 1947.

(207) Kyriienko, P. I.; Larina, O. V.; Popovych, N. O.; Soloviev, S. O.; Millot, Y.; Dzwigaj, S.

Effect of the Niobium State on the Properties of NbSiBEA as Bifunctional Catalysts for Gas- and Liquid-Phase Tandem Processes. *J. Mol. Catal. A Chem.* **2016**, *424*, 27–36.

(208) Ordomsky, V. V.; Sushkevich, V. L.; Ivanova, I. I. Study of Acetaldehyde Condensation Chemistry over Magnesia and Zirconia Supported on Silica. *J. Mol. Catal. A Chem.* **2010**, *333* (1–2), 85–93.

(209) Sushkevich, V. L.; Ivanova, I. I.; Tolborg, S.; Taarning, E. Meerwein-Ponndorf-Verley-Oppenauer Reaction of Crotonaldehyde with Ethanol over Zr-Containing Catalysts. *J. Catal.* **2014**, *316*, 121–129.

(210) Trejda, M.; Wojtaszek, A.; Floch, A.; Wojcieszak, R.; Gaigneaux, E. M.; Ziolek, M. New Nb and Ta-FAU Zeolites - Direct Synthesis, Characterisation and Surface Properties. *Catal. Today* **2010**, *158* (1–2), 170–177.

(211) Wang, Y.; Lewis, J. D.; Roman-Leshkov, Y. Synthesis of Itaconic Acid Ester Analogues via Self-Aldol Condensation of Ethyl Pyruvate Catalyzed by Hafnium BEA Zeolites. *ACS Catal.* **2016**, *6* (5), 2739–2744.

(212) Dzwigaj, S.; Millot, Y.; Che, M. Ta(V)-Single Site BEA Zeolite by Two-Step Postsynthesis Method: Preparation and Characterization. *Catal. Letters* **2010**, *135* (3–4), 169–174.

(213) Ushikubo, T. Recent Topics of Research and Development of Catalysis by Niobium and Tantalum Oxides. *Catal. Today* **2000**, *57* (3–4), 331–338.

(214) Luo, H. Y.; Lewis, J. D.; Román-Leshkov, Y. Lewis Acid Zeolites for Biomass Conversion: Perspectives and Challenges on Reactivity, Synthesis, and Stability. *Annu. Rev. Chem. Biomol. Eng.* **2016**, *7* (1), 663–692.

(215) Corma, A.; Llabrés i Xamena, F. X.; Prestipino, C.; Renz, M.; Valencia, S. Water Resistant, Catalytically Active Nb and Ta Isolated Lewis Acid Sites, Homogeneously Distributed by Direct Synthesis in a Beta Zeolite. *J. Phys. Chem. C* **2009**, *113* (26), 11306–11315.

(216) Gunther, W. R.; Michaelis, V. K.; Griffin, R. G.; Roman-Leshkov, Y. Interrogating the Lewis Acidity of Metal Sites in Beta Zeolites with 15N Pyridine Adsorption Coupled with MAS NMR Spectroscopy. *J. Phys. Chem. C* **2016**, *120* (50), 28533–28544.

(217) Boronat, M.; Corma, A.; Renz, M.; Viruela, P. M. Predicting the Activity of Single Isolated Lewis Acid Sites in Solid Catalysts. *Chem. - A Eur. J.* **2006**, *12* (27), 7067–7077.

(218) Sushkevich, V. L.; Vimont, A.; Travert, A.; Ivanova, I. I. Spectroscopic Evidence for Open and Closed Lewis Acid Sites in ZrBEA Zeolites Spectroscopic Evidence for Open and Closed Lewis Acid Sites in ZrBEA Zeolites. *J. Phys. Chem. C* **2015**, *119* (31), 17633–17639.

(219) Sushkevich, V. L.; Ivanova, I. I. Ag-Promoted ZrBEA Zeolites Obtained by Post-Synthetic Modification for Conversion of Ethanol to Butadiene. *ChemSusChem* **2016**, *9* (16), 2216–2225.

(220) Harris, J. W.; Cordon, M. J.; Iorio, J. R. Di; Vega-vila, J. C.; Ribeiro, F. H.; Gounder, R. Titration and Quantification of Open and Closed Lewis Acid Sites in Sn-Beta Zeolites That Catalyze Glucose Isomerization. *J. Catal.* **2016**, *335*, 141–154.

(221) Jehng, J.-M.; Wachs, I. E. Molecular Structures of Supported Niobium Oxide Catalysts under Ambient Conditions. *J. Mol. Catal.* **1991**, *67* (3), 369–387.

(222) Braga, V. S.; Dias, J. a; Dias, S. C. L.; De Macedo, J. L. Catalyst Materials Based on Nb 2 O 5 Supported on SiO 2 −Al 2 O 3 : Preparation and Structural Characterization. *Chem. Mater.* **2005**, *17* (3), 690–695.

(223) Baltes, M.; Kytökivi, A.; Weckhuysen, B. M.; Schoonheydt, R. A.; Van Der Voort, P.; Vansant, E. F.; Kyto, A.; Weckhuysen, B. M.; Schoonheydt, R. A.; Voort, P. Van Der; et al. Supported Tantalum Oxide and Supported Vanadia-Tantala Mixed Oxides: Structural Characterization and Surface Properties. *J. Phys. Chem. B* **2001**, *105* (26), 6211–6220.

(224) Burke, P. A.; Ko, E. I. Acidic Properties of Oxides Containing Niobia on Silica and Niobia in Silica. *J. Catal.* **1991**, *129* (1), 38–46.

(225) Tanabe, K.; Okazaki, S. Various Reactions Catalyzed by Niobium Compounds and Materials. *Appl. Catal. A, Gen.* **1995**, *133* (2), 191–218.

(226) Li, L.; Cani, D.; Pescarmona, P. P. Metal-Containing TUD-1 Mesoporous Silicates as Versatile Solid Acid Catalysts for the Conversion of Bio-Based Compounds into Valuable Chemicals. *Inorganica Chim. Acta* **2015**, *431*, 289–296.

(227) Kurmach, M. M.; Larina, O. V.; Kyriienko, P. I.; Yaremov, P. S.; Trachevsky, V. V.; Shvets, O. V.; Soloviev, S. O. Hierarchical Zr-MTW Zeolites Doped with Copper as Catalysts of Ethanol Conversion into 1,3-Butadiene. *ChemistrySelect* **2018**, *3* (29), 8539–8546.

(228) Chen, Y.; Fierro, J. L. G.; Tanaka, T.; Wachs, I. E. Supported Tantalum Oxide Catalysts: Synthesis, Physical Characterization, and Methanol Oxidation Chemical Probe Reaction. *J. Phys. Chem. B* **2003**, *107* (22), 5243–5250.

(229) Hattori, H. Heterogeneous Basic Catalysis. *Chem. Rev.* **1995**, *95* (3), 537–558.

(230) Cadran, N.; Chaumonnot, A. Ta-Nb Catalyst for the Production of 1,3-Butadiene. WO2017009108 A1, 2017.

(231) Larina, O. V.; Kyriienko, P. I.; Soloviev, S. O. Effect of Lanthanum in Zn-La(-Zr)-Si Oxide Compositions on Their Activity in the Conversion of Ethanol into 1,3-Butadiene. *Theor. Exp. Chem.* **2016**, *52* (1), 51–56.

(232) Larina, O. V.; Kyriienko, P. I.; Soloviev, S. O. Ethanol Conversion to 1,3-Butadiene on ZnO/MgO-SiO2 Catalysts: Effect of ZnO Content and MgO:SiO2 Ratio. *Catal. Letters* **2015**, *145* (5), 1162–1168.

(233) Marceau, E.; Carrier, X.; Che, M.; Clause, O.; Marcilly, C. Ion Exchange and Impregnation. *Handb. Heterog. Catal.* **2008**.

(234) Sushkevich, V. L.; Ivanova, I. I.; Taarning, E. Ethanol Conversion into Butadiene over Zr-Containing Molecular Sieves Doped with Silver. *Green Chem.* **2015**, *17* (4), 2552–2559.

(235) Olsbye, U.; Svelle, S.; Bjørgen, M.; Beato, P.; Janssens, T. V. W.; Joensen, F.; Bordiga, S.; Lillerud, K. P. Conversion of Methanol to Hydrocarbons : How Zeolite Cavity and Pore Size Controls Product Selectivity Angewandte. **2012**, 5810–5831.

(236) Boronat, M.; Concepción, P.; Corma, A.; Navarro, M. T.; Renz, M.; Valencia, S.

Reactivity in the Confined Spaces of Zeolites: The Interplay between Spectroscopy and Theory to Develop Structure–Activity Relationships for Catalysis. *Phys. Chem. Chem. Phys.* **2009**, *11* (16), 2876.

(237) Higgins, S.; DeSisto, W.; Ruthven, D. Diffusive Transport through Mesoporous Silica Membranes. *Microporous Mesoporous Mater.* **2009**, *117* (1–2), 268–277.

(238) Lari, G. M.; Dapsens, P. Y.; Scholz, D.; Mitchell, S.; Mondelli, C.; Pérez-Ramírez, J. Deactivation Mechanisms of Tin-Zeolites in Biomass Conversions. *Green Chem.* **2016**, *18* (5), 1249–1260.

(239) Larlus, O.; Valtchev, V. P. Control of the Morphology of All-Silica BEA-Type Zeolite Synthesized in Basic Media. *Chem. Mater.* **2005**, *17* (4), 881–886.

(240) Larlus, O.; Valtchev, V. Synthesis of All-Silica BEA-Type Material in Basic Media. *Microporous Mesoporous Mater.* **2006**, *93* (1–3), 55–61.

(241) Bourgeat-Lami, E.; Fajula, F.; Anglerot, D.; Couriers, T. Single-Step Dealumination of Zeolite-Beta Precursors for the Preparation of Hydrophobic Adsorbents. *Microporus Mater.* **1993**, *1* (4), 237–245.

(242) Dzwigaj, S.; Peltre, M. J.; Massiani, P.; Davidson, A.; Che, M.; Sen, T.; Sivasanker, S.; Mas, S. Incorporation of Vanadium Species in a Dealuminated b Zeolite. *Chem. Commun.* **1998**, No. 1, 87–88.

(243) Wang, C.; Zheng, M.; Li, X.; Li, X.; Zhang, T. Catalytic Conversion of Ethanol into Butadiene over High Performance LiZnHf-MFI Zeolite Nanosheets. *Green Chem.* **2019**, *21* (5), 1006–1010.

(244) Rouquerol, J.; Avnir, D.; Fairbridge, C. W.; Everett, D. H.; Haynes, J. M.; Pernicone, N.; Ramsay, J. D. F.; Sing, K. S. W.; Unger, K. K. Recommendations for the Characterization of Porous Solids (Technical Report). *Pure Appl. Chem.* **1994**, *66* (8), 1739–1758.

(245) Zhao, D.; Zhang, F.; Tu, B.; Yang, H.; Yu, C.; Yan, Y.; Meng, Y. Understanding Effect of Wall Structure on the Hydrothermal Stability of Mesostructured Silica SBA-15. *J. Phys. Chem. B* **2005**, *109* (18), 8723–8732.

(246) Xu, Y.; Liu, Z.; Han, Z.; Zhang, M. Ethanol/Acetaldehyde Conversion into Butadiene over Sol–Gel ZrO 2 –SiO 2 Catalysts Doped with ZnO. *RSC Adv.* **2017**, *7* (12), 7140–7149.

(247) GOLDWASSER, J. Studies of Acid-Base-Catalyzed Reactions XIV. Isomerization of Butene over La2O3 and ZnO. *J. Catal.* **1981**, *71* (1), 53–63.

(248) Ribeiro, F. H.; Von Wittenau, A. E. S.; Bartholomew, C. H.; Somorjai, G. A. Reproducibility of Turnover Rates in Heterogeneous Metal Catalysis: Compilation of Data and Guidelines for Data Analysis. *Catal. Rev. - Sci. Eng.* **1997**, *39* (1–2), 49–76.

(249) Cadran, N.; Chaumonnot, A. CATALYST Ta-Nb FOR THE PRODUCTION OF 1, 3-BUTADIENE. US20180200696A1, July 19, 2018.

(250) Szukiewicz, W. Method for Producing Butadiene, September 12, 1944.

(251) Natta, G.; Rigamonti, R. Studio Roentgenografico e Chimico Dei Catalizzatori Usati per La Produzione Del Butadiene Dall'alcool. *Chim. Ind.* 1947, pp 239–243.

(252) Sergei Vasiljevich Lebedev. FR 665917. FR 665917, 1929.

(253) Sergei Vasiljevich Lebedev. GB 331482. GB 331482, 1930.

(254) Angelici, C.; Velthoen, M. E. Z.; Weckhuysen, B. M.; Bruijnincx, P. C. A. Effect of Preparation Method and CuO Promotion in the Conversion of Ethanol into 1,3-Butadiene over SiO 2 -MgO Catalysts. *ChemSusChem* **2014**, *7* (9), 2505–2515.

(255) Kvisle, S.; Aguero, A.; Sneeden, R. P. A. Transformation of Ethanol into 1,3-Butadiene over Magnesium Oxide/Silica Catalysts. *Appl. Catal.* **1988**, *43* (1), 117–131.

(256) Hanspal, S.; Young, Z. D.; Shou, H.; Davis, R. J. Multiproduct Steady-State Isotopic Transient Kinetic Analysis of the Ethanol Coupling Reaction over Hydroxyapatite and Magnesia. *ACS Catal.* **2015**, *5* (3), 1737–1746.

(257) Chung, S.-H.; Angelici, C.; Hinterding, S. O. M.; Weingarth, M.; Baldus, M.; Houben, K.; Weckhuysen, B. M.; Bruijnincx, P. C. A. Role of Magnesium Silicates in Wet-Kneaded Silica–Magnesia Catalysts for the Lebedev Ethanol-to-Butadiene Process. *ACS Catal.* **2016**, *6* (6), 4034–4045.

(258) López, T.; Gomez, R.; Llanos, M.; López-Salinas, E. Acidic–Base Properties of Silica–Magnesia Sol–Gel Mixed Oxides: Use of 2 Butanol as Test Reaction. *Mater. Lett.* **1999**, *38* (4), 283–288.

(259) Ochoa, J. V.; Bandinelli, C.; Vozniuk, O.; Chieregato, A.; Malmusi, A.; Recchi, C.; Cavani, F.; Velasquez Ochoa, J.; Bandinelli, C.; Vozniuk, O.; et al. An Analysis of the Chemical, Physical and Reactivity Features of MgO–SiO 2 Catalysts for Butadiene Synthesis with the Lebedev Process. *Green Chem.* **2015**, *18* (6), 1653–1663.

(260) Nilius, N.; Sterrer, M.; Heyde, M. *Defects at Oxide Surfaces*; 2015; Vol. 58.

(261) Di Cosimo, J. I.; Díez, V. K.; Apesteguía, C. R. Base Catalysis for the Synthesis of α,β-Unsaturated Ketones from the Vapor-Phase Aldol Condensation of Acetone. *Appl. Catal. A Gen.* **1996**, *137* (1), 149–166.

(262) Chusuei, C. C.; Meier, D. C.; Wayne Goodman, D. Atomic-Scale Chemical and Electronic Structure Studies of Well-Defined Metal Oxide Surfaces. In *The Chemical Physics of Solid Surfaces*; 2001; pp 373–408.

(263) Zhang, M.; Gao, M.; Chen, J.; Yu, Y. Study on Key Step of 1,3-Butadiene Formation from Ethanol on MgO/SiO2. *RSC Adv.* **2015**, *5* (33), 25959–25966.

(264) Larichev, Y. V; Moroz, B. L.; Zaikovskii, V. I.; Yunusov, S. M.; Kalyuzhnaya, E. S.; Shur, V. B.; Bukhtiyarov, V. I. JPC,C071119427-XPS and TEM-RuMgO-Ru-CsMgO.Pdf. **2007**, 9427–9436.

(265) Karasuda, T.; Aika, K. Characterization of Electron Deficient Oxide Ion of Heat Treated MgO for Activation of Methane. *Bull. Chem. Soc. Jpn.* **1998**, *71* (8), 1999–2003.

(266) Ardizzone, S.; Bianchi, C. L.; Fadoni, M.; Vercelli, B. Magnesium Salts and Oxide: An XPS Overview. *Appl. Surf. Sci.* **1997**, *119* (3–4), 253–259.

(267) Khairallah, F.; Glisenti, A. XPS Study of MgO Nanopowders Obtained by Different Preparation Procedures. *Surf. Sci. Spectra* **2007**, *13* (1), 58–71.

(268) Ruiz, J. R.; Jiménez-Sanchidrián, C.; Hidalgo, J. M.; Marinas, J. M. Reduction of Ketones and Aldehydes to Alcohols with Magnesium-Aluminium Mixed Oxide and 2-Propanol. *J.*

Mol. Catal. A Chem. **2006**, *246* (1–2), 190–194.

(269) Larina, O. V.; Kyriienko, P. I.; Trachevskii, V. V.; Vlasenko, N. V.; Soloviev, S. O. Effect of Mechanochemical Treatment on Acidic and Catalytic Properties of MgO-SiO2 Composition in the Conversion of Ethanol To 1,3-Butadiene. *Theor. Exp. Chem.* **2016**, *51* (6), 387–393.

(270) Angelici, C.; Meirer, F.; van der Eerden, A. M. J.; Schaink, H. L.; Goryachev, A.; Hofmann, J. P.; Hensen, E. J. M.; Weckhuysen, B. M.; Bruijnincx, P. C. A. Ex Situ and Operando Studies on the Role of Copper in Cu-Promoted SiO 2 –MgO Catalysts for the Lebedev Ethanol-to-Butadiene Process. *ACS Catal.* **2015**, *5* (10), 6005–6015.

(271) He, R.; Men, Y.; Huang, X.; Wang, J.; Li, S.; Wang, X. Interaction of Ethanol with MgO-SiO_2 Catalysts Studied by TPD Techniques. *Chem. Lett.* **2018**, cl.180474.

(272) Larina, O. V.; Kyriienko, P. I.; Soloviev, S. O. Effect of the Addition of Zirconium Dioxide on the Catalytic Properties of ZnO/MgO-SiO2 Compositions in the Production of 1,3-Butadiene from Ethanol. *Theor. Exp. Chem.* **2015**, *51* (4), 244–249.

(273) Sekiguchi, Y.; Akiyama, S.; Urakawa, W.; Koyama, T. R.; Miyaji, A.; Motokura, K.; Baba, T. One-Step Catalytic Conversion of Ethanol into 1,3-Butadiene Using Zinc-Containing Talc. *Catal. Commun.* **2015**, *68*, 20–24.

(274) Kovařík, B. Einfluss Der Hydrothermalen Bedingungen Auf Die Aktivität Der Lebedjew-Katalysatoren. *Collect. Czechoslov. Chem. Commun.* **1959**, *24* (4), 1260–1267.

(275) Natta, G.; Rigamonti, R. X-Ray and Chemical Examination of Catalysts Used in the Manufacture of Butadiene from Alcohol. *Chim. Ind.* **1947**, *29*, 239–243.

(276) Cui, Z. M.; Chen, Z.; Cao, C. Y.; Song, W. G.; Jiang, L. Coating with Mesoporous Silica Remarkably Enhances the Stability of the Highly Active yet Fragile Flower-like MgO Catalyst for Dimethyl Carbonate Synthesis. *Chem. Commun.* **2013**, *49* (54), 6093–6095.

(277) Angelici, C. Ethanol-to-Butadiene Conversion over SiO2-MgO Catalysts: Synthesis-Structure-Performance Relationships, Utrecht University, 2015.

(278) Cai, D.; Zhu, Q.; Chen, C.; Hu, S.; Qin, P.; Wang, B.; Tan, T. Fermentation–Pervaporation–Catalysis Integration Process for Bio-Butadiene Production Using Sweet Sorghum Juice as Feedstock. *J. Taiwan Inst. Chem. Eng.* **2017**, *0*, 1–7.

(279) Chen, L.; Si, Z.; Wu, X.; Weng, D.; Ran, R.; Yu, J. Rare Earth Containing Catalysts for Selective Catalytic Reduction of NOx with Ammonia: A Review. *J. Rare Earths* **2014**, *32* (10), 907–917.

(280) Hussein G A M. Rare Earth Metal Oxides_ Formation, Characterization and Catalytic Activity Thermoanalytical and Applied Pyrolysis Review. *J. Anal. Appl. Pyrolysis* **1996**, *37*, 111–149.

(281) Mekhemer, G. A. H. Surface Structure and Acid-Base Properties of Lanthanum Oxide Dispersed on Silica and Alumina Catalysts. *Phys. Chem. Chem. Phys.* **2002**, *4* (21), 5400–5405.

(282) Frey, A. M.; Karmee, S. K.; de Jong, K. P.; Bitter, J. H.; Hanefeld, U. Supported La2O3 and MgO Nanoparticles as Solid Base Catalysts for Aldol Reactions While Suppressing Dehydration at Room Temperature. *ChemCatChem* **2013**, *5* (2), 594–600.

(283) Boukha, Z.; Fitian, L.; López-Haro, M.; Mora, M.; Ruiz, J. R.; Jiménez-Sanchidrián, C.; Blanco, G.; Calvino, J. J.; Cifredo, G. A.; Trasobares, S.; et al. Influence of the Calcination Temperature on the Nano-Structural Properties, Surface Basicity, and Catalytic Behavior of Alumina-Supported Lanthana Samples. *J. Catal.* **2010**, *272* (1), 121–130.

(284) Zhao, Y.; Li, S.; Wang, Z.; Wang, S.; Wang, S.; Ma, X. New ZnCe Catalyst Encapsulated in SBA-15 in the Production of 1,3-Butadiene from Ethanol. *Chinese Chem. Lett.* **2019**, 3–6.

(285) Zhao, Y.; Li, S.; Wang, Z.; Wang, S.; Wang, S.; Ma, X. New ZnCe Catalyst Encapsulated in SBA-15 in the Production of 1,3-Butadiene from Ethanol. *Chinese Chem. Lett.* **2019**, 3–6.

(286) Ohnishi, R.; Akimoto, T.; Tanabe, K. Pronounced Catalytic Activity and Selectivity of MgO-SiO2-Na2O for Synthesis of Buta-1,3-Diene from Ethanol. *J. Chem. Soc. Chem. Commun.* **1985**, *70* (22), 1613–1614.

(287) La-Salvia, N.; Lovón-Quintana, J. J.; Valença, G. P. Vapor-Phase Catalytic Conversion of Ethanol into 1,3-Butadiene on Cr-Ba/MCM-41 Catalysts. *Brazilian J. Chem. Eng.* **2015**, *32* (02), 489–500.

(288) Otomo, R.; Kosugi, R.; Kamiya, Y.; Tatsumi, T.; Yokoi, T. Modification of Sn-Beta Zeolite: Characterization of Acidic/Basic Properties and Catalytic Performance in Baeyer-Villiger Oxidation. *Catal. Sci. Technol.* **2016**, *6* (8), 2787–2795.

(289) Martínez, A.; Peris, E. Non-Oxidative Methane Dehydroaromatization on Mo/HZSM-5 Catalysts: Tuning the Acidic and Catalytic Properties through Partial Exchange of Zeolite Protons with Alkali and Alkaline-Earth Cations. *Appl. Catal. A Gen.* **2016**, *515*, 32–44.

(290) Ammoury, M.; Katryniok, B.; Heyte, S.; Paul, S.; Dumeignil, F.; Capron, M.; Pomalaza, G.; Shimizu, K. Ethanol-to-Hydrocarbons Reaction Catalysed by Ion-Exchanged ZSM-5 Zeolites; 8th International Symposium on Acid-Base Catalysis: Rio de Janeiro, Brazil.

(291) Yashima, T.; Suzuki, H.; Hara, N. Decomposition of 2-Propanol over Alkali Cation Exchanged Zeolites. *J. Catal.* **1974**, *33* (3), 486–492.

Chapter 2 Experimental Protocols and Techniques

2.1. Catalyst synthesis

2.1.1. Synthesis of Zn-Ta-TUD-1

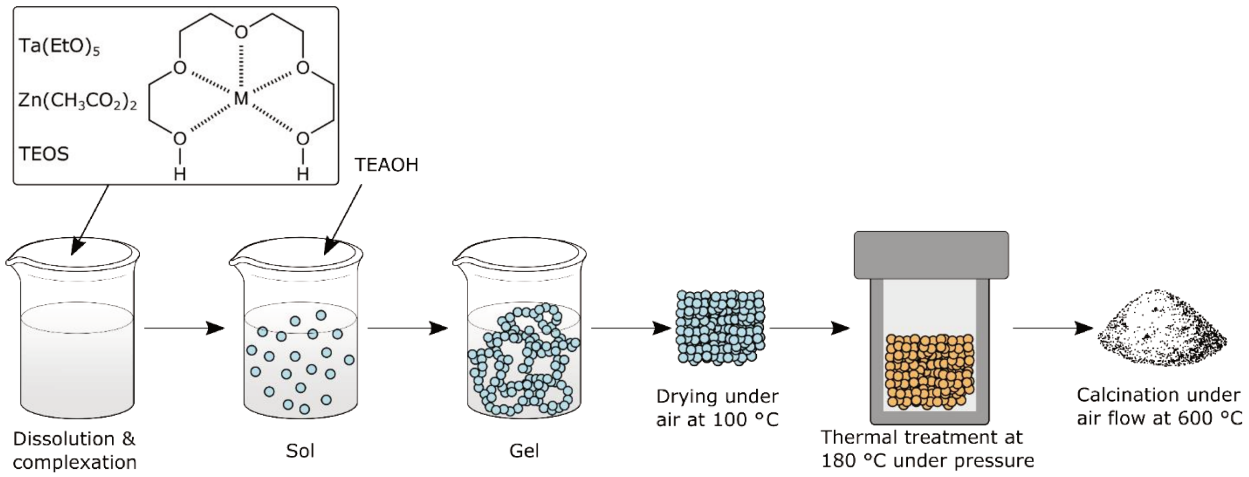

Figure 2.45 Synthesis process of Zn-Ta-TUD-1.

The TUD-1 synthesis method was used to prepare mesoporous silica catalysts with highly dispersed Zn(II) and Ta(V) phases.[1] In a typical synthesis, 69.7 mg of zinc acetate dehydrate (Acros Organics, 98^{+}%) and optical grade tantalum ethoxide (Alfa Aeser, 99.95%) were dissolved in 20 mL of absolute ethanol contained in a 50 mL beaker. To this beaker were added 1.7360 g of etratethyl orthosilicate (Agros Organics, 98%) and the solution was stirred for 5 minutes with a magnetic stirrer. 1.7262 g of tetraethylene glycol (Agros Organics, 99.5%) were added to the solution, which was stirred for 1 hour. 1.7492 g of an aqueous solution of tetraethyl ammonium hydroxide (Aldrich, 35 wt. %) were rapidly added to the solution without stirring to avoid the formation of a precipitate, resulting in the formation of a biphasic colorless transparent mixture. This mixture was homogenized by stirring, affording a colorless gel, which was left to age for 24 hours. The gel was dried overnight at 373 K, forming a shrinked xerogel with a glassy orange appearance. The xerogel was gently ground to a fine beige powder, which was placed in a Teflon-lined autoclave. The autoclave was heated at 353 K for 24 hours in a preheated oven. After letting the autoclave cool down to room temperature, a darkened, sticky powder was obtained. Starting from room temperature, this powder was calcined at 873 K under a 0.3 mL/min air flow in a tubular reactor for 10 hours; the heating ramp was 1 K/min. A fine white powder was thus obtained. Samples have been labelled ZTT, PB and RSM in the following chapters.

2.1.2. Synthesis of Zn-Ta/SiBEA and Zn-Ta/SiO_2

The incipient wetness impregnation method was used to prepared two catalysts with the same Si:Zn:Ta ratio as the catalyst described above with different supports. The first support used was dealuminated β zeolite, the second was commercial silica. The impregnation medium used ethanol.

β zeolite (Zeolyst International, CP814C) was dealuminated following the procedure by Bourgeat Lami *et al.*[2] After calcination under static air at 673 K for four hours, 500 mg of zeolite were dispersed in 50 mL of nitric acid (VWR chemicals, 64%). The suspension was stirred and heated to 353 K for four hours. After coolingto room temperature, the sample was recovered by filtration. Several washing with deionized water and recovery by centrifugation followed. The recovered solid was dried at 343 K overnight.

Amorphous fumed silica (Alfa Aeser, surface area 205 – 245 $m^2 \cdot g^{-1}$) was pretreated as per the method described by Afanasev *et al.*[3] 20 g of silica were mixed with 100 mL of deionized water until forming a homogeneous slurry, which was dried at 343 K over 2 days.

After impregnation with an ethanolic solution of zinc acetate dehydrate (Acros Organics, 98$^+$%) and optical grade tantalum ethoxide (Alfa Aeser, 99.95%), the wet solids were aged for three hours in an oven maintained at 303 K. The resulting solids were calcined under static air at 873 K for 10 hours with a ramp of 1 K/min.

2.1.3. Synthesis of SiO_2 supported catalysts

The high-throughput screening study described in section 2.3.3. tested 32 catalysts, which were using CatImpreg, a high-throughput synthesis machine of the RealCat platform at the École Centrale of Lille in Villeneuve-d'Ascq, France (http://realcat.ec-lille.fr/). These catalysts consisted of a variety of silica-supported mixed metal oxides.

As above, amorphous fumed silica (Alfa Aeser, surface area 205 – 245 $m^2 \cdot g^{-1}$) was pretreated to ease its handling during the automated synthesis. 20 g of silica were mixed with 100 mL of deionized water until forming a homogeneous slurry, which was dried at 343 K over 2 days. The resulting solid was ground and sieved to 120 mesh sized granules.

Wet impregnation was automated using the CatImpreg machine to introduce specified amounts of metal salts. Pretreated silica was mixed with solutions of the desired active phase and stirred for 6 hours, at which point the solvents were removed under vacuum within the apparatus. The resulting powders were calcined under static air to form the desired metal oxides. The elements chosen for this screening were Zr, Hf, V, Nb, Ta, La, Ce, Cu and Zn. Bimetallic, trimetallic and pentametallic samples were thus prepared; their composition was verified with X-ray fluorescence and is listed in the Annex 7.1. Deionized water was used as solvent in every instance, except for Ta. Since $TaCl_5$ precipitated in water, absolute ethanol was instead used.

Several materials were prepared with the zinc silicate hemimorphite as a substitute for ZnO. The synthesis of hemimorphite was adapted from a patented large-scale production method[4]. In short, sodium metasilicate (44-47%, Sigma Aldrich) was suspended in water under stirring. To this suspension were added an aqueous solution of $Zn(NO_3)_2 \cdot 6H_2O$ (≥98%, Sigma Aldrich) and a highly concentrated aqueous solution of NaOH (≥98%, Sigma Aldrich). The resulting white suspension was left to stir at 90 °C for 24 hours, after which it was filtered, washed with water repeatedly and dried. The structure of each batch of zinc silicate was verified using the powdered X-ray diffraction (XRD) technique by comparing it with a reference diffractogram taken from the University of Arizona Mineral Museum.

Hemimorphite-containing catalysts were prepared by wet-kneading the mineral with the aforementioned silica-supported catalysts in water. After recovery by centrifugation, the resulting powders were dried and calcined at 623 K.

2.2. Physico-chemical characterizations

2.2.1. N_2 physisorption

Specific surface area, pore diameter distribution and porous volume of catalysts were determined by N_2 physisorption.[5] 200 – 300mg of samples were outgassed at 150 ºC under vacuum for 6 hours and then exposed to a nitrogen gas atmosphere at 77 K using a Micrometric Tristar II instrument. The surface area was calculated using the Brunauer, Emmet & Teller (BET) method, which considers the amount of physisorbed N_2 as a function of relative pressure. The Barrett-Joyner-Halenda (BJH) method was used to calculate the pore volume-size distribution.[6] It is based on the Kelvin pore filling model. Pore volume and size are iteratively calculated during the

desorption gases in completely filled pores. At each step, capillary evaporation occurs; pore volume and diameter are related to the desorbed volume of gas desorbed and the thickness of the remaining adsorbed layer—the BJH radius is the sum of the Kelvin radius and the thickness of the adsorbate layer. All calculations were performed by the Tristar II 3020 software provided with the apparatus. Discussion of pores were made based on the IUPAC classifications as defined by their respective diameters: $d < 2$ nm for micropores, $2 \leq d \leq 50$ nm for mesopores and $d > 50$ nm for macropores.[7]

2.2.2. Inductively coupled plasma atomic emission spectroscopy (ICP-AES)

Elemental analysis of the as-synthesized ZTT samples was performed using inductively coupled plasma atomic emission spectroscopy (ICP-AES). Some experiments were conducted using a 720-ES ICP-OES (Agilent) instrument available at the aforementioned REALCAT platform. The instrument was calibrated using certified standard solutions. 10 mg of samples were dissolved 10 mg of dried and ground catalyst samples in concentrated acid ($HF:HNO_3$ = 1:3, v:v). Each sample solution was sonicated overnight in an ultrasonic cleaner, heated to 50 °C before dilution in 20 mL of ultrapure water and subsequent analysis. Other samples were analyzed at the *« Spectrométrie par torche à plasma »* platform of the Research Federation Michel-Eugène Chevreul hosted by the LASIR laboratory. 50 mg of catalysts were dissolved in a heated mixture of HF and HNO_3 (2:1 v:v), followed by the addition of H_3BO_3 and homogenization prior to analysis.

2.2.3. X-ray Diffraction (XRD)

Powder XRD was used to verify the crystalline phase of hemimorphite and zeolite as well as the presence of crystalline metal oxide particles. Experiments were carried out at room temperature with a Brüker D8 apparatus using Cu-Kα1 a source (λ = 1.5406 Å). A step of 0.02° with an acquisition time of 0.5 s was used.

2.2.4. X-ray Photoelectron Spectroscopy (XPS)

XPS measurements were carried out to determine the surface composition and chemical state of TUD-1 samples. Experiments were carried out with a Kratos AXIS Ultra DLD spectrometer using a monochromatic Al Kα radiation (1486.6 eV) operating at 225 W (15 mA, 15 kV). High-resolution spectra were collected using an analysis area of ≈300 µm × 700 µm and a 40 eV pass energy. Instrument base pressure was 5×10^{-10} Torr. The Kratos charge neutralizer system was applied in every instance.

The binding energies were corrected taking the C 1s peak corresponding to C–C/C–H type bonding at 284.8 eV as a reference. The C 1s, Ta 4d, Zn 2p and Zn Auger LMM spectra were analyzed using the CasaXPS software (version 2.2.16, Casa Software Ltd.). Spectra decomposition and quantification was performed after a Shirley type background subtraction and Gaussian–Lorentzian profiles with 30/70 Gaussian/Lorentzian proportion were used.

2.2.5. Fourier Transformed Infrared Spectroscopy (FTIR)

2.2.5.1. Attenuated Total Reflectance FTIR (ATR-FTIR)

The structural and compositional properties of TUD-1 samples were investigated *via* ATR-FTIR. IR spectra of powdered samples were obtained using a Nicolet iS50 FT-IR spectrometer from Thermo-Fisher equipped with an iS50 ATR sampling station. 50 scans over a scanning range of 4000 and 200 cm^{-1} with a resolution of 2 cm^{-1} were acquired.

2.2.5.2. FTIR of Chemisorbed Pyridine

The acid character of TUD-1 catalysts was characterized by monitoring the chemisorption of pyridine (Fischer, general purpose grade). Samples were prepared into self-supporting circular wafers with 2 cm diameters and loaded into a custom-made vacuum-sealable quartz apparatus coupled with a Nicolet Protege 460 infrared spectrometer fitted with an MCT detector (4 cm^{-1}). Samples were outgassed under vacuum (10^{-1} mbar) at 673 K for 1 hour prior to pyridine adsorption. The surfaces of catalysts were saturated at room temperature with pyridine. Desorption under vacuum was performed at 423 K, 523 K, 623 K and 723 K. IR spectra were acquired prior and during every step of the experiment. Acid sites were quantified based on the integrated IR bands using extinction coefficient found in the literature and the Beer-Lambert law.43

2.2.6. Temperature-Programmed Reduction (TPR)

H_2-TPR was used to study the reducibility of Zn and Ta-containing TUD-1 samples. Experiments were conducted with a Micromeritics Autochem 2920. Typically, 100 mg of catalyst were pretreated at 673 K under argon atmosphere. After cooling to room temperature, samples were heated to 1373 K (10 $K \cdot min^{-1}$) and exposed to a 50 $mL \cdot min^{-1}$ flow of 5% H_2 in argon. Hydrogen consumption was monitored by a thermal conductivity detector coupled with the apparatus.

2.2.7. Temperature-Programmed Desorption (TPD)

The number and strength of acid and basic sites of TUD-1 catalysts were characterized by TPD experiments using NH_3 and CO_2 as probes, respectively. A Micrometrics Autochem 2920 apparatus equipped with a Pfeiffer mass spectrometer. 100 mg of samples were saturated at room temperature for 30 minutes using a 50 mL/min flow of 5% NH_3 or CO_2 in He. Afterwards, desorption was conducted with a programmed heat ramp of 10 K/min until 1173 K were attained. The desorbed probes were quantified using the calibrated mass spectrometer.

2.2.8. Electron microscopy

2.2.8.1. High-angle Annular Darkfield imaging-Scanning Transmission Electron Microscopy (HAADF-STEM)

HAADF-STEM was also on a FEI Titan themis 300, equipped with a C_s probe corrector and a High-efficiency Super-X detector (EDX). At 300 kV in HRSTEM mode, it was possible to reach a resolution of 0.7 Å. This technique was used to characterize the surface of TUD-1 catalysts at the nanometric scale, notably the size of metal oxide particle. Energy dispersive X-spectroscopy (EDX) was also performed to obtain details on the nature of elements incorporated within the silica framework.

2.2.8.2 High-Resolution Transmission Electron Microscopy (HR-TEM)

The morphological properties of TUD-1 catalysts were studied with a TECNAI electron microscope operating at 200 kV. Samples were deposited onto holey-carbon copper grids.

2.2.9. Thermogravimetric Analysis-Differential Scanning Calorimetry (TGA-DSC)

The weight of compounds retained within the pores of spent catalysts and the thermicity of the desorption/combustion processes were characterized by TGA and DSC, respectively. Experiments were conducted with a TA Instrument SDT-Q600 under an air flow of 100 ml/min; samples were heated from room temperature to 973 K with a ramp of 10 K/min using alumna as a reference.

2.2.10 UV-Vis Diffuse-Reflectance Spectroscopy (UV-Vis-DRS)

UV-Vis diffuse reflectance spectroscopy was used to characterize the coordination state of metals incorporated within the as-synthesized TUD-1 catalysts. The spectra were acquired at room temperature using a Lambda 650 Perkin-Elmer spectrophotometer equipped with an integrating

sphere. Recoding ranged between 200 and 800 nm with a step of 0.2 nm with a slit width of 1 nm. $BaSO_4$ was used as standard. Reflectance spectra were converted using the Kubelka-Munk function $f(R) = (1 - R)^2/2R$.[8]

2.3. Catalytic Reactions

2.3.1. Catalyst testing

A Multi-R apparatus from TeamCat Solutions was used to evaluate the performances of prepared catalysts in the ethanol-to-butadiene reaction. This machine is a high-throughput equipment for heterogeneous catalyst screening. It consists of 4 parallel fixed-bed reactors heated independently with a single reactant feed distributed into equal inlet flows using a splitter. He was used as carrier gas passed through a heated bubbler containing ≥99.8 % ethanol. The ethanol flowrate and the bubbler's temperature were adjusted using Antoine's law to afford a 20 mL/min flow with 4.5% ethanol concentration per reactor.

Between 10 to 50 mg of catalysts were loaded into fritted glass reactors and were sandwiched between two 300 mg lawyers of 125 µm SiC to ensure their presence within the isothermal zone of the reactor and to allow ethanol to attain reaction temperature. An independently controlled valve enables selecting the output of each reactor for analysis, which outputs were analyzed with an online Agilent 7890 A equipped with an FID detector. The latter was calibrated to measure the concentration of ethanol, butadiene, acetaldehyde, crotonaldehyde, ethylene, propylene, butenes, diethyl ether and acetone.

Ethanol conversion (X, %, equation 1), the selectivity towards each product (S_i, %, equation 2), the molar yield of each product (Y_i, %, equation 3) and the productivity in butadiene (P_{BD}, $g_{BD} \cdot g_{cat}^{-1} \cdot h^{-1}$, equation 4) were used to describe catalytic activity. The carbon balance for each test was calculated by dividing the sum of carbon moles detected in the output flow with the molar amount of carbon introduced as ethanol.

$$X = \frac{c_{EtOH,in} - c_{EtOH,out}}{c_{EtOH,in}} \cdot 100 \qquad (1)$$

$$S_i = \frac{c_{i,out}}{c_{EtOH,in} - c_{EtOH,out}} \cdot 100 \qquad (2)$$

$$Y_i = X \cdot S_i \quad (3)$$

$$P_{BD} = X \cdot S_{BD} \cdot WHSV_{EtOH} \cdot 0.587/100 \quad (4)$$

2.3.2. Selective poisoning Study

A pyridine poisoning study was conducted in a steady-state fixed-bed glass reactor of 0.5 cm in diameter at 623 K. Ethanol was fed by pumping absolute ethanol with an HPLC pump into a vaporizer heater at 473 K into which 30 mL/min of He was flow and fed into the reactor. $WHSV_{EtOH}$ of 0.3 $h^{-1}$was used. After 1 hour on stream, the feed was switched to an ethanol-pyridine mixture containing 5 mol.% of pyridine (Fisher, 99%). After 1 hour of pyridine co-feeding, the feed was returned to pure ethanol. The concentration of reactants in the reactor output was monitored an online Agilent 7890 A equipped with an FID detector.

2.3.3. High-Throughput Screening Study

The high-throughput experiments for screening and kinetic studies were conducted using a Flowrence unit from Avantium (Netherlands) at the REALCAT platform of the Ecole Centrale of Lille. The Flowrence apparatus consists of 16 parallel fixed-bed reactors. These reactors are individually equipped with a liquid and gas inlet, and divided between four blocks, each with independent temperature control (Figure 2.46). The output of each reactor can be analyzed by means of a multi-position valve which directs automatically the desired effluent to an online GC (Agilent GC- 2010 Plus) equipped with a 30 m x 0.25 mm x 0.25 µm Zebron ZB-5MS column and an FID detector calibrated for the products of ethanol conversion.

D. C.; Datye, A. K. .; Niemantsverdriet, J. W.; Butz, T.; Engelhardt, G.; et al. Characterization of Solid Catalysts: Sections 3.1.1– 3.1.3. In *Handbook of Heterogeneous Catalysis*; Wiley-VCH Verlag GmbH: Weinheim, Germany; pp 427–582.

(6) Barrett, E. P.; Joyner, L. G.; Halenda, P. P. The Determination of Pore Volume and Area Distributions in Porous Substances. I. Computations from Nitrogen Isotherms. *J. Am. Chem. Soc.* **1951**, *73* (1), 373–380.

(7) Van Donk, S.; Janssen, A. H.; Bitter, J. H.; De Jong, K. P. Generation, Characterization, and Impact of Mesopores in Zeolite Catalysts. *Catal. Rev. - Sci. Eng.* **2003**, *45* (2), 297–319.

(8) Kubelka, P.; Munk, F. Ein Beitrag Zur Optik Der Farbanstriche (Contribution to the Optic of Paint). *Zeitschrift fur Tech. Phys.* **1931**, *12*, 593–601.

Chapter 3 Effect of Support on Zn-Ta Catalysts

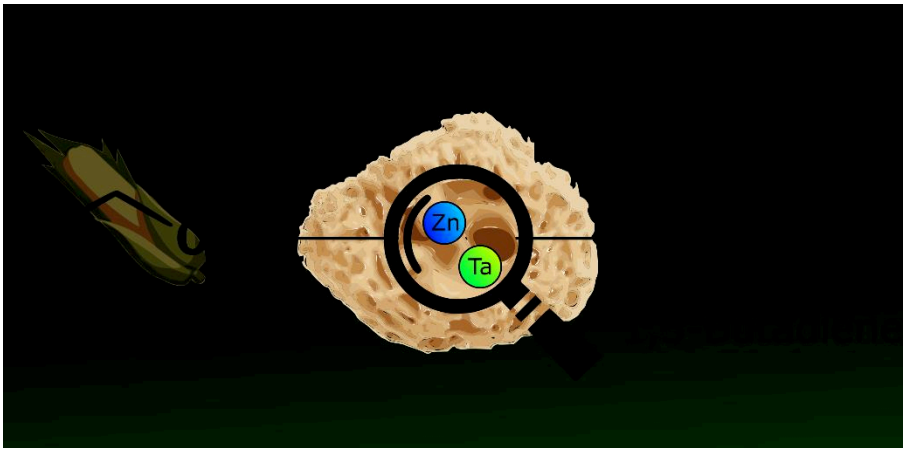

Abstract

High performances in the conversion of ethanol to *1,3*-butadiene were achieved with a Zn(II) and Ta(V) catalyst supported on TUD-1, a mesoporous silica. Selectivity reached 73% after 3 h at 94% conversion. At increased ethanol flow, initial productivity rose to 2.45 $g_{1,3\text{-BD}}.g_{cat}^{-1}.h^{-1}$, which remained stable during 60 h on stream, making it the most productive catalyst according to the literature. Preliminary characterization suggests morphological and acid properties contribute to these exceptional performances.

Preface

This chapter is based on the following manuscript: "ZnTa-TUD-1 as an easily prepared, highly efficient catalyst for the selective conversion of ethanol to 1,3-butadiene", which was accepted and published as a communication in the journal Green Chemistry on the 8th of June 2018 (Pomalaza, G.; Vofo, G.; Capron, M.; Dumeignil, F. Green Chem. **2018**, 20 (14), 3203–3209.).

Some context is needed to understand the decisions that have led to this work. First, the choice of using zinc and tantalum as catalysts stems from the results of the previously mentioned screening study in which 32 catalysts were tested in the Lebedev process. The internal report comparing the catalytic performances of each sample can be found Annex 7.1. It details how the Zn-Ta outperformed all other silica-supported bimetallic and trimetallic catalysts at equimolar metal content. As a result, Zn-Ta catalysts were further investigated with the aim of preparing catalysts with high butadiene productivity.

Second, the choice of TUD-1 as catalyst support was not arbitrary. As discussed in the introduction of the chapter, Lee *et al.* had identified mesocellular siliceous foam as a suitable catalyst for preparing a Zr-based catalyst, which was at the time the most productive in the literature. TUD-1 was ultimately chosen due to its easy and hasty synthesis compared to other mesocellular siliceous foams.

Finally, the initial work on Zn-Ta-TUD-1 was conducted by Giovanni Vofo, a master's student from the University of Lille whom I supervised for a period of 6 months. He conducted a small-scale screening of synthesis parameters which I later expanded upon, as discussed in Chapter 4. Although the experimental work presented here is mine, his screening study identified an approximate Zn-to-Ta ratio that led to high butadiene yield. I am grateful for his contribution.

3.1. Introduction

1,3-butadiene (herein referred to as *1,3*-BD) is considered the most economically important unsaturated C_4 compound; it is indeed crucial to the manufacturing of several polymers, such as synthetic rubber.[1,2] *1,3*-BD is predominantly extracted from the C_4 fraction following ethylene manufacturing *via* the steam cracking of naphtha.[1,2] Because of scarcity issues and environmental concerns, sustainable on-purpose production methods for *1,3*-BD are of topical interest. Bioethanol can be obtained from renewable sources.[3] For this reason, the catalytic conversion of ethanol (EtOH) to *1,3*-BD is attracting much attention, despite being an old technology.[4] Recent research has focused on increasing *1,3*-BD yield and productivity through catalyst design, with the aim of turning the ethanol-to-butadiene (ETB) reaction into an economically viable process.[5]

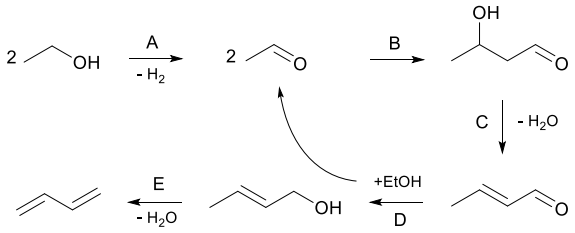

Figure 3.47 Main reaction pathway leading to *1,3*-butadiene. Reaction steps are: (A) ethanol dehydrogenation; (B) aldol condensation; (C) dehydration; (D) Meerwein–Ponndorf–Verley-Oppenaur (MPVO) reaction; (E) dehydration.[6]

Owing to its complex mechanism (Figure 3.47), the ETB reaction requires multifunctional catalysts; most illustrated steps occur on different catalytic sites, generally provided by combining metals and/or metal oxides possessing the appropriate chemical properties. For instance, acid sites are suitable for the aldol coupling and dehydration reactions (steps B, C and E in Figure 3.47).[6,7] Ethanol dehydrogenation and aldol coupling, also known as aldolization (steps A and B in Figure 3.47) can occur on basic sites.[8,9] Metal nanoparticles are also suitable for step A.[10] Furthermore, maximizing *1,3*-BD formation necessitates a catalyst with an adequate balance of such properties.[11] Otherwise, alternative reaction pathways may be favored, leading to the formation of undesired byproducts, such as ethylene or butanol.[12]

Recent improvements in the design of catalysts for the ETB reaction have yielded high-performing materials.[4] The combination of supported Lewis-acidic metal oxides [Zr(IV), Hf(IV), Ta(V) or Nb(V)] with dehydrogenation promoters (Ag, Cu) has afforded highly active

catalysts.[13–15] The use of mesoporous catalyst carriers was also demonstrably increased catalytic stability and *1,3*-BD selectivity.[14,16,17] Recently, Lee *et al*. designed a highly selective and stable zirconia catalyst supported on mesocellular siliceous foam.[14] They attributed the performances of their catalyst to two factors: *(i)* uniform tridimensional mesoporous supports, enabling efficient mass transfer and excellent resistance to coke, and *(ii)* highly dispersed active metal oxides. The benefits of mesoporous morphology to the catalytic performances were also observed by others.[16–18] Yet, this strategy is underutilized, with many recent works preferring tried-and-tested microporous zeolite supports, such as dealuminated zeolite beta.[13,19] Perhaps the time-consuming synthesis of mesoporous materials, such as mesocellular siliceous foam and SBA-15, including the post-synthesis modifications needed to introduce an active phase, hinders their use and study.

In this work, we report the facile preparation and study of a Zn(II) and Ta(V) catalyst supported on mesoporous TUD-1, achieving the aforementioned high performance-driving factors highlighted by Lee *et al*.[14] TUD-1 is a sponge-like mesoporous silica with an irregular three-dimensional pore system.[20] This material has found many applications as a support for heterogeneous catalysts due to its numerous practical advantages. Its structural properties are easily tuned following the preparation of a precursor gel by adjusting the duration of its hydrothermal treatment. This way, siliceous foam with mesopores ranging from 2 to 20 nm and with specific surface areas between 300 and 900 m^2/g can be obtained. Furthermore, metals or metal oxides are easily dispersed within the silica framework through a simple modification of the one-pot synthesis. This way, bimetallic or bi-metal oxide systems are effortlessly synthesized to take advantage of synergetic effects between two different active phases.[20] In addition, TUD-1 catalysts are usually highly active while showing a remarkable hydrothermal stability.[20–25] The key to TUD-1's versatility and straightforward preparation is the use of a chelating agent during the gelification process, which doubles as a structure directing agent. By chelating precursor ions prior to gelification, it also ensures an excellent degree of dispersion during the oxidizing calcination, which frees the agent and condenses the silica, simultaneously generating mesopores *via* steric hindrance.

Although both Zn(II) and Ta(V) have been used separately in other ETB catalysts, they are seldom reported together. Zinc oxide is cited as a promoter of ethanol dehydrogenation.[26,27]

Tantalum oxide was shown to reach remarkable selectivity when converting mixtures of ethanol with acetaldehyde.[16,28,29] In the present work, when supported on TUD-1, stable *1,3*-BD selectivity peaking at 73 % for an EtOH conversion of 96 % was achieved (T: 400 °C, $WHSV_{EtOH}$: 5.3 h^{-1}, TOS: 3 h). Productivity is also exceptionally high and stable, despite the high ethanol flow employed, outperforming any other formulation disclosed so far in the direct conversion to *1,3*-BD at comparable conditions.

3.2. Experimental

3.2.1. Catalysts preparation

A catalyst consisting of Zn(II) and Ta(V) supported on TUD-1 (labelled ZnTa-TUD-1) was synthesized with tetraethylene glycol as a chelating agent in a one-pot procedure based on a sol-gel methodology as found in the literature.[24] The appropriate amounts of Zn and Ta salts (zinc acetate dehydrate and tantalum ethoxide) were first dissolved in absolute ethanol with a Zn:Ta molar ratio of 1.5. Tetraethyl orthosilicate (TEOS) was added drop-wise to the ethanol solution while stirring. The chelating agent was subsequently added in a similar fashion. After 1 h of stirring, an aqueous solution of tetraethyl ammonium hydroxide (35 wt.%) was added dropwise to the mixture under vigorous stirring, which was maintained for 2 h. A clear gel was obtained and left to age at room temperature for 24 h. The aged gel was dried at 100 °C for 24 h before being gently ground to a white powder and subjected to a hydrothermal treatment in a Teflon-lined stainless-steel autoclave for 24 h at 180 °C. The resulting brown powder was calcined at 600 °C in a tubular quartz reactor for 10 h with a temperature ramp of 1 °C.min^{-1} and an air flow of 0.3 L.min^{-1}. A fine white powder was ultimately recovered.

For comparison, additional catalysts with the same amounts of Zn and Ta were prepared. In one case, zeolite BEA from Zeolyst international (CP814C) was dealuminated following a procedure detailed in the literature.[30] In another, fumed silica (Alfa Aeser) was used. In both cases, the appropriate amounts of Zn and Ta were introduced *via* incipient wetness impregnation (IWI) using the same precursor salts as those used in the preparation of the TUD-1-based catalyst. Drying and calcination according to the procedure described above followed, resulting in white powders in both cases. The as-obtained benchmark catalysts were labelled ZnTa/deBEA and $ZnTa/SiO_2$, respectively.

3.2.2. Catalyst testing

Catalytic activity tests were carried out with a Multi-R® apparatus from Teamcat Solutions SAS.[31] Multi-R® is a high-throughput equipment for heterogeneous catalysts screening. This device consists of 3 main components: the feed, the reaction section and the analytical system. The gaseous feed is split and fed into 4 reactors using a splitter provided by the manufacturer. The machine is adjusted so that every reactor receives an equal inlet flow in terms of gas composition and flowrate. Catalysts are loaded in specific liners with sintered glass filters and inserted in the device, acting as fixed-bed reactors. The temperature of each reactor is controlled independently. Their output is analysed with an online GC (Agilent 7890 A) equipped with a FID detector calibrated to detect and quantify the major products of the reaction, *i.e. 1,3*-BD, acetaldehyde (AcH), ethylene ($C_{2=}$), propylene, etc.). Choosing from the output of one reactor to another is done by an independently controlled valve.

Reaction temperature was set at 400 °C with a pressure of 1 atm. Catalysts were ground and sieved to 120 mesh-sized granules; 30 mg of catalyst were loaded in the glass reactors and held in place using SiC. Ethanol was introduced into the splitter and then each reactor by passing helium through a bubbler containing ≥ 99.8 % ethanol maintained at 25 °C. EtOH vapour concentration was set at 4.5 vol.%. Helium flow and catalyst mass were adjusted to provide a weighted hourly space velocity ($WHSV_{EtOH}$) of 2, 5.3 and 8 h^{-1}.

Catalyst regeneration was carried out the same reactors, under synthetic air with a flow of 10 $ml.min^{-1}$ for a period of 6 hours at 400 °C.

Catalytic activity was characterized by the conversion of ethanol (X, %), the selectivity towards each product (S_i, %), the molar yield of each product (Y_i, %) and the productivity in *1,3*-BD ($P_{1,3\text{-BD}}$, $g_{1,3\text{-BD}}.g_{cat}^{-1}.h^{-1}$). Each value was calculated according to the following formulas:

$$X = \frac{c_{EtOH}^0 - c_{EtOH}}{c_{EtOH}^0} \cdot 100$$

$$S_i = \frac{c_i}{c_{EtOH}^0 - c_{EtOH}} \cdot 100$$

$$Y_i = X \cdot S_i$$

$$P_{1,3-BD} = X \cdot S_{1,3-BD} \cdot WHSV_{EtOH} \cdot 0.587/100$$

Where c_{EtOH} is the amount of carbon moles from EtOH entering the reactor, c_i is the amount of carbon moles detected for a given product *i*, the 0.587 coefficient represents the 100 % mass yield of butadiene and $WHSV_{EtOH}$ represents the mass flow of ethanol per mass of catalysts (expressed as $g_{EtOH}.g_{cat}^{-1}.h^{-1}$). The carbon balance (*CB*) for each test was calculated by dividing the sum of carbon moles detected with the molar amount of carbon introduced as EtOH in percentage.

3.2.3. Characterization

Physisorption experiments were performed at −196 °C on a Micromeritics Tristar II instrument. Before analysis, a known mass of solid (~ 50–200 mg) was outgassed under vacuum at 150 °C for 6 h. Specific surface area (S_{BET}) could then be calculated using the B.E.T. equation on the linear part of the B.E.T. plot (P/P_0=0.1–0.25). Average pore volume (V_p) was measured from the adsorption branch of the isotherm, at a P/P_0 value of 0.98. The mean pore diameter (D_p) was calculated by applying the Barrett-Joyner-Halenda model on the desorption branch of the isotherm.

Powder X-ray diffraction (XRD) high angles patterns were recorded on a Bruker AXS D5005 diffractometer using a CuK_α radiation (λ = 1.54184 Å) as an X-ray source in the 2θ range from 10 to 50° with a step of 0.05° (integration time of 8 s).

Elemental analysis was performed with the catalysts using inductively coupled plasma-optic emission spectroscopy 720-ES ICP-OES (Agilent) with axial viewing and simultaneous CCD detection. The quantitative determination of metal content in the catalysts was made based on the analysis of certificated standard solution. The analytes were prepared by dissolving 10 mg of dried and ground catalyst samples in concentrated acid ($HF:HNO_3$=1:3, v:v). Each sample solution was stirred overnight in an ultrasonic cleaner heated to 50 °C before dilution in 20 mL of ultrapure water and analysis.

Acid sites were quantified using NH_3-temperature programmed desorption (NH_3-TPD). The measurements were performed on calcined samples of known masses with a Micrometrics Autochem 2920 apparatus coupled with a Pfeiffer mass spectrometer (MS). NH_3 adsorption was performed at room temperature during 30 min using a NH_3 flow consisting of 5 % NH_3 in 95 %

He). Desorption was performed until 900 °C (ramp of 10 °C.min^{-1}) and held for 30 min in He (30 mL.min^{-1}).

3.3. Results & Discussion

Table 3.9 Catalytic performances of Zn(II) and Ta(V) on TUD-1, dealuminated BEA and SiO_2 in *1,3*-BD production at 400 °C, $WHSV_{EtOH}$ of 5.3 h^{-1} after 3 h.

Sample	*X*, %	$S_{1,3\text{-BD}}$, %	S_{AcH}, %	$S_{C2=}$, %	$Y_{1,3\text{-BD}}$, %	$P_{1,3\text{-BD}}$, [a]	*CB*,%
ZnTa-TUD-1	94	73	18	10	69	2.13	102
ZnTa/deBEA	95	59	25	8	56	1.74	95
ZnTa/SiO2	94	48	34	4	45	1.40	95

[a] *1,3*-Butadiene productivity in $g_{1,3\text{-BD}}.g_{cat}^{-1}h^{-1}$.

Table 3.10 Metal loading and molar ratio in the studied samples.

Sample	Si/Zn	Si/Ta	Zn/Ta	Formula
ZnTa-TUD-1	16.5	29.6	1.79	$Zn_{6.1}Ta_{3.4}$-TUD-1
ZnTa/deBEA	18	30.3	1.67	$ZnT_{5.6}Ta_{3.3}$/deBEA
ZnTa/SiO_2	19.2	31	1.61	$Zn_{5.2}Ta_{3.2}/SiO_2$

We benchmarked the performances of ZnTa-TUD-1 in terms of *1,3*-BD selectivity and *1,3*-BD productivity against those of common materials: abundant publications on the Lebedev process employ dealuminated zeolite and silica-supported catalysts prepared through impregnation. *1,3*-BD selectivity demonstrably reflected the suppression of undesired byproducts, the presence of which being detrimental to the viability of bio-based processes.[32] Productivity is also hailed as an important indicator of industrial relevancy, unproductive catalysts obviously preventing a robust economic viability.[33] Carbon balance was within 95 and 105% over the course of the experiments and considered as satisfactory. The results are reported in Table 3.9.

EtOH conversion was equally high on all the catalysts, reaching 94-95%. *1,3*-BD selectivity depended on the catalyst, peaking at 73 % over ZnTa-TUD-1. This value is relatively high considering the elevated ethanol flow ($WHSV_{EtOH}$: 5.3), most articles reporting experimental conditions below 2 h^{-1}.[4] Conversely, selectivity over ZnTa/deBEA and ZnTa/SiO_2 was respectively 10 and 20 percentage points smaller. This disparity was mirrored in the higher selectivity towards AcH observed with both. These remarkable results are ostensibly attributed to the choice of catalyst carrier, possibly to its intrinsic properties or its synthesis procedure. To adequately investigate this assumption, the three samples were prepared with equal amounts of Zn(II) and Ta(V). Elemental analysis of Si, Ta and Zn in the prepared catalysts was conducted using ICP-OES, indicating that all the three catalysts containing similar amounts of oxide phase

and Zn/Ta ratio (Table 3.10). This excludes the possibility that the performance difference observed stemmed from uneven amounts of active phases.

Table 3.11 Morphological properties obtained by N_2 physisorption.

Sample	S_{BET}[a], $m^2.g^{-1}$	Pore vol.[a], $cm^3.g^{-1}$	Average pore diameter, nm
ZnTa-TUD-1	640	2.20	13.6
ZnTa/deBEA	501	0.60	6.0
ZnTa/SiO_2	185	0.82	16.05

[a] Specific surface area [b] Pore volume, measured at P/P_0 = 0.98.

Carrier morphology has been shown to influence catalytic activity in the ETB reaction. Jones *et al*. observed an increase in *1,3*-BD selectivity by up to 17 percentage points when the pore size diameter of a silica support was increased from 6 nm to 15 nm.[17] Likewise, Chae *et al.* also noted an initial benefit to increasing pore size diameter from 2.5 nm to 10.9 nm when using SBA-15 as a catalyst carrier. However, these became modest after 10 h on stream due to deactivation.[16] As stipulated by Lee *et al*., large and uniform pore sizes contribute to a stable catalytic activity.[14] Furthermore, Jones *et al*. also have drawn a direct correlation between specific surface area and *1,3*-BD yield.[34,35] These observations highlight the importance physical properties have in the ETB reaction, which were promptly investigated. Table 3.11 summarizes the results obtained by N_2 physisorption regarding the morphology of the catalysts prepared. ZnTa-TUD-1 possessed the expected morphological features: a large specific surface area (300-900 $m^2.g^{-1}$), a large porous volume and mesopores (2-20 nm).[20] Figure 3.S1 indicates that the pore size distribution is uniform, peaking at around 18 nm, with a full width at half maximum of 6.2 nm. Conversely, ZnTa/deBEA had a large specific surface, but smaller pore volume and diameter, the distribution of which was uneven. Figure 3.S1 illustrates how it ranges from nanopores inherent to zeolitic materials to mesopores formed during the dealumination process. ZnTa/SiO_2 had larger average pore diameter compared to the TUD-1 sample, but much smaller specific surface area and pore volume. Part of the inferior performances can be attributed in part to a lack of uniform mesopores in the case of zeolite-supported catalyst and the smaller specific surface area of the silica-supported catalyst. However, other factors should also be taken in consideration.

Table 3.12 Amount of acid sites measured by NH_3-TPD expressed by weight and surface units

Sample	Nb of acid sites per weight ($mmol.g^{-1}$)	N° of acid sites per surface ($mmol.m^{-2}$)
ZnTa-TUD-1	0.88	563
ZnTa/deBEA	0.43	213
ZnTa/SiO_2	0.17	30

Sushkevich and Ivanova have identified a direct correlation between the amount of Zr(IV) Lewis acid sites and the *1,3*-BD rate of formation.[13] In their study of the reaction mechanism, they propose that Lewis acid sites such as those brought by Ta(IV) catalyze every reaction step subsequent to the initial ethanol dehydrogenation step (aldol condensation, MPVO reaction and alcohol dehydration).[6] Since aldol condensation has been identified as the rate-limiting step, the observed accumulation of AcH suggests that the disparity in selectivity is related to the acidic Ta(V) phase. The amount and strength of acidic sites on the three catalysts were characterized by NH_3-TPD. Desorption profiles are illustrated in Figure 3.S2 and the results are summarized in Table 3.12. Figure 3.S2 suggests the existence of a single type of acid sites covering a broad range of strengths in each catalyst, as evidenced by the single broad peaks at 260 °C. The combination of Zn(II) with Ta(V) may explain the absence of acid sites desorbing at higher temperatures, *i.e.*, of stronger acid sites; some authors have reported a passivation of strong acidity upon the introduction of zinc oxide.[15,36] Despite containing equal amounts of Ta and Zn, the total amount of acid sites per gram differed according to the catalyst carrier used. ZnTa-TUD-1 possessed the double of acid sites than ZnTa/deBEA and five times more than ZnTa/SiO_2.

Figure 3.48 Correlation curve between 1,3-BD selectivity (T: 400 °C, $WHSV_{EtOH}$: 5.3 h^{-1}, P: 1 atm, TOS: 3 h) and total surface acidity.

A correlation between the amount of acid sites and selectivity towards *1,3*-BD after 3 h on stream was observed (Figure 3.48). Considering that silicate-supported Ta(IV) is predominantly Lewis acidic when reacting with alcohols, these results are in line with the current theory regarding the ETB mechanism.[29] The amount of Ta being identical on each catalyst, this suggests

that the dispersion was more successful using the TUD-1 methodology—thereby creating more isolated acid sites. ZnTa/deBEA was prepared using a method that generates isolated Ta(V) sites. However, it was successfully reported for Ta wt.% of 1, 2 and 3.[29,37] In this work, the Ta loading reaches 10 wt.%, which may have proved too much for proper dispersion using IWI. TUD-1 synthesis appears to be better suited for dispersing high active phase loadings.

Figure 3.49 XRD patterns of synthesized Zn(II) & Ta(V) catalysts

Powder XRD diffractograms of the synthesized samples (Figure 3.49) did not show the presence of bulk crystalline ZnO or Ta_2O_5, suggesting only an absence of large extra framework metal oxides particles. In addition, the diffractograms of ZnTa-TUD-1 and ZnTa/SiO_2 both possessed the broad bands around 15-30°, common on amorphous siliceous materials. Bands typical of the BEA structure on the diffractogram of ZnTa/deBEA—similar to those observed with other Ta-containing dealuminated BEA—confirms that the carrier retained its zeolite framework throughout the dealumination and impregnation processes.[37]

Figure 3.50 Performances of ZnTa-TUD-1 , ZnTa/deBEA and ZnTa/SiO_2 over a 20 h period (T: 400 °C, $WHSV_{EtOH}$: 5.3 h^{-1}, P: 1 atm).

Additional tests with the three synthesized materials were conducted to measure their stability, as deactivation commonly plagues the performances of ETB catalysts. Figure 3.50 compares the conversion and selectivity to the three major products over ZnTa-TUD-1, ZnTa/deBEA and ZnTa/SiO_2 over 20 h of reaction. Each catalyst suffered from a similar loss of activity in converting EtOH (about 10 percentage points in 20 h). The *1,3*-BD selectivity also dropped over time, with AcH selectivity increasing as a result, suggesting that coke deposits gradually poison the active acid sites. The rate of deactivation in terms of *1,3*-BD selectivity depended on the material. ZnTa-TUD-1 fell 7 percentage points over 20 h, whereas ZnTa/deBEA and ZnTa/SiO_2 decreased by 13 and 12 percentage points, respectively. Ostensibly, the stability of the TUD-1 catalyst is attributable to its uniform, three-dimensional mesopores.[14]

Deactivation of ZnTa-TUD-1 was again tested. At $WHSV_{EtOH}$ of 8 h^{-1}, *1,3*-BD selectivity was initially 66, losing 13 percentage points over the course of 60 hours (Figure 3.5). Ethanol conversion also decreased by 15 percentage points, whereas AcH selectivity grew steadily to around 35% before stabilizing at around TOS of 40 h. At TOS of 3 h, *1,3*-BD productivity is 2.45 $g_{1,3\text{-BD}}.g_{cat}^{-1}.h^{-1}$. A preliminary regeneration attempt was conducted at 400 °C under air in an attempt to remove coke deposits responsible for deactivation. Figure 3.S4 illustrates how ethanol conversion, acetaldehyde selectivity and ethylene selectivity were returned to their initial values. However, *1,3*-BD selectivity was only partially recovered and continued the trend of deactivation following 15 hours of reaction under the same conditions. These results suggest that carbonaceous species are partly responsible for the loss of catalytic activity. With regards to *1,3*-BD selectivity, deactivation may either be caused by species requiring different, possibly harsher calcination conditions or that the nature of the active site is compromised during the reaction/regeneration procedure. Work is ongoing to understand this phenomenon.

Compared to the performances reported in the literature, ZnTa-TUD-1 fared well: the other two most productive ETB catalysts (hierarchical MgO-SiO_2 from Men *et al.* and ZnY/deBEA from Li *et al.*) lost their selectivity toward *1,3*-BD faster than ZnTa-TUD-1.[19,39] Starting with a *1,3*-BD selectivity of 77%, MgO-SiO_2 (T: 450 °C, $WHSV_{EtOH}$: 4.1 h^{-1}) lost 13 percentage points in 20 h.[39] ZnY/deBEA (T: 400 °C, $WHSV_{EtOH}$: 7.9 h^{-1}) decreased by 20 percentage points in 10 h from an initial selectivity of 63 %.[19] Figure 3.S5 illustrates the productivity of the three catalysts as the reaction progresses. Figure 3.S6 compares *1,3*-BD productivity observed on ZnTa-TUD-1 with the other top 10 most productive catalysts found in the literature at the different $WHSV_{EtOH}$ each were tested. Admittedly, the difference in reaction conditions makes a direct comparison partiality inaccurate, as we have demonstrated that $WHSV_{EtOH}$ affects catalytic performances. Nevertheless, these figures indicate that ZnTa-TUD-1 is the most selective and stable catalyst at high ethanol flow, boasting a *1,3*-BD productivity of 2.45 $g_{1,3\text{-BD}}.g_{cat}.h^{-1}$ after 3 hours. To the best of our knowledge, this makes it the most productive catalyst recorded.

3.4. Conclusions

ZnTa-TUD-1 was revealed as a highly selective catalyst for the conversion of ethanol to *1,3*-butadiene. Its simple preparation method allows us, in a one-pot operation, both to disperse the

active phase within the support and to generate a mesoporous morphology beneficial to its catalytic activity. This does away with pre and post-synthesis procedures commonly used for introducing metal oxides such as ion-exchange, mechanical mixing, urea hydrolysis or impregnation[13,14,19], but also for generating mesopores, such as zeolites dealumination. In addition, the mesopores are formed using environmentally friendly chelating agents that double as structure-directing agents.

A remarkable selectivity towards BD of 73 % was observed with ZnTa-TUD-1 after 3 h on stream at 400 °C, which was tied with the total amount of surface acid sites. Using a $WHSV_{EtOH}$ of 5.3 h^{-1} combined with the aforementioned selectivity, a *1,3*-BD productivity reaching 2.13 $g_{1,3\text{-}BD}.g_{cat}.h^{-1}$ was attained. Raising the $WHSV_{EtOH}$ to 8 h^{-1} decreased *1,3*-BD yield, but increased overall *1,3*-BD productivity to 2.45 $g_{1,3\text{-}BD}.g_{cat}.h^{-1}$, an unprecedented value according to the literature. Because productivity is considered a key factor in making the ETB process compete with petroleum-derived *1,3*-butadiene, these performances are very promising and important. Additionally, the catalyst proved to be remarkably stable for a period of 60 hours—a phenomenon ostensibly attributed to its morphology.[14] Regeneration under air to remove deposed carbonaceous species was only partially successful, but is undergoing improvements.

Further synthesis is ongoing to optimize the highly tuneable TUD-1 catalyst. Additionally, a complete characterization of the catalytic system is in progress to fully grasp how its physicochemical properties are tied to the performances observed.

3.5. Notes and References

(1) Dahlmann, M.; Grub, J.; Löser, E. Butadiene. In *Ullmann's Encyclopedia of Industrial Chemistry*; Wiley-VCH Verlag GmbH & Co. KGaA: Weinheim, Germany, 2011; Vol. 100 C, pp 1–24.

(2) Sun, H. N.; Wristers, J. P. Butadiene. In *Kirk-Othmer Encyclopedia of Chemical Technology*; John Wiley & Sons, Inc.: Hoboken, NJ, USA, 2002; Vol. 4.

(3) Kosaric, N.; Duvnjak, Z.; Farkas, A.; Sahm, H.; Bringer-Meyer, S.; Goebel, O.; Mayer, D. Ethanol. In *Ullmann's Encyclopedia of Industrial Chemistry*; Wiley-VCH Verlag GmbH & Co. KGaA: Weinheim, Germany, 2011; pp 1–72.

(4) Pomalaza, G.; Capron, M.; Ordomsky, V.; Dumeignil, F. Recent Breakthroughs in the Conversion of Ethanol to Butadiene. *Catalysts* **2016**, *6* (12), 203.

(5) Jones, M. Catalytic Transformation of Ethanol into 1,3-Butadiene. *Chem. Cent. J.* **2014**, *8* (1), 53.

(6) Sushkevich, V. L.; Ivanova, I. I. Mechanistic Study of Ethanol Conversion into Butadiene over Silver Promoted Zirconia Catalysts. *Appl. Catal. B Environ.* **2017**, *215*, 36–49.

(7) Makshina, E. V; Dusselier, M.; Janssens, W.; Degrève, J.; Jacobs, P. A.; Sels, B. F. Review of Old Chemistry and New Catalytic Advances in the On-Purpose Synthesis of Butadiene. *Chem. Soc. Rev.* **2014**, *43*, 7917–7953.

(8) Ordomsky, V. V.; Sushkevich, V. L.; Ivanova, I. I. Study of Acetaldehyde Condensation Chemistry over Magnesia and Zirconia Supported on Silica. *J. Mol. Catal. A Chem.* **2010**, *333* (1–2), 85–93.

(9) Chieregato, A.; Velasquez Ochoa, J.; Bandinelli, C.; Fornasari, G.; Cavani, F.; Mella, M. On the Chemistry of Ethanol on Basic Oxides: Revising Mechanisms and Intermediates in the Lebedev and Guerbet Reactions. *ChemSusChem* **2015**, *8* (2), 377–388.

(10) Shimizu, K. I.; Sugino, K.; Sawabe, K.; Satsuma, A. Oxidant-Free Dehydrogenation of Alcohols Heterogeneously Catalyzed by Cooperation of Silver Clusters and Acid-Base Sites on Alumina. *Chem. - A Eur. J.* **2009**, *15* (10), 2341–2351.

(11) Angelici, C.; Velthoen, M. E. Z.; Weckhuysen, B. M.; Bruijnincx, P. C. A. Influence of Acid–Base Properties on the Lebedev Ethanol-to-Butadiene Process Catalyzed by SiO2–MgO Materials. *Catal. Sci. Technol.* **2015**, *5* (5), 2869–2879.

(12) Angelici, C.; Velthoen, M. E. Z.; Weckhuysen, B. M.; Bruijnincx, P. C. A. Effect of Preparation Method and CuO Promotion in the Conversion of Ethanol into 1,3-Butadiene over SiO 2 -MgO Catalysts. *ChemSusChem* **2014**, *7* (9), 2505–2515.

(13) Sushkevich, V. L.; Ivanova, I. I. Ag-Promoted ZrBEA Zeolites Obtained by Post-Synthetic Modification for Conversion of Ethanol to Butadiene. *ChemSusChem* **2016**, *9* (16), 2216–2225.

(14) Cheong, J. L.; Shao, Y.; Tan, S. J. R.; Li, X.; Zhang, Y.; Lee, S. S. Highly Active and Selective Zr/MCF Catalyst for Production of 1,3-Butadiene from Ethanol in a Dual Fixed Bed Reactor System. *ACS Sustain. Chem. Eng.* **2016**, *4* (9), 4887–4894.

(15) De Baerdemaeker, T.; Feyen, M.; Müller, U.; Yilmaz, B.; Xiao, F. S.; Zhang, W.; Yokoi, T.; Bao, X.; Gies, H.; De Vos, D. E. Bimetallic Zn and Hf on Silica Catalysts for the Conversion of Ethanol to 1,3-Butadiene. *ACS Catal.* **2015**, *5* (6), 3393–3397.

(16) Kim, T. W.; Kim, J. W.; Kim, S. Y.; Chae, H. J.; Kim, J. R.; Jeong, S. Y.; Kim, C. U. Butadiene Production from Bioethanol and Acetaldehyde over Tantalum Oxide-Supported Spherical Silica Catalysts for Circulating Fluidized Bed. *Chem. Eng. J.* **2014**, *278*, 217–223.

(17) Jones, M.; Keir, C.; Iulio, C.; Robertson, R.; Williams, C.; Apperley, D. Investigations into the Conversion of Ethanol into 1,3-Butadiene. *Catal. Sci. Technol.* **2011**, *1* (2), 267.

(18) Klein, A.; Palkovits, R. Influence of Structural Parameters on the Conversion of Ethanol into 1,3-Butadiene Using Mesoporous Zeolites. *Catal. Commun.* **2016**, *91*, 72–75.

(19) Dai, W.; Zhang, S.; Yu, Z.; Yan, T.; Wu, G.; Guan, N.; Li, L. Zeolite Structural Confinement Effects Enhance One-Pot Catalytic Conversion of Ethanol to Butadiene. *ACS Catal.* **2017**, *7* (5), 3703–3706.

(20) Telalović, S.; Ramanathan, A.; Mul, G.; Hanefeld, U. TUD-1: Synthesis and Application of a Versatile Catalyst, Carrier, Material…. *J. Mater. Chem.* **2010**, *20* (4), 642.

(21) Li, L.; Cani, D.; Pescarmona, P. P. Metal-Containing TUD-1 Mesoporous Silicates as Versatile Solid Acid Catalysts for the Conversion of Bio-Based Compounds into Valuable Chemicals. *Inorganica Chim. Acta* **2015**, *431*, 289–296.

(22) Lima, S.; Antunes, M. M.; Fernandes, A.; Pillinger, M.; Ribeiro, M. F.; Valente, A. A. Acid-Catalysed Conversion of Saccharides into Furanic Aldehydes in the Presence of Three-Dimensional Mesoporous Al-TUD-1. *Molecules* **2010**, *15* (6), 3863–3877.

(23) Maheswari, R.; Pachamuthu, M. P.; Anand, R. Copper Containing TUD-1: Synthesis, Characterization and Catalytic Behavior in Liquid-Phase Oxidation of Ethylbenzene. *J. Porous Mater.* **2012**, *19* (1), 103–110.

(24) Ramanathan, A.; Carmen Castro Villalobos, M.; Kwakernaak, C.; Telalovic, S.; Hanefeld, U. Zr-TUD-1: A Lewis Acidic, Three-Dimensional, Mesoporous, Zirconium-Containing Catalyst. *Chem. - A Eur. J.* **2008**, *14* (3), 961–972.

(25) Yan, W.; Ramanathan, A.; Patel, P. D.; Maiti, S. K.; Laird, B. B.; Thompson, W. H.; Subramaniam, B. Mechanistic Insights for Enhancing Activity and Stability of Nb-Incorporated Silicates for Selective Ethylene Epoxidation. *J. Catal.* **2016**, *336*, 75–84.

(26) Larina, O. V.; Kyriienko, P. I.; Soloviev, S. O. Ethanol Conversion to 1,3-Butadiene on ZnO/MgO-SiO2 Catalysts: Effect of ZnO Content and MgO:SiO2 Ratio. *Catal. Letters* **2015**, *145* (5), 1162–1168.

(27) Hayashi, Y.; Akiyama, S.; Miyaji, A.; Sekiguchi, Y.; Sakamoto, Y.; Shiga, A.; Koyama, T.; Motokura, K.; Baba, T. Experimental and Computational Studies of the Roles of MgO and Zn in Talc for the Selective Formation of 1,3-Butadiene in the Conversion of Ethanol. *Phys. Chem. Chem. Phys.* **2016**, *18* (36), 25191–25209.

(28) Toussaint, W. J.; Dunn, J. T.; Jackson, D. R. Production of Butadiene from Alcohol. *Ind. Eng. Chem.* **1947**, *39* (2), 120–125.

(29) Kyriienko, P. I.; Larina, O. V.; Soloviev, S. O.; Orlyk, S. M.; Dzwigaj, S. High Selectivity of TaSiBEA Zeolite Catalysts in 1,3-Butadiene Production from Ethanol and Acetaldehyde Mixture. *CATCOM* **2016**, *77*, 123–126.

(30) Bourgeat-Lami, E.; Fajula, F.; Anglerot, D.; Couriers, T. Single-Step Dealumination of Zeolite-Beta Precursors for the Preparation of Hydrophobic Adsorbents. *Microporus Mater.* **1993**, *1* (4), 237–245.

(31) Dumeignil, F.; PAUL, S.; Duhamel, L.; FAYE, J.; Miquel, P.; CAPRON, M.; Dubois, J. L. Dispositif d'évaluation d'au Moins Un Critère de Performance de Catalyseurs Hétérogènes. WO2015118263 A1, 2015.

(32) Patel, A. D.; Meesters, K.; den Uil, H.; de Jong, E.; Blok, K.; Patel, M. K. Sustainability Assessment of Novel Chemical Processes at Early Stage: Application to Biobased Processes. *Energy Environ. Sci.* **2012**, *5* (9), 8430.

(33) Lewandowski, M.; Babu, G. S.; Vezzoli, M.; Jones, M. D.; Owen, R. E.; Mattia, D.; Plucinski, P.; Mikolajska, E.; Ochenduszko, A.; Apperley, D. C. Investigations into the Conversion of Ethanol to 1,3-Butadiene Using MgO:SiO2 Supported Catalysts. *Catal.*

Commun. **2014**, *49*, 25–28.

(34) Da Ros, S.; Jones, M. D.; Mattia, D.; Pinto, J. C.; Schwaab, M.; Noronha, F. B.; Kondrat, S. A.; Clarke, T. C.; Taylor, S. H. Ethanol to 1,3-Butadiene Conversion by Using ZrZn-Containing MgO/SiO 2 Systems Prepared by Co-Precipitation and Effect of Catalyst Acidity Modification. *ChemCatChem* **2016**, *8* (14), 2376–2386.

(35) Geus, J. W.; van Dillen, A. J. Preparation of Supported Catalysts by Deposition-Precipitation. In *Preparation of Solid Catalysts*; Wiley-VCH Verlag GmbH: Weinheim, Germany, 2008; pp 460–487.

(36) Baylon, R. A. L.; Sun, J.; Wang, Y. Conversion of Ethanol to 1,3-Butadiene over Na Doped ZnxZryOz Mixed Metal Oxides. *Catal. Today* **2014**, *259*, 446–452.

(37) Dzwigaj, S.; Millot, Y.; Che, M. Ta(V)-Single Site BEA Zeolite by Two-Step Postsynthesis Method: Preparation and Characterization. *Catal. Letters* **2010**, *135* (3–4), 169–174.

(38) Da Ros, S.; Jones, M. D.; Mattia, D.; Schwaab, M.; Noronha, F. B.; Pinto, J. C. Modelling the Effects of Reaction Temperature and Flow Rate on the Conversion of Ethanol to 1,3-Butadiene. *Appl. Catal. A Gen.* **2017**, *530*, 37–47.

(39) Huang, X.; Men, Y.; Wang, J.; An, W.; Wang, Y. Highly Active and Selective Binary MgO–SiO 2 Catalysts for the Production of 1,3-Butadiene from Ethanol. *Catal. Sci. Technol.* **2017**, *7* (1), 168–180.

3.6. Supplementary Information

Figure 3.S1 Pore size distribution of synthesized samples

Figure 3.S2 Normalized NH_3-TPD profiles for ZnTa-TUD-1, ZnTa/deBEA and ZnTa/SiO_2

Chapter 4 Optimization of Zn-Ta-TUD-1 Synthesis

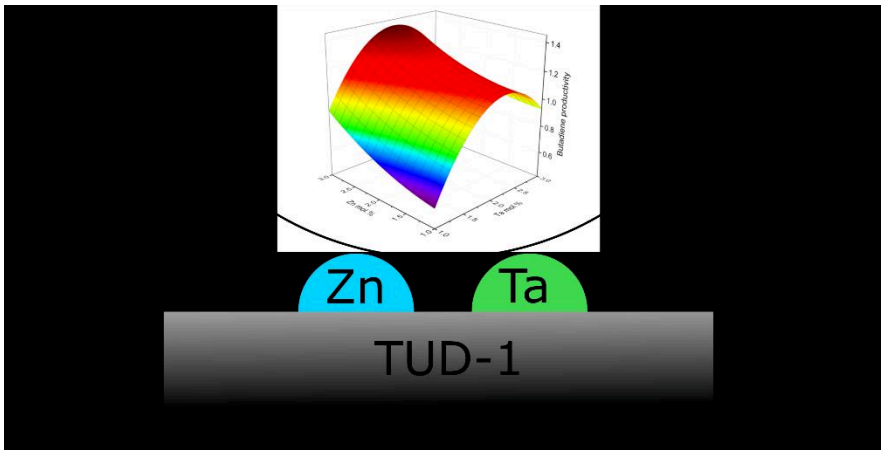

Abstract

The synthesis method of a zinc-tantalum catalyst supported on three-dimensional mesoporous silica with high specific surface area was studied. Its activity in the conversion of ethanol to butadiene was optimized using the Design of Experiment approach. A Plackett-Burman screening design identified the important preparation parameters, notably the ratio of Zn to Ta. It was subsequently optimized using the Response Surface Methodology, affording a highly active catalyst.

Preface

This chapter is based on the following manuscript: “Improving the BD productivity of Zn-Ta-TUD-1 using the Design of Experiments methodology” by Pomalaza, G., Capron, M., Dumeignil, F. which will be submitted to the Applied Catalysis A journal. Experiments and statistical interpretation were performed by Guillaume Pomalaza. The document was review by Mickaël Capron and Franck Dumeignil.

Motivation for this work stems from some issues encountered with the synthesis of Zn-Ta-TUD-1. Although the catalyst described in the previous chapter could be reproduced, the synthesis method was found to be highly sensible to various parameters, making the tuning of its properties difficult. One notable issue was the unwanted recurrent precipitation of the metal salts during the addition of the alkaline agent as part of the sol-gel synthesis. To ensure a reproduceable and practical preparation method, the following study was performed. This way, an optimal catalyst could be synthesized and used for further investigation

4.1. Introduction

The Lebedev process, the conversion of ethanol to 1,3-butadiene (BD), is being considered as a sustainable alternative to hydrocarbon steam cracking. The latter which currently produces 95% of BD—the world's most consumed diolefin.[1–6] Not only does the Lebedev process use a widely available feedstock derivable from biomass, it is also much more selective towards BD than steam cracking.[1] Selectivity comes into play when considering the purity needed by polymerization catalytic processes used to synthesize rubber from BD.[5–7] However, to financially compete with fossil-based routes, the Lebedev process requires—amongst other things—better performing catalysts.[8,9]

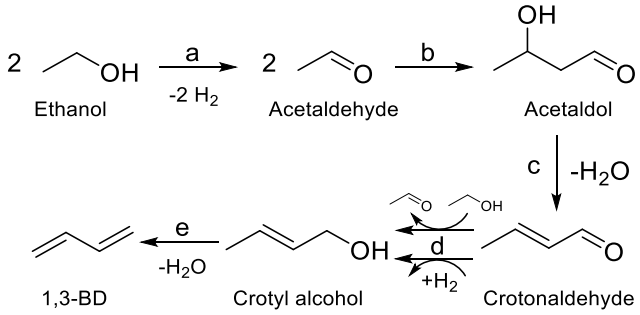

Figure 4.1 Generally accepted mechanism for the conversion of ethanol to 1,3-butadiene. Reaction steps: (a) ethanol dehydrogenation; (b) aldol condensation of acetaldehyde; (c) acetaldol dehydration; (d) MPVO reaction; (e) crotyl alcohol dehydration.

Silica-supported metal and metal oxide mixtures have demonstrated high catalytic activity in the Lebedev process [1,4]. Their performances are owed to the multi-functionality provided by the combination of different metals or metal oxides, each possessing complementary chemical properties required to catalyze the multi-step ethanol-to-butadiene reaction (Figure 4.1). A balance between these properties has been cited as the key to maximizing BD production.[10] We found through a preliminary rough screening study (not published) that silica-supported Zn and Ta yielded the largest amount of BD compared with the other transition metals tested, *e.g.*, Al, V, Cu, Ga, Zr, Nb,Hf, La, and Ce. In addition, catalyst structural properties have been linked to superior catalytic activity in the Lebedev process: high active phase dispersion [11–15], large specific surface areas,[15,16] three-dimensional mesoporous morphology[8,11,17] were all found to improve catalytic performances in metrics such as BD productivity, BD selectivity and resistance to coke deactivation.

In the present work, we sought to improve the performances of the Lebedev process by tuning the synthesis of catalysts possessing the important physical and chemical properties mentioned above. To do so, the procedure developed at the Delft University of Technology to synthesize mesoporous silica (TUD-1) was used.[18] TUD-1 materials have a three-dimensional sponge-like mesoporous morphology and many advantages over conventional mesoporous catalyst carriers.[19,20] They boast a simple, yet cost-effective one-pot synthesis based on the sol-gel process, with tunable pore size and specific surface area, ranging from 2 – 50 nm and 400 – 1000 m^2/g, respectively. TUD-1 materials are also reported to have a high hydrothermal stability, which suits them well for processes involving the dehydration of alcohol at high temperature. Furthermore, metals are easily introduced and dispersed within the silica framework with minor adaptation of the preparation procedure.[20] A key component of the TUD-1 synthesis is the addition of an organic chelating agent during the sol-gel process: it forms complexes of the metal and silica precursors, insuring their homogeneous dispersion throughout the preparation by preventing cluster formation; it also acts as a structure-directing agent to produce the sponge-like morphology when the silica precursor condenses during thermal treatment of the gel.[20,21] Catalysts with a highly dispersed active phase, a large specific surface area and a mesoporous morphology for the Lebedev process can thus be obtained. However, despite its simplicity, the TUD-1 preparation procedure needs to be treated carefully: the effects of several synthesis parameters are unclear in the literature, which may cause unexpected result when scientists attempt to adapt the method for their own purposes. Furthermore, authors working with TUD-1 sometimes omit to justify their preferences when adapting the synthesis method. One instance we encountered was the use of tetraethyl ammonium hydroxide (TEAOH) as an alkalizing agent during the sol-gel process. Although descripted as optional in the original paper by Jansen et al. [18] most scholars resort to it, undoubtedly due to its role as gelation catalyst. However, the quantity in relation to silica precursor amount appears to arbitrarily change from one publication to another [19,22,23]. Parameters we found to change depending on the publication were the calcination method[22,24] and solvent used,[19,22,25–27] amongst other.

The objective of our work was thus two-fold: to prepare a catalyst Zn-Ta-TUD-1 catalyst highly active in the Lebedev process, as well as sorting and understanding the effect of certain synthesis variables on the morphology of bimetallic TUD-1. These goals were achieved using a Design Of Experiment (DOE) methodology combined with mathematical and statistical

techniques which allow the modeling of dependent responses to the independent variables of a process. Such models can be used for process optimization, but also for statistical interpretation in order to study the influence exerted by each independent variable on the selected response. First, a Plackett-Burman (PB) experimental design was used to identify important variables of the Zn-Ta-TUD-1 synthesis and their impact on BD productivity, specific surface area and pore size. It is a two-level factorial design of experiment that allows the screening of $n - 1$ factors in a maximum of n experiments, where n is the number of runs and a multiple of four.[28,29] This highly economical design is ideal for studying processes that are expensive or time-consuming, but comes at the cost of screening resolution, meaning only the main effects of each variables can be calculated. With a better understanding of the Zn-Ta-TUD-1 synthesis, the catalyst was further optimized for BD productivity using a three-level factorial design of experiment combined with the response surface methodology (RSM), a mathematical-statistical technique used in engineering for experiment design and process optimization.[28,30–32] In this case, only two independent variables were selected—Zn and Ta concentration in the catalyst—enabling a more descriptive study of their effect on BD productivity. Catalytic testing and characterization of the morphological properties were performed to gather the experimental data needed for empirical modelling.

4.2. Materials and Methods

4.2.1. Reagents and Materials

For the synthesis of Zn-Ta-TUD-1, two sources of each metal were used alternatively: tantalum chloride (Alfa Aeser, 99.8%) or optical grade tantalum ethoxide (Alfa Aeser, 99.95%), and zinc chloride (Acros Organics, 97+%) or zinc acetate dehydrate (Acros Organics, 98+%). Two different chelating agents were used: triethanol amine (or $TEAH_3$, Acros Organic, 99+%) or tetraethylene glycol (or TEG, Agros Organics, 99.5%). Tetratethyl orthosilicate, (or TEOS, Agros Organics, 98%) was the silica precursor. Tetraethyl ammonium hydroxide (or TEAOH, Aldrich, 35 wt. % in water) was used as the alkalizing agent to catalyze gelation. Ethanol (Aldrich, 99.8%) was used as the solvent for the synthesis and as reactant during catalytic testing.

Thermal treatment of the dried gel was performed in a 35 mL PTFE-lined autoclave from the Parr Instrument Company. Calcination under air flow was done in a quartz tubular reactor and under static air in a muffled oven.

4.2.2. Characterization

Catalyst structures were characterized with nitrogen physisorption experiments at -196 °C using a Micromeritics Tristar II instrument. Prior to analysis, 50–200 mg of catalyst were outgassed under vacuum at 150 °C for 6 hours. Specific surface area (S_{BET}) was calculated with the Brunauer–Emmett–Teller (BET) method. The Barret-Joyner-Halenda model was used to calculate the pore diameter (D_p) distribution using the desorption isotherm.

Transmission electron microscopy (TEM) was used to characterize the microstructure of selected Zn-Ta-TUD-1 samples with a FEI Tecnai G2 transmission electron microscope operated at 200 kV.

4.2.3. Catalytic Testing

Ethanol conversion was performed with a Multi-R® apparatus from Teamcat Solutions SAS,[33] which is a high-throughput equipment for heterogeneous catalyst screening. Four glass reactors can be used simultaneously, with the gaseous feed being calibrated to ensure an equal inlet flow using a splitter; the reactor outputs were analyzed with an online Agilent 7890 A equipped with an FID detector. An independently controlled valve enables selecting the output of each reactor for analysis.

Catalyst testing was performed at 350 °C and a pressure of 1 atm. Each catalyst was ground and sieved to 120 mesh granules, 30 mg of which were loaded in glass reactors and kept in place with SiC. To feed the reactors with ethanol, He was used as a carrier gas. It was passed through a bubbler containing ≥99.8 % ethanol, set at pressure and temperature to afford vapor concentration of 4.5% according to the Antoine's law. Weighted hourly space velocity of ethanol ($WHSV_{EtOH}$) was set to5.3 h^{-1} by adjusting the inlet flow and catalyst mass.

Ethanol conversion (X, %), the selectivity towards each product (S_i, %), the molar yield of each product (Y_i, %) and the productivity in butadiene (P_{BD}, $g_{BD} \cdot g_{cat}^{-1} \cdot h^{-1}$) were used to describe catalytic activity—equation 1, 2, 3,and 4 respectively, where c_i represents the number of carbon moles measured for a given compound i. These values were recorded after 1 hour on stream, after

initial stabilization of the reactor output. The carbon balance (CB) for each test was calculated by dividing the sum of carbon moles detected with the molar amount of carbon introduced as ethanol and found to range between 95 – 105 %.

$$X = \frac{c_{EtOH,in} - c_{EtOH,out}}{c_{EtOH,in}} \cdot 100 \quad (1)$$

$$S_i = \frac{c_{i,out}}{c_{EtOH,in} - c_{EtOH,out}} \cdot 100 \quad (2)$$

$$Y_i = X \cdot S_i \quad (3)$$

$$P_{BD} = X \cdot S_{BD} \cdot WHSV_{EtOH} \cdot 0.587/100 \quad (4)$$

4.2.4. General Zn-Ta-TUD-1 Synthesis

The default TUD-1 preparation method was inspired by the work of Pescarmona et al.[26,34,35] However, we substituted 2-propanol—the original solvent—by ethanol as the former failed to adequately dissolve some metal precursors. In a typical synthesis, TEOS and the metal precursors were added to 30 mL of ethanol under vigorous stirring at room temperature. After obtaining a clear solution, the chelating agent was added dropwise while stirring; if $TEAH_3$ was used, it was first dissolved in water with 1:11 molar ratio. The mixture was left to stir for 1 hour, resulting in a clear solution. TEAOH, 35 wt.% in water, was added dropwise to the clear solution under vigorous stirring. During this step, the solution quickly became white and opaque, before returning to a clear, colorless solution, which was further stirred for 2 hours. This sol was left to age for 24 hours, resulting in gelation. The obtained gel was dried overnight at 100 °C, resulting in a solid, transparent xerogel with varying shades of dark orange. It was gently ground to a fine powder and placed in a Teflon-lined autoclave for a thermal treatment at 180 °C during 6 to 48 hours. The ensuing solid—a sticky power reminiscent of brown sugar—was calcined at 600 °C for 10 hours.

4.2.5. Plackett-Burman Screening Study

XLstat, an add-on for the Microsoft Excel® software, was used to generate the Plackett-Burman design used for studying the effects of the synthesis parameters on the properties and activity of Zn-Ta-TUD-1 and analyze the responses obtained experimentally (Table 4.13). XLstat can model the effect of each parameter (also known as variable or factor) of a given response by

fitting a first-order polynomial function of the studied parameters (equation 5) with the experimental response

$$Y_j = \beta_0 + \sum_{i=1}^{k} \beta_i \cdot X_i + \varepsilon \qquad (5)$$

where Y_j is the fitted response, β_0 the model intercept, β_i is the linear coefficient of independent variable i with X_i its level, k the number of involved variables, and ε the residual error. Equation 5 was solved using the least square method, which is a multiple regression technique that fits mathematical models to experimental data by minimizing the value of residuals between experimental and fitted responses. Quality of fit and model significance were established by the coefficient of determination (R^2) and Fischer's F-test, respectively. The obtained statistical results showed the medialization to be statistically acceptable for further study.

Table 4.13 Plackett-Burman experimental design used for studying the main effects of Zn-Ta-TUD-1 synthesis variables.

Run no.	Cat. name	Variable											Responses		
		Zn:Ta	Si:M	ThTr	TaPr	ZnPr	ChAg	Alk:Si	ChOrd	StiDW	CalcM	CalcR	Y_{PBD}	Y_{SBET}	Y_{Dp}
1	PB1	+	+	-	+	+	+	-	-	-	+	-	0.583	341	18.7
10	PB2	-	+	+	-	+	+	+	-	-	-	+	1.089	336	25.3
11	PB3	+	-	+	+	-	+	+	+	-	-	-	0.644	424	28.3
2	PB4	-	+	-	+	+	-	+	+	+	-	-	1.139	747	3
6	PB5	-	-	+	-	+	+	-	+	+	+	-	0.748	516	7
4	PB6	-	-	-	+	-	+	+	-	+	+	+	0.753	228	25.11
5	PB7	+	-	-	-	+	-	+	+	-	+	+	0.669	401	26
3	PB8	+	+	-	-	-	+	-	+	+	-	+	0.745	505	15.9
7	PB9	+	+	+	-	-	-	+	-	+	+	-	0.640	486	12.6
8	PB10	-	+	+	+	-	-	-	+	-	+	+	0.912	601	11.9
9	PB11	+	-	+	+	+	-	-	-	+	-	+	1.181	740	6.6
12	PB12	-	-	-	-	-	-	-	-	-	-	-	1.602	739	10.7

Variable signification: Zn:Ta, the zinc-to-tantalum molar ratio; Si:M, the silica-to-total-metal ratio; ThTr, the thermal treatment time; TaPr, nature of the Ta precursor; ZnPr, nature of the Zn precursor; ChAg, nature of the chelating agent; Alk:Si, the TEAOH-to-Si ratio; ChOrd, the order of chelation; StiDW, Dropwise addition of TEAOH with stirring; CalcM, calcination method; CalcR, calcination ramp.

The effect of each variable was judged according to their statistical significance, which was assessed with an analysis of variance (ANOVA) performed with XLstat. For each response, this required transforming three of the eleven variables into 'dummy' variables to reach the minimum variable-to-observation ratio required for statistical analysis. Variables were considered 'dummy' when the contribution of their coefficient to the response model was less than 1%. The ANOVA afforded standardized main effects of variables, which are t-statistics that test the null hypothesis, *e.g.*, that the effect of a variable on the response is 0.

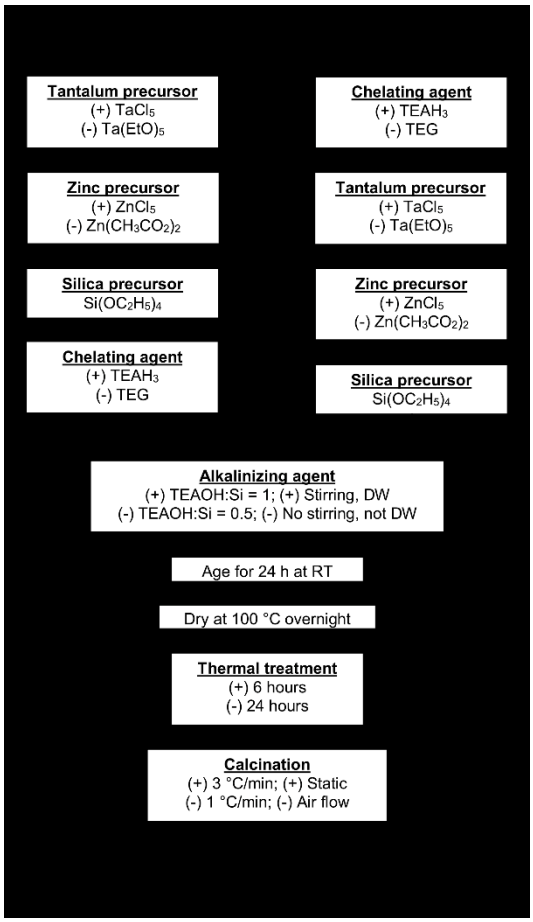

Figure 4.2 Preparation scheme of Zn-Ta-TUD-1; (+) and (-) signs represent the levels of the Plackett-Burman experimental design.

BD productivity (Y_{BD}) was chosen as the first response to model due to its industrial importance.[2,36] BET specific surface (Y_{SBET}) and average pore diameter (Y_{Dp}) were selected as responses due to their importance as morphological properties of catalyst carriers. The choice of synthesis variables was based on the literature concerning both the Lebedev process and TUD-1 catalysts, as well as preliminary experiments (not shown). The Zn-to-Ta (Zn:Ta) and total Si-to-metal molar ratios (Si:M) in the precursor gel were selected due to the reported importance of balanced active phases in catalysts for the Lebedev process.[10,13,16,37–39] The nature of the metal precursors, was reported as influential on TUD-1 morphology,[19] but also on activity in the Lebedev process.[40] In this case, zinc chloride and zinc acetate hydrate were selected as levels for the zinc precursor parameter (ZnPr). Tantalum chloride and tantalum ethoxide were chosen as tantalum precursors (TaPr). Thermal treatment (ThTr) duration is reported as an important TUD-1 synthesis parameter because of its influence on morphology.[20–22] The TEAOH-to-Si mole ratio

in the precursor gel (Alk:Si), the type of chelating agent (ChAg) and the choice of calcination method (CalcM) were selected due to the ambiguity in the literature regarding their influence. For instance, TEAOH is described as optional,[18] yet is used in most publications, without an optimal ratio being reported.[19,22,23] The calcination temperature ramp (CalcR) and the need for a drop-wise addition of TEAOH under vigorous stirring (StiDW) were investigated as potential time-saving measures. The order by which the chelating agent was added to the precursor solution (ChOrd) with regards to the metal precursor was also investigated out of curiosity. Figure 4.2 illustrates the Zn-Ta-TUD-1 synthesis methods used in the PB experiment, as well as the different levels of all parameters with the exception Zn:Ta and Alk:Si.

Table 4.14 Level of variables in the Plackett-Burman experiment of Zn-Ta-TUD-1 synthesis

Variable	Unit	Symbol	-	+
Zn-to-Ta ratio	n/a	Zn:Ta	2	5
Silica-to-metal ratio	n/a	Si:M	16	8
Thermal treatment duration	Hour	ThTr	6	24
Nature of Ta precursor	n/a	TaPr	$Ta(EtO)_5$	$TaCl_5$
Nature of Zn precursor	n/a	ZnPr	$Zn(CH_3CO_2)_2$	$ZnCl_5$
Nature of chelating agent	n/a	ChAg	TEG	$TEAH_3$
TEAOH-to-Si ratio	n/a	Alk:Si	0.5	1.0
Order of chelation addition step	n/a	ChOrd	Before metal	After metal
Dropwise addition of TEAOH with stirring	n/a	StiDW	No	Yes
Calcination method	n/a	CalcM	Under air flow	Under static air
Calcination temperature ramp	°C/min	CalcR	1	3

Choosing the two levels of each factor, represented by + and – in Table 4.13, was largely a matter of preliminary experimentation with the TUD-1 and the result of our unpublished screening study previously mentioned. Table 4.14 lists the levels of each variable investigated in the Zn-Ta-TUD-1 synthesis; Figure 4.2 illustrates these levels in relation to the Zn-Ta-TUD-1 preparation procedure. Experiments were performed in random order to minimize errors and biases.

4.2.6 Response Surface Methodology

RSM is a technique that encompasses multi-variant experimental design, statistical modelling and process optimization. It is generally performed in three steps: (1) DOE, (2) response surface modelling through regression and (3) optimization of the response.[41] The XLstat software was used for all three steps. RSM was used to optimize the productivity in BD (Y_{PDB}) by establishing its relationship to two independent variables: Zn and Ta molar content in Zn-Ta-TUD-1, Zn mol.% and Ta mol.% respectively. The variables were selected after the PB screening study

showed that the Zn:Ta molar ratio had a significant effect on the activity of the catalyst. In addition, the Zn-Ta-TUD-1 preparation method used corresponded to the best performing procedure identified by screening, which was equivalent to that used for sample PB12 in Table 4.13.

Table 4.15 Three-level factorial design and corresponding levels of variable for the optimization of Zn-Ta-TUD-1 preparation to maximize butadiene productivity and the corresponding experimental responses.

Run no.	Catalyst name	Variable				Y_{PBD} ($g_{BD}g_{cat}h^{-1}$)
		Ta mol.%		Zn mol.%		
2	RSM1	-1	1 %	-1	1 %	0.555
5	RSM2	0	2 %	-1	1 %	1.048
4	RSM3	1	3 %	-1	1 %	0.978
9	RSM4	-1	1 %	0	2 %	0.715
7	RSM5	0	2 %	0	2 %	1.188
8	RSM6	1	3 %	0	2 %	0.939
1	RSM7	-1	1 %	1	3 %	0.849
6	RSM8	0	2 %	1	3 %	1.456
3	RSM9	1	3 %	1	3 %	1.150

For a single-response, two-variable experiment, a three-level full factorial design was found suitable, as it did not require many experiments, yet provided a reasonable amount of information.[32] The three levels used were symbolized by -1, 0, 1. Table 4.15 lists the experimental design, the corresponding experimental values for each level and the Y_{PBD} response obtained via catalytic testing. Experiments were performed in random order to minimize errors and biases.

Response surface modelling was performed by an empirical quadratic model of the response (Equation 6) to the experimental data using the least square root method.

$$Y_j = \beta_0 + \sum_{i=1}^{k} \beta_i \cdot x_i + \sum_{i=1}^{k} \beta_{ii} \cdot x_i^2 + \sum_{i<j}^{k} \beta_{ij} \cdot x_i \cdot x_j + \varepsilon \qquad (6)$$

where Y_j is the fitted response, β_0 the model intercept, β_i is the linear coefficient of independent variable i with x_i its input factor, and k the number of involved variables, β_i is the quadratic coefficient of variable i, β_{ij} is the linear interaction coefficient between variable i and j, and ε the residual error. Goodness of fit of the model was evaluated with R^2 and its significance with Fischer's F-test. Contrarily to the modelling used in the PB experiment, the introduction of second-order terms allows the study of variable interaction effects. The relevance of each coefficient was judged according to the t-statistics resulting from an ANOVA.

Optimization, *e.g.*, finding the variable level providing the theoretical maximum response, was performed using the method of steepest ascent, which is available due to the model being limited to a single response.[28]

4.3. Results and Discussion

4.3.1. Plackett-Burman Screening

4.3.1.1. Statistical Interpretation

The coded value of experimental points representing the variables of the Zn-Ta-TUD-1 synthesis and the corresponding responses are listed in Table 4.13. For each response—BD productivity, BET surface area and average pore diameter—a first-order polynomial equation was generated and fitted to the experimental data. Accuracy of fit and F-test results (Table 4.S1) indicate that all three models explain >94% of the response variation and are overall significant at 95% confidence level. An association test of the studied responses with Pearson-type correlation was performed at 95% confidence level. The correlation matrix can be found in Table 4.S1.

The calculated linear coefficient β_i of every independent variable i can be used to estimate their influence on each response. A more rigorous interpretation considers the standardized main effects, which are the t-values of variable effects computed with the ANOVA of the models.[29] Two criteria were used to judge the importance of each variable: the t-value limit at confidence level of 95% (α = 0.05) and the Bonferroni limit, which tests the null hypothesis at more conservative confidence level.[29] Factors with standardized effects above the t-value limit were interpreted as likely to be significant; above the Bonferroni limit, variables were considered significant.[29,42] Below the t-value limit, variables were deemed unlikely to be significant.

Pareto charts of standardized effects are simple bar charts, but a useful visualization tool to quickly interpret the results of factorial screening studies through. By plotting the t-value and Bonferroni limits, the significant of each variable of the Zn-Ta-TUD-1 synthesis can be easily assessed. The length of each bar also indicates the relative weight of each variable. The effects each experimental level of the synthesis parameters had on the responses were also considered. For a given response, dashed bars indicate that the low level (–) of the parameter afforded the greater response value comparatively. Contrarily, dash-less bars indicate that the high level (+)

gave a higher response. Pareto charts of standardized effects of Zn-Ta-TUD-1 synthesis on BD productivity, S_{BET} and Dp are illustrated in Figure 4.3.

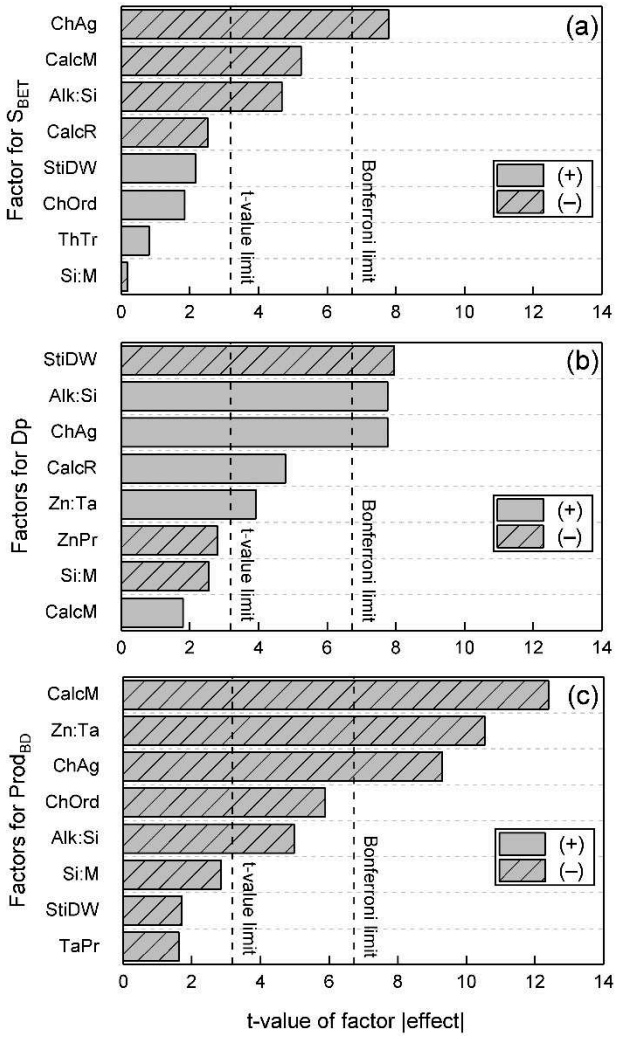

Figure 4.3 Pareto chart of standardized effects each TUD-1 synthesis has on the selected responses: (a) butadiene productivity; (b) BET specific surface area; (c) Average pore diameter. In comparing both levels, dashed bars indicate that the low level of the parameter gave the highest response; dash-less bars indicate the high level resulted in the highest response.

4.3.1.2. Zn-Ta-TUD-1 Morphology

The results of N_2 porosimetry with the catalysts prepared according to the PB design are listed in Table 4.13. These confirm the formation of mesoporous materials with high surface area. As Table 4.13 indicates, BET specific surface area (Y_{BET}) ranged between 228 and 747 m^2g^{-1} and

average pore diameter (Y_{Dp}) varied between 3.0 and 25.1 nm. This degree of irregularity in terms of morphological properties is consistent with the high tunability of TUD-1 materials.

In the original paper introducing the TUD-1 synthesis procedure, Jansen *et al*. explained how the mesoporous morphology could be tuned.[18] By adjusting the thermal treatment duration of the silica xerogel, pore diameter and specific surface area could be modified, with the value of each characteristic being inversely proportional to one another as a function of time—lengthening treatment time reducing specific surface area and increasing mesopore size. Similar observations were made with metal-containing TUD-1 materials when time was the only synthesis variable.[21]

The xerogel is an organic-inorganic hybrid in which the chelating agent and its metal complexes are homogeneously dispersed.[21] Upon heating, silica particles grow and organic species agglomerate, shaping the mesoporous framework by steric hindrance. In theory, lengthening the heating period promotes the organic agglomeration,[43] resulting in larger, but fewer agglomerates for silica to condense around. The morphological consequence of this phenomenon is larger pores, but a reduced specific surface area. This trade-off between the two morphological properties as a result of thermal treatment time is well established.[18,20,43]

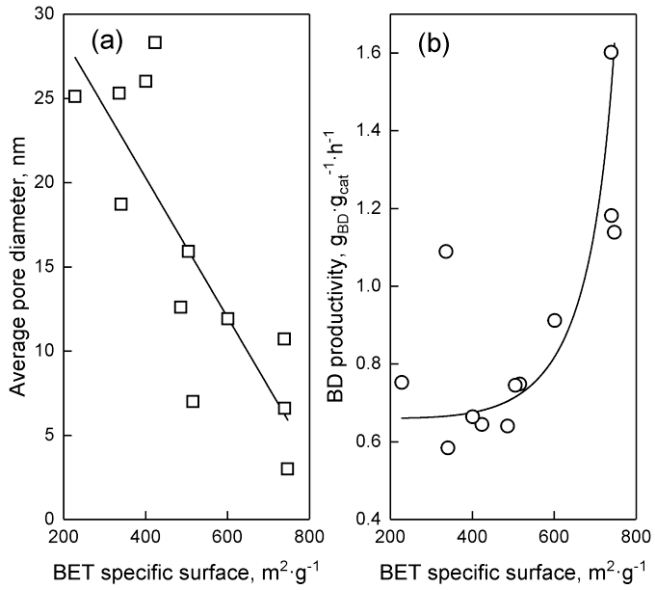

Figure 4.4 Relationship between BET specific surface area and (a) the average pore diameter, (b) BD productivity of PB series of catalysts.

Surprisingly, the statistical analysis of the effects exerted by the 11 variables of the Zn-Ta-TUD-1 synthesis under study (Figure 4.3) found thermal treatment time not to influence BET

specific surface area or the average mesopore size. Nevertheless, the association test () indicated a strong inverse correlation between the two morphological properties. In other words, the trade-off between surface area and pore size typical of TUD-1 still took place but was the subject of variables other than thermal treatment time. Figure 4.4 (a) illustrates this relationship. The type of chelating agent and TEAOH:Si ratio in the precursor gel were identified as statistically significant variables influencing both morphological properties. According to the literature, $TEAH_3$ and TEG play the identical dual role of precursor chelating and structure directing agents, with the former being the predominant choice in TUD-1 synthesis.[20] However, no study could be found that directly compared both molecules. Interestingly, TEG led to larger specific surface area and $TEAH_3$ to larger pores. This is consistent with the fact the latter has a larger molar volume than TEG, both when determined empirically at 25 °C and using Connolly's molecular surface package.[44] since equimolar amounts were used in the synthesis of Zn-Ta-TUD-1. Incidentally, greater quantities of TEAOH—used for catalyzing the gelation process and introduce micropores within the framework—was correlated with bigger pore diameter at the expense of surface area, although no micropores could be detected by N_2 porosimetry. The additional organic matter within the precursor gel likely increases the size of structure-shaping agglomerates during the thermal treatment. Consequently, the use of TEOH should be limited to gelation catalysis, as its structure-directing properties could be fulfilled by the less expensive, safer chelating agents.

Other synthesis variable studied showed significant effect on the morphological properties of Zn-Ta-TUD-1 (Figure 4.3). However, these were not reciprocal between both responses studied. Considering the inverse correlation observed, two possibilities main explain this discrepancy: these variables exclusively affected one of the morphological properties independently of the other; interaction effects between variables also influencing TUD-1 morphology could not be estimated due to the low degree of freedom of PB designs.[28] The most important synthesis parameter identified to only affect pore size was the TEAOH addition procedure during the sol-gel process. Most authors indicate TUD-1 should be prepared by adding TEAOH drop-wise under vigorous stirring and left stirring for up to two hours until a clear gel is obtained. Surprisingly, directly pouring TEOH consistently afforded a clear colorless gel, whereas the traditional method occasionally resulted in milky mixtures, which have been observed elsewhere.[23,43] In the sol-gel methodology, the basic catalyst feed rate controls the silica precursor hydrolysis and

condensation kinetics; higher feed rates have been associated to faster particle growth.[45] Consequently, the influence of the TEAOH addition method on the morphology of Zn-Ta-TUD-1 may be owed to the change in gelation kinetics it induces. Why this effect is statistically significant only for the average pore diameter remains to be answered.

4.3.1.3. BD productivity

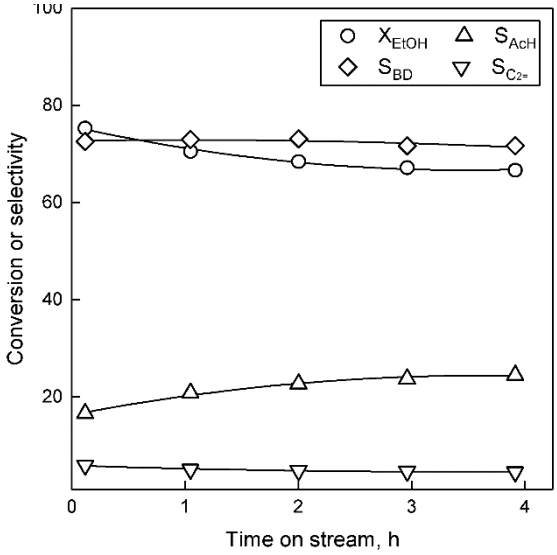

Figure 4.5 Conversion and selectivity towards major products of ethanol conversion on PB12 over time. T = 350 C, P = 1 atm, $WHSV_{EtOH}$ = 5.3 h^{-1}. EtOH: ethanol. AcH: acetaldehyde. $C_{2=}$: ethylene.

The catalytic performances of Zn-Ta-TUD-1 catalysts prepared according to PB design varied significantly in terms of productivity (Table 4.15). In a typical test, ethanol was converted to predominantly three products: BD, acetaldehyde and ethylene; 1–3 % yield consisted of diethyl ether, propylene, 1-butanol and butenes. Selectivity towards the three main products depended on the catalyst used. The best performances were achieved with PB12: its activity is depicted in Figure 4.5. As illustrated, BD selectivity reached 70%, a value comparable to many of the best catalysts found in the literature.[4] Although BD selectivity remained stable, deactivation took place, as evidenced by the decreasing ethanol conversion. Nevertheless, remarkable BD productivity was achieved.

As previously indicated, several authors have associated the morphology of studied materials and their performances in the Lebedev process.[8,11,16,17] Association tests of BD productivity with specific surface area and average pore diameter were performed. Accordingly, a Pearson-type

correlation between BD productivity and specific surface area at 95% confidence interval was found (**Error! Reference source not found.**); although statistically significant, it is unlikely that t he correlation is linear, as a better fit was found with a quadratic equation (Figure 4.4 (b)). Similar correlations have been reported by other scholars for this reaction.[16] In fact, it is well-established that greater surface area allows for a better accessibility to active sites and is often considered a desirable feature of catalysts. Contrarily to Jones et al.[8] and Palkovits et al.[17] who reported improvements in BD yield with increasing pore size, no correlation could be found between the average pore diameter and BD productivity on Zn-Ta-TUD-1. This can be explained by the trade-off between S_{BET} and Dp mention in section 4.3.1.2.: the benefits of greater pore size may be cancelled due to the loss in specific surface area, suggesting the latter to be the most important morphological property of the two for maximization BD formation. Consequently, it is unsurprising that two of the most influential factors on S_{BET}, the nature of the chelating agent and the calcination method, were also statistically significant on BD productivity, as depicted by Figure 4.3 (c).

The only factor with no impact on TUD-1 morphology, but significantly influential on BD productivity was the Zn-to-Ta molar ratio. Zinc oxide is well-established for catalyzing the dehydrogenation of ethanol and tantalum oxide can perform the conversion of ethanol-acetaldehyde mixtures of BD. However, many authors have reported that a subtle balance must be struck between the dehydrogenating and condensation promoters, as the active sites are also known to catalyze undesirable side-reaction. This theory is given statistical evidence through the results of our PB screening. The fact that the Zn-to-Ta molar ratio was statistically insignificant on synthesis procedure with regards to the resulting morphological properties further indicates that it is solely attributable to the chemical properties of Zn-Ta-TUD-1.

Further increase in BD productivity proceeded by tuning the synthesis of Zn-Ta-TUD-1. Of all significant preparation parameters identified by the PB design experiment, the Zn-to-Ta ratio was selected for the RSM experiment. To accommodate a two-variable design, Zn-to-Ta was split into the molar amount of each element, thereby providing information of the effect of low metal content. All other variables were set to their low-level setting, as Figure 4.3 shows them to improve BD productivity. Incidentally, this corresponds to the procedure used to synthesize PB12, except for the ratio and amount of Zn and Ta.

4.3.2. Response Surface Methodology

4.3.2.1. Statistical Interpretation

The obtained response listed in Table 4.15 was correlated with independent variables Zn mol.% and Ta mol.% using the quadratic equation, Eq. (6). The least square regression method was used to fit the experimental data to Eq. (6), resulting in the model below:

$$Y_{PBD} = 1.191 + 0.146 \cdot X_1 + 0.156 \cdot X_2 + 0.059 \cdot X_1^2 - 0.366 \cdot X_2^2 - 0.031 \cdot X_1 \cdot X_2 \quad (7)$$

where X_1 is Zn mol.% and X_2 is Ta mol.%. Validity of the model was tested through statistical means (Table 4.S2**Error! Reference source not found.**). The coefficient of determination and its adjusted form, 0.971 and 0.924, respectively, showed that the experimental results were well represented by the model. ANOVA of the model indicated an F-value of 20.347 and a p-value below 0.05; theses statistical results demonstrated the significance and adequacy of the model.

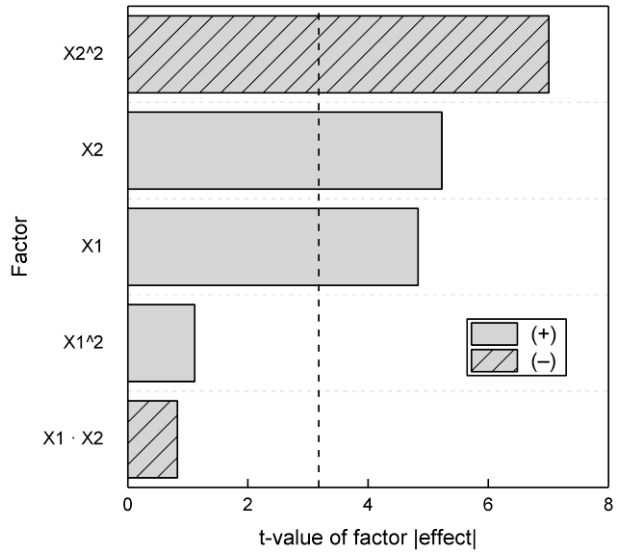

Figure 4.6 Pareto chart of the standardized main and interaction effects the Zn and Ta content have on the BD productivity of Zn-Ta-TUD-1. X1 = Zn mol.%; X2 = Ta mol.%. In comparing both levels, dashed bars indicate that the low level of the parameter gave the highest response; dash-less bars indicate the high level resulted in the highest response.

The importance of each factor on the response (BD productivity) was assessed by comparing their standardized effect to the minimum t-value at 95% confidence interval. The Pareto chart depicted in Figure 4.6 reveals the most important factors. The main effect of Zn and Ta content were found to be important, naturally suggesting both elements contribute to the catalytic activity of Zn-Ta-TUD-1. However, no interaction effect could be discerned between the two variables;

this implies Zn and Ta—although both required for forming BD—do not have a synergy effect that can be discerned using our quadratic model. Only the squared effect of Ta loading was significant, but also negative. This can be interpreted as a non-linear detrimental effect of Ta mol.% on BD productivity.

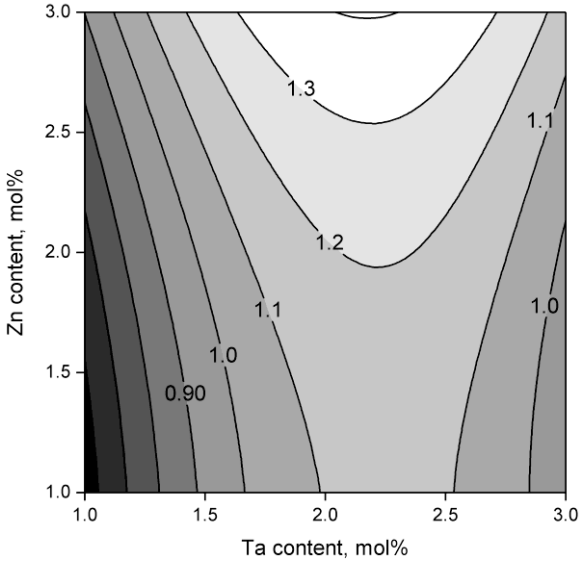

Figure 4.7 Contour plot obtained by the RSM representing BD productivity versus Zn and Ta loading in TUD-1. BD productivity increases from dark to light on the gray scale. Reaction conditions: 350 °C, $WHSV_{EtOH}$ of 5.3 h^{-1}, TOS of 1 h.

The two-dimensional contour plot of BD productivity corroborated with Zn and Ta loading is shown in Figure 4.7; it is the visual representation of the quadratic response model, Eq. 7. A noticeable plateau effect with regards to the Ta loading can be deduced from its shape.[32] reflecting the squared negative effect noted above. A linear relation between BD productivity with Zn content within the experimental region can also be observed. The method of steeped ascent indicated BD productivity can be maximized with a catalyst containing 3 mol.% of Zn and 2.2 mol.% of Ta. However, the elliptical shape of the response maxima suggests the true optimal value to be outside the experimental region with regards to Zn content. Incidentally, PB12—synthesized for the screening experiment with a loading of 4 mol.% Zn and 2.1 mol.% Ta—showed a BD productivity of 1.60 $g_{BD}.g_{cat}^{-1}.h^{-1}$. Consequently, the optimal Zn-Ta-TUD-1 catalyst should have a Zn content between 3 and 4 mol.%. Ta content between 2 and 2.2 mol.% was found optimal with the method of steepest ascent. This amounts to a Zn-to-Ta ratio between 1.5 and 2.

4.3.2.2. RSM Series Characterization

The TUD-1 preparation has been described as an easy way to homogeneously disperse metals within a mesoporous silica framework.[20] Optimization of Zn-Ta-TUD-1 synthesis to maximize its activity in the Lebedev process afforded highly active materials. To verify that the materials prepared were comparable to those found in the literature, thereby confirming the success of the synthesis method used, characterization was performed.

N_2 porosimetry results (Table 4.S3) indicated the final Zn-Ta-TUD-1 method afforded materials with an average BET surface area of 661±41 $m^2 \cdot g^{-1}$, indicative of its repeatability. Average pore size diameter of 9.8±1.5 nm was obtained, with an outlier at 7.0 nm. Interestingly, no correlation between BET surface area and activity could be observed. This suggested the metal content becomes the predominant factor once specific area is large enough, *e.g.*, ≥600 $m^2 \cdot g^{-1}$at which point this morphological property appears to no longer be an issue.

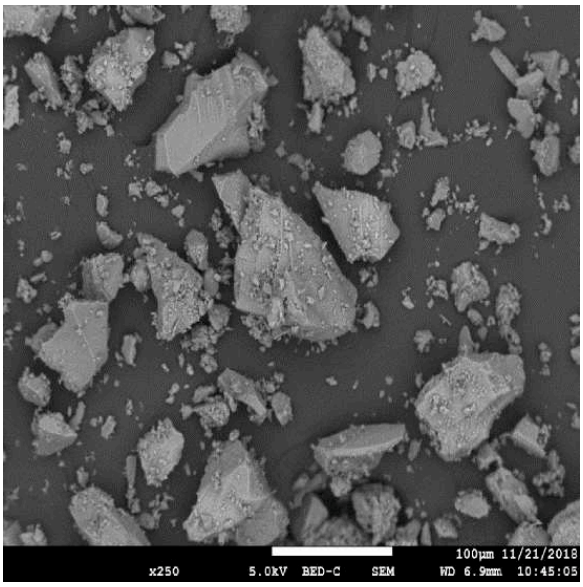

Figure 4.8 SEM images at different magnifications of Zn-Ta-TUD-1 prepared during the RSM experiment.

SEM images typical of samples prepared during the RSM experiments are shown in Figure 4.8. The results are similar to those reported in the literature for M-TUD-1 at low metal loading.[22,27,35,46–48] Zn-Ta-TUD-1 consisted of <100 µm particles apparently without a well-defined morphology. At high magnification, the catalyst surface is shown to be rough and

irregular, typical of the sponge-like morphology resulting from the agglomeration of silica particles formed during the synthesis procedure.[20,21,49]

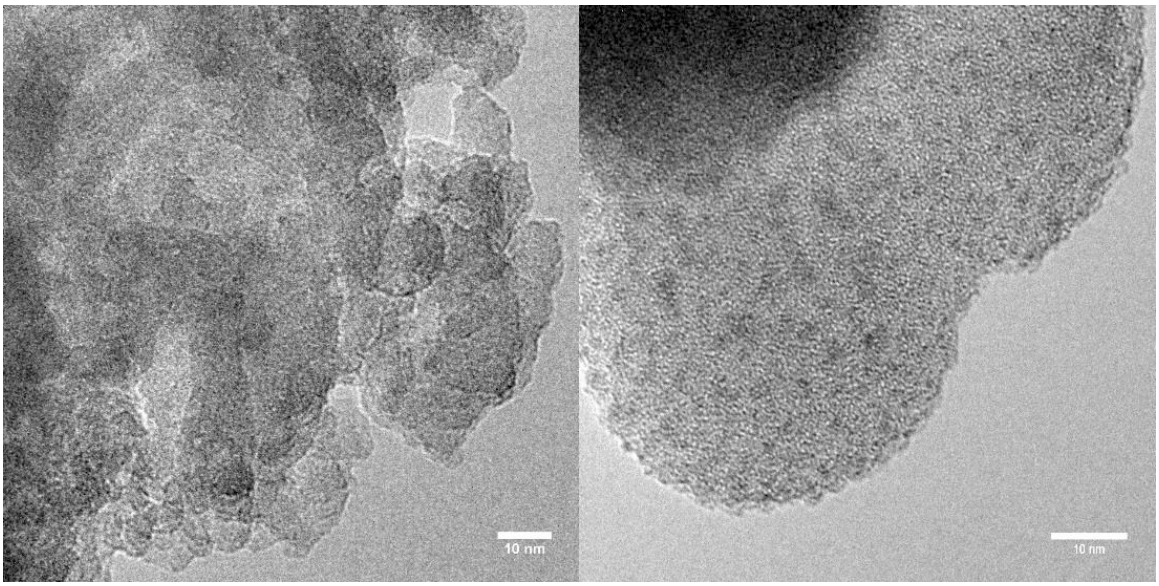

Figure 4.9 HR-TEM images of Zn-Ta-TUD-1 prepared during the RMS experiment. Left: RSM9 image taken immediately. Right: the same area of RSM9 after irradiation under electron beam for 5 minutes.

Figure 4.9 illustrates HR-TEM images of RSM series Zn-Ta-TUD-1 catalysts. Inspection of various samples confirmed the sponge-like 3D structure with "worm-like" pores characteristic of TUD-1 materials.[20,23] The absence of discernable metal oxide nanoparticles suggests Zn and Ta were completely isolated within the carrier framework. Their presence was confirmed by energy-dispersive X-ray spectroscopy. Furthermore, nanoparticles could be detected upon electron irradiation of the samples, which provoked the degradation of silica and metal oxide agglomeration (Figure 4.9, right, and Figure 4.S1).[50,51]

4.4. Conclusion

The effect of various parameters in the synthesis of Zn-Ta-TUD-1 materials on their morphology and ability to convert ethanol to BD was studied using designs of experiments. A Placket-Burman screening design coupled with mathematical modelling and statistical tools identified the most important preparation variables for attaining high BD productivity and understanding their effect on surface area and pore size. Response surface methodology was used

to optimize BD productivity by tuning the Zn and Ta content of catalysts prepared according to the most suitable procedure resulting from the screening study.

We found the nature of the chelating agent to play a statistically significant role on the morphology of Zn-Ta-TUD-1. Use of TEG—a sterically smaller molecule—resulted in larger surface area and smaller average pore diameter than $TEAH_3$. There existed a trade-off situation between the two structural properties depending on the agent used and the total amount of organic species present in the precursor gel. Ostensibly, the difference manifests itself during the structure shaping process taking place under thermal treatment. Choosing a favorable chelating agent may be an alternative to tuning the thermal treatment duration for obtaining desirable morphologies, the common practice with TUD-1 material. New chelating agents and their effect should also be investigated.

Substituting the drop-wise addition under stirring of TEAOH for rapid pouring influenced pore size, likely due to changes in the gelation kinetics. It showed great reproducibility in obtaining materials with large surface area ($\geq$600 $m^2 \cdot g^{-1}$) and mesopores diameters averaging 10.5 nm. In practical terms, this finding enables time saving during the synthesis. However, a more thorough study of the gelation kinetics with better controlled alkalizing agents addition rates is advised.

Besides the chelating agent, high BD productivity required a balanced Zn:Ta ratio and calcination of the samples under air. RSM optimization of Zn and Ta loadings further indicated the optimal content of Ta was between 2 and 2.2 mol.%. Maximum BD productivity required a Zn content between 3 and 4 mol.%. Despite finding no mathematical evidence of interaction between the amount of Zn and Ta, the results highlight the need for a balanced quantity of each element for maximizing BD production. This observation coincides with other findings of the literature which concluded that the multi-step reaction of the Lebedev process requires catalysts with balanced properties, often obtaining by tuning their different components.[10,16,37]

4.5. References

(1) Makshina, E. V; Dusselier, M.; Janssens, W.; Degrève, J.; Jacobs, P. A.; Sels, B. F. Review of Old Chemistry and New Catalytic Advances in the On-Purpose Synthesis of Butadiene. *Chem. Soc. Rev.* **2014**, *43*, 7917–7953.

(2) Cespi, D.; Passarini, F.; Vassura, I.; Cavani, F. Butadiene from Biomass, a Life Cycle Perspective to Address Sustainability in the Chemical Industry. *Green Chem.* **2016**, *18* (6), 1625–1638.

(3) Farzad, S.; Mandegari, M. A.; Görgens, J. F. Integrated Techno-Economic and Environmental Analysis of Butadiene Production from Biomass. *Bioresour. Technol.* **2017**, *239*, 37–48.

(4) Pomalaza, G.; Capron, M.; Ordomsky, V.; Dumeignil, F. Recent Breakthroughs in the Conversion of Ethanol to Butadiene. *Catalysts* **2016**, *6* (12), 203.

(5) Sun, H. N.; Wristers, J. P. Butadiene. In *Kirk-Othmer Encyclopedia of Chemical Technology*; John Wiley & Sons, Inc.: Hoboken, NJ, USA, 2002; Vol. 4.

(6) Dahlmann, M.; Grub, J.; Löser, E. Butadiene. In *Ullmann's Encyclopedia of Industrial Chemistry*; Wiley-VCH Verlag GmbH & Co. KGaA: Weinheim, Germany, 2011; Vol. 100 C, pp 1–24.

(7) Angelici, C.; Velthoen, M. E. Z.; Weckhuysen, B. M.; Bruijnincx, P. C. A. Effect of Preparation Method and CuO Promotion in the Conversion of Ethanol into 1,3-Butadiene over SiO 2 -MgO Catalysts. *ChemSusChem* **2014**, *7* (9), 2505–2515.

(8) Jones, M.; Keir, C.; Iulio, C.; Robertson, R.; Williams, C.; Apperley, D. Investigations into the Conversion of Ethanol into 1,3-Butadiene. *Catal. Sci. Technol.* **2011**, *1* (2), 267.

(9) Ezinkwo, G. O.; Tretyakov, V. P.; Aliyu, A.; Ilolov, A. M. Fundamental Issues of Catalytic Conversion of Bio-Ethanol into Butadiene. *ChemBioEng Rev.* **2014**, *1* (5), 194–203.

(10) Angelici, C.; Velthoen, M. E. Z.; Weckhuysen, B. M.; Bruijnincx, P. C. A. Influence of Acid–Base Properties on the Lebedev Ethanol-to-Butadiene Process Catalyzed by SiO2–MgO Materials. *Catal. Sci. Technol.* **2015**, *5* (5), 2869–2879.

(11) Kim, T. W.; Kim, J. W.; Kim, S. Y.; Chae, H. J.; Kim, J. R.; Jeong, S. Y.; Kim, C. U. Butadiene Production from Bioethanol and Acetaldehyde over Tantalum Oxide-Supported Spherical Silica Catalysts for Circulating Fluidized Bed. *Chem. Eng. J.* **2014**, *278*, 217–223.

(12) Cheong, J. L.; Shao, Y.; Tan, S. J. R.; Li, X.; Zhang, Y.; Lee, S. S. Highly Active and Selective Zr/MCF Catalyst for Production of 1,3-Butadiene from Ethanol in a Dual Fixed Bed Reactor System. *ACS Sustain. Chem. Eng.* **2016**, *4* (9), 4887–4894.

(13) Sushkevich, V. L.; Ivanova, I. I.; Ordomsky, V. V.; Taarning, E. Design of a Metal-Promoted Oxide Catalyst for the Selective Synthesis of Butadiene from Ethanol. *ChemSusChem* **2014**, 2527–2536.

(14) Tripathi, A.; Faungnawakij, K.; Laobuthee, A.; Assabumrungrat, S.; Laosiripojna, N. Catalytic Activity of Bimetallic Cu-Ag/MgO-SiO2 toward the Conversion of Ethanol to 1,3-Butadiene. *Int. J. Chem. React. Eng.* **2016**, *14* (5), 945–954.

(15) Dagle, V. L.; Flake, M. D.; Lemmon, T. L.; Lopez, J. S.; Kovarik, L.; Dagle, R. A. Effect of the SiO 2 Support on the Catalytic Performance of Ag/ZrO 2 /SiO 2 Catalysts for the Single-Bed Production of Butadiene from Ethanol. *Appl. Catal. B Environ.* **2018**, *236* (May), 576–587.

(16) Da Ros, S.; Jones, M. D.; Mattia, D.; Pinto, J. C.; Schwaab, M.; Noronha, F. B.; Kondrat, S. A.; Clarke, T. C.; Taylor, S. H. Ethanol to 1,3-Butadiene Conversion by Using ZrZn-Containing MgO/SiO 2 Systems Prepared by Co-Precipitation and Effect of Catalyst Acidity Modification. *ChemCatChem* **2016**, *8* (14), 2376–2386.

(17) Klein, A.; Palkovits, R. Influence of Structural Parameters on the Conversion of Ethanol into 1,3-Butadiene Using Mesoporous Zeolites. *Catal. Commun.* **2016**, *91*, 72–75.

(18) Jansen, J. C.; Shan, Z.; Marchese, L.; Zhou, W.; Puil, N. v d; Maschmeyer, T. A New Templating Method for Three-Dimensional Mesopore Networks. *Chem. Commun.* **2001**, No. 8, 713–714.

(19) Ramanathan, A.; Carmen Castro Villalobos, M.; Kwakernaak, C.; Telalovic, S.; Hanefeld, U. Zr-TUD-1: A Lewis Acidic, Three-Dimensional, Mesoporous, Zirconium-Containing Catalyst. *Chem. - A Eur. J.* **2008**, *14* (3), 961–972.

(20) Telalović, S.; Ramanathan, A.; Mul, G.; Hanefeld, U. TUD-1: Synthesis and Application of a Versatile Catalyst, Carrier, Material…. *J. Mater. Chem.* **2010**, *20* (4), 642.

(21) Saad, M. S. H. M. Functionalized TUD-1 : Synthesis , Characterization and (Photo-)

Catalytic Performance, Universiteit Van Hewan, 2005.

(22) Lima, S.; Antunes, M. M.; Fernandes, A.; Pillinger, M.; Ribeiro, M. F.; Valente, A. A. Acid-Catalysed Conversion of Saccharides into Furanic Aldehydes in the Presence of Three-Dimensional Mesoporous Al-TUD-1. *Molecules* **2010**, *15* (6), 3863–3877.

(23) Ranoux, A.; Djanashvili, K.; Arends, I. W. C. E.; Hanefeld, U. B-TUD-1: A Versatile Mesoporous Catalyst. *RSC Adv.* **2013**, *3* (44), 21524–21534.

(24) Imran, G.; Poomalai, M. Catalytic Activity of MnTUD-1 for Liquid Phase Oxidation of Ethylbenzene with Tert -Butyl Hydroperoxide. **2012**, 677–682.

(25) Karmakar, B.; Sinhamahapatra, A.; Panda, A. B.; Banerji, J.; Chowdhury, B. Ga-TUD-1: A New Heterogeneous Mesoporous Catalyst for the Solventless Expeditious Synthesis of Aminonitriles. *Appl. Catal. A Gen.* **2011**, *392* (1–2), 111–117.

(26) Li, L.; Cani, D.; Pescarmona, P. P. Metal-Containing TUD-1 Mesoporous Silicates as Versatile Solid Acid Catalysts for the Conversion of Bio-Based Compounds into Valuable Chemicals. *Inorganica Chim. Acta* **2015**, *431*, 289–296.

(27) Hamdy, M. S.; Berg, O.; Jansen, J. C.; Maschmeyer, T.; Moulijn, J. A.; Mul, G. TiO2 Nanoparticles in Mesoporous TUD-1: Synthesis, Characterization and Photocatalytic Performance in Propane Oxidation. *Chem. - A Eur. J.* **2006**, *12* (2), 620–628.

(28) Natrella, M. NIST/SEMATECH e-Handbook of Statistical Methods. **2010**.

(29) Madinger, J.; Whitcomb, P. J. *DOE Simplified*; Productivity Press, 2017; Vol. 24.

(30) Zougagh, M.; Rudner, P. C.; De Torres, A. G.; Cano Pavôn, J. M. Application of Doehlert Matrix and Factorial Designs in the Optimization of Experimental Variables Associated with the On-Line Preconcentration and Determination of Zinc by Flow Injection Inductively Coupled Plasma Atomic Emission Spectrometry. *J. Anal. At. Spectrom.* **2000**, *15* (12), 1589–1594.

(31) Lundstedt, T.; Seifert, E.; Abramo, L.; Thelin, B.; Nyström, Å.; Pettersen, J.; Bergman, R. Experimental Design and Optimization. *Chemom. Intell. Lab. Syst.* **1998**, *42* (1–2), 3–40.

(32) Bezerra, M. A.; Santelli, R. E.; Oliveira, E. P.; Villar, L. S.; Escaleira, L. A. Response Surface Methodology (RSM) as a Tool for Optimization in Analytical Chemistry. *Talanta* **2008**, *76* (5), 965–977.

(33) Dumeignil, F.; PAUL, S.; Duhamel, L.; FAYE, J.; Miquel, P.; CAPRON, M.; Dubois, J. L. Dispositif d'évaluation d'au Moins Un Critère de Performance de Catalyseurs Hétérogènes. WO2015118263 A1, 2015.

(34) Li, L.; Korányi, T. I.; Sels, B. F.; Pescarmona, P. P. Highly-Efficient Conversion of Glycerol to Solketal over Heterogeneous Lewis Acid Catalysts. *Green Chem.* **2012**, *14* (6), 1611.

(35) Neves, I. C.; Botelho, G.; Machado, A. V.; Rebelo, P.; Ramôa, S.; Pereira, M. F. R.; Ramanathan, A.; Pescarmona, P. Feedstock Recycling of Polyethylene over AlTUD-1 Mesoporous Catalyst. *Polym. Degrad. Stab.* **2007**, *92* (8), 1513–1519.

(36) Makshina, E. V.; Janssens, W.; Sels, B. F.; Jacobs, P. A. Catalytic Study of the Conversion of Ethanol into 1,3-Butadiene. *Catal. Today* **2012**, *198* (1), 338–344.

(37) Chung, S.-H.; Angelici, C.; Hinterding, S. O. M.; Weingarth, M.; Baldus, M.; Houben, K.; Weckhuysen, B. M.; Bruijnincx, P. C. A. Role of Magnesium Silicates in Wet-Kneaded Silica–Magnesia Catalysts for the Lebedev Ethanol-to-Butadiene Process. *ACS Catal.* **2016**, *6* (6), 4034–4045.

(38) Larina, O. V.; Kyriienko, P. I.; Soloviev, S. O. Effect of Lanthanum in Zn-La(-Zr)-Si Oxide Compositions on Their Activity in the Conversion of Ethanol into 1,3-Butadiene. *Theor. Exp. Chem.* **2016**, *52* (1), 51–56.

(39) Kyriienko, P. I.; Larina, O. V.; Soloviev, S. O.; Orlyk, S. M.; Calers, C.; Dzwigaj, S. Ethanol Conversion into 1,3-Butadiene by the Lebedev Method over MTaSiBEA Zeolites (M = Ag, Cu, Zn). *ACS Sustain. Chem. Eng.* **2017**, *5* (3), 2075–2083.

(40) De Baerdemaeker, T.; Feyen, M.; Müller, U.; Yilmaz, B.; Xiao, F. S.; Zhang, W.; Yokoi, T.; Bao, X.; Gies, H.; De Vos, D. E. Bimetallic Zn and Hf on Silica Catalysts for the Conversion of Ethanol to 1,3-Butadiene. *ACS Catal.* **2015**, *5* (6), 3393–3397.

(41) Panahi, P. N.; Salari, D.; Niaei, A.; Mousavi, S. M. Journal of Industrial and Engineering

Chemistry NO Reduction over Nanostructure M-Cu / ZSM-5 (M : Cr , Mn , Co and Fe) Bimetallic Catalysts and Optimization of Catalyst Preparation by RSM. *J. Ind. Eng. Chem.* **2013**, *19* (6), 1793–1799.

(42) Hesari, A.; Mohammad, P.; Fererdoon, A. H.; Mehdi, A. Statistical Evaluation of the Pertinent Parameters in Biosynthesis of Ag / MWf-CNT Composites Using Plackett-Burman Design and Response Surface Methodology. *Iran. J. Chem. Chem. Eng.* **2016**, *35* (2), 51–62.

(43) Shan, Z.; Jansen, J. C.; Zhou, W.; Maschmeyer, T. A1-TUD-1, Stable Mesoporous Aluminas with High Surface Areas. *Appl. Catal. A Gen.* **2003**, *254* (2), 339–343.

(44) Connolly, M. L.; Shell, M. P. W. The Molecular Surface Package. **1993**, *11*, 139–141.

(45) Rahman, I. A.; Vejayakumaran, P.; Sipaut, C. S.; Ismail, J.; Bakar, M. A.; Adnan, R.; Chee, C. K. An Optimized Sol-Gel Synthesis of Stable Primary Equivalent Silica Particles. *Colloids Surfaces A Physicochem. Eng. Asp.* **2007**, *294* (1–3), 102–110.

(46) Pachamuthu, M. P.; Srinivasan, V. V.; Maheswari, R.; Shanthi, K.; Ramanathan, A. Lewis Acidic ZrTUD-1 as Catalyst for Tert-Butylation of Phenol. *Appl. Catal. A Gen.* **2013**, *462–463*, 143–149.

(47) Yan, W.; Ramanathan, A.; Patel, P. D.; Maiti, S. K.; Laird, B. B.; Thompson, W. H.; Subramaniam, B. Mechanistic Insights for Enhancing Activity and Stability of Nb-Incorporated Silicates for Selective Ethylene Epoxidation. *J. Catal.* **2016**, *336*, 75–84.

(48) Pachamuthu, M. P.; Shanthi, K.; Luque, R.; Ramanathan, A. SnTUD-1: A Solid Acid Catalyst for Three Component Coupling Reactions at Room Temperature. *Green Chem.* **2013**, *15* (8), 2158.

(49) Ranoux, A.; Djanashvili, K.; Arends, I. W. C. E.; Hanefeld, U. B-TUD-1: A Versatile Mesoporous Catalyst. *RSC Adv.* **2013**, *3* (44), 21524.

(50) Jiang, N. Electron Beam Damage in Oxides: A Review. *Reports Prog. Phys.* **2016**, *79* (1), 016501.

(51) Martin, B.; Fl

SiO2. *Phys. Chem. Miner.* **1996**, *23* (7), 409–417.

4.6. Supplementary Information

Table 4.S1 Goodness of fit and ANOVA statistics for the polynomial response models resulting from the Placket-Burman experiment.

Statistical terms	Y_{prod}	Y_{SBET}	Y_{Dp}
R^2	0.993	0.997	0.988
Adj. R^2	0.974	0.914	0.955
Model F-value	53.002	15.640	26.731
Model p-value	0.004	0.023	0.009

Table 4.S2 Goodness of fit and ANOVA statistics for the quadratic model of butadiene productivity with Zn-Ta-TUD-1.

Statistical terms	Y_{prod}
R^2	0.971
Adj. R^2	0.924
Model F-value	20.347
Model p-value	0.016

Table 4.S3 Experimental results of N_2 porosimetry for Zn-Ta-TUD-1 samples prepared during the RSM experiment.

Sample	S_{BET} ($m^2 \cdot g^{-1}$)	Avg. pore diameter (nm)
RSM1	603	12.2
RSM2	679	7
RSM3	678	9.8
RSM4	598	9.5
RSM5	675	9.7
RSM6	672	9.6
RSM7	732	9.1
RSM8	658	11.9
RSM9	655	9.5

Figure 4.S1 Electron-induced sintering of Ta during HR-TEM analysis

Chapter 5 Properties and Activity of Zn-Ta-TUD-1

Abstract

A zinc and tantalum-containing mesoporous silica catalyst highly active and selective in the Lebedev process has been prepared using the one-pot TUD-1 methodology. Selectivity towards butadiene reached 60 - 70%, making Zn-Ta-TUD-1 one of the best performing catalysts in the literature. To rationalize these results and establish a structure-activity relationship, a series of similar catalysts were prepared and characterized. Nitrogen physisorption, XPS, ICP-AES, XRD, TEM, UV-vis spectroscopy, TGA NH_3-TPD, H_2-TPR and FT-IR techniques were used. The most active samples were found to possess a large specific surface area and highly dispersed metal oxide phase incorporated within the mesoporous silica matrix. In combination with catalytic testing, characterization also showed a direct correlation between the number of Lewis acid sites and butadiene yield, confirming the structure-activity relationship theory prevalent for the Lebedev process. Deactivation of Zn-Ta-TUD-1 was also studied using the same techniques to characterize the properties of spent catalysts. It was found that the accumulation of heavy carbonaceous species caused a reduction of specific surface area and pore size coinciding with the observed loss in activity. Nevertheless, the pores of TUD-1 were large enough to avoid total pore blockage and a high selectivity could be maintained for 72 hours.

Preface

This chapter is based on the following manuscript: “Insight into the activity and deactivation of Zn-Ta-TUD-1 in the Lebedev process” by Pomalaza, G., Simon, P., Addad, A., Capron, M. and Dumeignil F. which is intended for publication in the Green Chemistry journal following the International Symposium on Green Chemistry at La Rochelle in 2019 at which the results were presented. Guillaume Pomalaza conducted all the experiments detailed and data interpretation, with the exception of TEM/STEM, which was performed by Dr. Ahmmed Addad., and XPS, which was conducted by Dr. Pardis Simon, who also contributed to the interpretation of experimental results. The document was review by Mickaël Capron and Franck Dumeignil.

In this article, 5 Zn-Ta-TUD-1 samples were characterized. Some were prepared during the screening study detailed in the previous chapter.

Chapter 4	Chapter 5
RSM8	ZTT-1
PB9	ZTT-4
PB10	ZTT-5

5.1. Introduction

Catalytic conversion of ethanol for the manufacturing of chemicals is a promising alternative to fossil-based processes. The availability of ethanol, which is produced in the 100s of billions of litres yearly *via* the fermentation of biomass, makes it an attractive renewable feedstock.[1,2] Owing to its convertibility into a wide range of organic chemical commodities,[3] ethanol is expected to play an increasing role in replacing unsustainable hydrocarbon feedstocks.[4] Sun and Wang, who compiled a list of valuable chemicals obtainable from ethanol, showed that the development of catalytic processes is essential for making ethanol a viable alternative to fossil fuels.[3]

The Lebedev process, the conversion of ethanol to butadiene,[5,6] has attracted attention as an on-purpose technology for producing the world's most important conjugated diene in an environmentally sound fashion: Butadiene, which is essential to the automotive industry as the main feedstock for manufacturing the synthetic rubber used in tires,[7] predominantly comes from the steam cracking of naphtha.[8] However, this method was found unsustainable ecologically[9] and economically,[10] in part due to recent trends in the cracking feedstock.[11,12] This situation has spurred interest into the Lebedev process, which produces butadiene from gaseous ethanol *via* a catalytic reaction, and was in fact an important source of butadiene in the first half of the last century.[5] However, to compete financially with fossil-based routes, the Lebedev process must overcome performance limitations.[13,14]

Limitations to the Lebedev process are comparable to that of ethanol conversion reactions.[2,3] At relevant reaction conditions, the high reactivity of ethanol leads not only to the desired product and its intermediates, but also to large numbers of undesirable byproducts, including coke precursors susceptible to cause deactivation.[14,15] Low butadiene productivity could hinder the economic viability of the process,[13] but attaining high butadiene space-time yield by increasing the ethanol flow rate was found to coincide with lower selectivity.[16] Catalyst design can help overcoming these limitations by improving performances in the Lebedev process. However, this requires a better understanding of the structure-activity relationship so that new materials are tailored for optimal catalytic activity.[5]

Figure 5.10 Toussaint-Kagan mechanism for the conversion of ethanol to 1,3-butadiene. Reaction steps: (i) ethanol dehydrogenation; (ii) self-aldol condensation; (iii) dehydration of acetaldol; (iv) Meerwin-Ponndorf-Verley-Oppenaur (MPVO) reaction; (v) dehydration of crotyl alcohol.[6]

It is generally recognized that the ethanol-to-butadiene reaction mechanism depicted in Figure 5.10 requires a multi-functional catalyst.[5,6] However, establishing a clear relationship between the catalysts' properties and their performances is still a matter of debates.[17–19] While a substantial amount of insights have been acquired in the recent years, the rational design of catalysts to maximize butadiene formation remains limited.

Much attention has focused on the role of Lewis acid sites, also known as Lewis acid-base pairs, which have been proposed to catalyze the condensation of acetaldehyde to C_4 intermediates that lead butadiene.[20,21] Ivanova *et al*. established a direct correlation between the relative number of "open" Zr(IV) sites and initial butadiene formation using a supported silver-zirconium catalyst.[20,22,23] Since acetaldehyde condensation is often recognized as the rate-determining step,[20,24,25] their observation strongly supports the involvement of Lewis acid-base pairs in the reaction. Kyriienko *et al.* also reported a direct relationship between butadiene productivity and the relative amount of Lewis acid sites probed by $CDCl_3$ on Cu-doped Zr-containing zeolites.[26] Similar correlations have yet to be established on other materials, but there is strong evidence that Lewis acidity plays a role in other catalytic systems.[27]

Another crucial component of catalysts active in the Lebedev process is their ability to convert ethanol to acetaldehyde.[28] Several dehydrogenation promoters have been tested and their activity investigated: Ivanova *et al*. proposed a mechanism for dehydrogenation on silica-supported metallic silver;[20,29] Dagle *et al*. found silver particle size to be a crucial parameter;[30] Angelici *et al*. and Taifan *et al.* researched the activity and deactivation of copper on $MgO\text{-}SiO_2$;[14,31,32] Kyriienko *et al*. compared the promoter effect of Ag, Zn and Cu on Ta-containing zeolites, identifying the

latter as better suited for the Lebedev process.[33] Most likely, these promoters operate differently from one another, as implied by the different mechanisms proposed for ethanol dehydrogenation.

While neglected for long, recent articles on the topic of deactivation have provided new information that can be used for preparing catalysts with improved stability. Many authors argue that coke deposition naturally results in loss of activity.[24,34,35] Ostensibly, highly active acidic or basic sites are responsible for the formation polyaromatic carbonaceous species that block access to the active phase. Alternatively, Li *et al*. suggested that relatively lighter oxygenated cyclic species formed by the condensation of aldehydes poison the sites active for butadiene formation.[15] Sintering and changes in the active phase oxidation state have also been proposed.[31,32,36] As Taifan *et al*. demonstrated,[32] the deactivation mechanism depends on the type of catalyst used. Hence, the individual study of catalytic systems appears necessary.

In a previous issue of this journal, we published a short communication on our early findings concerning a zinc-tantalum catalyst introduced into TUD-1 mesoporous silica; it exhibited unprecedented activity and stability in the Lebedev process compared to the literature.[37] The performances of Zn-Ta-TUD-1 were compared with those of equivalent catalysts supported on dealuminated zeolite β and commercial silica, with TUD-1 found to be the best carrier to express high activity of the as-derived catalytic system. Better suited morphological properties and the TUD-1 synthesis process were seen as potential contributors to catalytic activity. In addition, a correlation between the number of acid sites probed by NH_3 and butadiene productivity of each catalyst tested was established, suggesting the conclusion of Ivanova *et al*.[17,22] that Lewis acid sites catalyze the aldol condensation of acetaldehyde leading to butadiene formation could also apply on our system.

The present work gives a detailed study of the Zn-Ta-TUD-1 catalytic system and its activity in the Lebedev process, unravelling fundamental aspects of the reaction by drawing a clear picture of the performances/structure/chemical properties relationship. A variety of techniques was employed to characterize the catalyst: N_2 physisorption, inductively coupled plasma atomic emission spectroscopy, X-ray powder diffraction, X-ray photoelectron spectroscopy, UV-Vis diffuse reflectance spectroscopy, infrared spectroscopy techniques, transmission electronic microscopy and temperature-programmed experiments. The as-obtained results confirmed the existence of Zn-Ta-TUD-1 as a mesoporous material with highly dispersed Zn(II) and Ta(V) phases.

A set of catalysts with varying metal loading and synthesis procedure were prepared and compared to especially investigate the structure-activity relationship. Notably, a direct correlation between the number Lewis acid sites probed by pyridine and the initial butadiene formation rate was established. This is the first account of such a relationship on a non-Zr catalyst. In addition, deactivation of Zn-Ta-TUD-1 during the Lebedev process was investigated by catalytic testing, surface-sensitive analytic techniques and other characterization methods. Reduction of the active phase was ruled out as a deactivation mechanism. Instead, deposition of carbonaceous species on the pore channels of the catalyst blocking the access to active sites appear to cause the loss of activity observed.

5.2. Experimental

5.2.1. Catalyst Preparation

Zn-Ta-TUD-1 with molar Si/Zn and Si/Ta ratios within 4–100 were synthesized using the procedure detailed in our previous article,[37] itself adapted from the TUD-1 methodology.[38,39] Briefly, the TUD-1 synthesis process involves the gelation by TEAOH of TEOS dissolved in ethanol with metal precursors complexed by tetraethylene glycol to ensure their dispersion. The resulting gel is dried and treated in a Teflon-lined autoclave at 180 °C, which creates the mesoporous morphology using tetraethylene glycol as a structure-directing agent. The resulting solid is calcined under air flow at 600 °C and ground and sieved to 125 μm, affording a white powder. The precursor gel were prepared with the following reagents: optical grade tantalum ethoxide (Alfa Aeser, 99.95%); zinc acetate dehydrate (Acros Organics, 98+%); tetraethylene glycol (or TEG, Agros Organics, 99.5%) was used as complexing agent; tetratethyl orthosilicate, (or TEOS, Agros Organics, 98%) was used silica precursor; tetraethyl ammonium hydroxide (or TEAOH, Aldrich, 35 wt. % in water) acted as the alkalizing agent; absolute ethanol (Aldrich, 99.8%) was used as solvent.

Table 5.16 Synthesis detail of Zn-Ta-TUD-1 catalysts, including the silica-metal molar ratio in the precursor gel and the concentration measured in the final product by ICP-AES. The duration of the thermal treatment in autoclave of the TUD-1 dried gel is also listed.

Catalyst	Si:Zn		Si:Ta		Treatment time (h)
	Gel	Product	Gel	Product	
ZTT-1	33.3	33.6	50	51.9	24
ZTT-2	50	46.8	100	94.3	6
ZTT-3	50	43.3	100	105.7	48
ZTT-4	16	4.5	24	20.3	24
ZTT-5	16	11.4	24	21.9	24

In total, 5 catalysts labelled ZTT were prepared. To achieve different properties, the synthesis method was modified with regards to the thermal treatment duration and calcination method. **Error! Reference source not found.** lists the synthesis details of the ZTT catalysts series. The f inal gel compositions before thermal treatment were: 1.0 TEOS : *x* Zn: *y* Ta : 0.5 TEAOH: 1.0 TEG, where *x* and *y* correspond to the ratios listed in Table 5.16. ZTT-1 was the primary subject of our investigation, as it the best performing catalyst.

To complete our study, TUD-1 materials with either Zn and Ta were prepared in the same way with the following ratios: Si:Zn = 33 and Si:Ta = 50. Hemimorphite, a zinc silicate, was also synthesized as instructed in the patent of Teles *et al.*[40]

5.2.2. Catalyst Characterization

N_2 physisorption at -196 °C with a Micrometric Tristar II instrument was used to study the morphological properties of the ZTT series, spent ZTT-1 and monometallic TUD-1 samples. Analysis was performed after outgassing 50 – 200 mg of powder at 150 °C for 6 hours. The Brunauer–Emmett–Teller (BET) and Barret-Joyner-Halenda (BJH) methods were used to calculate specific surface area (S_{BET}) as well as pore diameter (D_p) distribution and pore volume (P_{vol}).

Elemental analysis of the as-synthesized ZTT samples was performed using inductively coupled plasma atomic emission spectroscopy (ICP-AES). 50 mg of catalysts were dissolved in a heated mixture of HF, HNO_3 and H_3BO_3 prior to analysis.

Catalysts were analysed with X-ray powder diffraction (XRD) using a Brüker D8 apparatus using Cu-Kα1 a source (λ = 1.5406 Å). A step of 0.02 ° with an acquisition time of 0.5 was used.

Thermogravimetric analysis (TGA) and differential scanning calorimetric analysis (DSC) were performed with a TA Instrument SDT-Q600. Experiments proceeded under air flow (100 $mL \cdot min^{-1}$), where spent samples were heated up to 700 °C (10 $°C \cdot min^{-1}$). Alumina was used a reference.

X-ray photoelectron spectroscopy (XPS) experiments were carried out using an AXIS Ultra DLD Kratos spectrometer equipped with a monochromatic Al Kα radiation (1486.6 eV) operating at 225 W (15 mA, 15kV). Binding energies were calibrated according to the C 1s core level set at 284.8 eV. Spectra of C 1s, O 1s, Zn 2p, Zn LMM and Ta 4d were analysed using the CasaXPS software.[41] Spectra decomposition was performed *via* mixed Gaussian-Lorentzian peak fitting; semiquantitative analysis was performed after a Shirley-type background subtraction.

UV-Vis diffuse reflectance spectra of the as-synthesized catalysts were acquired at room temperature using a Lambda 650 Perkin-Elmer spectrophotometer equipped with an integrating sphere. Recoding ranged between 200 and 800 nm at a step of 0.2 nm with a slit width of 1 nm. $BaSO_4$ was used as standard. Reflectance spectra were converted using the Kubelka-Munk function $f(R) = (1 - R)^2/2R$.[42]

Attenuated total reflection infrared (ATR-IR) spectra of the synthesized catalysts were recorded using a Nicolet iS50 FT-IR spectrometer from Thermo-Fisher equipped with an iS50 ATR sampling station. 50 scans over a scanning range of 4000 and 200 cm^{-1} with a resolution of 2 cm^{-1} were recorded.

High-resolution transmission electron microscopy (HR-TEM) images were obtained using a TECNAI electron microscope operating at 200 kV. Samples were deposited onto holey-carbon copper grids.

High-angle annular darkfield imaging during TEM has been performed on a FEI Titan themis 300, equipped with a C_s probe corrector and a High-efficiency Super-X detector (EDX). At 300 kV in HRSTEM mode it is possible to reach a resolution of 0.7 Å.

Infrared spectra were recorded during pyridine adsorption-desorption experiments using a Nicolet Protege 460 infrared spectrometer fitted with an MCT detector (4 cm^{-1}). Outgassing at 400 °C under vacuum (10^{-1} mbar) for 1 hour preceded each experiment. Pyridine (Fischer, general purpose grade) adsorption took place at room temperature up to saturation coverage. Desorption under vacuum was performed at 150 °C, 250 °C, 350 °C and 450 °C. IR spectra were acquired

prior and during every step of the experiment. Acid sites were quantified based on the integrated IR bands using extinction coefficient found in the literature.[43]

Acid site number and strength was evaluated by temperature-programmed desorption using ammonia as a probe (NH_3-TPD). The experiments were performed on a Micrometrics Autochem 2920 apparatus equipped with a Pfeiffer mass spectrometer. NH_3 was adsorbed over 100 mg of catalyst at room temperature for 30 minutes using a 50 $mL \cdot min^{-1}$ flow of 5% NH_3 in He. A ramp of 10 $°C \cdot min^{-1}$ until 900 °C was used to desorb NH_3.

Temperature-programmed reduction (H_2-TPR) was used to study the reducibility of the catalysts with a Micromeritics Autochem 2920 coupled with a with a thermal conductivity detector. The samples were heated to 1100 °C (10 $°C \cdot min^{-1}$) while being reduced using a 50 $mL \cdot min^{-1}$ flow of 5% H_2 in argon.

5.2.3. Catalytic, Poisoning and Stability Tests

Catalytic testing was performed with a Multi-R® apparatus from Teamcat Solutions SAS,[44] which is a high-throughput device for heterogeneous catalyst screening. Four glass reactors are used simultaneously with the gaseous reactant feed calibrated by a splitter that ensured an equal inlet flow. Reactor outputs were analysed online with an Agilent 7890 A equipped with an FID detector. An independently controlled valve selected the output of each reactor for analysis.

Comparison the different catalysts in the ZTT series and monometallic TUD-1 was performed at 350 °C and a pressure of 1 atm. Each sample was ground and sieved to 120 mesh granules. 30 mg were loaded in glass reactors and held in place with SiC. He was passed through a bubbler containing ≥99.8 % ethanol, set at pressure and temperature to afford vapor concentration of 4.5% according to the Antoine's law and fed into the reactors. Weighted hourly space velocity of ethanol ($WHSV_{EtOH}$) was adjusted to 5.3 h^{-1} by tuning the inlet flow rate and catalyst mass.

Catalytic deactivation tests were performed at 400 °C at a $WHSV_{EtOH}$ of 5.3 h^{-1} with ZTT-1 using the Multi-R® apparatus. Rather than interrupting the reaction to sample some of the spent catalyst for analysis, 5 reactions were scheduled and conducted were conducted in parallel to provided catalysts after 1.5, 6, 24, 48 and 72 hours on stream. Samples were kept under N_2 until characterization.

A pyridine poison study was conducted in a steady-state fixed bed glass reactor at 350 °C. Ethanol was fed by pumping absolute ethanol with an HPLC pump into a vaporized maintained at 200 °C into which 30 mL/min of He was flow and fed into the reactor. $WHSV_{EtOH}$ of 0.3 $h^{-1}$was used. After 1 hour on stream, the feed was switched to an ethanol-pyridine mixture containing 5 mol.% of pyridine (Fisher, 99%); the reactor lines were kept above 125 °C to avoid condensation. After 1 hour of pyridine co-feeding, the feed was returned to pure ethanol. The reactor output was monitored with an online GC-FID.

Ethanol conversion (X, %), the selectivity towards each product (S_i, %), the molar yield of each product (Y_i, %) and the molar productivity of butadiene (P_{BD}, $mmol_{BD}\cdot g_{cat}^{-1}\cdot h^{-1}$) were used to describe catalytic activity—equation (1, (2, (3 and (4 respectively, where ci represents the number of carbon moles measured for a given compound i. These values obtained by extrapolating the values obtained over time on stream to t = 0. The carbon balance (CB) for each test was calculated by dividing the sum of carbon moles detected with the molar amount of carbon introduced as ethanol and found to range between 95 – 105 %.

$$X=\frac{c_{EtOH,in}-c_{EtOH,out}}{c_{EtOH,in}}\cdot 100 \quad (1)$$

$$S_i=\frac{c_{i,out}}{c_{EtOH,in}-c_{EtOH,out}}\cdot 100 \quad (2)$$

$$Y_i=X\cdot S_i \quad (3)$$

$$P_{BD}=X\cdot S_{BD}\cdot WHSV_{EtOH}\cdot 0.1087 \quad (4)$$

5.3. Results and Discussion

5.3.1. Structural Properties

N_2 physisorption of ZTT-1, 2 and 3 showed Type IV physisorption isotherm with an H2 type hysteresis loop indicative of their mesoporous morphology (Figure 5.S2);[45] the nitrogen intake plateau above 0.9 P/P_0 further suggested an absence of macropores.[46] ZTT-4 and 5 with high metal loading instead showed nitrogen adsorption beyond 0.9 P/P_0 with H1 hysteresis loop, implying the presence of macropores and a different mesoporous morphology (Figure 5.S2).[46] At high metal loadings (10–60 wt.%), the TUD-1 synthesis results in extra-framework metal nanoparticles that typically reduce pore size by obstruction.[46,47]

Table 5.17 Morphological properties of Zn-Ta-TUD-1 catalysts obtained by N_2 physisorption.

Catalyst	S_{BET} (m^2/g)	$V_{p,\,BJH}$ (cm^3/g)	$D_{P,\,BJH}$ (nm)
ZTT-1	658	2.45	11.9
ZTT-2	702	1.49	7.0
ZTT-3	394	2.47	27.7
ZTT-4	486	0.79	12.6
ZTT-5	601	1.29	11.9
ZTT-1*	324	0.98	9.1

*Spent catalyst after 72 hours on stream.

The morphological characteristics of Zn-Ta-TUD-1 calculated using the BET and BJH methods are listed in Table 5.17. ZTT-1 possessed a large specific surface area of 658 $m^2 \cdot g^{-1}$, a porous volume of 2.45 $cm^3 \cdot g^{-1}$ and a mesopore diameter averaging 11.9 nm; as illustrated in Figure 5.S3**Error! Reference source not found.**, pore size distribution was narrow. Comparatively, ZTT-2 exhibited a larger surface area, but smaller pores due to the shorter thermal treatment time; the longer treatment duration of ZTT-3 resulted in the opposite effect.[39] At higher metal loading, the treatment time had similar effect on the morphological properties, but porous volume was overall smaller, possibly due to the greater amount of metal inside the catalysts.

The presence and amounts of Zn and Ta into the series of ZTT catalysts were confirmed and evaluated, respectively, by ICP-AES (Table 5.16). As evidenced by the observed Si:Zn and Si:Ta ratios, the TUD-1 synthesis method efficiently introduced the desired amount of active phase at metal loading below 5.0 mol.%. At higher loadings, *e.g.*, 27.2 and 13.3 mol.% for ZTT-4 and 5, respectively, metal content deviated significantly from the target values. The TUD-1 preparation method is known to have loading limits dependent on the type of metal beyond which incorporation is less successful.[39]

XPS was used to determine the oxidation state of Zn and Ta in Zn-Ta-TUD-1; the results obtained with ZTT-1 are depicted in Figure 5.11. The two peaks of Figure 5.11 (a) at 1046.0 eV and 1022.8 eV in the Zn $2p_{1/2}$ and $2p_{3/2}$ range suggested the presence of Zn(II), as the binding energy (BE) of the latter peak was close to the expected value for oxidized zinc compounds, *e.g.*, 1022.1 – 1022.7 eV.[48,49] However, distinguishing Zn(II) from its metallic form is ambiguous due to the small BE difference (< 1 eV) between the two states. The oxidation state was confirmed by inspecting the X-ray induced Zn LMM Auger peak, as the greater kinetic energy (KE) shift that separates Zn(II) from its metal form allowed a clear identification.

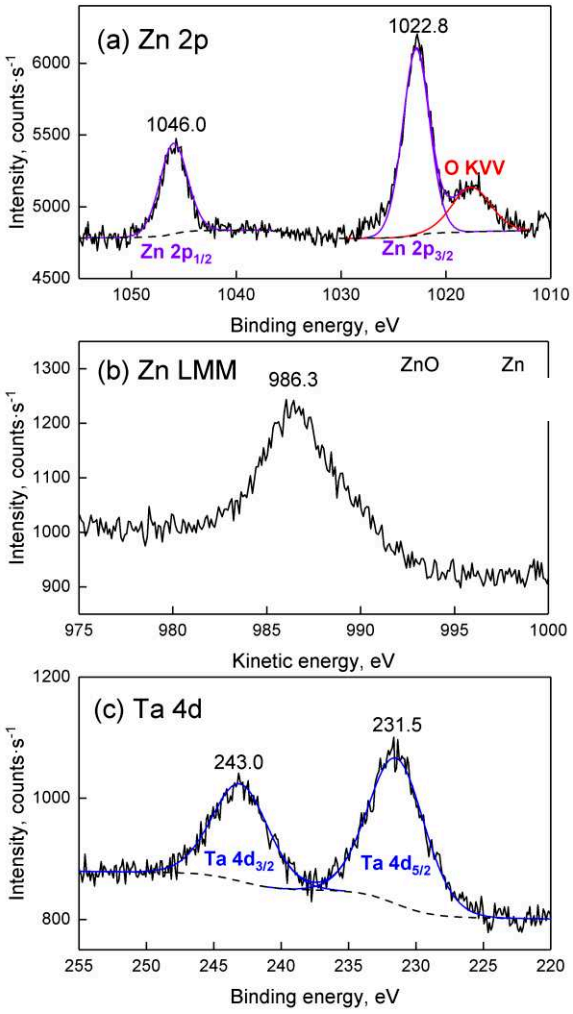

Figure 5.11 XPS spectra of ZTT-1 for (a) Zn 2p (b), Zn $L_3M_{4,5}M_{4,5}$[50] and (c) Ta 4d regions.

A Wagner plot—which plots the kinetic energy of a selected Auger peak as a function of measured binding energies of specifics photoelectron peaks for different compounds with the same element—was used to investigate the chemical state of Zn(II) in Zn-Ta-TUD-1.[51] Modified Auger parameters—defined as the sum between the Auger KE of a core level and the BE of the corresponding core-level—can be used to compare and classify different chemical environments.[52] As depicted in **Error! Reference source not found.Error! Reference source not found.**, the mo dified Auger parameter of Zn(II) in ZTT-1 of 2009.1 eV is closer to that of natural zinc minerals, such as hemimorphite and willemite or $Zn(OH)_2$.[53,54] This indicates the chemical environment of Zn(II) is similar to that of zinc silicates, notably of hemimorphite supported on SiO_2,[53] suggesting it is incorporated within the silica matrix of ZTT-1, rather than as extra-framework oxide particles.

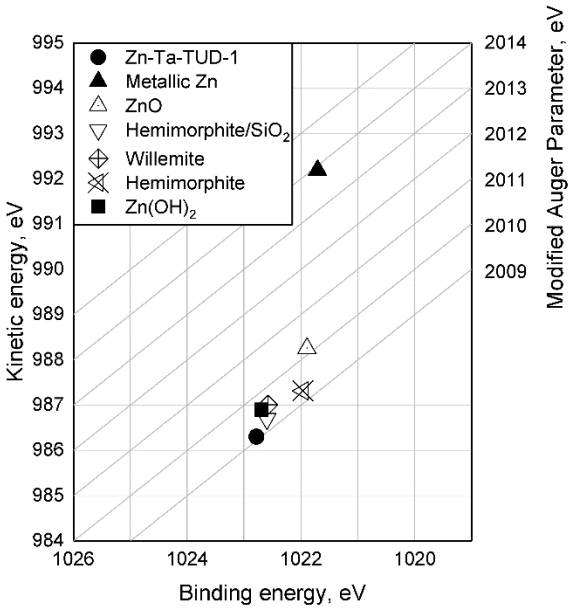

Figure 5.12 Wagner plot for Zn compounds comparing Zn-Ta-TUD-1 to those found in the literature.[53,54]

Regarding the Ta 4d core level (Figure 5.2(d)), a doublet peak is presents corresponding to Ta $4d_{5/2}$ and $4d_{3/2}$ contribution. The Ta $4d_{5/2}$ BE (243.0 eV) is consistent with that of Ta_2O_5,[55] suggesting the presence of Ta(V) in ZTT-1. Contrarily to recent publications on similar materials,[33,56] quantification of Ta was not performed with Ta 4f peak due to the interference by O 2s signals.

The Kerkhof-Moulijn (K-M) model was employed to study the dispersion state of Zn(II) and Ta(V) by analyzing the XPS results.[57–59] The K-M model predicts the XPS relative intensity of a homogeneously supported phase, *e.g.*, the "promoters", and its catalyst carrier according to Eqn (5):

$$\left(\frac{I_p}{I_s}\right)_{XPS} = \left(\frac{p}{s}\right)_b \cdot \frac{D_p}{D_s} \cdot \frac{\sigma_p}{\sigma_s} \cdot \frac{\beta_2}{2} \cdot \frac{\left(1+e^{-\beta_2}\right)}{\left(1-e^{-\beta_2}\right)} \cdot \frac{\left(1-e^{-\alpha_1}\right)}{\alpha_1} \qquad (5)$$

where $(p/s)_b$ is the bulk atomic ratio between promoter and support, σ_p/σ_s is the relative photoelectron cross section, β are dimensionless support thickness parameters, D is the detector efficiency for the given element and α_1 is the dimensionless particle size parameter. Cross sections for Zn 2p, Ta 4d and Si 2p were obtained from the relative sensitivity factor library available in Kratos Analytical.[60] The detector efficiency of each parameter can be further defined as:

$$\beta_1 = \frac{t}{\lambda_{ss}}, \quad \beta_2 = \frac{t}{\lambda_{ps}}, \quad \alpha_1 = \frac{d}{\lambda_{pp}}, \tag{6}$$

where t is the empirical thickness of the support, estimated from its density and specific surface area as $t = 2/\rho_s \cdot S$, and d is the average particle size. The mean free path of escaping electrons (λ) was calculated according to the Tanuma, Powell and Penn formula[61] using the QUASES-IMFP-TPP2M software.[62]

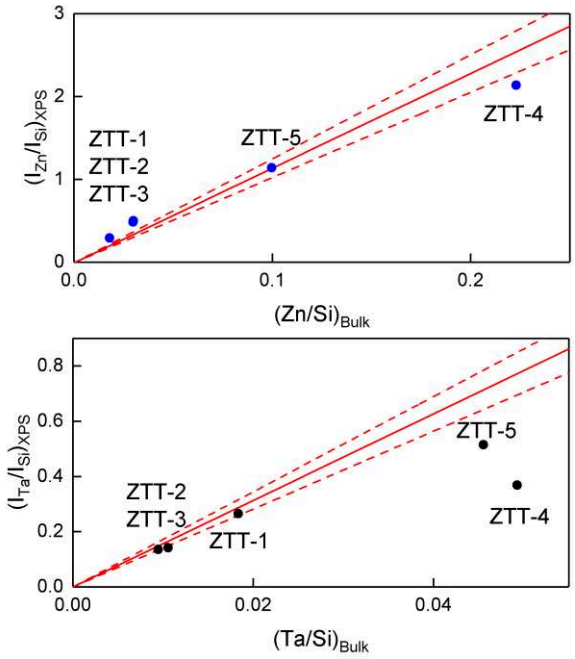

Figure 5.13 Comparison between the experimental and calculated intensity ratios of (a) Zn/Si and (b) Ta/Si versus the bulk ratios according to the model of Kerkhof and Moulijn.[57] The dashed red lines represent a 10% error on the calculated value.

Figure 5.13**Error! Reference source not found.** represents the experimental XPS intensity ratios (a) Zn/Si and (b) Ta/Si as a function of the bulk ratio determined by ICP-AES; the experimental points are compared to the red lines representing the theoretical intensity ratio predicted by the K-M model corresponding to the monolayer limit where $(1 - e^{-\alpha l})/\alpha_1 = 1$, that is to say maximum dispersion of the supported phase. It should be noted that the monolayer limit implies only the monolayer thickness of the promoter phase, not its monatomic dispersion. According to Léon,[58] monatomic and monolayered clusters give the same effect in the model. Experimental XPS intensities below the monolayer limit indicate that the promoter phase exist in three-dimensional particles heterogeneously dispersed on the surface of the support.[57]

Figure 5.13 (a) shows that only ZTT-4, with a 22.3% atomic loading of Zn, was below the monolayer limit, indicating that ZnO nanoparticles were formed. Concerning ZTT-1 and other catalysts, the experimental ratio obtained by XPS was either within or above the monolayer limit. It is unclear why ratios over the maximum dispersion prediction were obtained. We suggest the similitude between the photo-emitted electron escape path of Zn and the thickness of SiO_2 layers to be the source of this discrepancy, as it implies that not all the emitted Zn electrons could be seen by XPS. Nevertheless, the absence of extra-framework ZnO particles as shown by UV-Vis spectroscopy (*vide infra*) suggests that Zn(II) is in the state of maximum dispersion defined by the K-M model. In the case of Ta(V), Figure 5.13 (b) shows that ZTT-1, 2 and 3, with total atomic content of Ta below 2% were within the monolayer limit of the K-M, indicating their high degree of dispersion. Interestingly, the case of ZTT-4 denotes how, in bimetallic TUD-1 catalyst, the detrimental effect of high metal loading on dispersion is not self-contained to each individual metal: the larger Zn content resulted in a greater deviation of the Ta(V) points from the K-M model compared to ZTT-5 despite having similar Ta mol.% loading—4.6 and 4.9 %, respectively. Optimization of α_1—the dimensionless particle size parameter—indicates that the effective particle size of the latter two is 3.3 and 0.9 nm, respectively. This observation corroborates the limitation of TUD-1 synthesis that high dispersion can only be achieved up to a certain metal loading.[39]

XRD patterns of as-prepared ZTT catalysts showed a broad peak at 2θ around 25°, typical of amorphous silica (Figure 5.S4). Moreover, the diffractogram suggested the absence of crystalline ZnO or Ta_2O_5 particles, even at higher metal loadings. This suggests that the metal oxides are either poorly crystalized and/or highly dispersed in the silica phase.

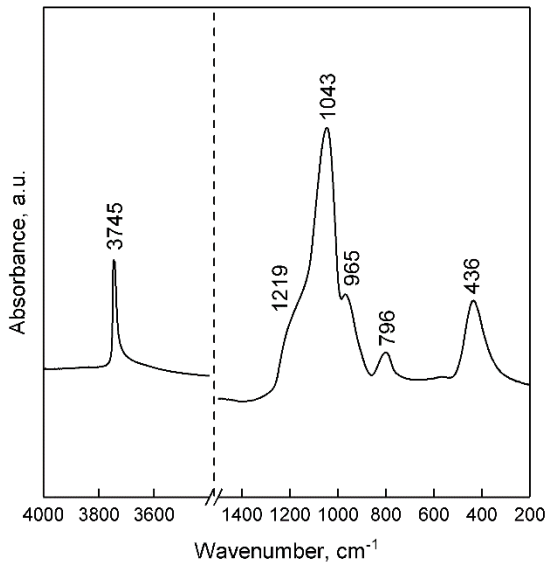

Figure 5.14 ATR-FTIR of ZTT-1 between 4000 and 200 cm^{-1}.

The ATR FTIR spectra of ZTT-1 showed the *v*(O-H) band at 3747 cm^{-1} typical of isolated silanol groups (Figure 5.14). Other signals typical of silica can be found in the 1500-200 cm^{-1} region: bands at 1043 and 1219 cm^{-1} are due to the asymmetric stretching vibrations of Si–O–Si; symmetric stretching vibration of Si–O–Si results in the band at 796 cm^{-1}; the band at 436 cm^{-1} is owed to O–Si–O bending vibrations. The absorption at 965 cm^{-1} could be generated by the stretching vibrations of Si–O–M[63,64] and/or terminal silanol groups. Recently, a band at 3721 cm^{-1} was identified on tantalum catalysts highly dispersed on silica and assigned to *v* Ta-OH; it was correlated with a superior activity in the conversion of ethanol-acetaldehyde mixtures to butadiene.[65] As it lacked this feature, ZTT-1 may not possess hydroxyl grounds bonded to Ta(V).

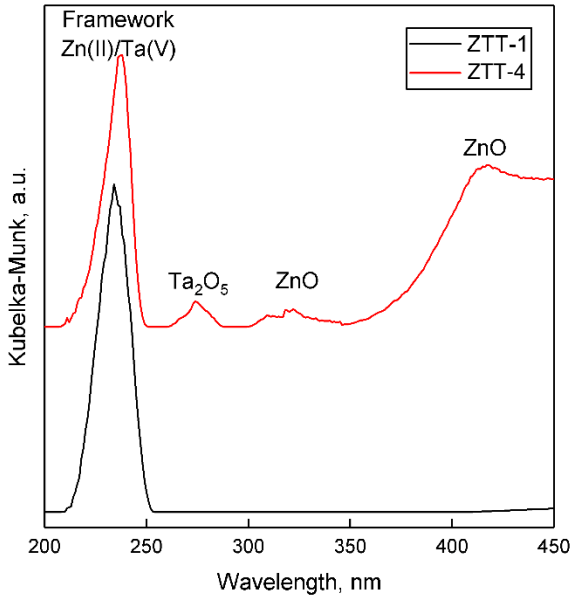

Figure 5.15 DR UV-Vis spectra of selected ZTT samples with two different metal contents. ZTT-1: 3.0 mol.% Zn, 1.9 mol.% Ta. ZTT-4: 22.3 mol.% Zn, 4.9 mol.% Ta

DRS UV-Vis analysis was used to verify the incorporation of Zn(II) and Ta(V) within the mesoporous silica framework. Figure 5.15 represents the UV-Vis spectra of ZTT 1 and ZTT 4 for comparison. ZTT-1 is characterized by an intense band centered at 233 nm. According to the literature, such a signal can be attributed to the charge transfer between silica lattice oxygen and transition metals, notably tetrahedral TaO_4 species dispersed on silica,[66,67] as well as tetrahedral Zn(II) incorporated within silicates.[68–70] The sharp band at 216 – 221 nm indicative of monoatomic Ta(V)[33,71–73] or Zn(II)[33] in silicates was not observed, but could be contained as the shoulder of the main signal. These results suggest that tantalum and zinc exist in Zn-Ta-TUD-1 as single-atom sites or small oxide domains contained within the mesoporous silica framework, likely in their tetrahedral form. Bandgap transitions typical of ZnO and Ta_2O_5 at 360 – 390 nm[74–76] and 260 – 275 nm,[21,56,67] respectively, were absent on samples with low metal loadings, excluding their presence in bulk form. With a higher metal loading, ZTT-5 showed signals at 275 nm, assigned to extra-framework Ta_2O_5. It also showed a band at 318 nm, which has been identified as extra-framework ZnO inside zeolites.[33] In addition, the strong signal at 415 nm can also be associated with ZnO nanoparticles;[77,78] size effects explain the significant red shift in contrast to the bulk oxide.[79] Interestingly, ZTT-5 also exhibited the band indicative of incorporated metal oxide clusters at 233 nm,[67,69] implying that the synthesis process did not generate a uniform particle size distribution. Monometallic TUD-1 samples showed exclusively the band at 233 nm (Figure 5.S5).

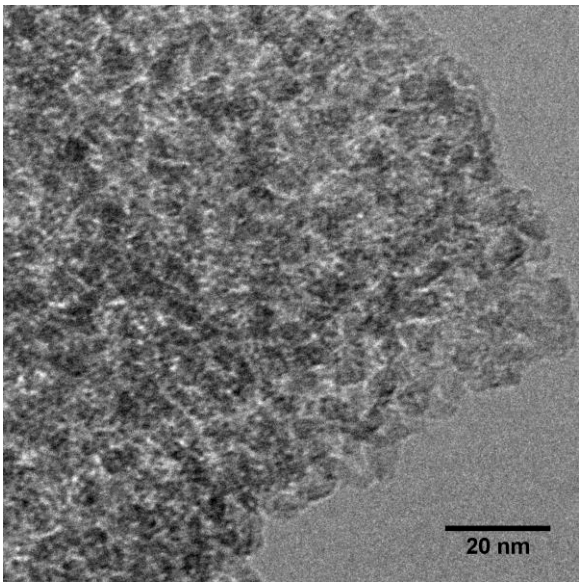

Figure 5.16 HR-TEM images of ZTT-1.

HR-TEM of ZTT-1 depicted in Figure 5.16confirmed the sponge-like mesoporous morphology of TUD-1 materials.[39] Moreover, no oxide particles could be detected, further confirming homogeneous incorporation of Zn(II) and Ta(V) inside the catalyst carrier.

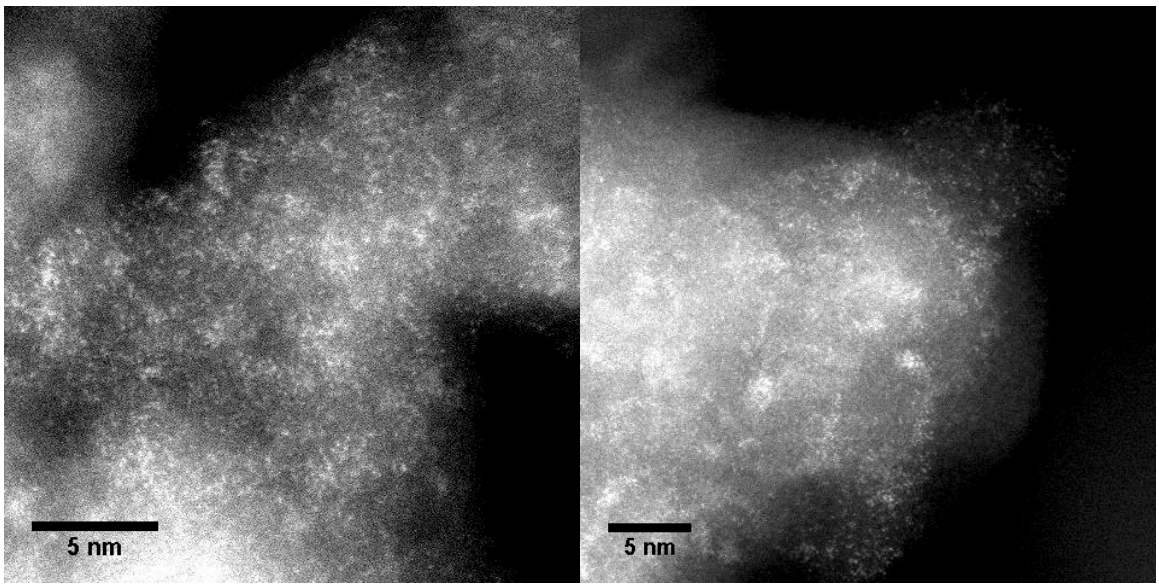

Figure 5.17 HAADF-STEM images of ZTT-1.

HAADF-STEM was used to further investigate the structure of metals inside Zn-Ta-TUD-1. As illustrated in Figure 5.17, ZTT-1 consisted of mononuclear metal sites and small polymeric oxide clusters around 1 nm in diameter. These were attributed exclusively to Ta(V) as the Z contrast

between Si and Zn was too low to clearly identify the structure of Zn(II) within the mesoporous silica. Nevertheless, STEM-EDX mapping (Figure 5.18) confirmed the presence of Zn(II) and its strong degree of integration with the Ta(V) phase.

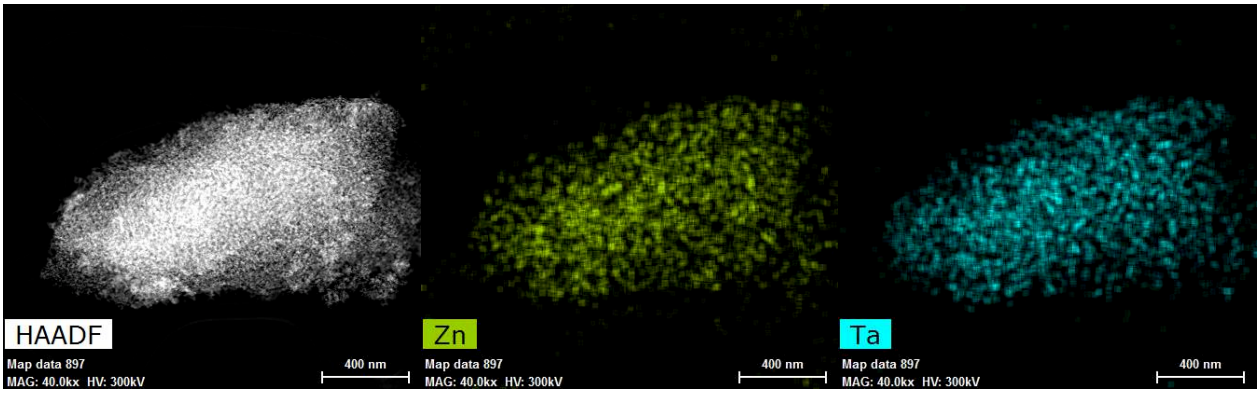

Figure 5.18 STEM-EDX mapping of ZTT-1.

Based on the combined characterization results, we can describe the structure of our best-performing Zn-Ta-TUD-1 catalysts. The mesoporous sponge-like morphology typical of TUD-1 materials was confirmed by HR-TEM. N_2 physisorption further provided the dimensions of pore diameter and specific surface; uniform pores between 6–20 nm were obtained together with high specific areas larger than 390 $m^2.g^{-1}$ and 658 $m^2.g^{-1}$ for the best performing catalyst. The carrier surface was confirmed to possess isolated silanol groups by IR spectroscopy. XPS revealed that below 5.0 mol.% of metal, Zn-Ta-TUD-1 catalysts were homogeneously dispersed over the silica surface in the form of metal oxides. HAADF-STEM indicated that Ta(V) in ZTT-1 existed in the form of mononuclear sites, along with polymeric oxide clusters no greater than 1 nm in diameter. UV-vis showed Ta(V) to be incorporated within the silica matrix with a band at 233 nm. According to the literature, such signal belongs to tetrahedral TaO_4 sites, as octahedral species were not detected.[67] The exact coordination of Zn(II) could not be determined, but UV-vis analysis found zinc oxide to be incorporated within the carrier matrix. Both phases were found to be thoroughly integrated within one another by EDX mapping.

5.3.2. Chemical Properties

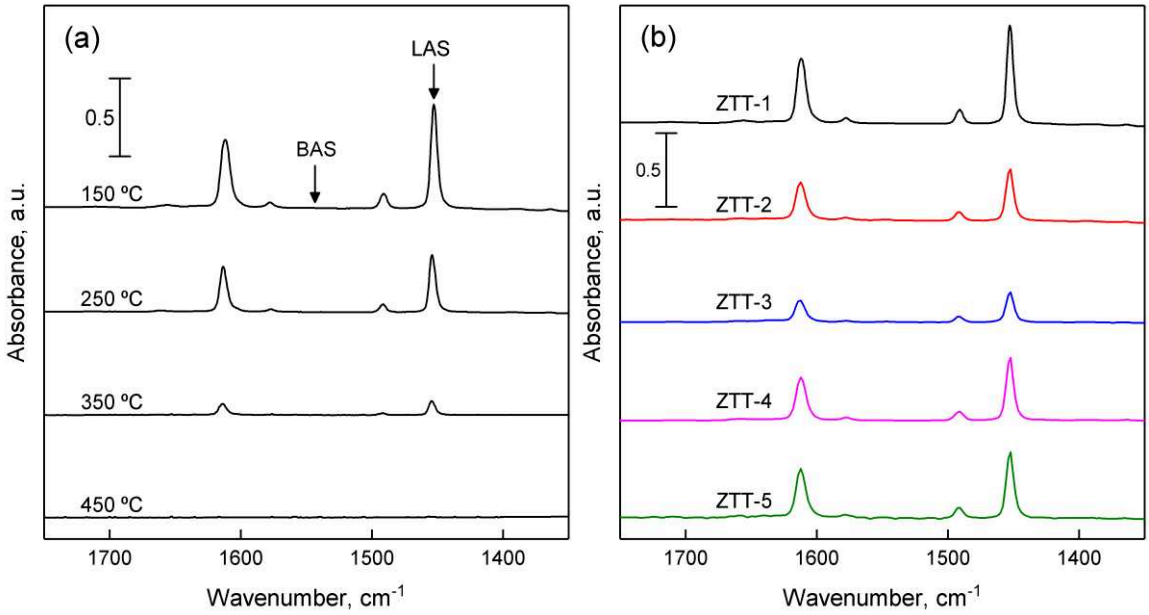

Figure 5.19 FTIR spectra of chemisorbed pyridine: (a) on ZTT-1 sample at different temperature; (b) on selected ZTT samples for comparison.

The surface acid properties of ZTT samples were analyzed using IR spectroscopy coupled with pyridine chemisorption. Figure 5.19 (a) depicts the results for the ZTT-1 sample at different desorption temperature. The bands detected at 1611, 1578 and 1454 cm^{-1} are due to pyridine coordinately bound on metal cations, *e.g.,* Lewis acid sites (LAS).[43,80] No signal at 1545 and 1638 cm^{-1} attributable to pyridinium ions formed on Brønsted acid sites (BAS) were observed. However, their presence on the surface of Zn-Ta-TUD-1 cannot be excluded: weak BAS have been detected using stronger basic probes on catalysts highly active in the Lebedev process.[23,33] Bands located at 1490 cm^{-1} can be attributed to both LAS and BAS. The progressive desorption of pyridine with increased temperatures entails the existence of LAS with different strengths on the surface of ZTT-1. Our results are similar to those observed over silicate-supported transition metals active in the Lebedev process, including the related Zn-Ta-SiBEA catalyst prepared by Kyriienko *et al*.[33]

Table 5.18 Quantification of Lewis acid sites on ZTT samples probed using pyridine-FTIR and calculated using the Beer-Lambert law.

Catalyst	LAS (mmol·g^{-1})	Zn (mol.%)	Ta (mol.%)
ZTT-1	0.276	3.1	1.9
ZTT-2	0.153	2.1	1.1
ZTT-3	0.101	2.3	1.0
ZTT-4	0.163	22.3	4.9
ZTT-5	0.199	8.8	4.6

As Figure 5.19 (b) illustrates, the selected ZTT samples also showed an absence of signal attributable to BAS. However, the intensity of the bands present differed, implying different amounts of LAS. Their quantification was performed using the Beer-Lambert law (Eqn (7)):

$$A = \frac{\varepsilon \cdot W \cdot C_w}{S} \quad (7)$$

where W (kg), C_w (mol kg^{-1}) and S (m^2) represent sample weight, probe concentration and disk area, respectively.[43,80] As listed in Table 5.18**Error! Reference source not found.**, the samples prepared for our comparative study had different numbers of LAS, which were not directly correlated with their metal content, notably at high loading. Most likely, the larger metal oxide particles formed at higher metal contents resulted in fewer acid sites, a phenomenon already observed elsewhere.[81] Despite having a lower metal content, ZTT-1, the most active catalyst, showed the highest concentration of LAS. This observation can be attributed to the high degree of dispersion confirmed by TEM and XPS.

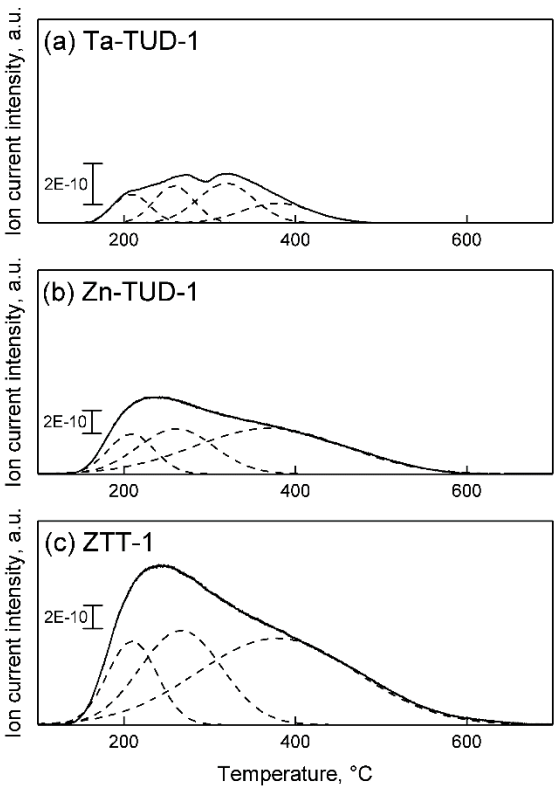

Figure 5.20 NH_3-TPD profiles of (a) Ta-TUD-1, (b) Zn-TUD-1, (c) ZTT-1.

The acid strength distribution of ZTT-1 was studied and compared to that of Zn-TUD-1 and Ta-TUD-1 using NH_3-TPD. As we previously reported, Zn-Ta-TUD-1 showed a single broad and asymmetric desorption peak indicative of a somewhat heterogeneous acid strength distribution (**Error! Reference source not found.**Figure 5.20(c)). Similar experiments on other bimetallic catalysts for the ethanol-to-butadiene reaction have shown comparable results,[82,83] although some authors were able to clearly identify acid sites of distinct strengths.[28,84] Gaussian decomposition of the NH_3-TPD profiles, although purely a mathematical tool, showed at least three hidden peaks centered at different temperatures, denoting the heterogeneous strength distribution, which can be classified as weak, medium and strong.[85] When contrasted with monometallic samples, the desorption profile of ZTT-1 more closely resembled that of Zn-TUD-1 (**Error! Reference source not found.**Figure 5.20(b)), revealing almost identical "hidden" peaks. Ta-TUD-1 showed more discernable peaks with similar desorption temperatures, except for a second medium-strength acid site centered at 320 °C absent on ZTT-1 (Figure 5.20(a)).

Table 5.19 Acid site strength distribution and quantification on selected catalyst according to their deconstructed NH_3-TPD profile.

Catalyst	Number of acid site ($mmol \cdot g^{-1}$)				
	Weak (205 ± 5 °C)	Medium 1 (261 ± 5 °C)	Medium 2 (320 °C)	Strong (382 ± 2 °C)	Total
ZTT-1	0.112	0.231	n/a	0.418	0.772
Zn-TUD-1	0.068	0.134	n/a	0.276	0.478
Ta-TUD-1	0.036	0.058	0.061	0.043	0.198

Nevertheless, comparing the sum of surface-derived acid sites amounts on each monometallic sample suggested both Zn(II) and Ta(V) contributed to the acid properties of ZTT-1 (Table 5.19). Interestingly, we did not observe the passivation of stronger acid sites by the presence of Zn as reported by other scholars on Zn-Hf and Zn-Zr catalysts.[28,36,86] Instead, the Zn(II) phase possessed additional stronger sites than Ta(V) when comparing each monometallic TUD-1 catalyst. The significantly different preparation methods used may explain this discrepancy. It should be noted that the dissimilar number of acid sites quantified by NH_3-TPD and pyridine-FTIR is not an uncommon phenomenon, and the difference in probe size and *pKa* may account for it.[80,87]

The observed LAS can be attributed to the Zn(II) and Ta(V) species, both having demonstrated Lewis characteristics when supported on silicates and studied with pyridine-FTIR analysis.[72,88,89] In Zn-Ta-TUD-1, Lewis acidity—the ability to accept a pair of electron—originates from the partial positive charge of the metal cations that comes about when its valence electrons covalently bound with the oxygen atoms of the framework, which becomes a Lewis basic site.[90] The resulting Lewis acid-base pairs can participate in a variety of organic reactions by interacting with electron-rich compounds, often *via* the cooperation of the acid and basic moiety.

Both zinc[91–94] and, more rarely, tantalum oxide[66] have been described as amphoteric materials. In fact, the necessity of basic or redox sites for converting ethanol first to acetaldehyde before BD has often been highlighted.[33,36,95] However, in our previous publication, we reported that CO_2-TPD of Zn and Ta-containing catalysts revealed little correlation between the basic properties of our samples and their performances;[37] the inadequacy of CO_2 for probing sites active in the Lebedev process reported by other scholars may be the cause.[82,96]

H2-TPR was also used to characterize the properties of catalysts capable of dehydrogenation reactions, as their reducibility can be related to activity.[97,98] In accordance with the literature, Ta-TUD-1 did not reduce in a hydrogen atmosphere even at 1100 °C.[66]

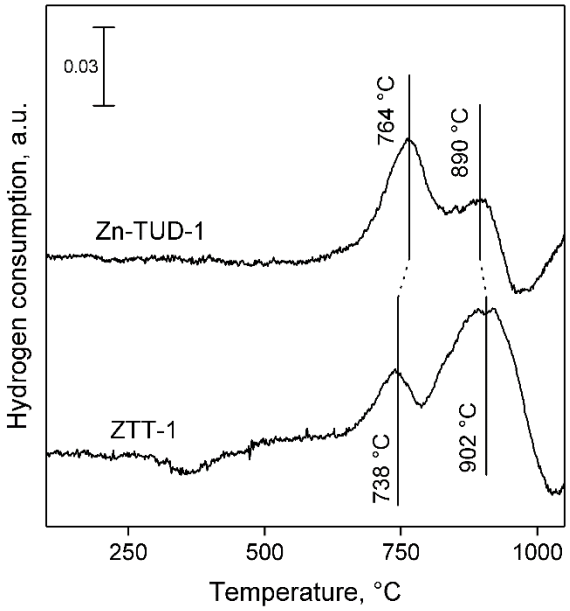

Figure 5.21 TPR profiles of Zn-TUD-1 and ZTT-1.

Figure 5.21 compares the H2-TPR profiles of Zn-TUD-1 and ZTT-1. In Zn-TUD-1, Zn(II) predominantly reduces at 764 °C, with a secondary signal around 890 °C. With ZTT-1, the presence of Ta(V) significantly lowers the reducibility of Zn(II), the major species now reducing at 902 °C, with a smaller signal at 738 °C. The reducibility of zinc can be affected by different factors. Pidko *et al.*found that zinc oxide supported on zeolites were less reducible the higher its degree of aggregation.[97] This explanation would indicate that the Zn(II) phase in Zn-TUD-1 was less aggregated than in ZTT-1, which was shown to be highly dispersed by XPS analysis. As the chemical environment can affect the reducibility of metal oxides,[85,98–101] another possibility is the presence of the Ta(V) phase lessening the reducibility of Zn(II).

5.3.3. Catalytic Activity

To perform the many steps in the conversion of ethanol to BD, catalysts require a combination of chemical properties. As stipulated by Ivanova *et al*., this is often achieved by combining metal oxides, each possessing part of the desired activity, most notably a dehydrogenation function and a condensation function.[95] It is assumed that the necessary dehydration steps are so thermodynamically favoured that the aforementioned active phases suffice.[5] In the case of our catalyst, Zn(II) and Ta(V) are the active phases. Zinc oxide, whether as a bulk phase or supported, can dehydrogenate and dehydrate short-chain alcohols.[92,93,98] Supported tantalum oxide has long been known to catalyse the conversion of ethanol-acetaldehyde mixtures to BD.[21,102–104] Both have

been used as components of catalysts for the Lebedev process, notably in the work of Kyriienko *et al.*, who supported the two phases on dealuminated zeolite.[33] Consequently, we proposed that, in Zn-Ta-TUD-1, the zinc phase provided the ability to catalyst of forming acetaldehyde from ethanol and the tantalum phase to condense it to precursors of BD.[37] Catalytic testing combined with characterization was employed to check this hypothesis.

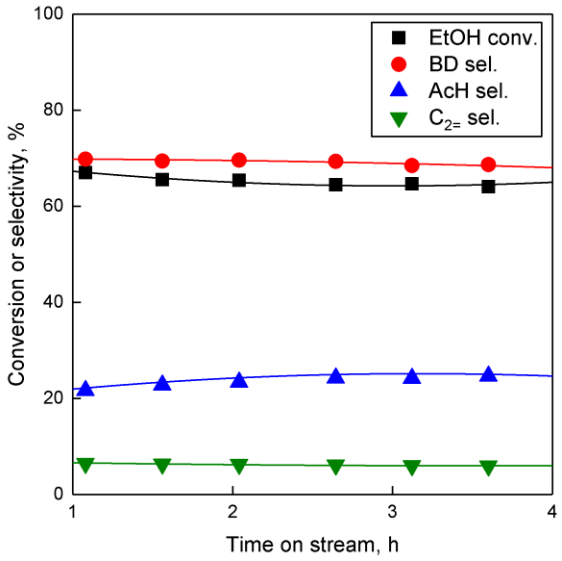

Figure 5.22 Conversion and selectivity towards major products of ethanol conversion on ZTT-1 over time. T = 350 C, P = 1 atm, $WHSV_{EtOH}$ = 5.3 h^{-1}.

The catalytic activity of Zn-Ta-TUD-1 under conditions aimed at maximizing BD productivity have formerly been reported.[37] As we previously noted, increasing contact time and temperature improves ethanol conversion and BD yield. In this work, temperature and ethanol space velocity were controlled allowing a better comparison between the selected catalysts by avoiding total ethanol conversion. At 350 °C and a $WHSV_{EtOH}$ of 5.3 h^{-1}, conversion did not exceed 67%. The performances exhibited by ZTT-1 under these conditions are depicted in Figure 5.22. It shows the main products were BD, acetaldehyde and ethylene—other compounds such as diethyl ether, propylene and crotonaldehyde accounted for less than 4% of products on a carbon basis. Ethanol conversion and product selectivity remained stable for the duration of catalytic test of 4 hour. Initial conversion and BD selectivity, which were obtained by extrapolation at TOS = 0 h, were 67.0 % and 68.1 %, respectively. Although the resulting BD yield was lower than at 400 °C,[37] BD selectivity is comparable to that of other well-performing catalysts found in the literature.[5,6]

Table 5.20 Initial catalytic performances in the Lebedev process of Zn-Ta-TUD-1 samples at 350 °C and $WHSV_{EtoH}$ of 5.3 h^{-1}.

Catalyst	X_{EtOH} (%)	BD S. (%)	AcH S. (%)	$C_{2=}$ S. (%)	CB (%)	BD Prod. $mmol \cdot gcat^{-1} \cdot h^{-1}$
ZTT-1	67.0	68.1	21.9	6.5	97.7	26.3
ZTT-2	53.6	42.8	24.6	24.1	95.4	13.2
ZTT-3	36.2	49.3	24.3	18.1	97.0	10.3
ZTT-4	40.6	50.6	40.0	7.1	99.1	11.8
ZTT-5	57.3	58.8	30.5	6.5	97.6	19.4

X_{EtOH}: ethanol conversion; BD S.: butadiene selectivity; AcH S.: acetaldehyde selectivity; $C_{2=}$ S. : ethylene selectivity; CB: carbon balance.

Catalytic test results for the other samples of the ZTT series are listed in Table 5.20. Evidently, performances differed from one catalyst to another, notably in terms of BD yield. This provided us with the opportunity to establish a relationship between the properties characterized and catalytic activity.

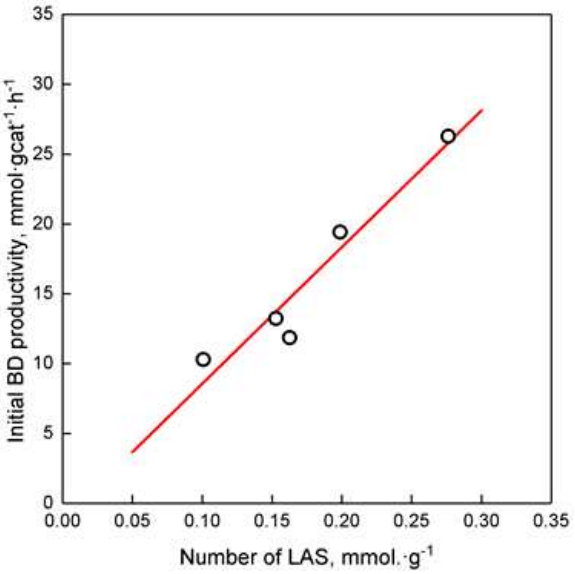

Figure 5.23 Initial butadiene productivity versus the number of Lewis acid sites on Zn-Ta-TUD-1 catalysts quantified by the FTIR of adsorbed pyridine.

As previously mentioned, Ivanova *et al*. established a correlation between the relative amount of 'open' Lewis acid sites on Zr-containing dealuminated zeolites, and the initial formation rate of BD.[17] For the first time, we report a similar correlation on zirconium-free catalyst. As illustrated in Figure 5.23, a linear correlation exists between the number of Lewis acid sites quantified by pyridine-FTIR (Table 5.18) and the initial productivity of BD (Table 5.20). The best fit was obtained with the quantification after desorption at 150 °C, suggesting that strong acid sites were not necessary. The aldol condensation is considered the rate-limiting step, partly evidenced by the

accumulation of acetaldehyde at high $WHSV_{EtOH}$.[20,24,37] Consequently, we propose that Lewis acid-base pairs found on Zn-Ta-TUD-1 are active sites for the aldol condensation of acetaldehyde that leads to BD.

Evidenced by the surface probing with NH_3 (Figure 5.20), both the Zn(II) and Ta(V) contribute to the to the surface acidity of Zn-Ta-TUD-1, which is predominantly Lewis acidic due the absence of pyridinium IR bands. As a result, it is unlikely that aldol condensation exclusively takes place on Lewis Ta(V) sites, despite its well-established condensation activity.[5,21,102,105] In agreement with Li *et al.*,[106] who studied the Lebedev mechanism on Zn-Y/SiBEA, Zn(II) is likely to contribute to the coupling activity of the catalyst. This conclusion is further reinforced by a linear correlation we previously observed between the total number of acid sites probed by NH_3 on Zn-Ta catalysts[37] and BD selectivity, highlighting the contribution of all acid sites.

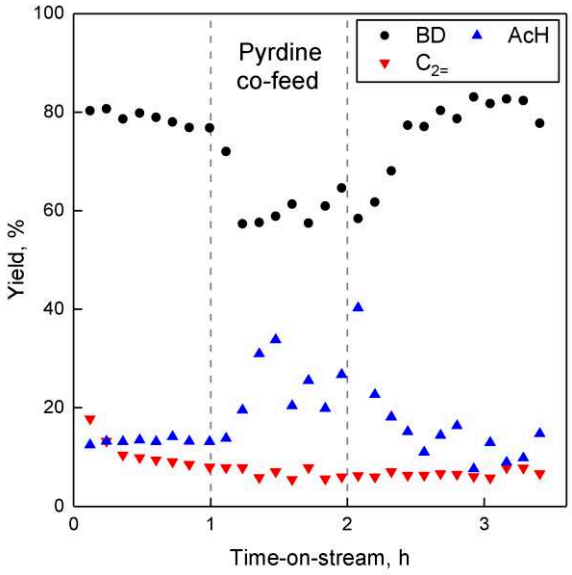

Figure 5.24 Pyridine poisoning reactivity test of the Lebedev process over ZTT-1 catalyst. The reaction was carried at 350 °C, WHSV of 0.3 h^{-1}. Concentration of pyridine in ethanol was 5 mol.%.

A poisoning study was performed to confirm the involvement of sites probed by pyridine in the conversion of ethanol to BD. The results are depicted in **Error! Reference source not found.**. I ntroducing pyridine into the reaction system caused a noticeable decrease BD yield. Together with the results of FTIR spectroscopy using pyridine as a probe (Figure 5.19), this experiment substantiates the involvement of metal cations in the reaction; the correlation observed in Figure 5.23. As catalytic activity was almost entirely recovered by switching back to a pure ethanol feed,

the involvement of acid sites strong enough to be irreversibly poisoned by pyridine at 350 °C must be limited. The small impact of pyridine co-feeding on the ethylene yield suggests that the basic probe does not poison sites responsible for ethanol dehydration. Similarly to other poison studies using basic probes,[19,107,108] acetaldehyde yield improved with the introduction of pyridine. On zinc oxide catalysts, the dehydrogenation of ethanol is believed to involve both moieties of Lewis acid-base pairs.[109] This suggests that both ethanol dehydrogenation and dehydration can take place on weaker acid sites less susceptible to poisoning by pyridine. Ostensibly, Lewis acid-base pairs are involved in every step of the ethanol-to-butadiene reaction. However, the possibility of hidden Brønsted sites and their participation cannot be disregarded.[19,33,36,110]

Table 5.21 Initial catalytic performances in the Lebedev process of monometallic TUD-1 catalysts, their mixture and hemimorphite, a zinc silicate. Major byproducts unaccounted for where diethyl ether, *1*-butanol, crotonaldehyde and ethyl acetate.

Catalyst	X_{EtOH} (%)	BD S. (%)	AcH S. (%)	$C_{2=}$ S. (%)
Zn-TUD-1	20.7	55.5	0.6	17.3
Ta-TUD-1	22.4	82.8	0.3	0.4
Zn+Ta-TUD-1	28.6	35.6	27.7	22.0
Hemimorphite	63.4	4.8	14.8	62.5

X_{EtOH}: ethanol conversion; BD S. : butadiene selectivity; AcH S.: acetaldehyde selectivity; $C_{2=}$ S. : ethylene selectivity.

To test the presumed role of Zn(II) and Ta(V), monometallic samples were tested under the same conditions (Table 5.21). Ta-TUD-1 exclusively formed products of ethanol dehydration, *e.g.*, ethylene and diethyl ether. These results agree with the literature on silica-supported Ta_2O_5 with highly dispersed oxide phases, as larger oxide particles generate dehydrogenation products from short-chain alcohols.[66] Surprisingly, Zn-TUD-1 predominantly formed ethylene and comparatively little acetaldehyde. Although the competition between alcohol dehydration and dehydrogenation on ZnO is known, we did not expect Zn-TUD-1 to exhibited so poor dehydrogenation capabilities. This observation questioned the role of Zn(II) in Zn-Ta-TUD-1. Hemimorphite—a zinc silicate known to promote ethanol dehydrogenation in catalysts for the Lebedev process—was investigated to exclude the possibility of error owed to our experimental set-; it formed significant amounts of acetaldehyde (Table 5.21). This confirmed what has been documented elsewhere: the chemical state of Zn(II) influences its catalytic activity.[93,98]

In the case of Zn-Ta-TUD-1, the synergism between Zn(II) and Ta(V) was investigated by testing the activity of both monometallic samples mechanically mixed together. As indicated in Table 5.21, this procedure noticeably increased acetaldehyde formation, but also overall activity in

the Lebedev process, indicative that more acetaldehyde was produced. Consequently, the proximity of the Zn(II) and Ta(V) phases in TUD-1 can be considered a prerequisite for the formation of BD, but also of acetaldehyde. As the NH_3 quantification of acid sites on ZTT-1 and both monometallic samples showed, the contribution between Zn(II) and Ta(V) cannot be attributed to the passivation of acid sites. Whereas several authors reported fewer strong acid sites upon introduction of a Zn(II) phase to transition metal oxides catalysts with Lewis acid characteristics,[28,36,86] the opposite effect was observed for Zn-Ta-TUD-1: Zn(II) was a major contributor to the overall acidity of the catalyst. A distinction between Zn-Ta-TUD-1 and other Zn-containing catalysts is the simultaneous incorporation of both metal oxide phases during the synthesis process. The passivation of acid sites may be partly owed to the post-synthesis method used, *i.e.*, impregnation or wet-kneading.

Explaining the discrepancy regarding the activity of Zn(II) is difficult, in part because the parameters that favour alcohol dehydrogenation over dehydration are not fully understood. For bulk ZnO, Drouilly *et al*. attributed its alcohol dehydrogenation activity to the presence of oxygen vacancies.[93,111] The structural properties of ZnO were also found to influence its activity with short-chain alcohol.[92,98,112] Unfortunately, fewer studies have been conducted regarding the activity of supported zinc oxide in dehydrogenation reactiosn,[113] and none could be found regarding ethanol dehydrogenation.

Clearly, the proximity with the Ta(V) phase is needed to enhance the dehydrogenation activity of Zn(II) when incorporated within TUD-1. This strongly suggests a synergism between the two phases. Judging from the H_2-TPR experiments (Figure 5.21), the presence of Ta(V) lowered the reducibility of Zn(II), implying change in the chemical state of the latter. Interestingly, the lower reducibility of bulk ZnO has been associated with superior activity in the dehydrogenation of alcohol versus dehydration.[98] Furthermore, lower reducibility of Zn aggregates was linked to a decreased basicity of the oxygen moiety in Lewis acid-base pairs. [97,114] Since strong basic sites are needed for alcohol dehydrogenation on such pairs,[115] the observed discrepancy may be explained by a change in the redox properties of Zn(II) induced by the presence of Ta(V). However, the exact nature of this synergistic effect remains to be elucidated.

5.3.4. Deactivation

There are strong economic incentives to limit the deactivation that occurs during the Lebedev process.[5,116,117] Understanding the deactivation mechanism would assist the design of more

resistant catalysts. While recent work has provided precious insights,[15,35,36] catalyst deactivation has not been fully understood, in part due to the multiplicity of materials and reaction conditions used.

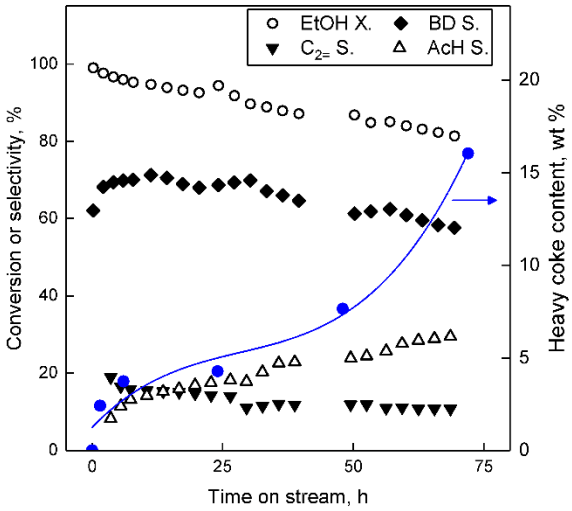

Figure 5.25 Ethanol conversion and product selectivity during the Lebedev process with ZTT-1 at 400 °C and $WHSV_{EtOH}$ of 5.3 h^{-1}. Only 25% of the data points are presented for increased clarity. The gap in data was caused by an unexpected shut down of the online-GC; the catalytic test itself was not compromised. The blue line indicates the accumulation of heavy coke content. $X_{EtOH:}$ ethanol conversion; BD S.: butadiene selectivity; AcH S.: acetaldehyde selectivity; $C_{2=}$ S. : ethylene selectivity.

Deactivation of Zn-Ta-TUD-1 was studied by testing ZTT-1 at 400 °C for a period of 70 hours and sampling the catalyst at various times on stream for analysis. The higher temperature was used to reflect reaction conditions more suitable for maximizing butadiene productivity. As shown in Figure 5.25, ethanol conversion decreased in a linear fashion. Selectivity towards BD initially increased and stabilized for the first 6 hours. Interestingly, it was mirrored by a fast loss in ethylene selectivity. This phenomenon may be explained by the initial poisoning of acid sites favourable to ethanol dehydration. BD selectivity peaked after six hours on stream and gradually decreased. This decline was compensated by an increase in acetaldehyde selectivity.

Coking has been identify major as source of deactivation during the conversion of ethanol to BD over many different catalysts.[19,24,34–36] Moreover, our team previously reported that calcination under air regenerated the catalytic activity of Zn-Ta-TUD-1—a possible sign of deactivation by coking.[37,117]

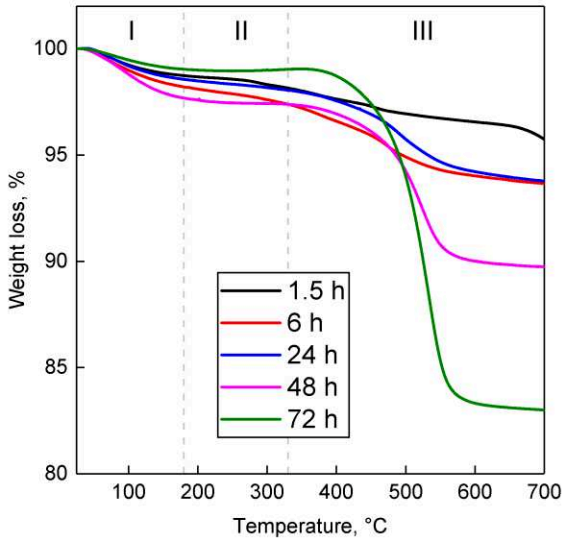

Figure 5.26 Thermograms of spent ZTT-1 at different TOS in the Lebedev process at 400 ºC and $WHSV_{EtOH\ of}$ 5.3 h^{-1}.

Coke deposits occurring in the Lebedev process on ZTT-1 were quantified by the TGA of spent catalysts after 1.5–72 hours on stream at 400 °C. The resulting thermograms (Figure 5.26) indicated the accumulation of removable matter with increased reaction time. Deposited substances were classified according the methodology of Liu *et al.*[118] into three temperature regions. Weight loss in region I (T < 180 °C) was assigned to water and volatile species, *e.g.*, reactants, intermediates and products. Region II (180 °C ≤ T ≤ 330 °C) was attributed to the loss of soft cokes—mobile, yet heavier carbonaceous species such as bulkier byproducts. The loss in region III (330 °C ≤ T) corresponded to the urther evidenced by the combined DSC-TGA analysis performed with ZTT-1 after 72 hours, which indicated an exothermal process took place beginning near 330 °C (Figure 5.S6). TGA results summarized in Table 5.S4 indicated that soft coke represented <1 % weight loss, a proportion which decreased after peaking at 6 h on stream. Heavy coke represented the greater fraction of substances accumulated; its content in ZTT-1 as a function of reaction time was plotted in Figure 5.25. As shown, heavy coke content rapidly increased during the first 6 hours of the reaction, coinciding with the stabilization of product selectivity mentioned previously. Beyond six hours, heavy coke content slowly increased as catalyst activity similarly decreased, implying the participation such specie in the deactivation process.

XPS was used to characterize the evolution of the surface of spent ZTT-1 as a function of time on stream. Bibby *et al.* developed a simple model for studying the coke deposition on catalyst pores

using XPS.[119] For materials with surface area larger than 200 $m^2 \cdot g^{-1}$, the dispersion of carbonaceous species within pore channels was proposed to proceed homogeneously following Eqn (8).

$$\left(\frac{C}{Si}\right)_{XPS} = \frac{wt}{12} \cdot \frac{100 - wt}{60} \quad (8)$$

where *wt* is the theoretical carbonaceous compound weight fraction, assuming the 100% silica support act as a solid solution; C and Si are the atomic percentages quantified by XPS using the C 1s and Si 2p peaks, respectively. Fresh ZTT-1 was used reference to estimate the quantity of atmospheric carbon pre-adsorbed.

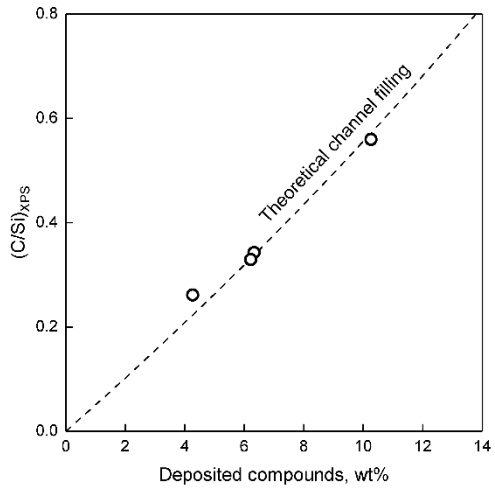

Figure 5.27 Measured C/Si ratio compared to the weight percent of carbonaceous species on spent ZTT-1 catalyst. The dashed line represents the C/Si function calculated assuming internal coke filling from a solid solution of carbon in SiO_2.[119]

In Figure 5.27, the resulting plot is compared to the atomic concentration of C and Si on ZTT-1 (TOS of 1.5 to 48 hours) versus TGA, where *wt* was assumed to be the total weight loss to account for trapped reactants. As illustrated, the model accurately predicted the relative XPS signal of carbon species inside ZTT-1 pore channels—disposition on the catalyst surface would have resulted in a drastic break-off from the theoretical line. Accordingly, the mesoporous structure of ZTT-1 accommodated the homogeneous deposition of carbonaceous compounds formed during the conversion of ethanol. Total pore blockage can disregarded a significant source of deactivation up to 48 hours, as no deviation from the theoretical model was observed. N_2 porosimetry confirmed that catalytic testing resulted in a reduction in average pore diameter, porous volume and specific surface area (Table 5.17).

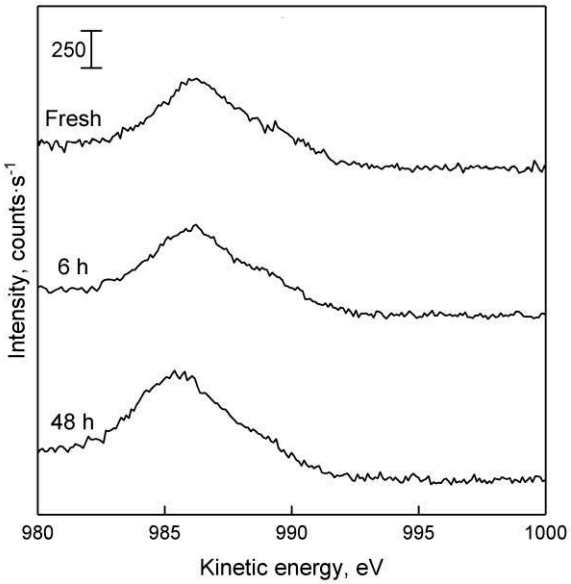

Figure 5.28 LMM Auger line of spent ZTT-1 with increasing time on stream during the Lebedev process. Dotted lines represent the appearance of Zn at different oxidation sate, as found in the literature. [50]

Recently, Villanueva Perales *et al.* proposed that the deactivation of their silica-supported hafnium-containing catalyst was owed to the *in situ* reduction of Zn(II) sites containing within hemimorphite—a zinc silicate used to promote ethanol dehydrogenation.[36] To verify whether this phenomenon took place with Zn-Ta-TUD-1, the Zn LMM Auger line of spent ZTT-1 was analyzed. Although the ethanol atmosphere of the Lebedev process can reduce metal oxides,[31,120] Figure 5.28 depicts how the oxidation state of Zn(II) in ZTT-1 was unaffected after several hours on stream. As expected, neither was Ta(V) (not shown). Consequently, we conclude that *in situ* reduction of the active phase is not a source of deactivation in Zn-Ta-TUD-1. Ostensibly, the low reducibility of Zn(II) in the presence of Ta(V) which was observed with H_2-TPR increased the resistance to deactivation of Zn-Ta-TUD-1.

Considering that the accumulation of heavy carbon species coincided with catalytic deactivation, we propose that the predominant deactivation mechanism is the formation and deposition of carbonaceous species inside the pores of Zn-Ta-TUD-1. Initially, there appears to be a selective poisoning of some active sites responsible for ethanol dehydration, as evidenced by the rapid change in selectivity the first 6 hours (Figure 5.25). However, the subsequent homogeneous channel filling indicated by the XPS analysis suggested the carbon deposition was not selective beyond that point. It also found that total pore blockage did not occur after 48 hours on stream.

Rather, the surface of pore channels was progressively filled with heavy carbon species, reducing the average pore diameter, porous volume and specific surface area. In this scenario, the loss of activity can be attributed to the physical inaccessibility of active sites. No change to the oxidation state of the metal oxide phase was observed by XPS, excluding it as a source of deactivation.

5.4. Conclusions

Zn-Ta-TUD-1 was shown to be one of the best performing catalyst in the production of butadiene from ethanol described in the literature. In the present study, a stable selectivity of 68% was achieved, which corroborates our previously that found the catalyst to be one of the most productive catalyst so far.[37] The TUD-1 preparation method allows for the one-pot synthesis of mesoporous materials with highly dispersed metal oxide phases. To verify the success of the synthesis method, 5 Zn-Ta-TUD-1 solids were synthesized with different metal loadings parameters, characterized and compared. For the best performing catalyst, N_2 porosimetry and TEM confirmed the foam-like mesoporous morphology expected of TUD-1 material. A combination of spectroscopy techniques revealed that the active phase consisted of highly dispersed Zn(II) and Ta(V) species incorporated within the silica matrix. TEM showed the Ta(V) phase to consist of mononuclear species and small metal oxide domains around 1 nm in diameter. This high degree of dispersion resulted in a strong concentration of Lewis acid sites. Contrarily, the TUD-1 synthesis could not be highly dispersed when 13 mol.% of metal were loaded in the synthesis, indicative of the method's limit. Instead extra-framework nanoparticles where formed, resulting in a lower Lewis acid site concentration despite the higher metal content.

A strong correlation between the initial productivity of BD and the concentration of Lewis acid sites in Zn-Ta-TUD-1 quantified with the IR spectroscopy of chemisorbed pyridine was established. Furthermore, a pyridine poison study confirmed the involvement of the probed sites in the condensation of acetaldehyde, which is recognized as the rate-determining step of the ethanol-to-butadiene reaction. Consequently, we propose that Lewis acid sites are the active sites in this reaction step. Characterization of the surface acidity suggested that both the Zn(II) and Ta(V) phases contributed to the condensation reactivity. Furthermore, synergy between Zn(II) and Ta(V) species was found necessary for enabling both the dehydrogenation of ethanol to acetaldehyde and its subsequent condensation.

The deactivation of Zn-Ta-TUD-1 was studied under reaction conditions intended to maximize butadiene productivity, *e.g.,* 400 ºC and $WHSV_{EtOH\ of}$ 5.3 h^{-1}. Analysis of spent catalysts recovered after 72 h runs revealed a significant accumulation of up to 16 wt.% of heavy carbonaceous species coinciding with the loss of catalytic activity. XPS revealed the deposition of carbon species proceeded homogeneously within the channels of the catalyst, which reduced its specific surface area, pore volume and pore size. Consequently, the deactivation mechanism appears to be the deposition of heavy carbon species within the catalyst, hindering the access to active sites. Total pore blockage and the reduction of the oxide active phase were dismissed as a source of deactivation.

5.5. References

(1) *OECD-FAO Agricultural Outlook 2017-2026*; OECD-FAO Agricultural Outlook; OECD, 2017.

(2) Abdulrazzaq, H. T.; Schwartz, T. J. *Catalytic Conversion of Ethanol to Commodity and Specialty Chemicals*; Elsevier Inc., 2018.

(3) Sun, J.; Wang, Y. Recent Advances in Catalytic Conversion of Ethanol to Chemicals. *ACS Catal.* **2014**, *4* (4), 1078–1090.

(4) Bozell, J. J.; Petersen, G. R. Technology Development for the Production of Biobased Products from Biorefinery Carbohydrates—the US Department of Energy's "Top 10" Revisited. *Green Chem.* **2010**, *12* (4), 539.

(5) Makshina, E. V; Dusselier, M.; Janssens, W.; Degrève, J.; Jacobs, P. A.; Sels, B. F. Review of Old Chemistry and New Catalytic Advances in the On-Purpose Synthesis of Butadiene. *Chem. Soc. Rev.* **2014**, *43*, 7917–7953.

(6) Pomalaza, G.; Capron, M.; Ordomsky, V.; Dumeignil, F. Recent Breakthroughs in the Conversion of Ethanol to Butadiene. *Catalysts* **2016**, *6* (12), 203.

(7) White, W. C. Butadiene Production Process Overview. *Chem. Biol. Interact.* **2007**, *166* (1–3), 10–14.

(8) Dahlmann, M.; Grub, J.; Löser, E. Butadiene. In *Ullmann's Encyclopedia of Industrial*

Chemistry; Wiley-VCH Verlag GmbH & Co. KGaA: Weinheim, Germany, 2011; Vol. 100 C, pp 1–24.

(9) Ren, T.; Patel, M. K.; Blok, K. Steam Cracking and Methane to Olefins: Energy Use, CO2emissions and Production Costs. *Energy* **2008**, *33* (5), 817–833.

(10) Plotkin, J. S. The Continuing Quest for Butadiene. American Chemical Society 2016.

(11) Amghizar, I.; Vandewalle, L. A.; Van Geem, K. M.; Marin, G. B. New Trends in Olefin Production. *Engineering* **2017**, *3* (2), 171–178.

(12) Bruijnincx, P. C. A.; Weckhuysen, B. M. Shale Gas Revolution: An Opportunity for the Production of Biobased Chemicals? *Angew. Chemie - Int. Ed.* **2013**, *52* (46), 11980–11987.

(13) Makshina, E. V.; Janssens, W.; Sels, B. F.; Jacobs, P. A. Catalytic Study of the Conversion of Ethanol into 1,3-Butadiene. *Catal. Today* **2012**, *198* (1), 338–344.

(14) Angelici, C.; Velthoen, M. E. Z.; Weckhuysen, B. M.; Bruijnincx, P. C. A. Effect of Preparation Method and CuO Promotion in the Conversion of Ethanol into 1,3-Butadiene over SiO 2 -MgO Catalysts. *ChemSusChem* **2014**, *7* (9), 2505–2515.

(15) Yan, T.; Yang, L.; Dai, W.; Wang, C.; Wu, G.; Guan, N.; Hunger, M.; Li, L. On the Deactivation Mechanism of Zeolite Catalyst in Ethanol to Butadiene Conversion. *J. Catal.* **2018**, *367*, 7–15.

(16) Da Ros, S.; Jones, M. D.; Mattia, D.; Schwaab, M.; Noronha, F. B.; Pinto, J. C. Modelling the Effects of Reaction Temperature and Flow Rate on the Conversion of Ethanol to 1,3-Butadiene. *Appl. Catal. A Gen.* **2017**, *530*, 37–47.

(17) Sushkevich, V. L.; Ivanova, I. I. Ag-Promoted ZrBEA Zeolites Obtained by Post-Synthetic Modification for Conversion of Ethanol to Butadiene. *ChemSusChem* **2016**, *9* (16), 2216–2225.

(18) Chung, S.-H.; Angelici, C.; Hinterding, S. O. M.; Weingarth, M.; Baldus, M.; Houben, K.; Weckhuysen, B. M.; Bruijnincx, P. C. A. Role of Magnesium Silicates in Wet-Kneaded Silica–Magnesia Catalysts for the Lebedev Ethanol-to-Butadiene Process. *ACS Catal.*

2016, *6* (6), 4034–4045.

(19) Taifan, W. E.; Baltrusaitis, J. In Situ Spectroscopic Insights on the Molecular Structure of the MgO/SiO 2 Catalytic Active Sites during Ethanol Conversion to 1,3-Butadiene. *J. Phys. Chem. C* **2018**, *122* (36), 20894–20906.

(20) Sushkevich, V. L.; Ivanova, I. I. Mechanistic Study of Ethanol Conversion into Butadiene over Silver Promoted Zirconia Catalysts. *Appl. Catal. B Environ.* **2017**, *215*, 36–49.

(21) Müller, P.; Burt, S. P.; Love, A. M.; McDermott, W. P.; Wolf, P.; Hermans, I. Mechanistic Study on the Lewis Acid Catalyzed Synthesis of 1,3-Butadiene over Ta-BEA Using Modulated Operando DRIFTS-MS. *ACS Catal.* **2016**, *6* (10), 6823–6832.

(22) Sushkevich, V. L.; Palagin, D.; Ivanova, I. I. With Open Arms: Open Sites of ZrBEA Zeolite Facilitate Selective Synthesis of Butadiene from Ethanol. *ACS Catal.* **2015**, *5* (8), 4833–4836.

(23) Sushkevich, V. L.; Vimont, A.; Travert, A.; Ivanova, I. I. Spectroscopic Evidence for Open and Closed Lewis Acid Sites in ZrBEA Zeolites Spectroscopic Evidence for Open and Closed Lewis Acid Sites in ZrBEA Zeolites. *J. Phys. Chem. C* **2015**, *119* (31), 17633–17639.

(24) Janssens, W.; Makshina, E. V.; Vanelderen, P.; De Clippel, F.; Houthoofd, K.; Kerkhofs, S.; Martens, J. A.; Jacobs, P. A.; Sels, B. F. Ternary Ag/MgO-SiO2 Catalysts for the Conversion of Ethanol into Butadiene. *ChemSusChem* **2015**, *8* (6), 994–1008.

(25) Kvisle, S.; Aguero, A.; Sneeden, R. P. A. Transformation of Ethanol into 1,3-Butadiene over Magnesium Oxide/Silica Catalysts. *Appl. Catal.* **1988**, *43* (1), 117–131.

(26) Kurmach, M. M.; Larina, O. V.; Kyriienko, P. I.; Yaremov, P. S.; Trachevsky, V. V.; Shvets, O. V.; Soloviev, S. O. Hierarchical Zr-MTW Zeolites Doped with Copper as Catalysts of Ethanol Conversion into 1,3-Butadiene. *ChemistrySelect* **2018**, *3* (29), 8539–8546.

(27) Zhu, Q.; Wang, B.; Tan, T. Conversion of Ethanol and Acetaldehyde to Butadiene over MgO–SiO $_2$ Catalysts: Effect of Reaction Parameters and Interaction between MgO and SiO $_2$ on Catalytic Performance. *ACS Sustain. Chem. Eng.* **2017**, *5* (1), 722–733.

(28) Baylon, R. A. L.; Sun, J.; Wang, Y. Conversion of Ethanol to 1,3-Butadiene over Na Doped ZnxZryOz Mixed Metal Oxides. *Catal. Today* **2014**, *259*, 446–452.

(29) Sushkevich, V. L.; Ivanova, I. I.; Taarning, E. Mechanistic Study of Ethanol Dehydrogenation over Silica-Supported Silver. *ChemCatChem* **2013**, *5* (8), 2367–2373.

(30) Dagle, V. L.; Flake, M. D.; Lemmon, T. L.; Lopez, J. S.; Kovarik, L.; Dagle, R. A. Effect of the SiO 2 Support on the Catalytic Performance of Ag/ZrO 2 /SiO 2 Catalysts for the Single-Bed Production of Butadiene from Ethanol. *Appl. Catal. B Environ.* **2018**, *236* (May), 576–587.

(31) Angelici, C.; Meirer, F.; van der Eerden, A. M. J.; Schaink, H. L.; Goryachev, A.; Hofmann, J. P.; Hensen, E. J. M.; Weckhuysen, B. M.; Bruijnincx, P. C. A. Ex Situ and Operando Studies on the Role of Copper in Cu-Promoted SiO 2 –MgO Catalysts for the Lebedev Ethanol-to-Butadiene Process. *ACS Catal.* **2015**, *5* (10), 6005–6015.

(32) Taifan, W. E.; Li, Y.; Baltrus, J. P.; Zhang, L.; Frenkel, A. I.; Baltrusaitis, J. Operando Structure Determination of Cu and Zn on Supported MgO/SiO 2 Catalysts during Ethanol Conversion to 1,3-Butadiene. *ACS Catal.* **2019**, *9* (1), 269–285.

(33) Kyriienko, P. I.; Larina, O. V.; Soloviev, S. O.; Orlyk, S. M.; Calers, C.; Dzwigaj, S. Ethanol Conversion into 1,3-Butadiene by the Lebedev Method over MTaSiBEA Zeolites (M = Ag, Cu, Zn). *ACS Sustain. Chem. Eng.* **2017**, *5* (3), 2075–2083.

(34) Kim, T. W.; Kim, J. W.; Kim, S. Y.; Chae, H. J.; Kim, J. R.; Jeong, S. Y.; Kim, C. U. Butadiene Production from Bioethanol and Acetaldehyde over Tantalum Oxide-Supported Spherical Silica Catalysts for Circulating Fluidized Bed. *Chem. Eng. J.* **2014**, *278*, 217–223.

(35) Zhang, M.; Tan, X.; Zhang, T.; Han, Z.; Jiang, H. The Deactivation of a ZnO Doped ZrO 2 –SiO 2 Catalyst in the Conversion of Ethanol/Acetaldehyde to 1,3-Butadiene. *RSC Adv.* **2018**, *8* (59), 34069–34077.

(36) Cabello González, G. M.; Murciano, R.; Villanueva Perales, A. L.; Martínez, A.; Vidal-Barrero, F.; Campoy, M.; González, G. M. C.; Murciano, R.; Perales, A. L. V.; Martínez, A.; et al. Ethanol Conversion into 1,3-Butadiene over a Mixed Hf-Zn Catalyst: A Study of

the Reaction Pathway and Catalyst Deactivation. *Appl. Catal. A Gen.* **2019**, *570* (July 2018), 96–106.

(37) Pomalaza, G.; Vofo, G.; Capron, M.; Dumeignil, F. ZnTa-TUD-1 as an Easily Prepared, Highly Efficient Catalyst for the Selective Conversion of Ethanol to 1,3-Butadiene. *Green Chem.* **2018**, *20* (14), 3203–3209.

(38) Jansen, J. C.; Shan, Z.; Marchese, L.; Zhou, W.; Puil, N. v d; Maschmeyer, T. A New Templating Method for Three-Dimensional Mesopore Networks. *Chem. Commun.* **2001**, No. 8, 713–714.

(39) Telalović, S.; Ramanathan, A.; Mul, G.; Hanefeld, U. TUD-1: Synthesis and Application of a Versatile Catalyst, Carrier, Material…. *J. Mater. Chem.* **2010**, *20* (4), 642.

(40) TELES, JOAQUIM HENRIQUE; RIEBER, NORBERT; BREUER, KLAUS; DEMUTH, DIRK; HIBST, HARTMUT; HAGEMEYER, A. Verfahren Zur Herstellung Eines Hemimorphit-Katalysators. EP1050510B1, 2003.

(41) Walton, J.; Wincott, P.; Fairley, N.; Carrick, A. Peak Fitting with CasaXPS: A Casa Pocket Book. **2010**.

(42) Kubelka, P.; Munk, F. Ein Beitrag Zur Optik Der Farbanstriche (Contribution to the Optic of Paint). *Zeitschrift fur Tech. Phys.* **1931**, *12*, 593–601.

(43) Tamura, M.; Shimizu, K.; Satsuma, A. Comprehensive IR Study on Acid/Base Properties of Metal Oxides. *Appl. Catal. A Gen.* **2012**, *433–434*, 135–145.

(44) Dumeignil, F.; PAUL, S.; Duhamel, L.; FAYE, J.; Miquel, P.; CAPRON, M.; Dubois, J. L. Dispositif d'évaluation d'au Moins Un Critère de Performance de Catalyseurs Hétérogènes. WO2015118263 A1, 2015.

(45) Sing, K. S. W.; Rouquerol, J. Characterization of Solid Catalysts: Physical Properties: Surface Area and Porosity. *Handb. Heterog. Catal.* **2008**, *2–5*, 427–439.

(46) Ramanathan, A.; Carmen Castro Villalobos, M.; Kwakernaak, C.; Telalovic, S.; Hanefeld, U. Zr-TUD-1: A Lewis Acidic, Three-Dimensional, Mesoporous, Zirconium-Containing Catalyst. *Chem. - A Eur. J.* **2008**, *14* (3), 961–972.

(47) Pachamuthu, M. P.; Srinivasan, V. V.; Maheswari, R.; Shanthi, K.; Ramanathan, A. Lewis Acidic ZrTUD-1 as Catalyst for Tert-Butylation of Phenol. *Appl. Catal. A Gen.* **2013**, *462–463*, 143–149.

(48) Dake, L. S.; Baer, D. R.; Zachara, J. M. Auger Parameter Measurements of Zinc Compounds Relevant to Zinc Transport in the Environment. *Surf. Interface Anal.* **1989**, *14* (1-2), 71–75.

(49) Barr, T. L.; Yin, M.; Varma, S. Detailed X-ray Photoelectron Spectroscopy Valence Band and Core Level Studies of Select Metals Oxidations. *J. Vac. Sci. Technol. A Vacuum, Surfaces, Film.* **1992**, *10* (4), 2383–2390.

(50) Rodriguez, J. A.; Jirsak, T.; Dvorak, J.; Sambasivan, S.; Fischer, D. Reaction of NO 2 with Zn and ZnO: Photoemission, XANES, and Density Functional Studies on the Formation of NO 3 . *J. Phys. Chem. B* **2002**, *104* (2), 319–328.

(51) Moretti, G. Auger Parameter and Wagner Plot in the Characterization of Chemical States by X-Ray Photoelectron Spectroscopy: A Review. *J. Electron Spectros. Relat. Phenomena* **1998**, *95* (2–3), 95–144.

(52) Michael Böttger, P. H.; Diplas, S.; Flage-Larsen, E.; Prytz, Y.; Finstad, T. G. Electronic Structure of Thermoelectric Zn-Sb. *J. Phys. Condens. Matter* **2011**, *23* (26), 1–5.

(53) Louis, C. Preparation of Coimpregnated Cu - Zn on Zn-Modified Silica : Influence of the Basicity Of. **2010**, 11140–11147.

(54) National Institute of Standards and Technology. NIST X-ray Photoelectron Spectroscopy Database, NIST Standard Reference Database Number 20 https://srdata.nist.gov/xps/Default.aspx.

(55) Garbassi, F.; Bart, J. C. J.; Petrini, G. XPS Study of Tellurium—Niobium and Tellurium—Tantalum Oxide Systems. *J. Electron Spectros. Relat. Phenomena* **1981**, *22* (2), 95–107.

(56) Kondo, J. N.; Yamazaki, H.; Ishikawa, A.; Osuga, R.; Takao, S.; Yokoi, T.; Kikkawa, S.; Teramura, K.; Tanaka, T. Monolayer Tantalum Oxide on Mesoporous Silica Substrate. *ChemistrySelect* **2016**, *1* (12), 3124–3131.

(57) Kerkhof, F. P. J. M.; Moulijn, J. A. Quantitative Analysis of XPS Intensities for Supported Catalysts. *J. Phys. Chem.* **1979**, *83* (12), 1612–1619.

(58) León, V. A Simplified Kerkhof-Moulijn Model for Dispersion Quantification from XPS Atomic Concentrations. *Surf. Sci.* **1995**, *339* (3), L931–L934.

(59) Nikolova, D.; Edreva-Kardjieva, R.; Grozeva, T.; Gouliev, G. *A COMPARATIVE STUDY OF XPS MODELS FOR PARTICLE SIZE DETERMINATION OF MOLYBDENUM SUPPORTED CATALYSTS*; 2006.

(60) Scofield, J. H. Hartree-Slater Subshell Photoionization Cross-Sections at 1254 and 1487 EV. *J. Electron Spectros. Relat. Phenomena* **1976**, *8* (2), 129–137.

(61) Tanuma, S.; Powell, C. J.; Penn, and D. R. Calculations of Electron Inelastic Mean Free Paths. V. Data for 14 Organic Compounds over the 50–2000 EV Range. *Surf. Interface Anal.* **1994**, *21* (3), 165–176.

(62) Tougaard, S. QUASES-IMFP-TPP2M: Database for Calculation of IMFPs by TPP2M Formula, Version 3.0. QUASES-Tougaard Inc, Odense, Denmark 2016.

(63) Camblor, M. A.; Corma, A. Infrared Spectroscopic Investigation of Titanium in Zeolites. A New Assignment of the 960 Cm-1 Band. **1993**, 557–559.

(64) Sasidharan, M.; Kiyozumi, Y.; Mal, N. K.; Paul, M.; Rajamohanan, P. R.; Bhaumik, A. Microporous and Mesoporous Materials Incorporation of Tin in Different Types of Pores in SBA-15 : Synthesis , Characterization and Catalytic Activity. *Microporous Mesoporous Mater.* **2009**, *126* (3), 234–244.

(65) Gaval, P. Catalysts for Butadiene Synthesis by Ostromyslensky Process Developed by Surface Organometallic Chemistry, Université Calude Bernard, 2018.

(66) Chen, Y.; Fierro, J. L. G.; Tanaka, T.; Wachs, I. E. Supported Tantalum Oxide Catalysts: Synthesis, Physical Characterization, and Methanol Oxidation Chemical Probe Reaction. *J. Phys. Chem. B* **2003**, *107* (22), 5243–5250.

(67) Baltes, M.; Kytökivi, A.; Weckhuysen, B. M.; Schoonheydt, R. A.; Van Der Voort, P.; Vansant, E. F.; Kyto, A.; Weckhuysen, B. M.; Schoonheydt, R. A.; Voort, P. Van Der; et

al. Supported Tantalum Oxide and Supported Vanadia-Tantala Mixed Oxides: Structural Characterization and Surface Properties. *J. Phys. Chem. B* **2001**, *105* (26), 6211–6220.

(68) Wang, L.; Sang, S.; Meng, S.; Zhang, Y.; Qi, Y.; Liu, Z. Direct Synthesis of Zn-ZSM-5 with Novel Morphology. *Mater. Lett.* **2007**, *61* (8–9), 1675–1678.

(69) Hur, S. G.; Kim, T. W.; Hwang, S. J.; Hwang, S. H.; Yang, J. H.; Choy, J. H. Heterostructured Nanohybrid of Zinc Oxide-Montmorillonite Clay. *J. Phys. Chem. B* **2006**, *110* (4), 1599–1604.

(70) Popova, M.; Trendafilova, I.; Szegedi, Á.; Mihály, J.; Németh, P.; Marinova, S. G.; Aleksandrov, H. A.; Vayssilov, G. N. Experimental and Theoretical Study of Quercetin Complexes Formed on Pure Silica and Zn-Modified Mesoporous MCM-41 and SBA-16 Materials. *Microporous Mesoporous Mater.* **2016**, *228*, 256–265.

(71) Ruddy, D. A.; Tilley, T. D. Kinetics and Mechanism of Olefin Epoxidation with Aqueous H 2O2 and a Highly Selective Surface-Modified TaSBA15 Heterogeneous Catalyst. *J. Am. Chem. Soc.* **2008**, *130* (33), 11088–11096.

(72) Trejda, M.; Wojtaszek, A.; Floch, A.; Wojcieszak, R.; Gaigneaux, E. M.; Ziolek, M. New Nb and Ta-FAU Zeolites - Direct Synthesis, Characterisation and Surface Properties. *Catal. Today* **2010**, *158* (1–2), 170–177.

(73) Dzwigaj, S.; Millot, Y.; Che, M. Ta(V)-Single Site BEA Zeolite by Two-Step Postsynthesis Method: Preparation and Characterization. *Catal. Letters* **2010**, *135* (3–4), 169–174.

(74) Lihitkar, P. B.; Violet, S.; Shirolkar, M.; Singh, J.; Srivastava, O. N.; Naik, R. H.; Kulkarni, S. K. Confinement of Zinc Oxide Nanoparticles in Ordered Mesoporous Silica MCM-41. *Mater. Chem. Phys.* **2012**, *133* (2–3), 850–856.

(75) Schröder, F.; Hermes, S.; Parala, H.; Hikov, T.; Muhler, M.; Fischer, R. A. Non Aqueous Loading of the Mesoporous Siliceous MCM-48 Matrix with ZnO: A Comparison of Solution, Liquid and Gas-Phase Infiltration Using Diethyl Zinc as Organometallic Precursor. *J. Mater. Chem.* **2006**, *16* (35), 3565–3574.

(76) Yoshida, H. Highly Dispersed Zinc Oxide Species on Silica as Active Sites for

Photoepoxidation of Propene by Molecular Oxygen. *J. Catal.* **2003**, *220* (1), 226–232.

(77) Jayachandraiah, C.; Krishnaiah, G.; Siva Kumar, K. Ce Induced Structural and Optical Properties of Ce Doped Zno Nanoparticles. *Int. J. ChemTech Res.* **2014**, *6* (6 SPEC. ISS.), 3378–3381.

(78) Hu, S.; Wang, B.; Zhu, M.; Ma, Y.; Lv, Z.; Wang, H. High-Performance 1D Type-II TiO 2 @ZnO Core-Shell Nanorods Arrays Photoanodes for Photoelectrochemical Solar Fuel Production. *Appl. Surf. Sci.* **2017**, *403*, 126–132.

(79) Kumar, S. S.; Venkateswarlu, P.; Rao, V. R.; Rao, G. N. Synthesis, Characterization and Optical Properties of Zinc Oxide Nanoparticles. *Int. Nano Lett.* **2013**, *3* (1), 30.

(80) Barzetti, T.; Selli, E.; Moscotti, D.; Forni, L.; Fisica, C.; Milano, U.; Golgi, V. C. Pyridine and Ammonia as Probes for FTIR Analysis of Solid Acid Catalysts. **1996**, *92* (ii), 1401–1407.

(81) Kyriienko, P. I.; Larina, O. V.; Popovych, N. O.; Soloviev, S. O.; Millot, Y.; Dzwigaj, S. Effect of the Niobium State on the Properties of NbSiBEA as Bifunctional Catalysts for Gas- and Liquid-Phase Tandem Processes. *J. Mol. Catal. A Chem.* **2016**, *424*, 27–36.

(82) Angelici, C.; Velthoen, M. E. Z.; Weckhuysen, B. M.; Bruijnincx, P. C. A. Influence of Acid–Base Properties on the Lebedev Ethanol-to-Butadiene Process Catalyzed by SiO2–MgO Materials. *Catal. Sci. Technol.* **2015**, *5* (5), 2869–2879.

(83) Patil, P. T.; Liu, D.; Liu, Y.; Chang, J.; Borgna, A. Improving 1,3-Butadiene Yield by Cs Promotion in Ethanol Conversion. *Appl. Catal. A Gen.* **2017**, *543* (January), 67–74.

(84) Gao, M.; Zhang, M.; Li, Y. Investigation into 1,3-Butadiene and Other Bulk Chemicals' Formation from Bioethanol over Mg–Al Catalysts. *RSC Adv.* **2017**, *7* (20), 11929–11937.

(85) Auroux, A. *Calorimetry and Thermal Methods in Catalysis*; Auroux, A., Ed.; Springer Series in Materials Science; Springer Berlin Heidelberg: Berlin, Heidelberg, 2013; Vol. 154.

(86) De Baerdemaeker, T.; Feyen, M.; Müller, U.; Yilmaz, B.; Xiao, F. S.; Zhang, W.; Yokoi, T.; Bao, X.; Gies, H.; De Vos, D. E. Bimetallic Zn and Hf on Silica Catalysts for the

Conversion of Ethanol to 1,3-Butadiene. *ACS Catal.* **2015**, *5* (6), 3393–3397.

(87) Corma, A.; Fornés, V.; Melo, F. V.; Herrero, J. Comparison of the Information given by Ammonia t.p.d. and Pyridine Adsorption-Desorption on the Acidity of Dealuminated HY and LaHY Zeolite Cracking Catalysts. *Zeolites* **1987**, *7* (6), 559–563.

(88) Connell, G.; Dumesic, J. A. The Generation of Brønsted and Lewis Acid Sites on the Surface of Silica by Addition of Dopant Cations. *J. Catal.* **1987**, *105* (2), 285–298.

(89) Corma, A.; Llabrés i Xamena, F. X.; Prestipino, C.; Renz, M.; Valencia, S. Water Resistant, Catalytically Active Nb and Ta Isolated Lewis Acid Sites, Homogeneously Distributed by Direct Synthesis in a Beta Zeolite. *J. Phys. Chem. C* **2009**, *113* (26), 11306–11315.

(90) Luo, H. Y.; Lewis, J. D.; Román-Leshkov, Y. Lewis Acid Zeolites for Biomass Conversion: Perspectives and Challenges on Reactivity, Synthesis, and Stability. *Annu. Rev. Chem. Biomol. Eng.* **2016**, *7* (1), 663–692.

(91) Tanabe, K.; Misono, M.; Hattori, H.; Ono, Y. *New Solid Acids and Bases: Their Catalytic Properties*; Elsevier, 1990.

(92) Vohs, J. M.; Barteau, M. A. Dehydration and Dehydrogenation of Ethanol and 1-Propanol on the Polar Surfaces of Zinc Oxide. *Surf. Sci.* **1989**, *221* (3), 590–608.

(93) Drouilly, C.; Krafft, J. M.; Averseng, F.; Lauron-Pernot, H.; Bazer-Bachi, D.; Chizallet, C.; Lecocq, V.; Costentin, G. Role of Oxygen Vacancies in the Basicity of ZnO: From the Model Methylbutynol Conversion to the Ethanol Transformation Application. *Appl. Catal. A Gen.* **2013**, *453*, 121–129.

(94) GOLDWASSER, J. Studies of Acid-Base-Catalyzed Reactions XIV. Isomerization of Butene over La2O3 and ZnO. *J. Catal.* **1981**, *71* (1), 53–63.

(95) Sushkevich, V. L.; Ivanova, I. I.; Ordomsky, V. V.; Taarning, E. Design of a Metal-Promoted Oxide Catalyst for the Selective Synthesis of Butadiene from Ethanol. *ChemSusChem* **2014**, 2527–2536.

(96) Ordomsky, V. V.; Sushkevich, V. L.; Ivanova, I. I. Study of Acetaldehyde Condensation

Chemistry over Magnesia and Zirconia Supported on Silica. *J. Mol. Catal. A Chem.* **2010**, *333* (1–2), 85–93.

(97) Almutairi, S. M. T.; Mezari, B.; Magusin, P. C. M. M.; Pidko, E. A.; Hensen, E. J. M. Structure and Reactivity of Zn-Modified ZSM-5 Zeolites: The Importance of Clustered Cationic Zn Complexes. *ACS Catal.* **2012**, *2* (1), 71–83.

(98) Perez-Lopez, O. W.; Farias, A. C.; Marcilio, N. R.; Bueno, J. M. C. The Catalytic Behavior of Zinc Oxide Prepared from Various Precursors and by Different Methods. *Mater. Res. Bull.* **2005**, *40* (12), 2089–2099.

(99) Li, J.-L.; Inui, T. Enhancement in Methanol Synthesis Activity of a Copper/Zinc/Aluminum Oxide Catalyst by Ultrasonic Treatment during the Course of the Preparation Procedure. *Appl. Catal. A Gen.* **1996**, *139* (1–2), 87–96.

(100) Zhang, X. R.; Wang, L. C.; Yao, C. Z.; Cao, Y.; Dai, W. L.; He, H. Y.; Fan, K. N. A Highly Efficient Cu/ZnO/Al2O3 Catalyst via Gel-Coprecipitation of Oxalate Precursors for Low-Temperature Steam Reforming of Methanol. *Catal. Letters* **2005**, *102* (3–4), 183–190.

(101) Hartmann, M.; Racouchot, S.; Bischof, C. Characterization of Copper and Zinc Containing MCM-41 and MCM-48 Mesoporous Molecular Sieves by Temperature Programmed Reduction and Carbon Monoxide Adsorption. *Microporous Mesoporous Mater.* **1999**, *27* (2–3), 309–320.

(102) Corson, B. B.; Stahly, E. E.; Jones, H. E.; Bishop, H. D. Butadiene from Ethyl Alcohol. *Ind. Eng. Chem.* **1949**, *41* (5), 1012–1017.

(103) Jones, H. E.; Stahly, E. E.; Corson, B. B. Butadiene from Ethanol. Reaction Mechanism. *J. Am. Chem. Soc.* **1949**, *71* (5), 1822–1828.

(104) Quattlebaum, W. M.; Toussaint, W. J.; Dunn, J. T. Deoxygenation of Certain Aldehydes and Ketones: Preparation of Butadiene and Styrene. *J. Am. Chem. Soc.* **1947**, *1491* (1915), 593–599.

(105) Jones, H. E.; Stahly, E. E.; Corson, B. B. Butadiene from Ethanol. Reaction Mechanism. *J. Am. Chem. Soc.* **1949**, *71* (5), 1822–1828.

(106) Yan, T.; Dai, W.; Wu, G.; Lang, S.; Hunger, M.; Guan, N.; Li, L. Mechanistic Insights into One-Step Catalytic Conversion of Ethanol to Butadiene over Bifunctional Zn–Y/Beta Zeolite. *ACS Catal.* **2018**, *8* (iv), 2760–2773.

(107) Niiyama, H.; Morii, S.; Echigoya, E. Butadiene Formation from Ethanol over Silica-Magnesia Catalysts. *Bull. Chem. Soc. Jpn.* **1972**, *45* (3), 655–659.

(108) Shylesh, S.; Gokhale, A. A.; Scown, C. D.; Kim, D.; Ho, C. R.; Bell, A. T. From Sugars to Wheels: The Conversion of Ethanol to 1,3-Butadiene over Metal-Promoted Magnesia-Silicate Catalysts. *ChemSusChem* **2016**, *9* (12), 1462–1472.

(109) Saad, L.; Riad, M. Characterization of Various Zinc Oxide Catalysts and Their Activity in the Dehydration-Dehydrogenation of Isobutanol. *J. Serbian Chem. Soc.* **2008**, *73* (10), 997–1009.

(110) Velasquez Ochoa, J.; Bandinelli, C.; Vozniuk, O.; Chieregato, A.; Malmusi, A.; Recchi, C.; Cavani, F. An Analysis of the Chemical, Physical and Reactivity Features of MgO-SiO2 Catalysts for Butadiene Synthesis with the Lebedev Process. *Green Chem.* **2015**.

(111) Drouilly, C.; Krafft, J.; Averseng, F.; Lauron-pernot, H. Origins of the Deactivation Process in the Conversion of Methylbutynol on Zinc Oxide Monitored by Operando DRIFTS. *Catal. Today* **2013**, *205*, 67–75.

(112) Vohs, J. M.; Barteau, M. A. Structure Sensitivity, Selectivity, and Adsorbed Intermediates in the Reactions of Acetone and 2-Propanol on the Polar Surfaces of Zinc Oxide. *J. Phys. Chem.* **1991**, *95* (1), 297–302.

(113) Aleksandrov, H. A.; Vayssilov, G. N.; Rösch, N. Heterolytic Dissociation and Recombination of H2 over Zn,H-ZSM-5 Zeolites-A Density Functional Model Study. *J. Mol. Catal. A Chem.* **2006**, *256* (1–2), 149–155.

(114) Pidko, E. A.; Santen, R. A. Van. Activation of Light Alkanes over Zinc Species Stabilized in ZSM-5 Zeolite : A Comprehensive DFT Study. **2007**, 2643–2655.

(115) Díez, V. K.; Apesteguía, C. R.; Di Cosimo, J. I. Acid-Base Properties and Active Site Requirements for Elimination Reactions on Alkali-Promoted MgO Catalysts. *Catal. Today* **2000**, *63* (1), 53–62.

(116) Bartholomew, C. H. Mechanisms of Catalyst Deactivation. *Appl. Catal. A Gen.* **2001**, *212* (1–2), 17–60.

(117) Moulijn, J. A.; van Diepen, A. E.; Kapteijn, F. Deactivation and Regeneration. In *Handbook of Heterogeneous Catalysis*; Wiley-VCH Verlag GmbH & Co. KGaA: Weinheim, Germany, 2008.

(118) Pradhan, A. R.; Wu, J. F.; Jong, S. J.; Tsai, T. C.; Liu, S. B. An Ex Situ Methodology for Characterization of Coke by TGA and 13C CP-MAS NMR Spectroscopy. *Appl. Catal. A Gen.* **1997**, *165* (1–2), 489–497.

(119) Sexton, B. A.; Hughes, A. E.; Bibby, D. M. An XPS Study of Coke Distribution on ZSM-5. *J. Catal.* **1988**, *109* (1), 126–131.

(120) Klein, A.; Keisers, K.; Palkovits, R. Formation of 1,3-Butadiene from Ethanol in a Two-Step Process Using Modified Zeolite-β Catalysts. *Appl. Catal. A Gen.* **2016**, *514*, 192–202.

5.6. Supplementary Information

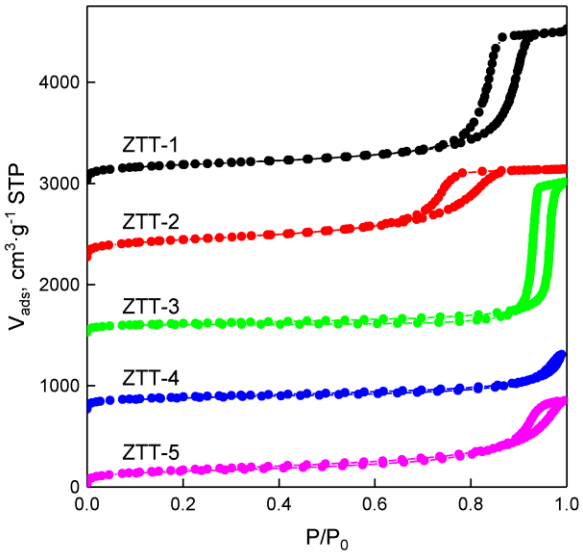

Figure 5.S2 N_2 adsorption-desoprtion isotherms for all as-prepared catalysts after degassing at 150 °C for 6 hours.

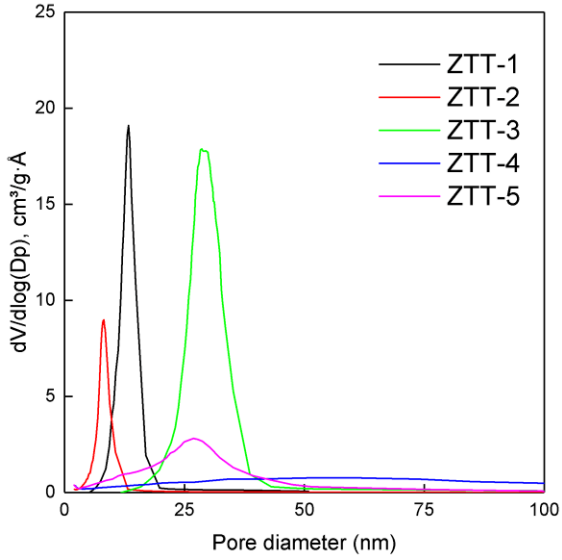

Figure 5.S3 Pore size distribution of ZTT samples

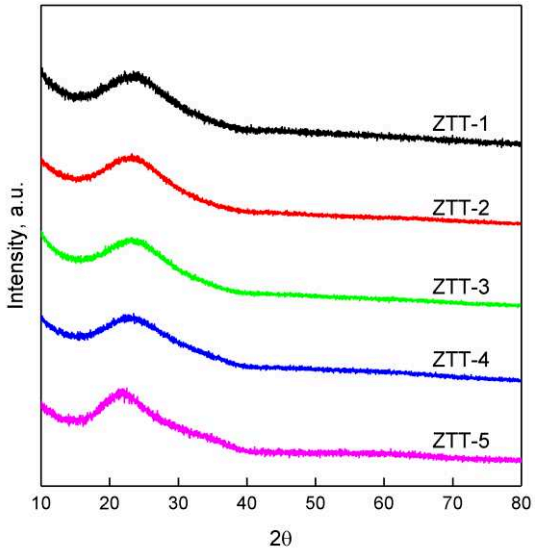

Figure 5.S4 X-ray diffractogram of Zn-Ta-TUD-1 samples.

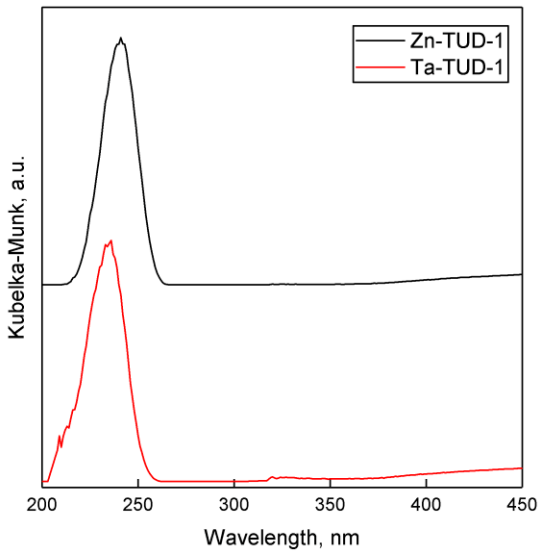

Figure 5.S5 UV-Vis of monometallic TUD-1 samples

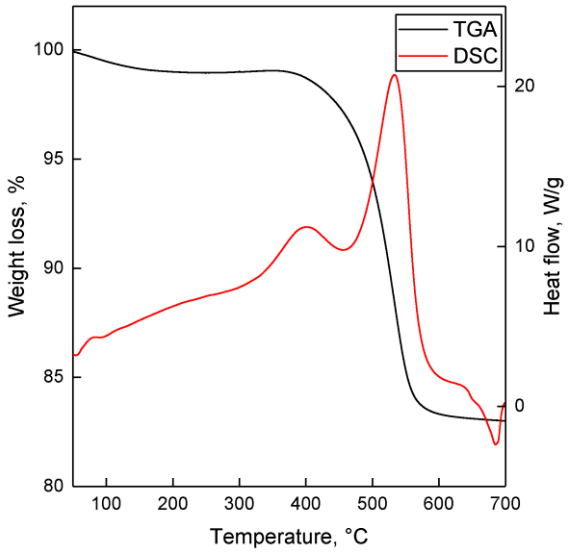

Figure 5.S6 TGA-DSC thermogram of spent ZTT-1 after 72 hours of reaction at 400 ºC and $WHSV_{EtOH\ of}$ 5.3 h^{-1}.

Table 5.S4 Composition of species trapped within spent ZTT-1 catalysts according to their weight determined by TGA. [118] Reaction at 400 ºC and $WHSV_{EtOH\ of}$ 5.3 h^{-1}.

TOS (h)	Volatile compounds (wt.%)	Light coke (wt.%)	Heavy coke (wt.%)	Total (wt.%)
1.5	1.3	0.6	2.4	4.3
6	1.8	0.8	3.7	6.3
24	1.4	0.5	4.3	6.2
48	2.3	0.3	7.6	10.3
72	1.2	0.0	16.0	17.2

Chapter 6 Conclusion and Outlook

6.1. Conclusion

This doctoral thesis describes the steps that were taken to develop a catalyst highly active in the conversion of ethanol to butadiene. As part of the H2CAT project funded by the Agence Nationale de la Recherche, the mission statement of this research was to prepare materials capable of high butadiene productivity in the Lebedev process.

Without prior experience in the subject, review of the literature was initially conducted to acquire knowledge of the reaction and the catalysts available. In section 7.2. of the appendix can be found the review that was first published in the first year of research. Because research on the conversion of ethanol to butadiene has rapidly progressed in recent years, the literature was monitored throughout the duration of this thesis. Chapter 1 is the result of this effort. It summarizes the different aspects of the reaction under study, notably the reaction mechanism, the influence of reaction conditions and the intricacies of the different catalytic systems.

The information gathered during the writing of the initial review coupled with preliminary experimental work, such as the reproduction of synthesis described in the scientific literature, served as the basis for conducting the initial screening study of 32 silica-supported catalysts—the internal report of which can be found in section 7.1. of the appendix. Although the large volume of materials prepared meant that their thorough characterization could not be done in a timely manner, it could be deduced from their activity in the Lebedev process that: (i) their chemical properties, influenced by type and proportion of metal oxide used, played a significant role; (ii) the Zn-Ta couple performed better than other metal combinations.

Having identified that Zn-Ta was more active than other catalysts tested, the next step was to determine if the support is an important factor to be considered. Preliminary testing of different supports found Zn-Ta incorporated in the mesoporous silica foam TUD-1 was capable of high butadiene yield. Chapter 3 investigates the influence of the catalyst carrier on the catalytic system performances. Zn-Ta-TUD-1 was compared to an equimolar amount of active phase dispersed on other catalyst supports, notably on dealuminated zeolite BEA. Other scholars had shown that dealuminated BEA could be impregnated to prepare catalysts very selective in converting ethanol to butadiene. Catalytic testing showed that Zn-Ta-TUD-1 performed better in the Lebedev process than the catalysts supported on dealuminated BEA and commercial silica; it yielded 13 and 24

percentage points more of butadiene, respectively. A comparison of the morphological characteristic determined by N_2 porosimetry of the three samples showed that Zn-Ta-TUD-1 possessed a larger specific surface area than the other two together with a mesoporous morphology, both of which had been linked with superior catalytic activity in the literature. Furthermore, quantification of the acid sites demonstrated that Zn-Ta-TUD-1 possess more acid sites, despite all three catalysts possessing similar metal loadings of transition metals, which are known to induce acidity when dispersed on silicate supports. The importance of acidity was highlighted by a direct correlation observed between the concentration of acid sites and butadiene selectivity. Since the activity of catalysts in the Lebedev process can decrease at high ethanol flow rate, hindering butadiene productivity, Zn-Ta-TUD-1 was subjected an ethanol high space velocity of 8 h^{-1} and tested at 673 K—conditions comparable to those used for the best performing catalysts found in the literature. Interestingly, Zn-Ta-TUD-1 not only performed moderately better in terms of productivity than these catalysts, it was also more resistant to deactivation over a period of 60 hours; productivity and stability are both desirable from an industrial point of view. It was also found that calcination under air could be used to recover the initial catalytic activity.

The synthesis method used to prepare Zn-Ta-TUD-1 had only been the subject of preliminary investigation. Although the preparation of TUD-1 materials is straightforward in practice, there were issues of repeatability, which we attributed to the effects of the many parameters involved. Chapter 4 describes the screening studies conducted to better understand the effect of these parameters and to find a suitable method to prepare highly active reproducible materials. 11 parameters were thus evaluated *via* the design of experiments method to consider their statistical impact on butadiene productivity, but also on the morphology of the final catalyst. Several parameters were found influential, notably the method of calcination and the nature of the chelating agent, but also the balance of Zn and Ta. The latter was further optimized in a second screening study, which relied on the optimized synthesis method. Ultimately, a Zn-to-Ta of 1.5 – 2.0 was found to achieve best performances in the conversion of ethanol to butadiene. Additionally, correlation between butadiene productivity and specific surface area was established. To achieve the best performances a specific surface area larger than 600 $m^2 \cdot g^{-1}$ and an average pore diameter between 10 – 12 nm was necessary.

Some of the best and worst catalysts of the screening study were characterized, in part to determine the chemical and physical properties of Zn-Ta-TUD-1 catalysts, but also to understand

its activity. Chapter 5 details the optimized synthesis method used to prepare a mesoporous material possessing the three-dimensional "foam-like" morphology expected of successful TUD-1 synthesis. Furthermore, the combination of spectroscopic techniques and microscopy indicated that the synthesis method formed highly dispersed Zn(II) and Ta(V) phases incorporated within the silica framework. As for Ta(V), it was found to exist as a mixture of isolated tetrahedral sites and monolayered clusters averaging 1 nm in diameter. The TUD-1 synthesis could not properly incorporate high metal loadings, resulting instead in the formation of extra-framework nanoparticles, which were less active. Butadiene formation rate was directly correlated with the concentration of Lewis acid sites quantified by the IR spectroscopy of pyridine. As a result, Lewis acid sites were identified as the active sites for the aldol condensation of the reaction. It was shown that the optimized catalyst possessed the most acid sites, which were assigned to both the Zn(II) and Ta(V) phases. The dehydrogenation activity could not been attributed to the presence of Zn(II) alone, as Zn-TUD-1 performed did not form significant amounts of acetaldehyde. Instead, the proximity of Zn(II) and Ta(V) was required, highlighting the synergy between the two components of the catalyst. A deactivation study of Zn-Ta-TUD-1 revealed that the main source of deactivation was the deposition of heavy carbonaceous species. Pore blockage was not a source of deactivation, ostensibly due to the mesoporous morphology of the catalyst.

In summary, the development of a Zn-Ta-TUD-1 catalyst with remarkable performances in the Lebedev process proceeded sequentially. First, a continuously updated review of the literature was conducted to acquire the necessary knowledge to begin research on the subject. Next, a screening study allowed the identification of a promising active phase. Investigating the effect of support on the performances of Zn-Ta revealed the potential of Zn-Ta-TUD-1 as a highly active, very productive catalyst. Screening studies were able to optimize the synthesis method to ensure reproducibility and high catalytic activity. Finally, the origin of this remarkable active was determined by characterization of Zn-Ta-TUD-1.

6.2. Outlook

As with all catalytic processes, there is room for improvement in both our fundamental understanding of the reaction mechanism and the structure-activity relationship. These aspects are all essential to attain the best possible performances required to industrialize the formation of butadiene from ethanol.

At present, there is a growing consensus on the reaction pathway. Yet, a number of questions remain to be answered regarding the molecular-level mechanism. Notably, the mechanism of the aldol condensation is point of contention. The discrepancies reported in the literature may be owed to the different types of catalysts used, but further investigation is required. *In situ* spectroscopic analysis, isotopic tracer studies and DFT calculations have all been used with success and should be expanded to other catalytic systems.

Concerning the structure-activity relationship, our results strongly support the crucial role of isolated Lewis acid sites in the condensation of acetaldehyde established by Ivanova *et al.*, indicating that their theory may be valid for catalytic systems other Zr. However, investigation at the molecular level should be conducted to establish the validity of this model. With regards to the activity of Zn-Ta-TUD-1, the origin of the dehydrogenating activity must be further investigated. Evidently, the presence of Zn(II) alone is not enough to explain the formation of acetaldehyde. So far, our result suggest synergism between Zn and Ta enabling ethanol dehydrogenation manifests itself in the reducibility of Zn(II). Yet, there remains to understand how exactly these two phases interact with one another and with incoming ethanol molecules. Two weaknesses of the characterization study should be overcome: first, the structure of the Zn(II) phase could have been better defined; second, the basic properties were not properly characterized, while it is known that amphoteric ZnO acts as a basic oxide in the presence of ethanol. Low-energy ion scattering is a technique which should have been used to study the surface chemistry and structure of Zn-Ta-TUD-1. It could reveal the degree of interaction between the two phases. Next, chemical probes other than controversial CO_2 could be used to investigate the influence of basic properties on the reaction.

For ethanol-to-butadiene processes to progress in the road to industrialization, the effect of reaction parameters should be further investigated. Recent studies on the influence of co-feeding water showed that crude bioethanol could be used, thereby reducing purification costs. Yet, a systematic study of its influence on activity and stability remains to be performed. A great gap in the ethanol-to-butadiene research is the lack of rigorous kinetic modelling of the effects of reaction conditions have on catalytic performances. Such a specific study could provide significant information on the reaction mechanism, but also enable simulation of the process. This latter would help in accurately evaluating the financial viability of the ethanol-to-butadiene reaction, which is the only way it could eventually be industrially implemented.

Appendix

7.1. Results of the catalytic tests

7.1.1 Hemimorphite-containing catalysts

In their original publication, De Vos *et al.* presented a highly active catalytic system obtained from the mechanical mixing of silica-supported HfO_2 with hemimorphite.[1] Although the team evaluated the activity of catalysts with various amounts of zinc silicate, it did not investigate the potential of hemimorphite with other metal oxides. In this work, HM was combined with several silica-supported metal oxides: HfO_2, ZrO_2, Ta_2O_5, Nb_2O_5, V_2O_5 and Ga_2O_3. They were prepared according to the methodology described in section 2.1 with the appropriate metal precursors using the CatImpreg machine. Except for hemimorphite itself, all metal oxides are in equivalent molar amounts unless otherwise noted.

Table 1. Catalytic results of HM containing catalysts ($WHSV_{EtOH}$: 2.37 h^{-1}, P: 1 atm, TOS: 3 – 6h)

Cat. ID	Catalyst name	350 °C		400 °C	
		X_{EtOH} (%)	S_{BD} (%)	X_{EtOH} (%)	S_{BD} (%)
1	14.5%HM 3.5%HfO_2/SiO_2	58.08	29.77	96.80	34.14
2	18%HM 7% HfO_2/SiO_2	58.32	36.36	97.67	37.43
3	14.5%HM 3.5%HfO_2/SiO_2 (mixed)	58.25	20.56	93.51	22.39
4	14.5%HM 2%ZrO_2/SiO_2	49.24	36.15	96.66	39.35
5	14.5%HM 4%Ta_2O_5/SiO_2	41.19	38.41	97.83	42.62
6	14.5%HM 2%Nb_2O_5/SiO_2	44.11	7.96	91.44	11.87
7	14.5%HM 1%VO_2/SiO_2	7.70	1.24	52.28	0.93
8	14.5%HM 3%Ga_2O_3/SiO_2	55.32	4.80	95.59	7.37

Catalyst #1 was prepared to mimic the catalysts described in the work of De Vos *et al*. It serves as a reference to compare the activity of other catalysts. It should be noted that the catalyst itself underperformed compared to the original catalyst described in the literature, in which a similar material reaches a BD selectivity of 71%, albeit at shorter TOS and at a $WHSV_{EtOH}$ of 0.64 h^{-1}. The effect of increasing the amount of acidic metal oxide (HfO_2) was evaluated with catalyst #2. Despite twice the amount of hafnium, only a marginal increase in selectivity towards BD was observed. The increase in potential acid sites leads to an increase in ethylene selectivity averaging 5% and an increased consumption of acetaldehyde. Considering the acid-base balance of the material, these results suggest that the Zn:Hf metal ratio of 7 is likely not optimal and further balancing is required.

In their original publication, De Vos *et al.* noted that the method used to mix hemimorphite with HfO_2/SiO_2 was critical, potentially leading poorly active materials. Catalyst #3 is an attempt to speed up the synthesis process by introducing hemimorphite during the impregnation step. As the results in Table 1 indicate, a noticeable drop in activity occurs when this shortcut is taken. Two explanations: either HfO_2 impregnated on hemimorphite is inactive (as noted by De Vos *et al.*), thereby lowering the total amount of active sites, or the calcination process, which is performed at a higher temperature than the usual post-mixing calcination, distorts the crystalline morphology of the silicate, rendering it less active. The X-ray diffractogram of catalyst #3 excludes this last option, as it reveals that the morphology of hemimorphite is maintained. However, it also reveals the presence of an unidentified phase (indicated by the arrows in figure 4) which does not belong to the zinc silicate and is absent in other catalysts. Identifying signals in the 15 –30 ° range is difficult due to the broad signal attributable to amorphous silica, which hides weaker signals.

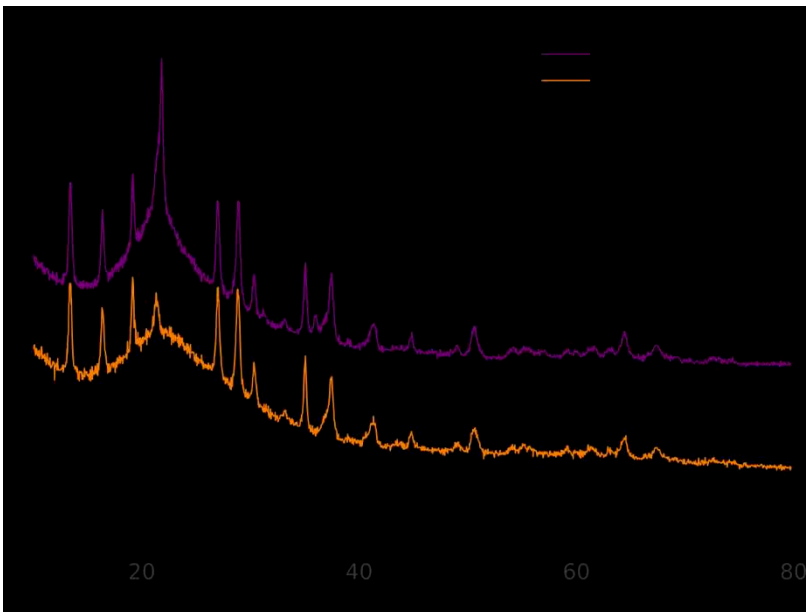

Figure 4. X-ray diffractograms of catalyst #1 and #3 compared with pure hemimorphite

The contribution to the catalytic activity by the nature of the acidic metal oxide was evaluated by substituting Hf with several other species. Zr (catalyst #4) was found to be slightly more selective towards BD than Hf, albeit at the cost of overall activity. A survey of the literature indicates that both metal oxides share similarities in terms of chemical properties. In the context of silica-supported catalysts, Zr(IV) and Hf(IV) act as Lewis sites.[2] Contrarily to the claims made by De VOs *et al.*, the 'softness' of hafnium did not reduce ethylene production; at both temperatures, the Hf-containing catalyst resulted in a slightly higher selectivity towards ethylene (e.g., 14.75%

for catalyst #1 and 12.75% for catalyst #4 at 350 °C). There does not appear to be an obvious advantage over one or the other metal oxide.

Catalyst #5 used tantalum oxide as a source of acidity. At 350 °C, the material was more selective towards BD but slightly less active in the conversion of ethanol. At 400 °C, ethanol conversion was maximized – as on most of the best performing catalysts; BD selectivity was also higher than over both Zr or Hf-containing catalysts, making it the most active ethanol-to-butadiene catalyst in this series. According to the literature, tantalum oxide is also a strong Lewis solid acid when dispersed over silica.[3,4] Furthermore, bulk tantalum oxide was noted to possess intrinsic redox properties and is a catalyst for the dehydrogenation of ethanol in itself – albeit an average one.[5] These properties may be responsible for the superior activity of Ta(V) for the production of BD, when dispersed on silica and mixed with hemimorphite. Some Ta-containing materials capable of converting ethanol mixed with acetaldehyde to BD have recently been reported.[3,6]

The activity of niobium was evaluated with catalyst #6. Nb is also a strong solid acid with particular properties, as its activity is highly dependent on numerous factors, such as the calcination temperature and its oxidation state.[4,7,8] At all temperatures, the Nb –containing catalyst was poorly selective towards BD but was nonetheless highly active in the formation of ethylene (between 20 and 40% selectivity), with significant amounts of unreacted acetaldehyde present (between 20 and 40% selectivity). Higher temperature leads to an increase in ethylene formation at the expense of acetaldehyde. Admittedly, due to its peculiar nature, a single catalyst is insufficient to evaluate the activity of Nb. Therefore, despite the seemingly poor results, the peculiar properties could be of interest for future research. For instance, Nb(V) possesses intrinsic properties for the conversion of ethanol to acetaldehyde when properly dispersed.[9] Nb-containing catalysts capable of converting ethanol mixed with acetaldehyde to BD have also recently been reported.[10]

The vanadium oxide-containing catalyst #7 was found to be poorly active. Accordingly, no report of active V-based catalysts was found in the literature, despite possessing Lewis acidic properties. However, poor selectivity towards BD is only part of the problem: ethanol conversion remained extremely low when compared to other catalysts, despite the significant presence of hemimorphite which is responsible of ethanol dehydrogenation. This means that the addition of V poisoned the active sites on the zinc silicate. Sodium vanadate being used as a precursor, it is possible that remaining Na poisoned the acidic sites, despite the washing procedure. Still, it does

not explain why ethanol dehydrogenation is also hindered, as successful catalysts containing Na have been reported.[11,12] The X-ray diffractogram of the as-synthesized material compared to that of hemimorphite (figure 5) indicates that the zinc silicate morphology is preserved during the preparation. With regards to Na poisoning, elemental analysis with XRF was fruitless, as the signals for sodium and zinc overlap. Other types of elemental analysis will be necessary to verify this hypothesis.

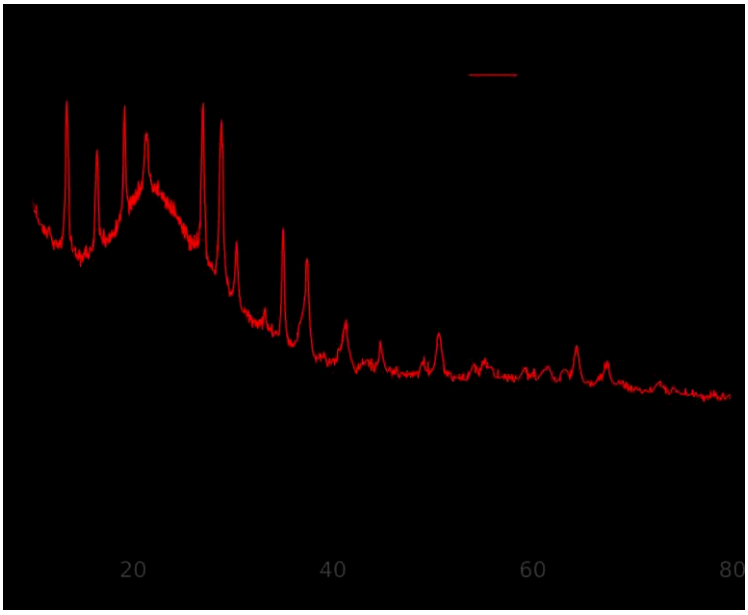

Figure 5. X-ray diffractograms of catalyst #7 compared with pure hemimorphite

The acidic gallium oxide was recently reported as a dopant for the $MgO\text{-}SiO_2$ catalytic system active in the ethanol-to-butadiene reaction.[13] Unfortunately, the Ga-containing catalyst #8 was poorly selective towards BD, yielding large amounts of ethylene. This may be the result of the acidic properties of gallium oxide. Silica-supported gallium oxide catalysts possess the required Lewis acid sites. But they also possess strong Brønsted acid sites, which have been recognized to be the main culprit behind the formation of ethylene due to their capacity for ethanol dehydration.[2,14] Although metal oxides such as ZrO_2 may also create Brønsted acid sites, when properly prepared, these display mostly Lewis acidity. The performances of catalyst #8 suggest that Brønsted acidity was the predominant property when gallium oxide is used.

7.1.2 Lanthanum oxide-based catalysts

Larina *et al.* have demonstrated the use of lanthanum oxide as a dopant for silica supported zinc-zirconium oxide catalysts.[15] The team argues that the addition of lanthanum oxide provides

basic active sites that increase C2 condensation, yielding high performing catalysts. To investigate the ability of lanthanum as part of a catalytic system, several catalysts inspired by the work of Larina *et al.*, including a reproduction of their most active catalyst prepared by wet impregnation outside of the CatImpreg platform (see catalyst #17 in table 2). In our study, the redox and acidic element of the original Zn-La-Zr-Si were replaced and catalytically tested.

Table 2. Catalytic results of La-based catalysts ($WHSV_{EtOH}$: 2.37 h^{-1}, P: 1 atm, TOS: 3 - 8 h)

Cat. ID	Catalyst name	350 °C		400 °C	
		X_{EtOH} (%)	S_{BD} (%)	X_{EtOH} (%)	S_{BD} (%)
9	2% ZnO_2 6% La_2O_3 2% ZrO_2/SiO_2	35.47	26.18	82.46	31.11
10	2% ZnO_2 3% La_2O_3 2% ZrO_2/SiO_2	36.79	32.94	86.68	34.36
11	2% ZnO_2 6% La_2O_3 4% ZrO_2/SiO_2	35.61	32.10	84.46	32.96
12	1% CuO 3% La_2O_3 2% ZrO2/SiO_2	16.75	11.81	40.48	14.03
13	2% ZnO_2 6% La_2O_3 1.4% Ga_2O3/SiO_2	24.00	24.39	70.95	19.29
14	2% ZnO_2 6% La_2O_3 3% HfO_2/SiO_2	42.57	29.21	89.72	32.40
15	2% ZnO_2 6% La_2O_3 3% Ta_2O_5/SiO_2	34.44	13.86	73.04	16.21
16	2% ZnO_2 6% La_2O_3 1.4% V_2O5/SiO_2	4.18	0.42	17.45	0.33
17	2% ZnO_2 7% La2O3 1% ZrO_2/SiO_2	31.80	55.37	81.36	46.56
18	3%HM 6%La2O3 2%ZrO_2/SiO_2	26.31	25.81	70.64	31.95
19	14.5%HM 6%La2O3 3.5%HfO_2/SiO_2	45.27	27.46	93.40	20.80
20	14.5%HM 3%La_2O_3/SiO_2	32.04	6.24	66.49	9.21

In the group of CatImpreg-prepared catalysts, catalyst 9 served as a reference as it closer to the metal content of the original catalyst prepared by Larina *et al.*[15] It severely underperformed compared to the activity reported in the literature – almost half the selectivity towards BD. One possible explanation may be found in the difference in synthesis method; whereas catalyst 9 was prepared by impregnation, the original material was mixed with zirconium salts. Nevertheless, some degree of activity was observed comparable to that of hemimorphite-containing catalysts.

The effect of the La content on catalytic activity was studied with catalyst 10. It had its total La content halved compared with catalyst 9. Despite an overall lower amount of metal oxides, the catalyst proved to be more active in all respects, albeit only slightly. Furthermore, catalyst 11, for which the Zr content was doubled and thus has the same La:Zr ratio as catalyst 10, displayed similar performances. It would appear that the La:Zr metal ratio reported by Larina *et al.* might not be

optimal. Further balancing could afford better performing catalysts. According to these results, a higher amount of Zr in relation to La could be beneficial.

For this category of catalytic system, zirconium oxide – believed to provide Lewis acid sites for the C2 condensation – was substituted by other metals: Hf, Ga, Ta, V. Of these, hafnium-containing catalyst 14 displayed higher selectivity and notably higher ethanol conversion under both temperatures. The superiority of hafnium oxide as a component of catalytic systems for this reaction was previously noted by De Vos *et al.*[1] It was attributed to its "softer" acidic properties. XRF results excluding the possibility of unequal molar amounts of metal oxides, the observed results can only be explained by a phenomenon either intrinsic to hafnium oxide or the method by which the catalyst was prepared. Other acidic metal oxides did not produce materials of interest. This is also true of tantalum oxide, despite the high activity observed in the case of the hemimorphite-containing catalysts (see table 1). Activity was overall lower than Zr or Hf-containing catalysts.

Zinc was substituted with copper as an alternative source of redox properties to enable the dehydrogenation of ethanol. Cu-containing catalyst 12 poorly converted ethanol and was mostly selective towards ethylene. Copper-containing catalysts and their issues are discussed below.

Catalyst 17 was meant as a closer reproduction of the original catalyst, with the same metal ratios. It was prepared out of CatImpreg by wet impregnation, a process that lasted 3 days – making it distinct from the other catalysts in this series. At both temperatures, catalyst 17 was significantly more selective towards BD. However, because this particular material was prepared under different conditions, this cannot simply be attributed to the slightly different metal-to-metal ratio; it makes the comparison with other catalysts inconclusive. Another distinction is that, contrarily to most CatImpreg-prepared materials, catalyst 17 suffers a non-negligible loss of selectivity towards BD at higher temperatures, along with the gallium-containing catalyst 13. One possible explanation for the gap in activity could be that the impregnation process performed with CatImpreg was too short to properly disperse the metal particles, as it is done by diffusion. Poorly dispersed particles are less active. Nevertheless, catalyst 17 one was of the most active materials tested in this screening.

Based on these results, further research will be oriented towards: understanding the activity gap between CatImpreg-prepared catalysts and the reproduction of the original catalyst, as the very similar metal ratios make it unlikely that the acid-base property balance is the only factor at play;

explaining the higher activity observed with hafnium oxide; investigating the effect of the Zr (or Hf)-to-La ratio and to find an optimal balance.

The role of lanthanum oxide as dopant was also evaluated by introducing it to the hemimorphite-mixed hafnium-based catalyst (e.g., Catalyst 1). Catalyst 18 proved to be poorly active when compared the undoped catalyst, especially at higher reaction temperature. Other catalysts containing both hemimorphite and lanthanum oxide were tested. Catalyst 18 was an attempt to replicate catalyst 9 substituting hemimorphite as the equimolar source of zinc. Unfortunately, the amount of zinc in catalyst 18 suffered from the same phenomenon of overabundant zinc – it ultimately had three times the amount of zinc when compared to catalyst 9. In catalyst 19 the amount of zinc silicate was similar to that of other hemimorphite-containing catalysts, essentially a La-doped catalyst 1. In the latter case, performances were inferior its undoped equivalent. This indicates that the doping effect of lanthanum is not straightforward an addition of active sites; it likely involves a synergic effect absent with the addition of hemimorphite. As for catalyst 18, BD selectivity was identical to the hemimorphite-less catalyst 9. However, ethanol conversion was lower, despite the total amount of zinc being three times higher. This suggests that zinc oxide is more active for ethanol dehydrogenation than hemimorphite.

The activity of lanthanum oxide with hemimorphite alone was tested with catalyst 20. Compared with the activity of acidic catalysts reported in table 1, catalyst 20 was only slightly selective towards BD and overall poorly performing at both temperatures. This observation highlights the dopant effect of lanthanum oxide, as observed in catalyst 17, suggesting that lanthanum oxide requires the presence of an acidic metal oxide to properly increase BD selectivity.

7.1.3 Cerium oxide-based catalysts

Cerium belongs to the lanthanide family and also possesses basic properties in addition to strong oxidative properties.[9] In the search of new catalytic materials, lanthanum was substituted by cerium following the same catalytic system as discussed in section 7.1.2 with the objective of comparing the catalytic activity of both metals under different catalytic systems.

Table 3. Catalytic activity of cerium-based catalysts ($WHSV_{EtOH}$: 2.37 h^{-1}, P: 1 atm, TOS: 3 – 8 h)

Cat. ID	Catalyst name	350 °C		400 °C	
		X_{EtOH} (%)	S_{BD} (%)	X_{EtOH} (%)	S_{BD} (%)
21	2% ZnO_2 6% CeO2 2% ZrO_2/SiO_2	35.10	32.16	85.02	32.37
22	14.5%HM 3%CeO_2/SiO_2	22.24	11.49	64.68	10.95

Comparing the Ce-containing catalyst 21 with catalyst 9 (table 2), the catalytic performances are almost identical – with Ce being slightly more BD selective. However, selectivity towards ethylene (not displayed) was higher on the cerium-based catalyst (at 350 °C, catalyst 9: 1% vs catalyst 2: 8%). Acetaldehyde selectivity was around 25% with both catalysts at 350 °C and 10% at 400 °C. Based on these results, cerium oxide does not offer an obvious advantage over lanthanum oxide.

The activity of cerium oxide alone with the zinc silicate hemimorphite was also evaluated in the form of catalyst 22. Again, the activity of cerium oxide is like that of lanthanum oxide, with the exception of a lower ethanol conversion at 350 °C. The selectivity towards the various main products is similar in most respects. As with the La-containing catalyst 20, when compared to those presented in table 1, these results again suggest that basic metal oxides are less active than their acidic counterparts when combined with zinc silicate.

7.1.4 Copper-doped catalysts

Copper-doped acidic oxide-based catalysts were also investigated. This category of catalyst is among the oldest tested catalysts in which copper dehydrogenates ethanol while the acidic oxides condense the C2 species. Throughout the tests performed, the recurring problem of copper-containing catalysts has been their extremely poor selectivity towards BD and high ethylene production (see table 4 and catalysts 12 in table 2). According to the literature, metallic copper is responsible for the conversion of ethanol into acetaldehyde, whereas the post-calcination materials contain copper oxide, easily evidenced by their distinctive blue color.[16,17] However, the literature recognizes that metallic particles are formed *in situ* by the reductive action of gaseous ethanol – several reported syntheses having reported by-passing the inconvenient reduction step with hydrogen that is common with silver-containing catalysts.[18] A characterization of the post-reaction material to determine the oxidation state of copper may provide an explanation if the latter was not properly reduced. In any case, these results demonstrate that using copper as the source of redox

properties is not as straightforward as the use of zinc, which does not require pre-treatment or is easily synthesized and mixed as its silicate form.

Table 4. Catalytic activity of Cu-containing catalysts ($WHSV_{EtOH}$: 2.37 h^{-1}, P: 1 atm, TOS: 3 -8 h)

Cat. ID	Catalyst name	350 °C			400 °C		
		X_{EtOH} (%)	S_{BD} (%)	$S_{C2=}$ (%)	X_{EtOH} (%)	S_{BD} (%)	$S_{C2=}$ (%)
23	1.5%CuO 4.1%ZrO_2/SiO_2	26.76	1.74	56.34	61.81	2.60	70.16
24	1.5%CuO 7.1%Ta_2O_5/SiO_2	13.67	2.70	61.21	48.00	1.05	68.43
25	1.5%CuO 6.8%HfO_2/SiO_2	14.66	43.19	8.27	52.67	25.46	8.53

Interestingly, of all materials tested, only the hafnium-containing catalyst 25 displayed what could be dubbed as 'average performances' -- i.e., above 30% selectivity towards BD, in spite of low ethanol conversion. No explanation for this phenomenon could be devised. However, it should be noted that the drastically lower selectivity towards ethylene when compared with the Zr-containing catalyst 23 and Ta-containing catalyst 24 is in agreement with the 'softer' acid explanation provided by De Vos et al. as explanation for their preference towards that particular element.[1]

7.1.5 Zinc & Copper-doped catalysts

In their 2011 paper, Jones *et al.* reported that silica-supported zirconium oxide could convert ethanol into BD when doped with both zinc and copper to provide redox properties.[19] Since, many other catalytic systems have involved the use of either copper or both zinc and copper to produce active materials.[1,20,21] Several materials combining these two elements with various acidic metal oxides to find new active catalysts. The results are displayed below in table 5.

Table 5. Catalytic activity of Zn & Cu-doped catalysts ($WHSV_{EtOH}$: 2.37 h^{-1}, P: 1 atm, TOS: 3-8 h)

Cat. ID	Catalyst name	350 °C		400 °C	
		X_{EtOH} (%)	S_{BD} (%)	X_{EtOH} (%)	S_{BD} (%)
26	2%ZnO 2%ZrO_2/SiO_2	33.37	30.32	88.78	37.51
27	1%CuO 2%ZnO 2%ZrO_2/SiO_2	36.89	27.98	84.81	34.77
28	1%CuO 2%ZnO 3.5%Ta_2O_5/ SiO_2	20.30	5.85	89.83	35.10
29	1%CuO 2%ZnO 3.5 %HfO_2/SiO_2	33.04	17.11	86.28	29.96
30	1%CuO 2%ZnO 1.5%Ga_2O_3/SiO_2	41.61	0.28	84.04	1.48
31	1%CuO 2%ZnO 6%Ga_2O_3/SiO_2	59.90	0.48	93.08	1.63
32	1%CuO 2%ZnO 6%La_2O_3 2%HfO_2 2%Ga_2O_3/SiO_2	34.88	3.82	71.64	7.64

When compared to catalysts containing only copper as the source of dehydrogenation active sites (table 4), catalysts such 27, 28 and 29 are definitely more active in the Lebedev process. These do not suffer from the excessive selectivity towards ethylene observed with catalysts 23, 24, 35. However, because the amount acidic metal oxide is different, it is impossible to draw a conclusion with regards to their compared activity. Nonetheless, which catalyst 26 was prepared as a copper-less equivalent of catalyst #27suggests that the addition of copper is detrimental to the catalytic activity of the material. Despite a slightly higher ethanol conversion rate, the additional presence of copper diminishes the selected towards the desired product at both reaction conditions. This is in agreement with other observations in which the addition or substitution of a metal by copper has led to a decrease in activity. The gallium-containing catalysts 30 and 31 also failed to yield any amount of BD, once again indicating that gallium oxide is unsuited to be a substitute to the traditional Lewis acidic zirconium oxide.

7.1.6 Summary & outlook

The screening study conducted has accomplished its goals as starting point for further research. Although it has revealed several interesting phenomena, it has also left several questions unanswered. Because solving all these issues might be time consuming, it would be wise to focus on the most important elements to come out of this study. What follows is a summary of the most notable observations and what could be done to exploit or understand them.

- The most active catalyst has been a combination of silica-supported tantalum oxide with hemimorphite (catalyst 5). In a subsequent reaction at the same conditions as those in table 1, it achieved the highest BD yield of 54.75% -- making it amongst the best performing catalysts when compared with the literature.[22]

- The use of lanthanum oxide as dopant with basic properties was demonstrated with catalyst 17, a confirmation of the works of Larina *et al*. However, the gap in activity between materials prepared by different means (e.g. catalyst 9 and 17) suggests that the synthesis method plays an important role in insuring high activity. Furthermore, the doping effect of La was found to require the presence of acidic metal oxide, resulting in otherwise poorly performing materials. In addition, these metal oxides had to be either ZrO_2 or HfO_2; other acidic oxides – even the highly active tantalum oxide mentioned above – did not fare well. To better understand this phenomenon, it is planned to study these materials using acid and

basic probes combined with Fourier-transformed infrared (FT-IR) spectroscopy in an attempt to deduce the explanation behind the disparity in activity.

- In terms of redox properties for the dehydrogenation of ethanol, copper has shown to be poorly active, despite recurring claims made in the literature. Many explanations will be investigated to elucidate this phenomenon. First, determining the oxidation state of copper during or after the reaction could explain its poor activity, as metallic copper – believed to be formed in situ by a reduction from ethanol – is the active species. It might be that copper was not reduced and thus not active. Temperature Programmed Reduction could also be used to gain further information on the reducibility of copper and its co-elements inside the synthesized catalysts, which could be used to modify the synthesis process to include a reduction step.

- Redox properties for the dehydrogenation of ethanol were successfully introduced using zinc – either in its oxide or in its silicate form. For an equal amount of zinc, the oxide form proved to be more active than its silicate equivalent. However, the silicate allowed materials to reach higher degrees of ethanol conversion. It is unclear which form of zinc is more advantageous: zinc oxide is easily introduced by impregnation, but this process might cause aggregation of zinc oxide particles at higher content, thereby reducing the total number of active sites; hemimorphite, although easily synthesized and mixed with active material, guarantees dispersed zinc active sites due to its crystalline structure, nevertheless requiring additional steps. Making a judgment between the two options will require additional experiments – namely to see if highly dispersed zinc active sites can be introduced by some other mean. For the time being, zinc remains the element of choice for the catalyzing the dehydrogenation of ethanol.

- Cerium oxide proved to be comparatively active to lanthanum oxide. With no obvious advantages between the two, it nonetheless offers the potential of an alternative basic dopant. In the immediate, testing cerium with other acidic metal oxides will be a priority. If the doping properties could be maintained with metal oxides other than HfO_2 or ZrO_2 (e.g. with the highly active tantalum oxide), it could produce great new materials. Other lanthanides should be investigated as well.

7.1.7. References

(1) De Baerdemaeker, T.; Feyen, M.; Müller, U.; Yilmaz, B.; Xiao, F. S.; Zhang, W.; Yokoi, T.; Bao, X.; Gies, H.; De Vos, D. E. Bimetallic Zn and Hf on Silica Catalysts for the Conversion of Ethanol to 1,3-Butadiene. *ACS Catal.* **2015**, *5* (6), 3393–3397.

(2) Sushkevich, V. L.; Ivanova, I. I. Mechanistic Study of Ethanol Conversion into Butadiene over Silver Promoted Zirconia Catalysts. *Appl. Catal. B Environ.* **2017**, *215*, 36–49.

(3) Kim, T. W.; Kim, J. W.; Kim, S. Y.; Chae, H. J.; Kim, J. R.; Jeong, S. Y.; Kim, C. U. Butadiene Production from Bioethanol and Acetaldehyde over Tantalum Oxide-Supported Spherical Silica Catalysts for Circulating Fluidized Bed. *Chem. Eng. J.* **2014**, *278*, 217–223.

(4) Ushikubo, T. Recent Topics of Research and Development of Catalysis by Niobium and Tantalum Oxides. *Catal. Today* **2000**, *57* (3–4), 331–338.

(5) Legendre, M.; Cornet, D. Catalytic Oxidation of Ethanol over Tantalum Oxide. *J. Catal.* **1972**, *25* (2), 194–203.

(6) Kyriienko, P. I.; Larina, O. V.; Soloviev, S. O.; Orlyk, S. M.; Dzwigaj, S. High Selectivity of TaSiBEA Zeolite Catalysts in 1,3-Butadiene Production from Ethanol and Acetaldehyde Mixture. *CATCOM* **2016**, *77*, 123–126.

(7) Nowak, I.; Ziolek, M. Niobium Compounds : Preparation , Characterization , and Application in Heterogeneous Catalysis. **1999**.

(8) Ziolek, M. Niobium-Containing Catalysts—the State of the Art. *Catal. Today* **2003**, *78* (1–4), 47–64.

(9) Nishimura, M.; Asakura, K.; Iwasawa, Y. New SiO2-Supported Niobium Monomer Catalysts for Dehydrogenation of Ethanol. *J. Chem. Soc. Chem. Commun.* **1986**, No. 22, 1660.

(10) Kyriienko, P. I.; Larina, O. V.; Popovych, N. O.; Soloviev, S. O.; Millot, Y.; Dzwigaj, S. Effect of the Niobium State on the Properties of NbSiBEA as Bifunctional Catalysts for Gas- and Liquid-Phase Tandem Processes. *J. Mol. Catal. A Chem.* **2016**, *424*, 27–36.

(11) Kozlowski, J. T.; Davis, R. J. Sodium Modification of Zirconia Catalysts for Ethanol Coupling to 1-Butanol. *J. Energy Chem.* **2013**, *22* (1), 58–64.

(12) Da Ros, S.; Jones, M. D.; Mattia, D.; Pinto, J. C.; Schwaab, M.; Noronha, F. B.; Kondrat, S. A.; Clarke, T. C.; Taylor, S. H. Ethanol to 1,3-Butadiene Conversion by Using ZrZn-Containing MgO/SiO 2 Systems Prepared by Co-Precipitation and Effect of Catalyst Acidity Modification. *ChemCatChem* **2016**, *8* (14), 2376–2386.

(13) Velasquez Ochoa, J.; Malmusi, A.; Recchi, C.; Cavani, F. Understanding the Role of Gallium as a New Promoter of MgO-SiO2 Catalysts for the Conversion of Ethanol into Butadiene. *ChemCatChem* **2017**.

(14) Karmakar, B.; Sinhamahapatra, A.; Panda, A. B.; Banerji, J.; Chowdhury, B. Ga-TUD-1: A New Heterogeneous Mesoporous Catalyst for the Solventless Expeditious Synthesis of Aminonitriles. *Appl. Catal. A Gen.* **2011**, *392* (1–2), 111–117.

(15) Larina, O. V.; Kyriienko, P. I.; Soloviev, S. O. Effect of Lanthanum in Zn-La(-Zr)-Si Oxide Compositions on Their Activity in the Conversion of Ethanol into 1,3-Butadiene. *Theor. Exp. Chem.* **2016**, *52* (1), 51–56.

(16) Ordomskiy, V. V.; Sushkevich, V. L.; Ivanova, I. I. One-Step Method for Butadiene Production, 2014.

(17) Angelici, C.; Meirer, F.; van der Eerden, A. M. J.; Schaink, H. L.; Goryachev, A.; Hofmann, J. P.; Hensen, E. J. M.; Weckhuysen, B. M.; Bruijnincx, P. C. A. Ex Situ and Operando Studies on the Role of Copper in Cu-Promoted SiO 2 –MgO Catalysts for the Lebedev Ethanol-to-Butadiene Process. *ACS Catal.* **2015**, *5* (10), 6005–6015.

(18) Klein, A.; Keisers, K.; Palkovits, R. Formation of 1,3-Butadiene from Ethanol in a Two-Step Process Using Modified Zeolite-β Catalysts. *Appl. Catal. A Gen.* **2016**, *514*, 192–202.

(19) Jones, M.; Keir, C.; Iulio, C.; Robertson, R.; Williams, C.; Apperley, D. Investigations into the Conversion of Ethanol into 1,3-Butadiene. *Catal. Sci. Technol.* **2011**, *1* (2), 267.

(20) Cheong, J. L.; Shao, Y.; Tan, S. J. R.; Li, X.; Zhang, Y.; Lee, S. S. Highly Active and Selective Zr/MCF Catalyst for Production of 1,3-Butadiene from Ethanol in a Dual Fixed Bed Reactor System. *ACS Sustain. Chem. Eng.* **2016**, *4* (9), 4887–4894.

(21) Sushkevich, V. L.; Ivanova, I. I.; Taarning, E. Ethanol Conversion into Butadiene over Zr-Containing Molecular Sieves Doped with Silver. *Green Chem.* **2015**, *17* (4), 2552–2559.

(22) Pomalaza, G.; Capron, M.; Ordomsky, V.; Dumeignil, F. Recent Breakthroughs in the Conversion of Ethanol to Butadiene. *Catalysts* **2016**, *6* (12), 203.

7.2. Recent Breakthroughs in the Conversion of Ethanol to Butadiene

catalysts

MDPI

Review

Recent Breakthroughs in the Conversion of Ethanol to Butadiene

Guillaume Pomalaza [1], Mickaël Capron [1], Vitaly Ordomsky [1,2] and Franck Dumeignil [1,*]

[1] University Lille, CNRS, Centrale Lille, ENSCL, University Artois, UMR 8181-UCCS-Unité de Catalyse et Chimie du Solide, F-59000 Lille, France; pomalaza.g@gmail.com (G.P.); mickael.capron@univ-lille1.fr (M.C.); italy.Ordomsky@univ-lille1.fr (V.O.)

[2] Eco-Efficient Products and Processes Laboratory (E2P2L), UMI 3464 CNRS-Solvay, Shanghai 201108, China

* Correspondence: franck.dumeignil@univ-lille1.fr; Tel.: +33-(0)3-20-43-45-38

Academic Editor: Yu-Chuan Lin

Received: 30 October 2016; Accepted: 6 December 2016; Published: 13 December 2016

Abstract: 1,3-Butadiene is traditionally produced as a byproduct of ethylene production from steam crackers. What is unusual is that the alternative production route for this important commodity chemical via ethanol was developed a long time ago, before World War II. Currently, there is a renewed interest in the production of butadiene from biomass due to the general trend to replace oil in the chemical industry. This review describes the recent progress in the production of butadiene from ethanol (ETB) by one or two-step process through intermediate production of acetaldehyde with an emphasis on the new catalytic systems. The different catalysts for butadiene production are compared in terms of structure-catalytic performance relationship, highlighting the key issues and requirements for future developments. The main difficulty in this process is that basic, acid and redox properties have to be combined in one single catalyst for the reactions of condensation, dehydration and hydrogenation. Magnesium and zirconium-based catalysts in the form of oxides or recently proposed silicates and zeolites promoted by metals are prevailing for butadiene synthesis with the highest selectivity of 70% at high ethanol conversion. The major challenge for further application of the process is to increase the butadiene productivity and to enhance the catalyst lifetime by suppression of coke deposition with preservation of active sites.

Keywords: butadiene; ethanol; acetaldehyde; ETB; condensation; catalyst; oxide

1. Introduction

1.1. Scope of the Review

1,3-butadiene (butadiene, BD or C_4H_6) is essential to the production of numerous elastomers, such as styrene-butadiene rubber, polybutadiene, acrylonitrile-butadiene-styrene and others [1–3]. It is also used as a reagent in organic chemistry, particularly in Diels-Alder reaction [2]. At present, butadiene is predominantly extracted from the C4 steam cracker fractions [2]. Because the butadiene yield depends largely on the nature of the feedstock of the steam cracker, butadiene production is susceptible to market instability or trends in the petroleum industry, notably the emergent use of shale gas, which may lead to BD shortages [4]. The scarcity of greenhouse gas-emitting fossil fuel reserves is another long-term issue with the current butadiene production method, both in terms of commercial and environmental sustainability. These matters have recently renewed an interest in the century-old heterogeneous catalytic conversion of ethanol to butadiene in which gaseous ethanol is primarily transformed to BD over multifunctional materials.

Scientific development in the production of ethanol from biomass, coupled with state subsidies and mandates, have greatly increased the global output and affordability of bioethanol. Due to its

limited use as a fuel for combustion engines, an excess of bioethanol is expected. For this reason, it is believed that ethanol would make an ideal platform molecule for the synthesis of value-added chemicals, namely butadiene [5]. A recent publication by Bell et al. has detailed the conditions under which the industrial use of butadiene from bioethanol would reduce greenhouse gas emissions; the key is believed to be the use of low-carbon emitting ethanol sources [3]. Another case study by Burla et al. has outlined that the conversion of ethanol and acetaldehyde into butadiene would be profitable under certain given circumstances; butadiene production in the Gulf coast of the USA can be expected to be very profitable as long as ethanol remains below \$3.0/gallon [6].

Despite having been successfully implemented in the past, it is recognized that productivity levels of current ethanol-to-butadiene technology are not yet sufficient to insure economic viability [7]. To meet the increasing demand for BD in the face of eventual scarcity, the aim of the ongoing scientific research is to improve the performances of the catalysts being developed.

In the literature, the ethanol-to-butadiene (ETB) reaction is referred to by different names due to the two processes by which it was historically industrialized. The one-step process (or Lebedev process) refers to the direct gas-phase conversion of ethanol to butadiene over active materials. The two-step process (or Ostromislensky process) refers to the conversion to butadiene of an ethanol/acetaldehyde gaseous mixture previously obtained by partial dehydrogenation of ethanol. Because the two processes have been recognized to undergo the same reaction pathway, both can be studied conjointly. BD synthesis through the one-step process usually results in the production of acetaldehyde as a byproduct of the reaction, which has to be recycled in the system in the case of implementation in an industrial process. Thus, even in the one step process it is necessary to test feeds containing acetaldehyde in order to assess the behavior of the catalytic system in acetaldehyde-containing mixtures, however, in lower amounts compared to the two-step process.

Having been discovered more than a century ago, research on the ETB reaction is abundant, but scattered over different time periods. Fortunately, the dispersed literature has been summarized in review articles [4,8–10]; the reader is referred to these publications for details concerning the history of the reaction, its fundamental principles, including mechanistic and thermodynamic considerations, the many catalytic systems studied and the issues regarding the design of new catalysts. Marked by the publication of "Investigation into the conversion of ethanol into 1,3-butadiene" in 2011 by Jones et al. [11] the pace of scientific progress in the field of the ethanol-to-butadiene conversion has accelerated, as illustrated in Figure 1, which indicates the number of publications on the ethanol-to-butadiene reaction in the recent years. The aim of this review is to bridge the gap between the previous reviews dating back to 2014 and the recent advances made in this field. By discussing the latest catalyst designs and characterization techniques, it is hoped that readers wishing to partake in this research can be made fully aware of the newest tools at their disposal to pursue the groundbreaking work accomplished in recent years.

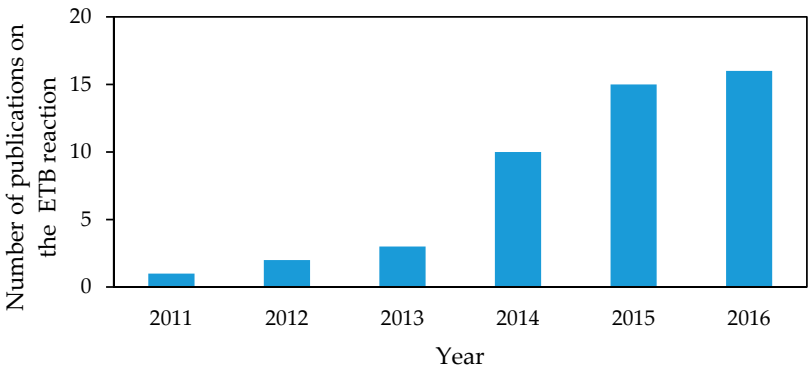

Figure 1. Number of publications dedicated to the ethanol-to-butadiene reaction in the recent years. ETB, ethanol-to-butadiene.

1.2. Reaction Details Reaction of Ethanol to Butadiene

1.2.1. Generalities Mechanism

Several mechanism explaining the transformation of a gaseous ethanol feed (or an ethanol/acetaldehyde feed) to butadiene have been proposed and debated; the reader is directed to the review article by Sels et al. for the detailed history of this subject [8]. Until recently, the issue was settled by the wide recognition of a mechanism involving the condensation of acetaldehyde as the origin of C4 species. However, based on their observation on purely basic MgO catalysts, Cavani et al. have recently proposed a new and self-consistent mechanism featuring an intermediate carbanion species in the formation of C4 molecules [12–14]. Both will be briefly discussed hereafter. Despite the debate between both mechanisms, the involvement of both ethanol and acetaldehyde in some steps of the reaction is well-established and not controversial [4,8,9]. In general, addition of acetaldehyde (in the two-step process) yields higher butadiene productivity [8]. The reaction can be summarized as a dehydrogenation, condensation, dehydration reaction (Figure 2) for the Lebedev process [14]. Additionally, thermodynamic considerations on the conversion of ethanol to butadiene have also been covered by Sels et al. and Weckhuysen et al. in great detail [8,9].

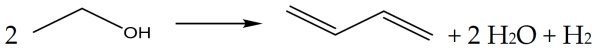

Figure 2. Stoichiometry of the ethanol-to-butadiene reaction.

1.2.2. The Kagan Mechanism

The generally recognized route to butadiene formation from ethanol was elaborated over decades by different scientific teams studying the kinetics of the reaction [8]. Because the current form of the mechanism was first proposed by Kagan et al.—subsequently modified by Niiyama et al., Natta et al. and Bhattacharyya et al., it is referred as such in the present paper to distinguish it from the alternative mechanism [4,9]. The complete reaction pathway is believed to proceed as follows (Figure 3): ethanol partially undergoes non-oxidative dehydrogenation, forming acetaldehyde (1); 3-hydroxybutanal (acetaldol) is produced by the adol condensation of two acetaldehyde molecules (2); acetaldol is dehydrated to acetaldehyde (3); crotonaldehyde is subjected to a Meerwein–Ponndorf–Verley–Oppenauer (MPVO) reduction involving ethanol, affording crotyl alcohol and acetaldehyde (4); crotyl alcohol is dehydrated to butadiene (5). The rate-limiting reaction is thought to vary depending on the chemical properties [8]. Over basic catalysts with poor redox properties, ethanol dehydrogenation is generally recognized as the limiting step. In the case of Lewis acids, it is thought to be the MPVO reaction that is the limiting step [8].

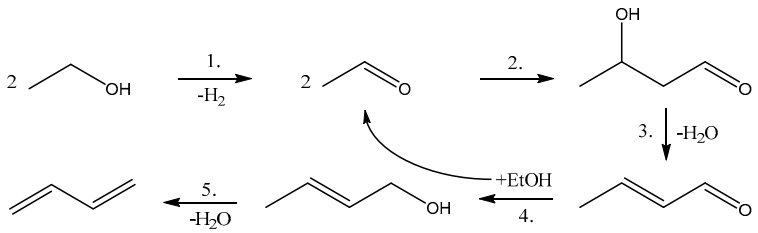

Figure 3. Generally accepted reaction pathway for the formation of butadiene from ethanol initially proposed by Kagan et al. [8].

Some issues with this mechanism have been identified by Cavani et al. in their latest book [14]. First, the supposed intermediate acetaldol is seldom detected amongst the products of the reaction, arguably due to its facile dehydration. Second, the engineers at Union Carbide Corporation have

reported that acetaldol was converted back to acetaldehyde when fed together with ethanol into a reactor packed with a 2% Ta/SiO_2 catalyst without producing butadiene [15]. This suggests that butadiene is produced through a different route, which does not involve the aforementioned intermediate. Nevertheless, because recent kinetic studies have repeatedly supported the validity of this pathway, it cannot be ruled out [16–19].

1.2.3. The Cavani Mechanism

The conversion of ethanol to 1-butanol—through the so-called "Guerbet reaction"—is believed to follow a similar pathway to that of the ETB mechanism indicated above [20–22]. C4 carbonaceous intermediates are thought to be formed by aldol condensation of acetaldehyde, like in the Kagan mechanism, with 1-butanol being formed in the absence of dehydration active sites. However, Meunier et al. have recently argued that aldol condensation was irrelevant [23]. Based on this possibility, Cavani et al. have investigated both reactions over purely basic MgO catalysts at short contact time and proposed new reaction pathways, supported by density functional theory (DFT) calculations, diffuse-reflectance infrared Fourier transform spectroscopy analysis (DRIFTS) and mass spectroscopy (MS) [12,14]. Briefly, the formation of crotonaldehyde was found to be kinetically consecutive to the formation 1-butanol and crotyl alcohol, the precursor to butadiene. Ethylene was also produced in the absence of acid sites, ethanol dehydration thus not being the exclusive pathway to this light olefin. Additionally, the conversion of acetaldol mixed with ethanol did not afford butadiene, but crotonaldehyde and acetaldehyde. A new reaction model was conceived to explain this inconsistency with the Kagan mechanism (Figure 4). According to this model based on observations over MgO, adsorbed ethanol may dissociate into acetaldehyde and hydrogen (1). Ethoxide species adsorbed on specific MgO defects could also undergo proton abstraction to form a carbanionic species stabilized by surface Mg cations (2). This carbanion would act as the main intermediate for the formation of the various products that are generated during an ETB reaction: if attacked by the carbanion, a neighboring adsorbed acetaldehyde molecule would transform into crotyl alcohol (3), which would go on to be dehydrated into BD (4); if attacked by the carbanion, a neighboring adsorbed ethanol molecule would instead form 1-butanol (5), which can be dehydrated into 1-butene (6); in the absence of neighboring molecule, the remaining hydroxy group of the carbanion would dissociate, resulting in ethylene (7).

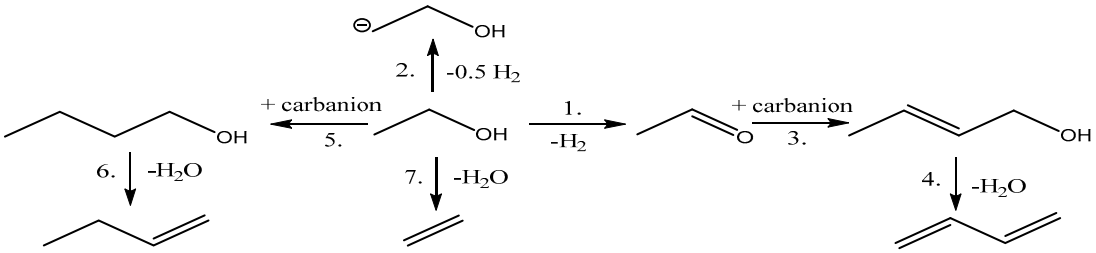

Figure 4. Novel reaction pathway for the formation of butadiene from ethanol proposed by Cavani et al. [12–14].

To the best of our knowledge, these very recent results have not been repeated by other teams. On the contrary, subsequent kinetic studies of the ETB reaction and the Guerbet reaction have reconfirmed the original pathways, albeit on other catalysts than MgO [17,18,22].

1.2.4. Byproducts

Gaseous ethanol can be easily converted to a wide variety of chemicals with the appropriate catalyst [5]. The product distribution is affected by several factors such as the reaction conditions. A difference in temperature alters the thermodynamics and kinetics of the process, possibly favoring

the formation of byproducts. The same is true for the contact time between the reagents and the catalyst [9,19,24]. Therefore, a careful optimization is required. The nature of the catalysts can also influence the nature and quantity of the byproducts depending on their chemical properties. For instance, silica-supported zirconium oxides were found to produce larger amounts of C_6+ hydrocarbon species as side products, presumably due to their trend to catalyze condensation reactions [16]. This issue is complicated by an incomplete understanding of the mechanism. For instance, the formation of ethylene, whether it is directly formed or obtained from diethyl ether cracking, is still a matter of debates and likely depends on the catalyst used [13]. Maximizing the butadiene yield also requires suppressing of the formation of such byproducts [25]. At many steps of the reaction, the intermediate may undergo an alternative pathway, thereby wasting carbon atoms on undesired products. However, the task is complex due to the ambiguity surrounding their formation. Another issue with the formation of several byproducts is the additional cost associated with their separation [25]. Nevertheless, a reaction network of the main byproducts, discussed elsewhere, is summarized in Figure 5 to illustrate the wide variety of species that can be expected and observed [8,16].

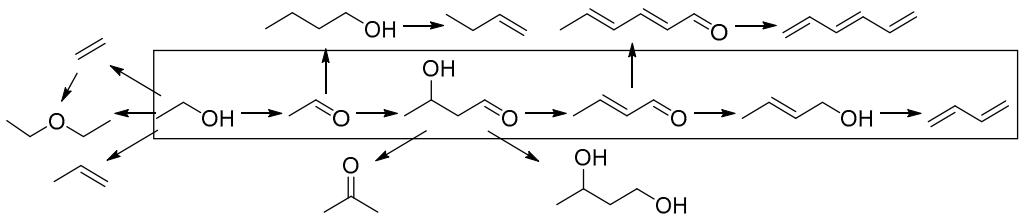

Figure 5. Reaction network of the main byproducts [8,16]. The Kagan mechanism intermediates and product are inboxed.

The main byproduct of the ETB reaction is ethylene, which is the result of ethanol dehydration or ether cracking over acid sites. However, dehydration itself cannot be entirely suppressed as it is required for the formation of butadiene after condensation reaction. Other important byproducts include: 1-butanol as a result of the Guerbet reaction, butenes from the dehydration of 1-butanol and propylene, possibly formed by acetone conversion or its own ethanol-to-propylene pathway, as well as C_5+ hydrocarbons resulting from the aldol condensation of crotonaldehyde [5,8,16].

1.3. Catalyst Design

Due to the variety of reaction steps involved, it is obvious that catalysts for the conversion of ethanol to butadiene must be multifunctional—regardless of the subscribed mechanism. Versatile catalysts have been obtained by mixing different materials to provide the required combined chemical properties. A survey of the literature indicates that active catalytic systems generally have acid, basic or redox properties, or a mixture thereof [8,16]. Redox and basic sites are thought to participate in the dehydrogenation of ethanol to acetaldehyde, while acid and basic active sites have been reported to be active in the reactions of condensation and dehydration [8,9,16]. Because of the complexity of the reaction, a difficult balance between these properties is necessary to achieve for high productivity. The amount of different active sites needs to be in appropriate proportions to avoid promotion of undesired side-reactions, such as dehydration of ethanol. However, definitive identification of the active sites on different catalytic systems remains an open question. As stated by Weckhuysen et al. and summarized by Ivanova et al., a key issue in the design of optimal catalysts is the understanding of the optimal catalytic functions (acid/base/redox), the structure-catalytic relationship and the balance between them [9,16].

Because of the long history of the ETB reaction, several catalytic systems have been proposed. Mixed oxides with either acid, basic and/or redox properties are a significant category of those. Bhattacharyya et al. have thoroughly investigated the potential of binary and ternary metal oxide

systems and discovered that a mixture of amphoteric alumina with basic and redox zinc oxide (Al_2O_3-ZnO (60:40)), is the most active catalyst (see Table 1) [26]. Other good catalysts included the mixture of alumina with basic magnesia or alumina with chromium oxide possessing redox properties. Another well investigated catalytic system is MgO-SiO_2, which is discussed in more details below.

Table 1. Catalytic performances of selected materials of the literature, including the best performing catalysts found in the articles reviewed in this paper.

ID	Catalyst	*T* (K)	*WHSV* (h^{-1})	EtOH/AA	*TOS* (h)	X_{EtOH} (%)	Y_{BD} (%)	P_{BD} $g_{BD} \cdot g_{cat}^{-1} \cdot h^{-1}$	Ref.
			Old catalytic systems						
1	Wet-kneaded MgO-SiO_2	623	0.15	-	-	50	42	0.06	[8]
2	Commercial MgO-SiO_2	713	0.3	-	-	70	48	0.06	[8]
3	2% Cr_2O_3-59% MgO-39% SiO_2	673	0.4	-	-	68	38	0.08	[8]
4	3% CuO-56% MgO-42% SiO_2	673	0.7	-	-	86	44	0.22	[8]
5	40% ZnO-60% Al_2O_3	698	1.5	-	-	94	56	0.50	[26]
6	20% MgO-80% Al_2O_3	698	1.5	-	-	-	48	0.40	[26]
7	40% Cr_2O_3-60% Al_2O_3	698	1.5	-	-	-	47	0.40	[26]
8	9.5% ZrO_2-90.5% SiO_2	698	1.0	-	-	-	23	0.13	[8]
9	Ag/ZrO_2/SiO_2	598	0.3	-	-	34	24	0.04	[16]
10	40% ZrO_2-60% Fe_2O_3	698	1.5	-	-	-	40	0.34	[26]
			Recent MgO-SiO_2 catalysts						
11	MgO-SiO_2 (WK)	698	1.1	-	4	~67 [a]	35	0.25	[27]
12	MgO-SiO_2 (MC)	673	1.0	-	-	41.2	23.6 [a]	0.14	[28]
13	3% Au/MgO-SiO_2	573	1.1	-	3.3	45	27 [a]	0.14	[3]
14	1% Ag/MgO-SiO_2	753	1.2	-	3.3	84	42	0.29	[29]
15	1% CuO/MgO-SiO_2	698	1.1	-	4	74	74 [a]	0.48 [a]	[25]
16	1.5% Zr-1% Zn/MgO-SiO_2	648	0.62	-	3	40	30.4	0.13	[30]
17	1.2% K/ZrZn/MgO-SiO_2	648	1.24	-	3	26	13.1	0.12	[30]
18	2% ZnO/MgO-SiO_2	648	1.0	-	3	84.6	45	0.26 [a]	[31]
19	1.2% Zn-Talc	673	8.4 [a]	-	7	41.6	21.5	1.1 [a]	[19]
			Recent Zr-containing catalysts						
20	3.5% Ag/Zr/BEA	593	1.2–3.0	-	3	-	-	0.59	[32]
21	2000 ppm Na/$Zn_1Zr_{10}O_n$	623	6.2	-	-	54.4	15.2 [a]	0.49	[33]
22	2% ZnO-7% La_2O_3/SiO_2-2% ZrO_2	648	1.0	-	3	80.0	60.0	0.71	[34]
23	2% ZrO_2/SiO_2 [b]	593	1.8	3.5	-	45.4	31.6	0.33 [a]	[35]
24	4.7% Cu/MCF + 2.7% Zr/MCF [b]	673	3.7	0.7–1.6	15	92	64.4 [a]	1.4	[36]
			Other recent catalytic systems						
25	HM-Hf/SiO_2	633	0.64	-	10	99	68.8	0.26	[37]
26	3% Ta/BEA [b]	623	0.8	3.7	4	58.9	43.1	0.20	[38]
27	0.7% Nb/BEA [b]	623	0.8	2.7	4	42.8	23.6	0.11	[39]
28	1.4% Cr-16% Ba/Al-MCM-41	723	3.1	-	10	80	22.4	0.40 [a]	[40]

[a] Value estimated according to Equations (1)–(4) based on the data available; [b] used a two-step. WHSV, weighted hourly space velocity in terms of ethanol mass flow; EtOH, ethanol; AA, acetaldehyde; TOS, time on steam.

Apart from mixed oxides, silica-supported Lewis acids for the two-step process have been studied by Corson et al. and Kagan et al. Metal oxides such as zirconium, tantalum, niobium, hafnium, thorium, uranium and titanium oxide were found to be highly active in the conversion of ethanol/acetaldehyde mixtures to butadiene. This was attributed to the ability of these Lewis acids to catalyze aldol condensation, MPVO and dehydration reactions [16].

Another aspect of catalyst design is the recurring use of promoters to tune the properties of the considered catalytic system. Promoters with redox properties (e.g., Ag, Cu, ZnO) have been repeatedly used to enhance the dehydrogenation of ethanol and increase the yield of butadiene in cases where these properties were absent or insufficient in the parent catalyst [4]. For instance, silica-supported tantalum oxide can become active for the Lebedev process with the use of copper to enable to conversion of ethanol to acetaldehyde [41]. The introduction of Lewis acid promoters such as ZrO_2 to improve the activity for the MPVO reaction has also been reported over basic catalysts. Alkali metals have been previously used to alter the acid properties by selective poisoning of acid sites or to introduce new basic properties into the catalyst. One notorious case is the introduction of

sodium oxide into MgO-SiO_2 by Ohnishi et al., which led to one of the best catalytic performance ever reported [42]. Unfortunately, a lack of experimental details seems to have casted some doubts on the validity of their observations [16].

1.4. Performances and Reaction Conditions

Although the economic viability of the ethanol-to-butadiene process is within reach, the current performances do not meet industrial requirements [43–45]. Researchers should therefore strive to design catalysts with improved catalytic performance. As outlined by Jones et al., the most industrially relevant measure of performance is butadiene productivity—meaning the amount of BD produced in relation to the amount of catalyst used over time (e.g., $g_{BD} \cdot g_{cat}^{-1} \cdot h^{-1}$) [7]. Another key factor is the nature and quantity of byproducts, the presence of which leads to decrease of the yield of butadiene and increase the separation costs [25]. In this paper, the catalytic performances will be discussed in terms of BD productivity ($g_{BD} \cdot g_{cat}^{-1} \cdot h^{-1}$), ethanol conversion (%), product selectivity (%) and product yield (%) in terms of molar carbon. The ethanol conversion was calculated according to Equation (1):

$$X\ (\%) = \frac{n^0_{EtOH} - n_{EtOH}}{n^0_{EtOH}} \times 100\% \quad (1)$$

where n^0_{EtOH} is the number of mole fed into the reactor and n_{EtOH} out of the reactor [34]. Selectivity is calculated by the following Equation (2):

$$S_{\ i}(\%) = \frac{n_i \times c_i}{2(n^0_{EtOH} - n_{EtOH})} \times 100\% \quad (2)$$

where n_i is number of moles of product i and c_i is the number of carbon atoms in product i (e.g., for BD it is equal to 4) [34]. The yield is calculated according to Equation (3):

$$Y_i\ (\%) = S_i \times X \div 100\% \quad (3)$$

Butadiene productivity is estimated using Equation (4):

$$Productivity = Y_{BD} \times WHSV \times 0.587 \div 100\%, \quad (4)$$

where WHSV is the weight hourly space velocity in $g_{EtOH} \cdot g_{cat}^{-1} \cdot h^{-1}$ and 0.587 is the mass ratio between ethanol and butadiene assuming 100% conversion [34].

Apart from its nature, the catalytic performances of a material are largely influenced by the conditions under which they operate. As mentioned above, a proper investigation of the ETB reaction should aim at identifying the best industrial conditions. Obviously, the key conditions are the reaction temperature, pressure and the reactant space velocity. The latter can be expressed in terms of weight hourly space velocity (WHSV), taking in account the mass of catalyst in relation to the mass of gaseous ethanol fed into the reactor. Apart from Bhattacharyya et al., all the publications have dealt with fix-bed reactors [46]. While some researchers have investigated the effect of pressure on the catalytic activity, the reaction is generally conducted at atmospheric pressure; the reviewed literature must be therefore assumed to occur at atmospheric pressure unless otherwise noted [19]. Another parameter that influences the reaction is the catalyst pre-treatment, usually done under inert atmosphere at high temperature to activate the material. Finally, the ratio of ethanol-to-acetaldehyde being fed in a reactor is a crucial factor of the two-step process, as it can influence the BD productivity and product distribution [18,36,41,47,48]. Since several papers have reported different optimal ratios, it is likely that this factor is governed by the nature of the catalytic system and the other reaction conditions.

The catalytic performances found in the literature have been compiled elsewhere [8]. The average results of the best catalysts can be summarized as follows: at temperatures between 573 and 673 K for WHSVs from 0.2 to 1.0 h^{-1}, butadiene selectivity is in the range from 40% to 60%, with a butadiene

yield from 30% to 40% [8]. Estimating BD productivity can be difficult due to omission of experimental details, however Jones et al. have suggested a minimum target for butadiene productivity of 0.15 $g_{BD} \cdot g_{cat}^{-1} \cdot h^{-1}$ before envisioning industrial application [7]. Another crucial factor of the reaction is the time-on-stream (TOS) stability, as costly regeneration is likely to have an impact of the viability of the process. Unfortunately, this parameter is also often ignored, painting an incomplete picture of the catalytic performances, as an undisclosed deactivation may prove to be problematic for industrial applications. When available, this paper will also indicate the TOS at which the activity was recorded. It has been repeatedly demonstrated that the main culprit behind catalytic deactivation was the formation of coke on the catalytic surface [4,36,47,49,50]. Table 1 highlights the performances of notable catalysts for the one-step process reported in the past hundred years to provide references to the readers (catalysts 1 to 10 in Table 1), as well as the catalytic systems reviewed in this work.

2. Catalytic Systems

2.1. Magnesium-Silica System

2.1.1. Introduction

Magnesia mixed with silica was first reported as an active catalyst for the direct conversion of ethanol to butadiene in 1944 by Szukiewicz [8]. It has been the subject of numerous investigations, making it the most studied catalyst for the ETB reaction. The reader is referred to the review of Sels et al. for a complete survey of the literature prior to 2014 [8]. This section will instead focus on the latest publications on the subject.

As previously stated, the ETB reaction requires multifunctional catalysts active for the various reactions steps believed to be involved: dehydrogenation, dehydration and condensation. The multi-functionality of magnesia-silica catalysts is attributed to the combination of basic and acid properties: the basicity of magnesium oxide is well established, while acidity is attributed to interactions between magnesium oxide and silica [13,29,51]. It has been repeatedly demonstrated that a careful balance of the chemical properties is necessary to maximize butadiene production [8]. In practice, this has often been done by varying the amount of Mg and Si in a material and is expressed by the molar Mg/Si ratio. Although the nature of the active sites is being debated, Kvisle et al. have demonstrated that catalytic activity requires interaction between the magnesia and silica [52]. One issue with the MgO-SiO_2 system is its susceptibility to deactivate due to coke formation most probably due to the strong basic properties of MgO [53].

Depending on the subscribed mechanism, several active sites and their functionalities have been proposed. Following the Kagan mechanism, basic sites resulting from defects on the MgO phase and Lewis acid-base pair Mg–O are thought to catalyze both the dehydrogenation of ethanol and the aldol condensation between acetaldehyde molecules (Figure 3, steps 1 and 2), incompletely coordinated Mg^+ ions, Mg–O–Si Lewis acid and Mg–O acid pairs would then catalyze MPVO reduction (Figure 3, step 4) [54]. The subsequent dehydration to produce butadiene would be catalyzed by acid sites present on the surface of the catalyst (Figure 3, step 5) [29]. In the case of the mechanism proposed by Cavani et al., the MgO surface instead hosts stable carbanions from proton abstraction of ethanol (Figure 4, step 2) [12,13]. Condensation of acetaldehyde with the carbanion leads to the synthesis of crotyl alcohol which dehydrates into butadiene over acid sites (Figure 3, steps 3 and 4). Over bare magnesium-silica, the rate-limiting reaction is thought to be the dehydrogenation of ethanol [24,31,52]. It explains the observed low productivity of butadiene over these catalysts (Table 1).

Recently, Baba et al. have studied the potential of Zn-containing talc as a catalyst [19,55]. Their findings also include observations relevant to the understanding of the magnesia-silica system. To understand the role of magnesia, they have compared the activity of two MgO catalysts prepared by calcination and by hydrothermal treatment. Surprisingly, hydrothermally-treated magnesia was capable of converting ethanol with a conversion of 36.6% and a selectivity of 47.1% towards butadiene at a WHSV of 0.19 h^{-1} at 673 K. At the same time, calcined MgO did not lead to the formation of BD,

an observation that had previously led several authors to conclude that acidity provided by SiO_2 was actually necessary [12,13,27,29,30]. Based on the XPS spectra of O_{1s} for both samples, a correlation was drawn between the formation of butadiene and the presence of a distinct oxygen species in the MgO phase. Baba et al. suggest that this feature plays a key role in the ETB reaction by being an active site for the MPVO reduction of crotonaldehyde to crotyl alcohol and production of acetaldehyde by heterolytic dissociation involving ethanol (Equation (5)).

$$CH_3CH_2OH + O\text{-}Mg\text{-}O\text{-}Mg \rightarrow O\text{-}Mg\text{-}H + H\text{-}O\text{-}Mg + CH_3CHO \quad (5)$$

2.1.2. Unpromoted MgO-SiO_2

Jones et al. have investigated the effect of the Mg-to-Si ratio in MgO-SiO_2 catalysts and its effect on catalytic properties [30,44]. MgO-SiO_2 was initially prepared by wet-kneading magnesium oxide and silica in water. Subsequently, co-precipitation at 298 K of magnesium nitrate and sodium silicate solutions was employed. For the sake of clarification, wet-kneading is defined as " ... a process in which two or more solid precursor materials are combined and stirred (mechanically or magnetically) thoroughly in a liquid medium." [27]. The highest butadiene yield has been observed over the catalyst with an optimal Mg/Si ratio above 3. ^{29}Si cross polarization magic-angle spinning solid-state nuclear magnetic resonance (CP MAS-SSNMR) spectra indicated that silicon atoms in the co-precipitated materials at low Si content consisted largely of Q1 species attributed to single-bridged Mg–O–Si magnesium silicates. XRD also indicated the existence of crystalline MgO in Si-deprived materials, but no correlations with activity have been observed. It was suggested that co-precipitation generated more Mg–O–Si linkages than wet-kneading. Interestingly, an uncalcined $Mg(OH)_2$-SiO_2 sample proved to be active in the conversion of ethanol to butadiene. The authors suggest that $Mg(OH)_2$ is also active for the dehydrogenation of ethanol and the aldol condensation, as XRD patterns of the spent catalyst indicate it was not oxidized in situ. The effect of pore size was also studied by using SiO_2 with different pore diameters in the preparation of the catalysts. The author reported a drop in ethanol conversion when silica possessing larger pore diameters (250 Å) were used. Preliminary investigations using deuteration indicated that acetaldehyde was converted back to ethanol over MgO-SiO_2 catalysts, which was confirmed by the presence of deuterium in the products of ethanol dehydration after having introduced deuterated acetaldehyde into the feed. A kinetic analysis of the reaction was also conducted: results from varying the contact time were in accordance with the Kagan mechanism [24]. Ethanol dehydrogenation was found to be the rate-limiting step at temperatures between 573 and 673 K over MgO-SiO_2 (Mg/Si = 1), while aldol condensation would be the slowest step at 723 K.

Weckhuysen et al. have studied the influence of the preparation method on the chemical properties of magnesia silica catalysts [25,27,51]. Wet-kneading, mechanical mixing and co-precipitation were investigated over a MgO-SiO_2 catalyst with a Mg/Si ratio of 1. Wet-kneading $Mg(OH)_2$ with spherical silica was found to produce a layered magnesium silicate phase, the presence of which was found to increase butadiene yield. Co-precipitation resulted in a thick amorphous magnesia silicate phase with high ethylene selectivity. Mechanical mixing produced materials with little interaction between the magnesia and silica phases, resulting in poor activity. The acid-base properties of the catalysts were studied using Fourrier transformed infrared (FTIR) spectroscopy coupled with chemisorption of pyridine and deuterated chloroform. It indicated the presence of Brønsted and Lewis acid sites, as well as basic sites of different strengths on the wet-kneaded catalysts. Excessive Lewis acidity and strong basic sites were detected on the co-precipitated materials, which explains the high selectivity to ethylene and the fast deactivation. The use of Hammett indicators further revealed that the catalysts was predominantly basic. TEM images and catalytic testing indicate a closer proximity between magnesia, silica and magnesium, which was correlated with greater catalytic activity. It was argued that a cooperation between acid and basic sites was involved in the ETB reaction. Thus, the best performing catalysts were prepared using nano-sized magnesia particles, which allowed a more intimate mixing between the phases. At 673 K with a WHSV of 1.1 h^{-1} for a TOS of 4 h, butadiene

yield of 35% was achieved, meaning a butadiene productivity of 0.25 $g_{BD} \cdot g_{cat}^{-1} \cdot h^{-1}$ (ID: 11 in Figures 15 and 16). A similarly prepared catalysts was found to be remarkably stable for a period of 24 h. More importantly, the interpretation of solid-state ^{1}H-^{29}Si CP MAS-SSNMR spectra revealed the existence of distinct magnesium silicates forming at the interface between magnesia and silica–namely anhydrous magnesium silicates, amorphous hydrous magnesium silicates and layered hydrous magnesium silicates. Based on the variation in signal intensity associated to each kind of magnesium silicate and by testing several wet-kneaded samples with different Mg/Si ratios, Weckhuysen et al. were able to directly correlate butadiene yield with the relative amount of layered hydrous magnesium silicates, expressed as the integrated area from the deconvoluted NMR spectra and scaled with number of scans (Figure 6, **left**). Additionally, the relative amount of amorphous hydrous magnesium silicates was directly correlated with ethylene yield (Figure 6, **right**). With these observations, the authors suggested that BD formation could occur on amphoteric layered hydrous magnesium silicates (talc, stevensite, lizardite) close to the MgO phase, while amorphous magnesium silicates contributed to ethanol dehydration, explaining the inferior performances observed with the co-precipitated samples. It was recognized that characterizing the chemical properties and activity of such phases is required to confirm this hypothesis. It should be noted that synthetic talc alone has been demonstrated to be poorly active in the ETB reaction, but was highly active once ethanol dehydrogenation was promoted [19].

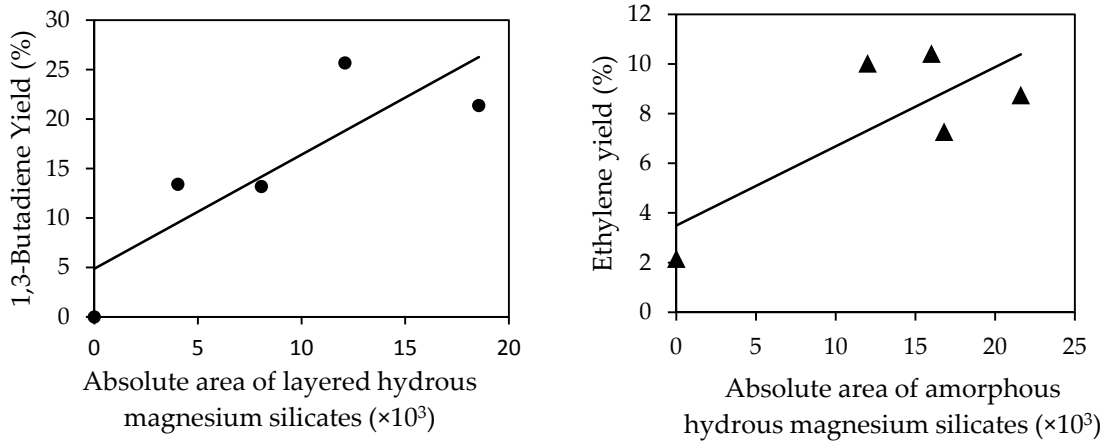

Figure 6. Direct correlations between 1,3-butadiene (**left**) and ethylene yield (**right**) and the absolute area detected by ^{1}H-^{29}Si CP MAS-SSNMR spectroscopy for layered hydrous magnesium silicates (**left**) and amorphous hydrous silicates (**right**), respectively. The areas were determined by scaling the integrals of the corresponding peaks with the number of scans. The data point $x = 0$ is the MgO_{nano} sample. Reprinted with permission from [27]. Copyright 2016, American Chemical Society.

A comparison between mechano-chemically (MC) mixed and wet-kneaded (WK) MgO-SiO_2 materials was also conducted by Kyriienko et al. [28]. For the MC mixing process, magnesium oxide and acid-treated commercial silica precursors were ball-milled using inert silicon nitride balls. Powdered XRD indicated the presence of crystalline magnesium silicate forsterite-like phase in the MC mixed sample absent for the wet-kneaded material. Similar phases were also detected for MgO-SiO_2 catalysts prepared by co-precipitation and wet-kneading with spherical silica [13,27]. Both materials also displayed intensive signals for crystalline MgO. IR spectra in the OH region revealed that MC mixing consumed Si–OH groups of silica. The authors argue that MC mixing generates localized amorphous magnesium silicates that become crystalline upon heating during the mixing process. Pyridine chemisorption measured by FTIR spectroscopy indicated the presence of weak and strong Lewis acid sites over both samples. However, these sites in MC material weaker. Despite having fewer acid sites and a lower surface area, the MC mixed catalysts turned to be more active and selective towards the formation of butadiene. Further, despite a higher ethanol conversion, the selectivity

towards dehydration products over MgO-SiO_2 (MC) was half that of MgO-SiO_2 (WK). The authors attribute this performance to the presence of weak Lewis acid sites capable of participating in the ETB reaction, but less favorable to ethanol dehydration, as well as superior redox properties originating from the crystalline magnesium silicate phase and the proximity between acid and base sites on the surface of the catalyst. At 673 K for a TOS of 8 h and a WHSV of 1 h^{-1}, the MC mixed sample displayed a BD yield of 23.7% and a productivity of 0.14 $g_{BD} \cdot g_{cat}^{-1} \cdot h^{-1}$ (ID: 12 in Figures 15 and 16).

The impact of mixing magnesia with different silica (SiO_2, COK-12 & MCM-41) to prepare catalysts for the ETB reaction was evaluated by Sels et al. [29]. MgO-SiO_2, MgO-COK-12 and MgO-MCM-41 were prepared by dry milling $Mg(OH)_2$ with the respective silicas based on a Mg/Si ratio of 2. To simulate the effect of impregnation, these materials were treated with water prior to calcination. In the case of MgO-SiO_2, this approach produced silica particles covered by magnesia flakes. Magnesium silicates were believed to be formed between the two phases. For the materials prepared with mesoporous molecular sieves, their morphology significantly changed by the wetting process. In both cases, a loss of their mesoporous structure and surface area was observed, which was explained by the migration of dissolved magnesium hydroxide into the pores during the wetting process. A collapse of the thin-walled framework was also thought to lead to the formation of amorphous magnesium silicates in the case of MCM-41. The wetting process also altered the surface chemistry of all catalysts. An increase in the amount of both Lewis acid sites and basic sites was observed when compared to the parent materials using FTIR spectroscopy and a thermal conductivity detector (TCD) with chemisorbed CO_2 and pyridine. The dispersions of dissolved Mg species could have resulted in additional defects in the magnesia phase, thus generating more basic sites. The dispersion of Mg over silica would also generate Lewis acid sites in the form of isolated Mg(II) cations. The presence of these features was supported by UV–Vis spectroscopy. However, no direct correlation between them and catalytic activity was found as all catalysts displayed very poor ethanol conversion. As discussed below, a silver promoter was used to overcome this problem. Ultimately, the use of COK-12 and MCM-41 produced inferior catalyst as their structure could not survive the preparation method, resulting in restricted access to the potential active sites, as well as reducing the amount of magnesium oxide by forming larger amounts of magnesium silicates.

To measure the validity of their new mechanism, Cavani et al. conducted several experiments using magnesia silica catalysts prepared by the sol-gel technique over a large range of Mg/Si ratios (from 1 to 30) [13]. The Mg/Si ratio was shown to have a significant impact on the structural and chemical properties of each catalysts. At Mg/Si ratios above 9, Si atoms were found to be well dispersed with the magnesia phase, as evidenced by ATR spectra. With Mg/Si ratios between 9 and 3, magnesium silicates were detected by both XRD and attenuated total reflectance, along with crystalline MgO. Only at a ratio of 1 were segregated silica and magnesia phases observed. In situ chemisorption of CO_2 measured by DRIFT spectroscopy showed correlation of basicity with Mg content. Conversably, NH_3-TCD indicated an increase in acidity associated with larger amounts of silica. These results suggest that the sol-gel technique promotes interaction between SiO_2 and MgO, but only at low Si content. The variation of the chemical and structural properties had a significant impact on the activity of the catalysts. At high Si content, ethanol conversion into ethylene was the main process (Figure 7). This was attributed to the presence of Mg–O–Si Lewis acid sites generated from the additional Si. The increase in basicity correlated with Mg content and led to an increase of the butadiene yield, despite a drop in ethanol conversion, as the selectivity towards butadiene increased with the Mg/Si ratio (Figure 7). This evidenced the role of the MgO phase in the dehydrogenation of ethanol. However, at a Mg/Si ratio of 30, the overall activity of the material was severely reduced, highlighting the necessity of some acid sites in the process. Interestingly, at low Si content, ethylene selectivity was low, but still detectable as a kinetically secondary product. This phenomenon was explained by the Cavani mechanism, in which the ethoxide carbanion formed on MgO forms ethylene by proton abstraction. An interesting phenomenon was observed when in situ acidity of the catalyst was measured by addition of water in the reactor feed. Pyridine-FTIR revealed an increase in the

number of Brønsted acid sites, which was believed to form during interaction between Lewis acid sites and water. Cavani et al. propose that these sites are responsible for the dehydration of ethanol and crotyl alcohol. This observation also means that ex situ characterization of the catalysts may not give an accurate depiction of the acid-base properties of a catalyst.

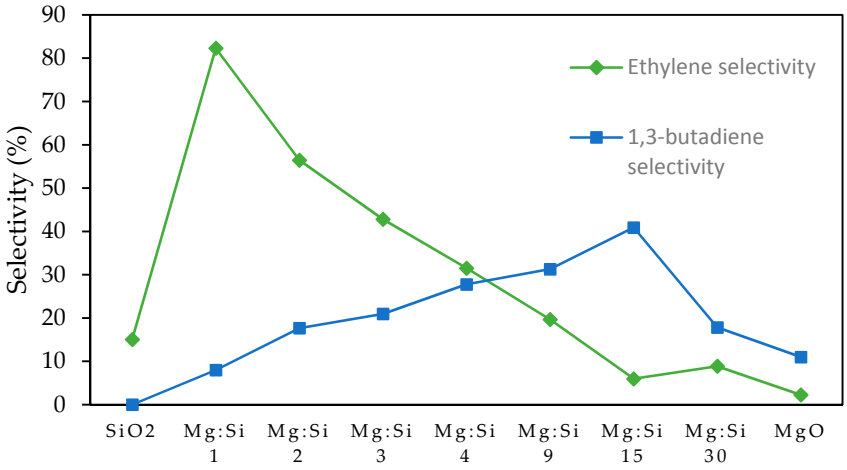

Figure 7. Effect of Mg-to-Si ratio on 1,3-butadiene selectivity and ethanol conversion for MgO-SiO_2 catalysts prepared by the sol-gel method (T = 673 K, contact time = 0.41 s). Reprinted with permission from [13]. Copyright 2016, Royal Society of Chemistry.

2.1.3. Metal-Promoted MgO-SiO_2

The capacity of noble metals to catalyze the non-oxidative dehydrogenation of ethanol is well established [56,57]. Bell et al. have recently investigated the promotion of ethanol dehydrogenation in the ETB reaction with gold nanoparticles over magnesia-silica catalyst [3]. The catalysts were prepared by impregnation of commercial silica gel with aqueous solutions of magnesium nitrate using IWI method. Materials with Mg/Si ratios from 0.15 to 6 were prepared, dried and calcined at 823 K for 3 h. Au was introduced using a modified deposition-precipitation (DP) method involving the addition of an aqueous solution of $HauC_{14}$ to MgO-SiO_2 samples. A pH of 8–10 was reached by adding urea, after which the mixture was dried and reduced under H_2. Surprisingly, for materials with Mg/Si ratios above 1, the DP procedure resulted in a disappearance of crystalline MgO and formation of an amorphous magnesium silicate hydrate phase. Transmission electron microscopy (TEM) coupled with energy dispersive spectroscopy (EDS) indicated that Mg and Si were distributed uniformly over the material, suggesting the complete transformation of bulk MgO to the amorphous magnesium silicate hydrate phase. The cause of this phenomenon was subsequently investigated. The authors proposed that silica reacts with water in the presence of HCl produced by hydrolysis of the gold chloride precursor with formation of the magnesium silicate phase. The role of Cl^- was evidenced by the absence of change when the gold precursor was substituted by Au(acetate) and confirmed by the use of HCl_{aq} with magnesium and silica, which also produced the magnesium silicate hydrate phase. The acid-base properties of the catalysts were studied by FTIR spectroscopy. Strong basic sites on the surface of the magnesium silicate were identified using CO_2 as probe molecule. Pyridine-FTIR indicated the presence of strong Lewis acid sites, but no Brønsted acid sites were detected. In terms of activity, the materials showed moderately high activity in the Lebedev process. Interestingly, decent ethanol conversion and high butadiene selectivity could be obtained at temperatures as low as 533 and 573 K. Increasing the temperature further only increased ethylene selectivity. High butadiene and acetaldehyde yield, but low selectivity towards dehydration products was reported at 40% ethanol conversion. The optimal catalyst was found to be 3% Au/MgO-SiO_2 with a Mg/Si ratio of 1. At 573 K for a WHSV of 1.1 h^{-1}, the butadiene yield was 20.5% and butadiene productivity was

0.14 $g_{BD} \cdot g_{cat}^{-1} \cdot h^{-1}$ (ID: 13 in Figures 15 and 16). To investigate the active sites of the catalyst, Bells et al. co-fed different reactants and measured their impact on butadiene formation. Unsurprisingly, the addition of acetaldehyde into the feed greatly increased butadiene selectivity. A ten-fold increase in butadiene formation was also observed when crotonaldehyde was co-fed with ethanol, suggesting aldol condensation to be the rate-limiting step. By feeding propionic acid with ethanol to poison the basic sites, it was observed that ethanol dehydrogenation and butadiene formation were suppressed. Although removing the poison from the feed allowed dehydrogenation to recover, butadiene yields remained low. Based on this observation, the authors argue that two different basic sites exist: weak basic sites involved in the dehydrogenation reaction and stronger basic sites active for the aldol condensation—assisted by strong-to-medium Lewis acid sites.

Sels et al. used a silver promoter to enhance performances of their MgO-SiO_2, MgO-COK-12 and MgO-MCM-41 catalysts—poorly active in the dehydrogenation of ethanol [29]. Supported Ag nanoparticles are well-known for their ability to dehydrogenate alcohols in the absence of oxidants [58,59]. Silver particles were introduced into the catalysts by aqueous impregnation with $AgNO_3$ and were subsequently calcined, but were not reduced prior to catalytic testing. Environmental scanning electron microscopy combined with energy diffraction analysis of X-rays clearly indicated that silver nanoparticles were dispersed over the silica phase of the catalysts. The impregnation process also altered the chemical properties of the materials compared to the wetting process. Impregnation reduced the total amount of basic sites. It also increased the relative amount of Lewis acid sites. These alterations were measured by CO_2-TCD and pyridine-FTIR. The first observation was attributed to the aggregation of $Mg(NO_3)_2$ species formed by the presence of NO_3^- counter-ions, resulting in large MgO particles possessing fewer basic surface defects. Indeed, the total basicity was shown to decrease with an increase of Ag content. Nevertheless, the overall number of basic sites increased compared to the materials that did not go through a wetting process, meaning Mg(II) dispersion could still occur, albeit at a lesser extent due to NO_3^- counter-ions. The increase in Lewis acid sites is explained by an increase in isolated Mg(II) sites on the silica as a result of the migration of Mg species. The authors also argue that Ag(I) contribute to the Lewis acidity of the material, but due to the likely reduction of silver under the reaction conditions, the quantification of Lewis acid sites could be inaccurate [60]. In terms of activity, a significant improvement was observed on all samples, but was more pronounced with MgO-SiO_2 and MgO-COK-12 than on MgO-MCM-41. The latter phenomenon is believed to occur as a result of the smaller pores of the molecular sieve, more susceptible to the negative effects of impregnation discussed above (pore blockage and structure collapse), ultimately hindering the access to silver active sites. The promotion of ethanol dehydrogenation shifted the limiting reaction to aldol condensation, as evidenced by the accumulation of acetaldehyde. However, excessive amount of silver lead to decrease in activity, likely due to the formation of large Ag particles [58]. Based on this observations, Sels et al. recommend an optimal amount of silver as 1–2 wt %. Ultimately, the most active catalyst was reported to be 1% Ag/MgO-SiO_2 with a BD yield of 42% and a productivity of 0.29 $g_{BD} \cdot g_{cat}^{-1} \cdot h^{-1}$ at 753 K for a WHSV of 1.2 h^{-1} after 200 min on stream (ID: 14 in Figures 15 and 16).

Weckhuysen et al. have investigated the addition of CuO to magnesia-silica materials [25,50,51]. The best catalyst was found to be 1 wt % CuO/MgO-SiO_2 prepared by impregnating the wet-kneaded magnesia-silica catalysts discussed above with copper salt using the IWI method. XRD indicated that copper was isolated over the catalyst surface. At 673 K with a WHSV of 1.1 h^{-1} for a TOS of 4 h this catalyst showed a total butadiene yield of 74% and a butadiene productivity of 0.48 $g_{BD} \cdot g_{cat}^{-1} \cdot h^{-1}$, a great improvement from the unpromoted material, which showed a total butadiene yield of 32% under the same conditions (ID: 15 in Figures 15 and 16). This increase in activity is primarily attributed to the redox properties of copper, which promotes the dehydrogenation of ethanol to acetaldehyde. A secondary contribution could come from the selective poisoning of the stronger acid sites by CuO. Interestingly, the promoter effect of CuO was more pronounced when it in contact with the magnesia phase—either by post-synthesis IWI or by co-precipitating CuO with MgO before wet-kneading in SiO_2. This improvement prompted an intensive study on the relation between the

two metal oxides using X-ray absorption near edge structure (XANES) and extended X-ray absorption fine structure (EXAFS). Ex situ analysis showed Cu(II) to be the predominant specie, existing as a distorted octahedral in a $Cu_xMg_{1-x}O$ solid solution. However, under reductive operando conditions at 698 K, a quasi-steady-state was quickly obtained with the introduction of ethanol during which approximately 60% of the total copper was reduced to its metallic state, 20% to its Cu^{1+} state and a final 20% remaining unchanged. The authors conclude that the metallic species was responsible for the dehydrogenation of ethanol, but that the remaining CuO could still contribute to the performances by poisoning the stronger acid sites. Contrarily to the bare catalyst that did not deactivate, a slight but constant deactivation was also observed with the copper-containing catalyst over a period of 24 h. Because no increase in the amount of Cu–Cu bonds was detected by X-ray adsorption spectroscopy (XAS), it was instead attributed to coke formation, and not metal aggregation.

2.1.4. Lewis Acid Promoted MgO-SiO_2

Jones et al. have investigated the use of mixed zinc and zirconium oxides as promoters for the MgO-SiO_2 catalysts mentioned above which were prepared by wet-kneading and co-precipitation at a variety of Mg-to-Si ratios [30,44]. 1.5 wt % Zr(IV) and 0.5 wt % Zn(II) were introduced by simultaneous aqueous impregnation with the appropriate salts, followed by calcination. Contrarily to other reports, Jones et al. tested the effect of not calcinating their MgO-SiO_2 catalysts before impregnation, a procedure which lead to a comparatively greater surface area when using the co-precipitation method. Compared to the bare catalysts prepared by wet-kneading, the addition of ZnO and ZrO_2 greatly improved the selectivity towards butadiene with a slight increase in ethanol conversion. Over MgO-SiO_2 catalysts, the rate-limiting reaction is believed to be ethanol dehydrogenation. When doped with zinc oxide, a change of the rate-limiting step to subsequent reactions can be expected to occurs, most notably to aldol condensation (according to the Kagan mechanism) due to the often observed accumulation of acetaldehyde and to kinetic studies [3,24,29]. In that case, the promotion of such a reaction would become beneficial. It was suggested that both zinc and zirconium oxides possessed the Lewis acidity believed to be capable of catalyzing the aldol condensation [11]. The increased performances of doped MgO-SiO_2 are suggested to be result of improved redox properties by ZnO and a promotion of aldol condensation by the zinc and zirconium oxide couple. Contrarily to their observations with the bare magnesia-silica catalysts where higher Mg content improved the activity for both the dehydrogenation and condensation reactions, Jones et al. found that the optimal Mg-to-Si ratio for Lewis promoted catalysts was of 1. ZrO_2 and ZnO are likely to disperse more readily over Mg–O–Si linkages to form smaller, more active particles. Therefore, MgO-SiO_2 catalysts with greater Si content would benefit more from the promoter effect. According to ^{29}Si MAS NMR results, co-precipitation was found to be more efficient at generating these linkages at a Mg/Si ratio of 1 when compared to wet-kneading. Furthermore, a drop in activity was observed at high Si content, suggesting a necessary contribution of magnesia to the process. A combination of the promoter effects provided by ZrO_2/ZnO and the increased dispersion resulting from the additional Mg–O–Si linkages is thought to be the origin of the superior performances of 1.5% Zr-0.5% Zn/MgO-SiO_2. At 648 K with a WHSV of 0.62 h^{-1} for a TOS of 3 h, the total butadiene yield was of 40% for a productivity of 0.13 $g_{BD} \cdot g_{cat}^{-1} \cdot h^{-1}$ (ID: 16 in Figures 15 and 16). The doped catalysts were further modified by introducing alkali metal (Na, K and Li) through impregnation, resulting in a suppression of ethanol dehydration, as well as an increase in butadiene and acetaldehyde selectivity, albeit at the expense of ethanol conversion (Figure 8). $CHCl_3$-FTIR indicated that alkali modification did not greatly alter the basicity of the catalysts, the changes in catalytic activity were therefore attributed to deactivation of stronger acid sites, as measured by NH_3-FTIR. Although the best alkali doped catalyst did not result in high butadiene yield, it nevertheless offers the possibility of recycling the large amounts of acetaldehyde produced, while benefiting from the reduced ethylene production. In that sense, the best performing catalyst was 1.2% K/1.5% Zr-0.5% Zn/MgO-SiO_2 with a combined butadiene-acetaldehyde selectivity of 72% (ID: 17 in Figures 15 and 16).

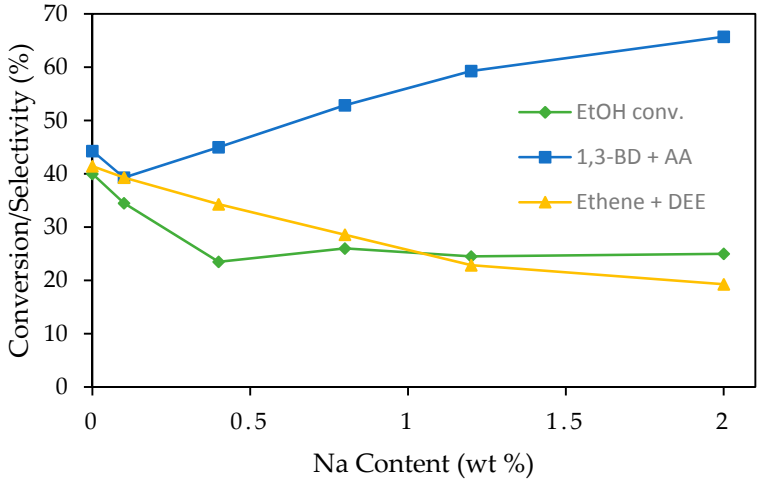

Figure 8. Effect of catalyst Na content on ethanol conversion and selectivity towards the main categories of products (T = 648 K, weight hourly space velocity of ethanol ($WHSV$) = 0.62 h^{-1}, time on stream (TOS) = 3 h). Reprinted with permission from [30]. Copyright 2016, John Wiley and Sons.

Kyriienko, Larina et al. have also investigated the use of zinc and zirconium as promoters for MgO-SiO_2 catalysts [31,61]. The effect of ZnO alone on the catalytic system was first studied [31]. MgO and silica gel mixed at different ratios were impregnated by zinc acetate solutions, dried and calcined for three hours. MgO and SiO_2 were also impregnated in the same way for comparison. Catalytic tests at temperatures ranging between 623 and 698 K and with WHSVs between 0.45 and 1.0 h^{-1}, along with characterization of the samples were conducted. Pyridine-FTIR revealed the existence of two types of Lewis acid sites on ZnO/MgO-SiO_2: one exclusive to MgO-SiO_2 and another resulting from the interaction between ZnO and SiO_2. The latter coincided with the pyridine chemisorption IR spectra over ZnO/SiO_2 and was found to gain in signal strength with ZnO/MgO-SiO_2 possessing larger amounts of Si. The dispersion of all elements of the catalysts was evidenced by XRD and XPS-EDS. In terms of catalytic activity, zinc oxide was found to improve the formation of butadiene of MgO-SiO_2 catalytic system. However, at higher Mg-content, ethanol conversion dropped from 56% to 32% and down to 10% over ZnO/MgO. Higher Si-content led to increase of ethanol dehydration products, a trend which continued over to ZnO/SiO_2 and attributable to the formation of new acid sites by zinc oxide on silica. As a result, the optimal Mg/Si ratio for the production of butadiene was found to be 1. At 648 K with a WHSV of 1.0 h^{-1} and a TOS of 3 h, 2% ZnO/MgO-SiO_2 had a reported yield of 45% and a productivity of 0.26 $g_{BD} \cdot g_{cat}^{-1} \cdot h^{-1}$ (ID: 18 in Figures 15 and 16). The improved performance of the material was attributed to the promotion of ethanol dehydrogenation by ZnO dispersed on the silica. The presence of equal amounts of magnesia and silica was necessary to properly catalyze the subsequent reaction steps. The addition of zirconium to the above system was evaluated in a following study [61]. Before impregnation with a zinc acetate solution, zirconium oxynitrate hydrate was mixed with pre-calcined MgO, SiO_2 and both, followed by the addition of water. In terms of activity, the addition of ZrO_2 to the mixture of SiO_2 and MgO doubled the conversion of ethanol without significantly altering the selectivity towards butadiene, ethylene or acetaldehyde. However, an increase of C_5+ side products was observed, attributed to the condensation of crotonaldehyde promoter by ZrO_2 and noted with similar catalysts [16]. The mixture of ZrO_2 with MgO-SiO_2 and SiO_2 formed new Lewis acid sites not observed on ZrO_2/MgO or bare magnesia-silica. The involvement of these additional sites is not evidenced, however the authors suggest they may improve acetaldehyde condensation due to a synergic effect with magnesia and silica. Surprisingly, the addition of ZnO to the ZrO_2-MgO-SiO_2 system did not significantly improve its performances, a phenomenon explained by a suppression of the acid sites believed participate in the reaction. This also explains the reduction of dehydration products. Surprisingly, the addition of ZnO

lead to significant improvements to the performances of ZrO_2-SiO_2, greatly increasing both ethanol conversion and selectivity towards butadiene, resulting in a better catalyst than ZnO/ZrO_2-MgO-SiO_2. At 648 K with a WHSV of 1.0 h^{-1} and a TOS of 3 h, 4% ZnO/6% ZrO_2-SiO_2 showed a butadiene yield of ~50%, resulting in a butadiene productivity of ~0.29 $g_{BD} \cdot g_{cat}^{-1} \cdot h^{-1}$. Silica-supported zirconium oxide with ethanol dehydrogenation promoters have been reported as highly active and are discussed below [11,16]. The discrepancy with the observations of Jones et al. can be explained by differences in the preparation methods.

2.1.5. Promoted Magnesium Silicate Minerals

Magnesium silicate clay minerals have also been used as catalysts for the conversion of ethanol to butadiene [8]. In particular, sepiolite was previously the subject of investigations, including modifications with Ag, Cu, Ni, Co, V and Zn [8,62–64]. Recently, Baba et al. have studied the potential of Zn-containing talc as a catalyst [19,55]. A thorough optimization of the experimental conditions was conducted. Ethanol conversion was found to greatly influence the product distribution: maximum butadiene selectivity and productivity was observed at an ethanol conversion of approximately 50%. In practice, ethanol conversion was purposefully maintained at 40%. Concerning the effect of catalyst preheating, it was found that heating the catalyst at 673 K for 8 h was optimal; higher temperatures and shorter periods were detrimental to butadiene production. The rate of butadiene formation was found to be proportional to ethanol pressure after decreasing it to 20 kPa with the product distribution only slightly affected—indicating the first-order nature of the reaction. The best performing catalyst was reported to be 1.2% Zn-talc, displaying a butadiene yield of 21.5% and a butadiene productivity of 1.01 $g_{BD} \cdot g_{cat}^{-1} \cdot h^{-1}$ at a WHSV of 8.39 h^{-1} and a temperature of 673 K (ID: 19 in Figures 15 and 16). To the best of our knowledge, this makes Zn-containing talc the most productive catalyst for the one-step process. The role of zinc in this system was also thoroughly investigated by means of characterization, reactivity tests and DFT studies. Modified talc was prepared by hydrothermally synthesizing talc in an autoclave with the addition of zinc precursors. The presence of zinc was found to significantly suppress the dehydration of ethanol. Over pure talc, the combination of ethylene and diethylether accounted for 77.5% of carboneous products; the addition of zinc lowered this value to a minimum of 6.4% at the reaction conditions described above. In return, selectivity towards acetaldehyde and butadiene greatly increased up until Zn concentration of approximately 2 wt %. This improvement observed was solely attributed to the promotion of ethanol dehydrogenation, as the reaction of an acetaldehyde feed revealed that the presence of zinc actually suppresses crotonaldehyde formation, which is the secondary product of aldol condensation. The effect of zinc incorporation on the chemical properties of talc was evaluated to explain the promoter effect. The substitution of magnesium by zinc in the octahedral sites of the talc lattice was evidenced by XRD. The binding energies of Mg_{2p}, Si_{2p} and O_{1p} were measured using XPS. Although Si and Mg were unaffected, the binding energy O_{1s} was reduced with increased zinc concentration isn talc. It was assumed that the introduction of Zn resulted in a decrease in the basicity of talc, correlating with the reduction of croton aldehyde formation observed as it is believed to occur on basic sites. The origin of the dehydrogenative properties of Zn-talc was investigated using DFT studies to estimate the chemical hardness of the material, according to the theory elaborated by Pearson and Parr [65]. In short, zinc introduction is believed to soften the chemical hardness of talc, turning into a soft Lewis acid with an increased electronic polarizability of its O atoms. Doing so would enhance dehydrogenation of ethanol by promoting hydride abstraction of the $–CH_2–O–$ group in surface ethoxide formed by ethanol chemisorption due to its soft Lewis basic nature. According to the theory of hard and soft acids and bases, the highly polarizable and low positively charged soft Lewis acids reacts more readily with low electronegative and high polarizable soft bases [66]. In this case, DFT computations were employed to estimate the alteration of chemical hardness based on bandgap between the highest occupied crystal orbital (HOCO) and lowest occupied crystal orbital (LUCO) energy levels of the crystal before and after the incorporation of zinc. The authors suggest that the concept of chemical hardness coupled with

computational calculations could be a useful tool to predict the promoting effect of dopants introduced in catalytic systems for the ETB reaction.

2.2. Zirconium Catalytic System

2.2.1. Introduction

Lewis acid catalysts consisting of silica-supported zirconium, tantalum and niobium oxide were investigated several decades ago for the Ostromislensky process by Toussaint et al. [67]. After a screening study, Jones et al. concluded that zinc and zirconium oxide on silica were active in the Lebedev process due to a combination of Lewis acidity and the capacity of ZnO to catalyze the dehydrogenation of ethanol [11]. Recently, Ivanova et al. outlined a novel approach to the design of catalysts for the Lebedev process. By combining metal oxides active in the aldol condensation and the MPVO reduction (ZrO_2, MgO, Al_2O_3, Nb_2O_5, TiO_2) with metal promoters capable converting ethanol to acetaldehyde (Ag, Cu, Ni) over silica, the team was able to produce highly active materials for the one-step process [16]. Early investigations having identified silver/zirconium system as the most active for the production of butadiene, it was thoroughly investigated. Such investigations include: the aldol condensation of acetaldehyde over silica-supported zirconium oxide, the dehydrogenation of ethanol over silica-supported silver and the MPVO reduction of crotonaldehyde over Zr-containing catalyst—all reactions believed to occur in the Kagan reaction pathway [54,59,68].

2.2.2. Catalysts for the One-Step Process

Ivanova et al. have investigated the use of ordered microporous zeolite beta polymorph A (BEA) and mesoporous MCM-41 as alternatives to silica to support their Ag and Zr(IV) catalytic system [69]. At equal amounts of silver and zirconium, the BEA-supported catalyst was found to slightly more active than the MCM-41 catalyst and significantly better than its silica-supported equivalent. The higher activity observed with molecular sieves was explained by the greater concentration of isolated Zr(IV) sites that could be obtained by directly incorporation during the synthesis procedure and evidenced by XPS and ^{29}Si MAS NMR, as opposed to the impregnation of silica, where zirconium is supposed to be in the form of ZrO_2. The butadiene yield also correlated with the amount of Lewis acid sites, identified by FTIR using deuterated acetonitrile ($CDCN_3$) and attributed to the isolated Zr(IV) sites. In all the samples, the dry impregnation with silver lead to the formation of 2–5 nm particles, the optimal particle size for the dehydrogenation of ethanol when supported over silica [58]. Although Ag/Zr/BEA and Ag/Zr/MCM-41 displayed similar activity, the latter generated more dehydration products due to the greater amount of surface silanol groups acting as Brønsted acid sites. The nature of Zr/BEA active sites was further investigated in subsequent studies [49,70]. Ivanova et al. argued that the configuration of Zr(IV) within the zeolite framework influenced the activity of the Lewis acid sites—a phenomenon comparable to the well-documented cases of Ti/BEA and Sn/BEA in which distinguishable "open" and "closed" Lewis acid sites have been demonstrated to exist [71–75]. The term open site refer to partially hydrolyzed metal ion sites linked by three M–O–Si bonds to the zeolite framework with one M–OH linkage (Figure 9) compared to closed sites fully coordinated in the zeolite framework by four M–O–Si bonds (Figure 9).

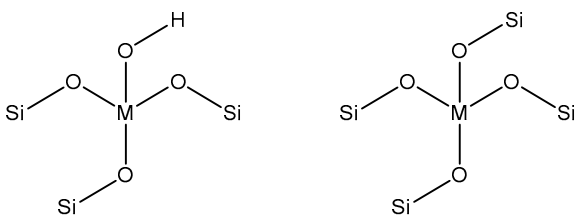

Figure 9. Distinct open (**left**) and closed (**right**) metal ion sites in M/BEA (M = Zr, Sn, Ti) [49,70–75].

The presence and role of open Zr sites was subsequently demonstrated on Zr/BEA prepared by hydrothermal synthesis according to the literature with $ZrOCl_2$ as a precursor [76]. Due to the subtle difference between open and closed sites, clearly identifying the nature of the Lewis acid site required the chemisorption of multiple molecular probes measured by FTIR spectroscopy. The presence of weak Brønsted acid sites could only be demonstrated by ditertbutylpyridine (DTBPy)-FTIR, a sensitive probe when compared to pyridine, which failed to show any Brønsted acidity at all. As bulk ZrO_2 shared similar bands, its signal was tentatively assigned to interaction with Zr–OH bonds. Contrarily to Ti/BEA, distinguishing between the open and closed Lewis acid could not be done using deuterated acetonitrile as a probe, as it only displayed a single signal for Zr/BEA Lewis acid sites. Carbon monoxide (CO) chemisorption at low temperature was used to address this issue. The progressive adsorption of CO unto the catalyst surface monitored by FTIR spectroscopy revealed the presence of two different Lewis acid sites—one strong, one weak—as well as the presence of an OH group, also attributed to a Zr–OH group and thought to belong to the open Lewis acid site. To demonstrate this, $CDCl_3$ was preadsorbed on Zr/BEA before adding CO at low temperature; this resulted in a significant suppression of the CO signals for Zr–OH and the strong Lewis acid site. It was therefore concluded that both signals belong to the same species: the open Lewis acid sites, and that $CDCl_3$ exclusively adsorbed unto it, sterically hindering the access to CO. Only the latter could properly distinguish between both sites. With a method to detect Zr open and closed sites, Ivanova et al. were able to compare their relative amounts with the formation of butadiene from ethanol obtained during catalytic testing [32,49]. A direct correlation between the relative number of open Lewis acid sites and the initial rate of butadiene production was observed (Figure 10). On the contrary, the relative amount of closed sites did not correlated with the conversion of ethanol, suggesting that they are either inactive or less active in the ETB reaction [49].

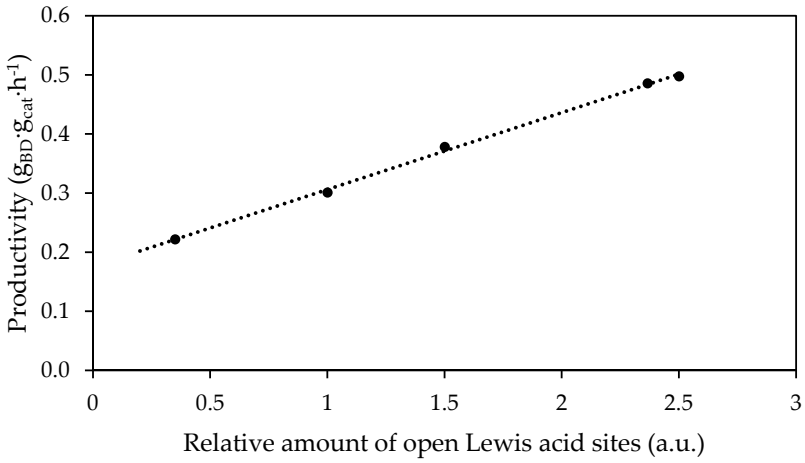

Figure 10. Correlation between the relative amount of open Lewis acid Zr sites with the rate of BD formation. Adapted from [32]. Copyright 2016, WILEY-VCH Verlag GmbH & Co. KGaA.

Having identified the nature of the active sites, Ivanova et al. focused on designing more active catalysts by maximizing the amount of open sites [32]. To this end, a new approach to the preparation of Ag/Zr/BEA was developed. By the post-synthetic treatment of dealuminated BEA zeolite with a DMSO solution of $ZrOCl_2$ under reflux conditions, catalysts containing only open Zr Lewis acid sites were obtained, as evidenced by the FTIR spectroscopy method described above. It was discovered that the grafting of zirconium ions over terminal silanol groups, which can be found on the surface of zeolites, led to the formation of the desired open Zr sites and that this particular post-synthetic treatment highly favoured the interaction between the dissolved precursor and such groups. Surprisingly, Zr was not grafted onto the silanol groups formed during the dealumination with nitric acid, the so-called "silanol nests", meaning these had little impact on the incorporation of

zirconium. These phenomena was evidenced FTIR spectroscopy in the O–H region, demonstrating a consumption of terminal silanol groups by the post-synthesis procedure, but not of silanol nests. Steric hindrance, diffusion limitations or energetic limitations were suggested as the cause of this preferential grafting. The relative amount of open Lewis sites was measured by CO-FTIR and correlated with the crystal size of zeolite—smaller crystals possess additional terminal silanol groups, resulting in greater amounts of open sites. In turn, ~1% Ag/Zr/BEA catalyst was significantly more active than those prepared by the traditional hydrothermal route. The most active amongst them was ~3.5% Ag/Zr/BEA with Si/Zr ratio of 75; it achieved a selectivity towards butadiene near 60% and a productivity of 0.58 $g_{BD} \cdot g_{cat}^{-1} \cdot h^{-1}$ (ID: 20 in Figures 15 and 16). This places the catalytic system designed by Ivanova et al. amongst the most productive currently recorded. Although the precise WHSV is not disclosed, it is indicated to be between 1.2 and 3.0 h^{-1}.

Wang et al. have studied the conversion of ethanol to butadiene over a zinc-zirconium mixed oxide catalytic system, adding sodium to alter its surface acidity and further studied the relation between the material's chemical properties and catalytic activity [77]. $Zn_xZr_yO_z$ was synthesized using commercial carbon as a hard template for impregnation with different amounts of dissolved zinc and zirconium precursors. The template was removed by calcination at 823 K for 20 h, affording a zirconia material over which zinc oxide is highly dispersed, according to XRD patterns. As per a previous publication by the same research team, such a material would also possess large mesopores [77]. As demonstrated with NH_3-TPD and pyridine-FTIR, varying the Zr/Zn ratio from 2 to 30 had a significant impact on the surface acidity of the catalytic system. On all samples, weak, medium and strong Brønsted and Lewis acid sites were detected. Decreasing the Zr/Zn ratio from 30 to 10 weakened the strength of the acidity, generating greater amounts of weak and medium sites at the expense of strong sites. This alteration mostly affect the Lewis acidity of the sample. Below a ratio of 10, the Brønsted acidity of the material was suppressed and the number of sites of all strength dropped. It was suggested that zinc oxide first passivates strong Lewis acids, then targets medium Brønsted acid sites. New Lewis acid sites could also be generated with sufficient interaction at oxygen vacancies of mixed zinc-zirconium oxide phase. These changes in surface chemistry were reflected in the catalytic activity of the samples: the loss of Brønsted and strong Lewis acid sites due to the suppression by zinc oxide was associated with a reduction in the quantity of dehydration products. It also led to the accumulation of acetaldehyde, which evidenced that the rate-limiting reaction step shifted from ethanol dehydration to aldol condensation due to the redox properties introduced by zinc oxide. However, at the highest Zn content, the overall ethanol conversion and butadiene selectivity dropped, suggesting that Brønsted acid sites might be necessary for the reaction. A catalyst without Brønsted acidity was prepared by incipient wetness impregnation to verify this possibility; it mostly produced acetaldehyde and crotonaldehyde, but little butadiene or ethylene. Although the authors argue that this observation demonstrates the role of Brønsted acid sites in the reaction, there is a possibility that different structural properties, namely the great surface area of the templated catalyst, might have played a role. Because the loss of Brønsted acid sites also suppressed ethylene formation, the alteration of surface chemistry with Na was attempted over the mixed oxide with a Zr/Zn ratio of 10. Evidenced by FTIR spectroscopy with molecular probes, the addition of sodium shifted the strength of acid sites from strong and medium to medium and weak. It also reduced the overall amount of sites with increased Na amount, while retaining both types of acidity. These changes greatly reduced ethanol dehydration, simultaneously increasing acetaldehyde and butadiene formation. The suppression of ethylene formation was attributed to the passivation of strong acid sites by Na-doping, while preserving sufficient medium-strength acid sites of both types to catalyze the desired reaction. Figure 11 illustrates the effect of Na doping at increasing amounts on the catalytic performance of the catalyst. For the catalytic testing of 2000 ppm $Zn_1Zr_{10}O_n$ at 623 K for a WHSV of 0.2 h^{-1}, ethanol conversion was 97% with a high selectivity towards butadiene of 47% and ethylene selectivity of 15.9%. In addition, the catalyst remained reasonably active at a high WHSV of 6.2 h^{-1} producing butadiene at a rate of 0.49 $g_{BD} \cdot g_{cat}^{-1} \cdot h^{-1}$ with an ethanol conversion of 54.4% and a BD selectivity of 28%. In terms

of stability, a 20% drop in ethanol conversion was observed over a period of 60 h, along with a slow decay of butadiene selectivity to the benefit of acetaldehyde formation. The deactivation was reversed with calcination under air, suggesting coke formation as its origin.

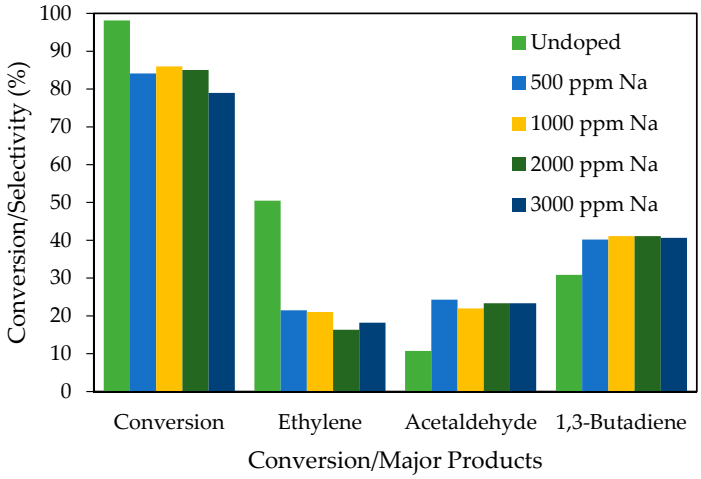

Figure 11. Effect of Na-doping on the conversion and selectivity towards major products on $Zn_1Zr_{10}O_n$ catalyst (T = 623 K, $WHSV$ = 0.2 h^{-1}). Reprinted with permission from [33]. Copyright 2014, Elsevier.

Kyriienko et al. have investigated the use of silica-supported lanthanum oxide as an active component of mixed oxide catalyst including zing and zirconium for the one-step conversion of butadiene [34]. Lanthanum was previously reported active for several of the reaction taking part in the Kagan mechanism, namely ethanol dehydrogenation, aldol condensation and the MPVO reduction [78–80]. Silica was prepared from treated commercial silica gel and was impregnated with lanthanum nitrate hexahydrate and/or zinc acetate solution by the incipient wetness impregnation (IWI) method. Zirconium was added to the mixture by wet-kneading zirconium oxynitrate with silica. The samples were subjected to catalyst activity testing at 648 K at a WHSV of 1.0 h^{-1}. At TOS of 3 h, 7% La_2O_3/SiO_2 was shown to catalyze the formation of butadiene with a selectivity of 23%. However, ethanol conversion remained low and dehydration products were the main products. The addition of zinc to this system increased ethanol dehydrogenation—evidenced by increased production of acetaldehyde and suppression of dehydration. When ZnO-La_2O_3/SiO_2 was mixed with zirconium, a significant increase in butadiene formation was observed. 2% ZnO-7% La_2O_3/SiO_2-2% ZrO_2 greatly increased ethanol conversion to 80% while keeping the selectivity towards dehydration products below 14%. Butadiene selectivity increased to 65.7% while acetaldehyde selectivity fell sharply, a sign of increased activity in the reaction believed to be aldol condensation. At 648 K for a WHSV of 2 h^{-1} and a TOS of 3 h, this material showed a butadiene yield of 60% and a productivity of 0.71 $g_{BD} \cdot g_{cat}^{-1} \cdot h^{-1}$, making it one of the best performing catalyst for the one-step process (ID: 20 in Figures 15 and 16). Additionally, the catalytic activity was maintained for 10 h. Acid and base surface properties of this system were characterized by pyridine-FTIR and pyrrol-FTIR. Signals believed to belong to basic sites were attributed to the addition of lanthanum oxide to silica while Lewis acid sites were assigned to the presence of zirconium, and to a lesser extent to lanthanum and zinc oxides interacting with the silica phase. Based on these observations, the authors explain that the high activity as a synergic effect between each component of the system: lanthanum oxide and zirconium oxide are thought to provide basic sites and Lewis acid sites respectively, while zinc oxide would promote the dehydrogenation of ethanol; the combination of acid, base and redox properties meet the criteria to catalyze the ETB reaction based on the Kagan mechanism. This conclusion is further supported by the high selectivity towards butadiene but poor ethanol conversion observed with 7% La_2O_3/SiO_2-2% ZrO_2, in which case the rate-limiting reaction should be the ethanol dehydrogenation.

2.2.3. Catalysts for the Two-Step Process

Han et al. have examined ZrO_2/SiO_2 catalysts for the Ostromislensky process. Using a sol-gel method with nitric acid to induce hydrolysis and gelification of tetraethyl orthosilicate (TEOS), different catalysts were prepared with ZrO_2 content going as high as 8.4 wt %. The gels were dried and calcined at 823 K for 6 h, affording mesoporous materials with large surface area that decreased with the increase in ZrO_2 content. Because no ZrO_2 phase was observed by XRD, it was assumed to be highly dispersed despite the high zirconium loading and further evidenced by TEM, which also revealed the catalyst possessed a leaf-like morphology. Brønsted and Lewis acid sites were detected by pyridine-FTIR spectroscopy, but only Lewis acid sites were shown to increase with higher zirconium content. The catalytic activity was measured according to three controlled parameters: temperature, WHSV and ethanol-to-acetaldehyde ratio. While increasing the temperature from 593 to 683 K promoted ethanol conversion, it also promoted butenes selectivity at the expense of butadiene formation. WHSV did not affect butadiene selectivity, but reduced ethanol conversion at lower contact time. An interesting effect observed at high zirconium loadings was an unexpectedly selectivity towards butenes, as high as 25%, when compared to other zirconium-based catalysts [16,32,69]. The ratio of ethanol/acetaldehyde had a significant influence on the formation of butenes. As shown on Figure 12, for the catalyst 2% Zr/SiO_2 at 593 K and WHSV of 1.2 h^{-1}, the selectivity towards butenes was higher than that of butadiene at high acetaldehyde content. At high ethanol content, the formation of BD increases. Interestingly, while the C4 yield (butadiene + butane) remains high under these various conditions, ethylene formation remained low. Although the authors do not speculate on the origin of the butenes species, it has been reported that butenes are not formed by hydrogenation of butadiene [16]. This would mean that sol-gel prepared ZrO_2 has some degree of activity in the Guerbet reaction and butenes are formed by the dehydration of 1-butanol or that some other pathway is involved. Alkali-doped ZrO_2/SiO_2 has been reported as active in the Guerbet reaction, however it is unlikely that an acidic material would preferably hydrogenate crotyl alcohol rather than dehydrate it without the presence of a dopant to suppress the acidity [21,81]. Because ZrO_2 is known for being amphoteric, the authors suggest that the great degree of dispersion together with interaction with the silica phase might have altered the acid-base properties of the oxide. Regardless of the explanation, at sufficient ethanol content in the feed, BD production was reasonable. The authors conclude that 2 wt % is an appropriate amount of ZrO_2 for the sol-gel synthesis, beyond which undesired active sites may be formed despite the metal's dispersion. The optimal catalysts, recorded at 593 K for a WHSV of 1.8 h^{-1} and a EtOH/AA ratio of 3.5 had a butadiene yield of 31.6% for a productivity of 0.33 $g_{BD} \cdot g_{cat}^{-1} \cdot h^{-1}$ after 3 h on stream (ID: 21 in Figures 15 and 16).

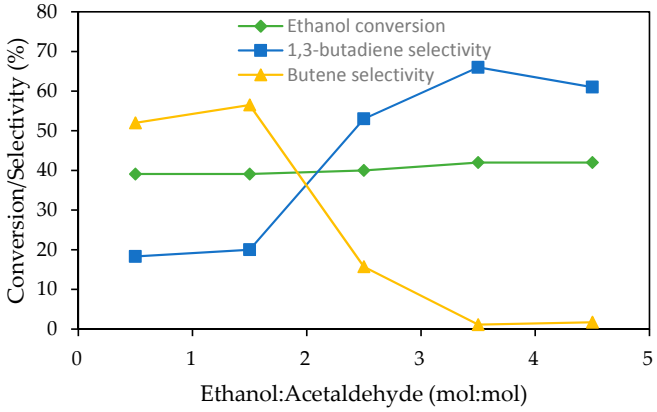

Figure 12. Effect of ethanol/acetaldehyde ratio in the feed over 2% Zr/SiO_2 (T = 593 K, $WHSV$ = 1.2 h^{-1}). Reprinted with permission from [35]. Copyright 2015, Royal Society of Chemistry.

Lee et al. used a connected double fixed reactor system with dedicated functionalities to achieve high butadiene production from ethanol. In the first reactor, a gaseous ethanol feed was converted over a copper-containing catalyst [36]. The second reactor was packed with zirconium-containing catalyst to convert the resulting ethanol-acetaldehyde mixture to butadiene. Both metal oxides were highly dispersed over mesocellular silica foam (MCF), a silica support possessing high surface area, high mesoporosity and ultra large, interconnected nanopores. MCF was prepared according to the procedure disclosed in the literature [82]. To achieve high dispersion of copper oxide over silica, an ion-exchange method was used. Zirconium oxide was introduced into the support by urea hydrolysis. In both cases, drying and a calcination at 773 K for 3 h followed. These methods afforded 4.7% Cu/MCF and 2.7% Cu/MCF. XRD and scanning transmission electron microscopes combined with energy-dispersive X-ray spectroscopy (STEM-EDX) indicated a high degree of dispersion for both active phases. N_2 physisorption and the BET method revealed that the large surface area and porous volume were preserved despite the synthesis procedure. Different types of commercial silica were also used as support for zirconium for comparison. As the temperature of each reactor could be adjusted separately, the first reactor was fine-tuned so as to produce an optimal ethanol-to-acetaldehyde ratio to feed into the second reactor, which was also optimized to maximize butadiene formation. The addition of water in the ethanol feed is a convenient way to measure whether a process is suited for the transformation of crude bioethanol, which contains some amount of it. Lee et al. therefore tested the effects of including 10% water with the ethanol into the first reactor. In turn, the optimal ethanol-to-butadiene ratio varied between 0.69 and 1.68, and depended on the WHSV or the presence of water. The latter had the effect of reducing the optimal ethanol-to-acetaldehyde ratio, meaning acetaldehyde was actually the most abundant species in the feed. After careful optimization, a butadiene yield of 64.4% and productivity of 1.4 $g_{BD} \cdot g_{cat}^{-1} \cdot h^{-1}$ for a WHSV of 3.7 h^{-1} after 15 h on stream was be obtained. The temperatures of the first and second reactors were respectively 523 and 673 K. In terms of productivity, these results are the highest found in the literature concerning the two-step process and the ethanol-to-butadiene conversion as a whole. Regarding the stability of this system, the high ethanol conversion and butadiene selectivity were slowly eroded over a period of tens of hours, but the system was successfully regenerated twice by heat treatment in air. Similarly to previously discussed publications, deactivation was attributed to coke formation. To explain the performances of their catalytic system, the authors argue that the high activity can attributed to the high dispersion of the metal oxides, while the large pores of the support help preventing mass-transfer issues and coking. This later conclusion is supported by the poor performances of catalysts supported on commercial silica, which lacks such morphological properties.

2.3. Other Catalytic Systems

Other Acid Catalysts

De Vos et al. have reported a novel silica-supported hafnium oxide mixed with zinc silicate catalyst yielding 68% butadiene with a productivity of 0.26 $g_{BD} \cdot g_{cat}^{-1} \cdot h^{-1}$ at 633 K with a WHSV of 0.64 h^{-1} for a TOS of 10 h [37]. Remarkably, ethylene selectivity remained below 10% despite ethanol conversion nearing 100%. These results were achieved after making several modifications to a $Cu_xZn_yZr_zO_n/SiO_2$ catalyst first reported by Jones et al. [11]. Initially, zirconium was substituted by hafnium for its softer acid properties with the aim to reduce ethylene formation. Hafnium was introduced into silica by aqueous impregnation before calcination. Hafnium-containing catalysts were first reported as notably active in the Orstromislensky process by Corson et al. and were studied by Corson et al. and Jones et al. [11,41]. This first modification more than halved ethylene selectivity, but only slightly improved butadiene yield. The second modification involved mixing the silica-supported hafnium oxide with the zinc silicate hemimorphite as a substitute for copper and zinc. Hemimorphite was previously reported to catalyze the addition of methanol to propene through the Zn^{2+} open sites found on its surface. The zinc silicate proved to be highly active in the formation of

acetaldehyde, but also to increase butadiene selectivity at the expense of ethylene when combined with Hf/SiO_2. Hemimorphite alone did not produce any butadiene. The increased activity is attributed to synergy between hafnium(IV) and hemimorphite resulting in the near disappearance of Brønsted acid sites, as measured by pyridine-FTIR and the activity of the zinc silicate in the dehydrogenation of ethanol. A notable feature of this catalyst is the importance of the synthesis method; to be fully active, hemimorphite had to be mixed in water with Hf/SiO_2 at room temperature, followed by calcination. All other approaches involving either reflux conditions or impregnation of hemimorphite with hafnium resulted in poorly active materials.

The activity of tantalum oxide was demonstrated by Corson et al. during the Second World War. Copper-doped silica-supported tantalum oxide was shown to be amongst the most active catalysts for the one-step conversion of ethanol [41]. In 2014, Chae et al. showed tantalum-containing ordered mesoporous silica were highly active for the two-step process [47]. More recently, Kyriienko et al. have reported the high selectivity of a tantalum-modified zeolite beta catalyst for the two-step process [38]. Tantalum(V)-single sites BEA zeolites were synthesized by 2-step post-synthesis method similar to that used in other articles discussed in this work. Briefly, dealumination of BEA zeolite was conducted using nitric acid to produce vacant silanol sites. Impregnation with varying amounts of tantalum ethoxide followed, affording samples believed to contain 1 and 3 wt % tantalum. The acid and basic properties of the modified zeolites were characterized by pyridine, pyrrol and $CDCl_3$-FTIR. These techniques suggested the presence of Lewis acid sites, and medium and weak basic sites. An absence of signals usually assigned to Brønsted acid sites was noted. With an ethanol feed alone, 1% Ta/BEA was active for the conversion of ethanol to butadiene. Selectivity towards butadiene at 623 K and WHSV of 0.8 h^{-1} was 28.9%. Acetaldehyde was also produced in notable amounts, attributable to the redox properties of Ta(V) [83]. Dehydration products were also generated in significant amounts. Higher Ta(V) content increased the formation of ethylene, a phenomenon the authors explain by the formation of closed tantalum sites bound to four silicon atoms, as described by Ivanova et al. in the case of Zr/BEA, which are believed to be less active in the formation of butadiene [49,70]. With an ethanol/acetaldehyde mixture, the catalysts proved to be much more selective towards the desired product. At 623 K, with an EtOH/AA ratio of 3.7 and for a WHSV of 0.8 h^{-1}, butadiene yield for 3% Ta/BEA was 43.1% after 4 h on stream with a productivity of 0.20 $g_{BD} \cdot g_{cat}^{-1} \cdot h^{-1}$. The authors argued that the system lacked redox properties for the dehydrogenation of ethanol, as acid-base properties are believed to be predominant over redox properties in the case of Ta/BEA materials.

Supported niobium oxide can possess redox and acidic properties depending on the nature of the support [84–86]. Niobium oxide was identified as active for the two-step process by Toussaint et al. in 1947 [48]. Ivanova et al. have reiterated this claim, adding that niobium—amongst other metals—could be used to produce butadiene from ethanol when properly promoted [53]. Kyriienko et al. have investigated niobium-modified zeolite BEA for the ETB reaction [39]. This was done in the context of a study on the effects of the metal's incorporation with the zeolite framework state on a gas- and liquid-phase tandem process. The catalysts were prepared in a two-step post-synthesis method: dealumination of BEA was conducted using nitric acid; niobium ions were introduced into T-vacant sites by impregnation using niobium ethoxide as precursor. Washing with deionized water, drying and calcination at 723 K for three hours followed these procedures. Samples containing 0.7 and 2.0 wt % were prepared in this manner. The mononuclear incorporation of Nb(V) into the zeolite framework for the 0.7% Nb/BEA was demonstrated using XRD, DR UV–Vis, MAS NMR and FTIR. 2.0% Nb/BEA was shown to possess both the mononuclear species—albeit in lower amounts—and extra-framework octahedral niobium oxide. Notably, the presence of polynuclear species was evidenced by the presence of specific signals on the DR UV–Vis spectrum. In terms of surface properties, pyridine-FTIR revealed the presence of mostly weak Lewis acid sites, with some medium and strong sites, on both samples. Di-*tert*-butyl pyridine-FTIR further indicated the presence of very weak Brønsted on the surface of the catalyst that could not detected with pyridine. Higher ethanol conversion, TOF and butadiene yield were observed on 0.7% Nb/BEA. However, ethylene

and diethyl ether yields were also higher. In fact, the combined selectivity towards both dehydration products was higher than the sum of those presumably resulting from the dehydrogenation route. Evidently, mononuclear Nb(V) species are more active for all reactions and side-reactions involved in the Lebedev process than extra-framework species. Nevertheless, the catalytic performance of Nb/BEA in the one-step process was under average when compared to many of the recent materials reported in the literature [7,29]. As with Ta/BEA discussed above, this phenomenon could be attributed to the lack of the redox properties or modification to suppress ethanol dehydration. The addition of acetaldehyde in the feed at an ethanol-to-acetaldehyde ratio of 2.7 further evidenced the better activity of mononuclear species, as all measures of activity (ethanol conversion, butadiene and ethylene yields) were higher despite lower metal content. At 623 K, with an EtOH/AA ratio of 2.7 and for a WHSV of 0.8 h^{-1}, butadiene yield over 0.7% Nb/BEA was of 23.6, for a productivity of 0.11 $g_{BD} \cdot g_{cat}^{-1} \cdot h^{-1}$. Despite the increase in performances from the addition of acetaldehyde, the performances of Nb/BEA remains poorer than similar Ta and Zr-containing catalysts, reconfirming a trend previously observed by Toussaint et al. (referred to by its former name columbium in their article) [38,48,69]. For this reason, it is improbable that niobium could be used as a viable substitute to zirconium or other Lewis solid acids.

La-Salvia et al. report the catalytic activity of acidic Al-MCM-41 modified with chromium and barium for the one-step conversion of ethanol to butadiene. MCM-41 is an ordered mesoporous silica with large surface area. Acidity was generated by the introduction of an aluminium precursor in the preparation procedure. The as-synthesized Al-MCM-41 was sequentially doped using barium and chromium IWI method. It was argued that barium would provide the acidic material with basic properties, while chromium would promote the ethanol dehydrogenation. Unmodified Al-MCM-41 was also kept for characterization and catalytic testing. As in the work of Sels et al., the ordered nature and structure of Al-MCM-41 did not survive the impregnation process. Powdered XRD and N_2 physisorption revealed the progressive collapse of Al-MCM-41 framework with each impregnation. Additionally, amorphous barium silicate was detected and supposed to block pore access. Although chromium oxide was not detected by XRD, changes in surface chemical properties suggest it was present as highly dispersed particles. CO_2 chemisorption indicated a progressive increase in the density of basic sites after the addition of each dopant–first barium, then chromium. In terms of activity, Al-MCM-41 and 16% Ba/Al-MCM-41 were highly active for the dehydration of ethanol. No butadiene was observed and acetaldehyde was exclusively detected in small amount over the barium-containing catalyst. The acidity of Al-MCM-41 is well established and the likely cause of the significant ethanol dehydration observed [87]. This suggests that the alkali nature of barium was either insufficient to curb this acidity or that the framework collapse reduced the accessibility to the barium-containing surface. The subsequent introduction of chromium greatly improved the activity of material. At 723 K for a WHSV of 3.07 h^{-1}, 1.4% Cr-16% Ba/Al-MCM-41 had a butadiene yield of 22.1% and a productivity of 0.40 $g_{BD} \cdot g_{cat}^{-1} \cdot h^{-1}$ after 10 h on stream, along with a significant increase in acetaldehyde selectivity. The role of Cr_2O_3 as promoter of ethanol dehydrogenation in the ETB reaction has been previously reported and is the likely reason for the increased production of butadiene [8,41]. As the activity of Cr/MCM-41 was not reported, it is difficult to the role of barium in this improvement or if Ba and Cr had any synergic contribution in that regard. It should be noted that chromium-containing amphoteric mixed oxides were reported as active for the ETB reaction, but not silica-supported Cr_2O_3, evidencing some contribution from MCM-41 and/or Ba [26,41]. A decrease in ethanol conversion is observed over a period of 24 h. Coke formation on the catalytic surface, evidenced by thermal gravimetric analysis, is the likely cause of this deactivation. So far, MCM-41 has proved to be a poor support for materials active in the conversion of ethanol to butadiene.

Palkovits et al. have approached the synthesis of butadiene from ethanol with a two-stage system. An ethanol/acetaldehyde mixture with a ratio of 4 was obtained during the first stage of the process. The second step concerned the conversion of this mixture to butadiene over modified zeolite BEA catalysts. Two catalysts were tested for the dehydrogenation of ethanol: Cu/SiO_2 and

Ag/SiO_2 prepared by IWI. Although only the copper catalyst was reduced under hydrogen flow, subsequent catalytic test of CuO/SiO_2 coupled with post-reaction characterization revealed that both silver and copper are readily reduced under an ethanol flow at the reaction temperature [50]. EtOH/AA ratio of 4 (20% acetaldehyde yield) was obtained over Cu/SiO_2 at 463 K and WHSV of 0.24 h^{-1} and remained highly stable over a period of 90 h on stream. No other product except acetaldehyde could be detected. On the contrary, Ag/SiO_2 suffered from deactivation in the first 20 h on stream before stabilizing. Furthermore, small quantities of side-products were detected, not unlike the observations of Ivanova et al. on similar a Ag/SiO_2 catalyst [59]. Because of its obvious benefits, Cu/SiO_2 was selected for the first stage of this process. The second stage of the process concerned the conversion of the ethanol/acetaldehyde feed to butadiene at 573 K. Palkovits et al. studied the relation between the acid and basic properties of modified zeolite BEA and the their catalytic activity. To change the acidity and basicity of the catalysts, the acidic zeolites with varied Al/Si ratios underwent several modifications: the acidity of the zeolites was passivated by the exchanging alkaline and earth alkaline ions (Ca^{2+}, K^+ and Cs^+) with the surface protons; basicity was introduced by impregnating the zeolites and alkali-modified zeolites with magnesium oxide; these magnesium-modified zeolites were further modified by the addition of different metal oxides (Al_2O_3, ZnO and NiO). The catalytic activity of these materials was evaluated at the ethanol/acetaldehyde ratio obtained previously and compared with their acid-base properties measured by NH_3 and CO_2-TPD respectively; the acid-based properties was represented by a ratio between the number of acid and basic sites, n_{acidic}/n_{baisc}. From this comparison, a correlation between the balance of acid and basic sites with the catalytic activity was obtained (Figure 13). Butadiene selectivity was correlated with a balance between the number of basic and acid sites at ratios approximating 1 (Figure 13A). However, it had to be achieved by the introduction of basic functions with MgO; passivation with alkali metals alone suppressed ethanol conversion, barely improving BD selectivity. On the contrary, selectivity towards dehydration products (ethylene and diethyl ether) was associated with an excess of acidity, expressed by a n_{acidic}/n_{baisc} ratio above 1 (Figure 13B). The ethanol conversion rate followed a similar trend, evidently the result of increased ethanol dehydration (Figure 13C). Based on these observations, the authors conclude that a balance between the acid and basic properties is essential. However, the correlations obtained did not distinguish between the nature and strength of the active and basic sites, therefore not providing an accurate assessment of the necessary properties to catalyze the reaction. Pyridine-FTIR indicated the presence of Brønsted acid sites on the zeolites with smaller Si/Al ratio, while greater Si/Al ratio materials displayed mostly signals for Lewis acid sites. Regardless of the type of acidity, ethylene selectivity remained above 88%, evidencing the necessity of additional chemical properties. The combination of MgO with alkali metals proved relatively successful, where it increased BD selectivity while maintaining a high ethanol conversion, suggesting that basic active sites are responsible for the production of acetaldehyde. Ultimately, the optimal catalyst was obtained by the introduction of basic MgO and further modified with ZnO to promote ethanol dehydrogenation. At 573 K, with a EtOH/AA ratio of 4 and for a GHSV of 96.0 h^{-1}, ZnO-MgO/BEA showed a BD yield of 33% butadiene. Due to a lack of reaction detail, it is difficult to compare these performances to other catalysts.

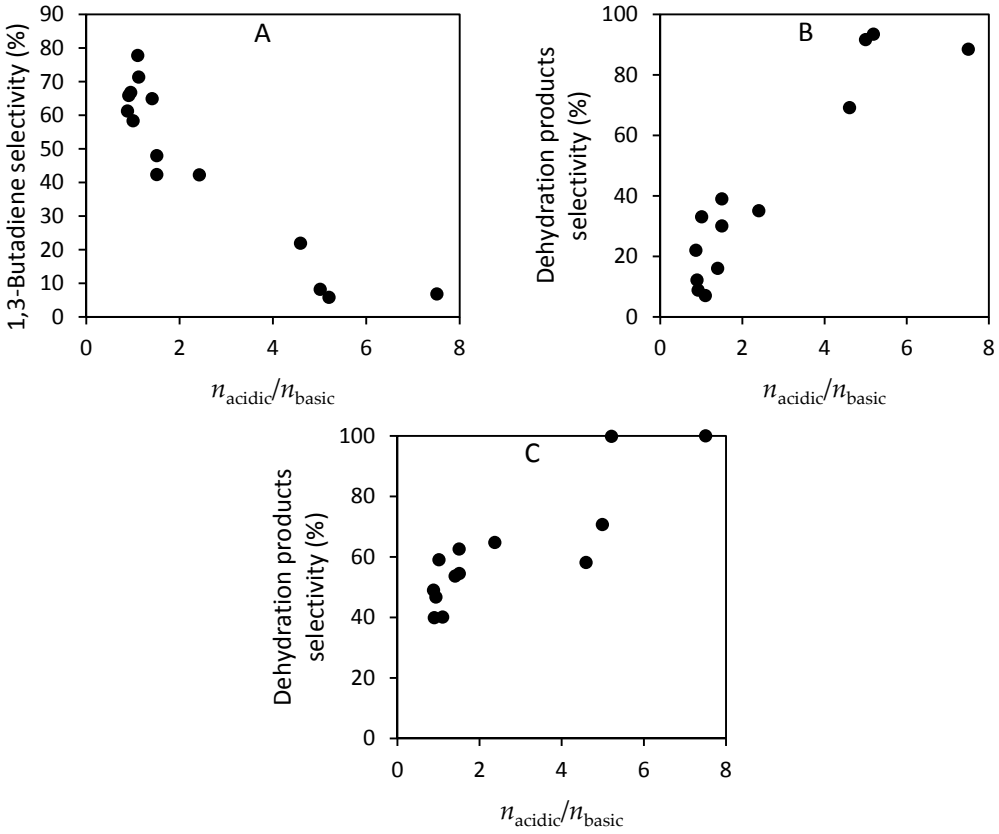

Figure 13. Correlation curves between the ratio between the number of acid and basic sites with: (**A**) 1,3-butadiene selectivity; (**B**) dehydration products selectivity; (**C**) ethanol conversion. Reprinted with permission from [60]. Copyright 2015, Elsevier.

3. Discussion

The production of 1,3-butadiene from renewable sources could address the sustainability issues associated with steam cracker extraction, the current method of choice. One such production process is the catalytic conversion of ethanol to 1,3-butadiene. The main advantage of this process is that it has successfully been implemented decades ago, before the petroleum based route. Some studies have already suggest that the one or two-step process could soon [3,6,43]. Industrial initiatives such as the Michelin project Biobutterfly suggest that biosourced butadiene is a possibility [88]. Accordingly, research on the subject has undergone a renaissance in the past few years: catalytic systems first discovered decades ago are being retested, new catalysts are being developed and the number of publications on the subject is growing at a considerable rate. The latest scientific investigations have focused on increasing the performances of catalytic materials either for the one-step or two-step process with the aim of improving their economic viability. A crucial target for improvement has been the productivity in butadiene, but also the reduction of non-recyclable byproducts. It is understood that catalytic activity requires a combination of either acid, basic and redox properties—the balance is thought to be the key to achieve high productivity. With each catalytic system also comes the use of various promoters to alter this balance or to introduce new functionalities, incidentally adding a new layer of complexity to the preparation of catalysts. Although significant progress has been made, aspects crucial to the rational design of new catalysts, namely the exact nature of some active sites, the true reaction mechanism and the optimal preparation methods have either not yet been fully elucidated or are still under debates. To solve this issue, researchers have sought to understand the relation between the chemical and structural properties of material and its catalytic activity—with various degrees of success. As highlighted by Sels et al. concerning MgO-SiO_2, a lack of "systematic

studies with advanced surface characterization tools in combination with catalytic measurements" has plagued the development and understanding of ETB reaction [8]. This review has highlighted the recent progress achieved in this field.

The issue with designing catalysts for the ethanol-to-butadiene reaction lies in the complexity of the reaction mechanism which requires different active sites. Because the chemical and structural properties that give rise to the catalytic activity are not fully understood, it becomes difficult to generate or balance these properties in a way that maximizes butadiene production. Only by systematic studies with advanced surface characterization tools in combination with catalytic measurements this issue might be resolved [8]. One such study can be found in the case of the Ag/Zr/BEA catalysts developed by Ivanova et al. in which a new highly active catalytic system for the Lebedev process was devised, carefully characterized until an active site could be identified, then rationally optimized (Figure 14). The first step of the development involved identifying and combining the chemical properties known to partake in the ethanol conversion to BD. While the activity of silica-supported ZrO_2 in the two-step process due to its Lewis acidity had been established decades before, it lacks the properties necessary to catalyze the first step of the Lebedev process [41,67]. This issue was resolved by the addition of silver which can dehydrogenate ethanol without an oxidant when supported on silica [58]. By combining both properties, a new catalytic system was created and proven to be superior to the combination of other metals and metal oxides—according to their patent [53]. The next step was to understand the relation between the chemical properties of the catalyst and its activity. Thus, both the activity of silver in the production of acetaldehyde, and of zirconium oxide in the MPVO reduction and acetaldehyde condensation were investigated [59,68]. The effect of the support on the activity of the catalyst was also investigated, which indicated that molecular sieves allowing for larger dispersion of the active phase increased the performance of the catalyst [69]. Zeolite BEA became the support of choice. Finally, an active site was recognized through a sequential chemisorption of $CDCl_3$ and CO measured by FTIR spectroscopy. This method allowed the distinction between closed and open Lewis acid sites within the zeolite framework; the latter was linearly correlated with butadiene formation. Ivanova et al. followed with the optimization of their catalysts by intentionally inducing the now-identified active sites. This was achieved using a novel method which involved the mixture of DMSO-dissolved $ZrOCl_2$ with dealuminated zeolite BEA under reflux conditions. It was suggested that the solvent prevented the aggregation of zirconium oxide, allowing the formation of isolated ion sites, while steric hindrance, diffusion limitations or energetic limitations were thought to cause of the preferential grafting as open Zr sites. With the addition of silver to Zr/BEA, one of the most productive catalysts was obtained. Although some subsequently reported catalysts were found to be more productive than Ag/Zr/BEA, their superiority is attributed to the use of new materials, not out of rational design. By systematically studying these materials, new and better catalytic systems could be devised.

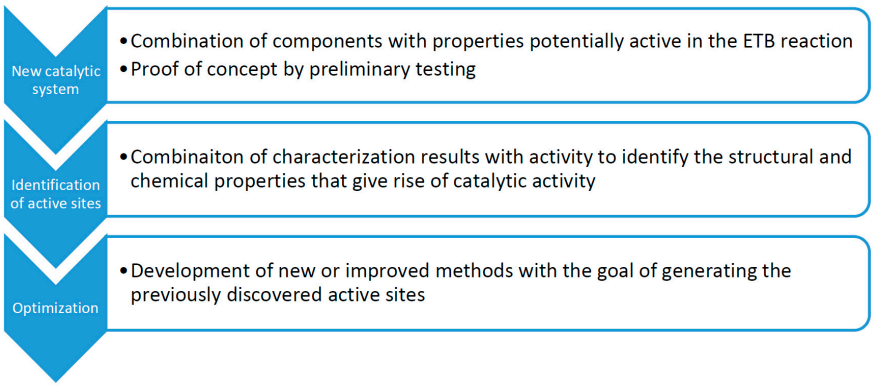

Figure 14. Development progress of Ag/Zr/BEA as exemplified by Ivanova et al.

Despite being the most investigated catalyst, the magnesia-silica system is still at the stage of pin-pointing the chemical and structural properties from which originates their activity. One issue is the difference in preparation method which significantly alters many of the features of the MgO-SiO_2 catalysts, making their comparison difficult, as evidenced by the different Mg-to-Si ratios being reported as optimal. In general, it is recognizes that a predominantly basic catalyst with some degree of acidity is the preferred balance to produce active materials [7,13,25,27,29,30,51]. Weckhuysen et al. have reported that sufficient amount of Lewis acid in the form of Mg–O–Si with small amounts of strong basic sites has led to the most active wet-kneaded catalysts [51]. They also concluded that a cooperation between acid and basic sites was involved in the condensation of acetaldehyde. Sels et al. have proposed that the strong basic sites present in the form of O^{2-} defects in the magnesia, while uncoordinated Mg(II) cations isolated in silica could participate in the dehydration reactions and MPVO reduction [29]. In the context of their mechanism, Cavani et al. have suggested that the reaction of acetaldehyde with the carbanion would occur on defects and edges of the MgO phase, while the dehydration of crotyl alcohol into butadiene would occur with Mg–O–Si Lewis acid sites transformed into Brønsted acid sites in the presence of water [13]. The most interesting observation has been that of Weckhuysen et al. concerning the activity of magnesium silicates [27]. Using ^{1}H-^{29}Si CP MAS-SSNMR, correlation between the relative amount of layered hydrous magnesium silicates formed during the interaction between magnesia and silica was linearly correlated with butadiene yield, while the relative amount of hydrous amorphous magnesium silicate was correlated with ethylene formation. Although additional characterization is required to clarify their properties and exact role in the reaction, it remains the first instance of a structural property being directly correlated with catalytic activity that could mark a beginning of rationally designed MgO-SiO_2 catalysts. Coincidently, Baba et al. investigated the activity of layered hydrous magnesium silicate-talc [19]. The team reported that synthetic talc alone did not lead to butadiene; however, it was found to be the most active catalyst after zinc was incorporated in the crystal lattice. A thorough investigation revealed that zinc did not promote any of the reaction steps besides ethanol dehydrogenation, suggesting talc alone was responsible for the high butadiene yield. Talc is an amphoteric material with proximate acid and basic sites, which are required to catalyze the ETB reaction, minus ethanol dehydrogenation [27]. It is possible that the active sites in MgO-SiO_2 system are the layered magnesium silicates with MgO providing the redox properties. In such case, the necessity of MgO and SiO_2 is dubious, as redox properties can more easily be introduced in talc with the use of dedicated promoters. The recent investigations on MgO-SiO_2 catalytic system indicate a shift away from characterization studies to the new preparation methods capable of generating active sites. Already, wet-kneading spherical silica with MgO particles and mechano-chemical mixing have been reported to generate layered magnesium oxides, which is active in the ETB reaction [3,27,28].

In the past few years, several materials, old and new, have been tested for either the one or two-step process, giving rise to new opportunities for the design of catalytic systems. For instance, many promoters of the nonoxidative dehydrogenation of ethanol to acetaldehyde have successfully been implemented in various catalytic systems. Metals such as gold, copper and silver have been used in the MgO-SiO_2 catalytic system and others. In the case of Cu/MgO-SiO_2, it was found that Cu disperses more readily on the magnesia phase than on silica, affecting its activity, while the opposite was true for Ag [29,50]. The introduction of Cu lead to a slow deactivation of the catalyst by coke formation that did not occur on the unpromoted catalyst. The catalytic activity of Au/MgO-SiO_2 was reportedly inferior to that of the other metals, but it is possible that the synthesis method, which led to the formation of amorphous magnesium silicate previously associated with ethylene formation, indivertibly lowered the selectivity towards butadiene. Measuring the activity of gold-modified catalyst without such phase could shed some light on this issue. Silica-supported Cu and Ag where also used as catalysts for the formation of acetaldehyde in the first step of the Ostromislensky process [36,60]. Of the two metals, copper was found to be the highly selective and stable, while silver deactivated and generated some amounts of byproducts [60]. It should be noted

however, that the loading of silver was of almost 10%, whereas the literature indicates that high metal loading is detrimental, recommending 5% instead [58]. Finally, metal promoters have been reported to be successfully reduced in situ by ethanol, potentially making a pre-treatment with hydrogen optional [32,50,60].

Zinc oxide was also used as promoter for the dehydrogenation of ethanol. It proved to greatly increase the activity of MgO-SiO_2 adding some Lewis acidity by interacting with silica [31]. Zinc oxide was also used to balance the acid properties of hard-templated ZrO_2 and silica-supported ZrO_2 while also providing the missing redox properties to the Lewis acidic materials [33,37]. The use of hemimorphite, a zinc silicate, combined with a silica-supported Lewis acid resulted in a highly selective catalyst; it simultaneously promoted the dehydrogenation of ethanol, reaching 100% ethanol conversion, while passivating the Brønsted acidity of the metal oxide, significantly lowering ethylene selectivity [37]. Although in the latter case, the specific origin of the high activity has not been identified, it appears that zinc-based promoters have the double effect of improving the redox properties of material, while also altering its acid properties to a greater extent than metal promoters.

Rather than tweaking the preparation method, the acid properties of a catalyst can be altered by a post-treatment with alkali metals [30,33,60]. Both Jones et al. and Wang et al. have reported the selective poisoning of the stronger acid sites on their zirconium-containing catalysts [30,33]. As a result, ethylene formation was significantly suppressed, boosting butadiene and acetaldehyde selectivity. Because acetaldehyde can be recycled and fed in the reactor again, alkali poisoning offers the opportunity of reducing the number of secondary products over acid-based catalysts. However, the poor results obtained with BEA-support alkali metals suggest that despite their basic properties, they do not participate as active sites in the ETB reaction [60].

The current study of Lewis acid catalysts discussed above has mostly focused on zirconium-containing materials, either supported on silica or a molecular sieve, but also as hard-templated bulk oxide [16,32,69]. However, several alternatives have been recently investigated. Originally evaluated together with zirconium decades ago, tantalum and niobium oxide have been revisited by Kyriienko et al., this time supported on zeolite BEA [38,39,48,67]. Both were found to lack the redox properties required to be active in the one-step process, but were reasonably active in the two-step process. Of the two, tantalum was found to be superior in activity and its productivity rivaled that of other zirconium catalysts tested in similar conditions [35]. On the contrary, niobium oxide could not be properly dispersed and displayed relatively poorer performances. These observations are in accord with a trend noted by Toussaint et al. concerning the activity of the three Lewis acids [48]. The substitution of zirconium by hafnium as the Lewis acid component of a catalyst resulted in a reduction of ethylene formation, while preserving a similar yield of butadiene [37]. This phenomenon was attributed to the softer acid properties of hafnium. When combined with hemimorphite, it proved to be a highly selective catalyst with high conversion rate. Hafnium offers the possibility of designing Lewis acid catalysts with lower selectivity towards dehydration products.

A recent publication by Kyriienko et al. suggest that lanthanum oxide may possess the basic properties required to catalyze the ETB reaction [34]. Their La-Zn-(Zr)-Si catalyst proved to be one of the most productive catalysts in the one-step process with stability up to 10 h. The combination of these oxides was argued to provide the redox, acid and basic properties required to catalyze the reaction. According to the authors, zinc oxide provided the redox properties, zirconium oxide the Lewis acidity and lanthanum oxide the basic properties. New opportunities could arise from this discovery, as lanthanum could be used to provide basicity to other catalytic systems.

The importance of the support was also highlighted in the reviewed literature. The most active catalyst was obtained by dispersing zirconium oxide over mesocellular silica foam [36]. The performance of this catalyst was attributed to the high degree of dispersion of ZrO_2 enabled by the great surface area of the support, and to the large, interconnect mesopores of MCF, which diminish the formation of coke and issues relating to the mass-transfer of reagents into the catalyst. Incidentally, the use of an incorrect support resulted in undesired properties. In particular, MCM-41 was shown to be

a poor support, as it structural integrity was repeatedly compromised by post-synthetic modifications, once as silica source for an MgO-SiO_2 catalyst, another time as an acidic support for Cr_2O_3 and BaO_2 [7,40]. In both case, the ordered mesoporous structure of the silicate was lost.

4. Conclusions

In this paper, the latest advances in the design of catalytic systems for the ethanol-to-butadiene reaction have been reviewed. The use of new components, as wells as a careful optimization of existing catalysts have allowed scientists to surpass the performances of previous catalytic systems. In particular, the productivity of butadiene under realistic industrial conditions (with large ethanol flow) has seen a dramatic increase in both one and two-step process [7]. Figure 15 gives a visual representation of the most productive catalysts reported in recent years. Considering that a large proportion of the numerous catalysts developed over the last decades could not reach a productivity of 0.150 $g_{BD} \cdot g_{cat}^{-1} \cdot h^{-1}$ (suggested as Jones et al. in 2012 as the minimum for industrial application), it illustrates the progress in ETB reaction.

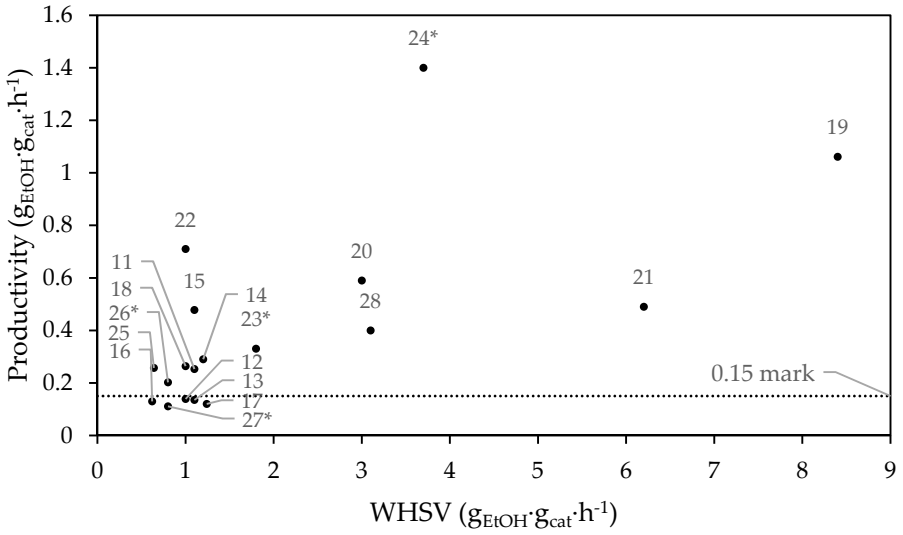

Figure 15. 1,3-Butadiene production versus weight hourly space velocity (WHSV) for the reviewed catalysts in reference to the ID number in Table 1. * indicates a result obtained from a two-step process.

Comparing Figure 16 below with a similar figure (Figure 14) found in the book chapter by Cavani et al. on this subject representing the performances in terms of yield of selected catalysts shows that the past 2 to 3 years have afforded as many highly active catalysts as the past 70 years combined [14]. This progress was accomplished both by the rational design of new catalytic systems, as well as the use of highly active new components, such as lanthanum oxide or mesoporous silica foam for the support of zirconium oxide. As illustrated, the majority of the catalysts showed a BD yield between 20% and 40%, which is in line with the performances reported in the literature. Nevertheless, several catalysts were able to go beyond, with two catalysts reaching values above 60%. Only the notorious catalyst be Ohnishi et al. and one catalyst Ivanova et al. had been reported to reach that point [14].

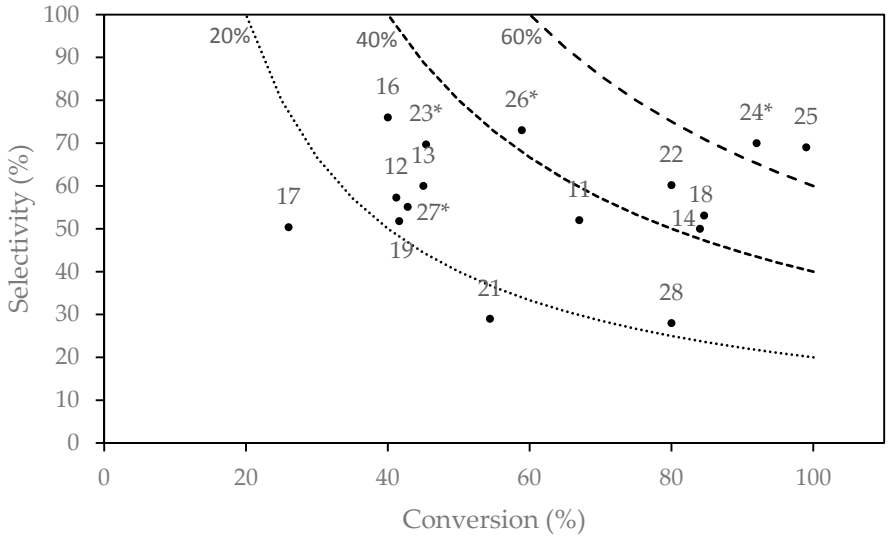

Figure 16. 1,3-Butadiene selectivity versus ethanol conversion for the reviewed catalysts in reference to the ID number in Table 1. * indicates a result obtained from a two-step process.

Many aspects of the ETB reaction still necessitate investigation. Obviously, settling the question of the reaction mechanism is a primordial objective, as is the establishment of clear link between certain properties and BD productivity; the identification of the active sites of each catalytic systems would enable a more rational design of new active materials. Another issue that has yet to be fully addressed is the effect of water in the system, as it would help predict the viability of using more affordable unpurified bioethenol. Already Cavani et al. have observed that additional water in the feed leads to the formation of new Brønsted acid sites from existing Lewis sites [13]. Lee et al. have also noted that the presence of water increases the need for acetaldehyde in the feed of the two-step process [36]. Another aspect that will grow in importance is the too-often ignored time-on-stream stability of the catalytic materials. Currently, it is believed the coke deposition is the principal source of deactivation [36,40,50,54]. As the performances of the catalysts improve, growing attention will be devoted to minimizing this phenomenon. With the old & new chemistry of the ETB reaction being currently investigated by several research teams, it is likely that the issues will be addressed in the near future and a transition from the laboratory to the industry scale is maybe now just a question of time.

Acknowledgments: Authors acknowledge the support from the French National Research Agency (ANR-15-CE07-0018-01). Chevreul Institute (FR 2638), Ministère de l'Enseignement Supérieur et de la Recherche, Région Nord–Pas de Calais and FEDER are acknowledged for supporting and funding partially this work.

Author Contributions: Guillaume Pomalaza wrote the paper; Franck Dumeignil, Vitaly Ordomsky and Mickaël Capron revised the paper.

Conflicts of Interest: The authors declare no conflict of interest.

References

1. Ouhadi, T.; Abdou-Sabet, S.; Wussow, H.-G.; Ryan, L.M.; Plummer, L.; Baumann, F.E.; Lohmar, J.; Vermeire, H.F.; Malet, F.L.G. Thermoplastic elastomers. In *Ullmann's Encyclopedia of Industrial Chemistry*; Wiley-VCH Verlag GmbH & Co. KGaA: Weinheim, Germany, 2014; pp. 1–41.
2. Dahlmann, M.; Grub, J.; Löser, E. Butadiene. In *Ullmann's Encyclopedia of Industrial Chemistry*; Wiley-VCH Verlag GmbH & Co. KGaA: Weinheim, Germany, 2011; Vol. 100 C, pp. 1–24.
3. Shylesh, S.; Gokhale, A.A.; Scown, C.D.; Kim, D.; Ho, C.R.; Bell, A.T. From sugars to wheels: The conversion of ethanol to 1,3-butadiene over metal-promoted magnesia-silicate catalysts. *ChemSusChem* **2016**, *9*, 1462–1472. [CrossRef] [PubMed]
4. Ezinkwo, G.O.; Tretyakov, V.P.; Aliyu, A.; Ilolov, A.M. Fundamental issues of catalytic conversion of bio-ethanol into butadiene. *ChemBioEng Rev.* **2014**, *1*, 194–203. [CrossRef]

5. Sun, J.; Wang, Y. Recent advances in catalytic conversion of ethanol to chemicals. *ACS Catal.* **2014**, *4*, 1078–1090. [CrossRef]
6. Burla, J.; Fehnel, R.; Louie, P.; Terpeluk, P. Two-Step Production of 1,3-Butadiene from Ethanol. Available online: http://repository.upenn.edu/cgi/viewcontent.cgi?article=1033&context=cbe_sdr (accessed on 12 December 2016).
7. Makshina, E.V.; Janssens, W.; Sels, B.F.; Jacobs, P.A. Catalytic study of the conversion of ethanol into 1,3-butadiene. *Catal. Today* **2012**, *198*, 338–344. [CrossRef]
8. Makshina, E.V.; Dusselier, M.; Janssens, W.; Degrève, J.; Jacobs, P.A.; Sels, B.F. Review of old chemistry and new catalytic advances in the on-purpose synthesis of butadiene. *Chem. Soc. Rev.* **2014**, *43*, 7917–7953. [CrossRef] [PubMed]
9. Angelici, C.; Weckhuysen, B.M.; Bruijnincx, P.C.A. Chemocatalytic conversion of ethanol into butadiene and other bulk chemicals. *ChemSusChem* **2013**, *6*, 1595–1614. [CrossRef] [PubMed]
10. Jones, M. Catalytic transformation of ethanol into 1,3-butadiene. *Chem. Cent. J.* **2014**. [CrossRef] [PubMed]
11. Jones, M.; Keir, C.; Iulio, C.; Robertson, R.; Williams, C.; Apperley, D. Investigations into the conversion of ethanol into 1,3-butadiene. *Catal. Sci. Technol.* **2011**, *1*, 267–272. [CrossRef]
12. Chieregato, A.; Velasquez Ochoa, J.; Bandinelli, C.; Fornasari, G.; Cavani, F.; Mella, M. On the chemistry of ethanol on basic oxides: Revising mechanisms and intermediates in the Lebedev and Guerbet reactions. *ChemSusChem* **2015**, *8*, 377–388. [CrossRef] [PubMed]
13. Ochoa, J.V.; Bandinelli, C.; Vozniuk, O.; Chieregato, A.; Malmusi, A.; Recchi, C.; Cavani, F. An analysis of the chemical, physical and reactivity features of $MgO–SiO_2$ catalysts for butadiene synthesis with the Lebedev process. *Green Chem.* **2016**, *18*, 1653–1663. [CrossRef]
14. Chieregato, A.; Ochoa, J.V.; Cavani, F. Olefins from biomass. In *Chemicals and Fuels from Bio-Based Building Blocks*; Wiley-VCH Verlag GmbH & Co. KGaA: Weinheim, Germany, 2016; pp. 1–32.
15. Jones, H.E.; Stahly, E.E.; Corson, B.B. Butadiene from ethanol. reaction mechanism. *J. Am. Chem. Soc.* **1949**, *71*, 1822–1828. [CrossRef]
16. Sushkevich, V.L.; Ivanova, I.I.; Ordomsky, V.V.; Taarning, E. Design of a metal-promoted oxide catalyst for the selective synthesis of butadiene from ethanol. *ChemSusChem* **2014**, *7*, 2527–2536. [CrossRef] [PubMed]
17. Gao, M.; Liu, Z.; Zhang, M.; Tong, L. Study on the mechanism of butadiene formation from ethanol. *Catal. Letters* **2014**, *144*, 2071–2079. [CrossRef]
18. Müller, P.; Burt, S.P.; Love, A.M.; McDermott, W.P.; Wolf, P.; Hermans, I. Mechanistic study on the Lewis acid catalyzed synthesis of 1,3-butadiene over Ta-BEA using modulated operando DRIFTS-MS. *ACS Catal.* **2016**, *6*, 6823–6832. [CrossRef]
19. Hayashi, Y.; Akiyama, S.; Miyaji, A.; Sekiguchi, Y.; Sakamoto, Y.; Shiga, A.; Koyama, T.; Motokura, K.; Baba, T. Experimental and computational studies of the roles of MgO and Zn in talc for the selective formation of 1,3-butadiene in the conversion of ethanol. *Phys. Chem. Chem. Phys.* **2016**, *18*, 25191–25209. [CrossRef] [PubMed]
20. Veibel, S.; Nielsen, J.I. On the mechanism of the Guerbet reaction. *Tetrahedron* **1967**, *23*, 1723–1733. [CrossRef]
21. Kozlowski, J.T.; Davis, R.J. Heterogeneous catalysts for the Guerbet coupling of alcohols. *ACS Catal.* **2013**, *3*, 1588–1600. [CrossRef]
22. Ho, C.R.; Shylesh, S.; Bell, A.T. Mechanism and kinetics of ethanol coupling to butanol over hydroxyapatite. *ACS Catal.* **2016**, *6*, 939–948. [CrossRef]
23. Scalbert, J.; Thibault-Starzyk, F.; Jacquot, R.; Morvan, D.; Meunier, F. Ethanol condensation to butanol at high temperatures over a basic heterogeneous catalyst: How relevant is acetaldehyde self-aldolization? *J. Catal.* **2014**, *311*, 28–32. [CrossRef]
24. Da Ros, S.; Jones, M.D.; Mattia, D.; Schwaab, M.; Barbosa-Coutinho, E.; Rabelo-Neto, R.C.; Bellot Noronha, F.; Carlos Pinto, J. Microkinetic analysis of ethanol to 1,3-butadiene reactions over $MgO–SiO_2$ catalysts based on characterization of experimental fluctuations. *Chem. Eng. J.* **2016**, *308*, 988–1000. [CrossRef]
25. Angelici, C.; Velthoen, M.E. Z.; Weckhuysen, B.M.; Bruijnincx, P.C. A. Effect of preparation method and CuO promotion in the conversion of ethanol into 1,3-butadiene over SiO_2–MgO catalysts. *ChemSusChem* **2014**, *7*, 2505–2515. [CrossRef] [PubMed]
26. Bhattacharyya, S.K.; Ganguly, N.D. One-step catalytic conversion of ethanol to butadiene in the fixed bed. II Binary- and ternary-oxide catalysts. *J. Appl. Chem.* **1962**, *12*, 105–110. [CrossRef]

27. Chung, S.-H.; Angelici, C.; Hinterding, S.O.M.; Weingarth, M.; Baldus, M.; Houben, K.; Weckhuysen, B.M.; Bruijnincx, P.C.A. On the role of magnesium silicates in wet-kneaded silica-magnesia catalysts for the Lebedev ethanol-to-butadiene process. *ACS Catal.* **2016**, *6*, 4034–4045. [CrossRef]
28. Larina, O.V.; Kyriienko, P.I.; Trachevskii, V.V.; Vlasenko, N.V.; Soloviev, S.O. Effect of mechanochemical treatment on acidic and catalytic properties of $MgO–SiO_2$ composition in the conversion of ethanol to 1,3-butadiene. *Theor. Exp. Chem.* **2016**, *51*, 387–393. [CrossRef]
29. Janssens, W.; Makshina, E.V.; Vanelderen, P.; De Clippel, F.; Houthoofd, K.; Kerkhofs, S.; Martens, J.A.; Jacobs, P.A.; Sels, B.F. Ternary $Ag/MgO–SiO_2$ catalysts for the conversion of ethanol into butadiene. *ChemSusChem* **2015**, *8*, 994–1008. [CrossRef] [PubMed]
30. Da Ros, S.; Jones, M.D.; Mattia, D.; Pinto, J.C.; Schwaab, M.; Noronha, F.B.; Kondrat, S.A.; Clarke, T.C.; Taylor, S.H. Ethanol to 1,3-butadiene conversion by using ZrZn-containing MgO/SiO_2 systems prepared by Co-precipitation and effect of catalyst acidity modification. *ChemCatChem* **2016**, *8*, 2376–2386. [CrossRef]
31. Larina, O.V.; Kyriienko, P.I.; Soloviev, S.O. Ethanol conversion to 1,3-butadiene on $ZnO/MgO–SiO_2$ catalysts: effect of ZnO content and $MgO:SiO_2$ ratio. *Catal. Lett.* **2015**, *145*, 1162–1168. [CrossRef]
32. Sushkevich, V.L.; Ivanova, I.I. Ag-promoted ZrBEA zeolites obtained by post-synthetic modification for conversion of ethanol to butadiene. *ChemSusChem* **2016**, *9*, 2216–2225. [CrossRef] [PubMed]
33. Baylon, R.A.L.; Sun, J.; Wang, Y. Conversion of ethanol to 1,3-butadiene over Na doped $Zn_xZr_yO_z$ mixed metal oxides. *Catal. Today* **2014**, *259*, 446–452. [CrossRef]
34. Larina, O.V.; Kyriienko, P.I.; Soloviev, S.O. Effect of lanthanum in Zn-La(-Zr)-Si oxide compositions on their activity in the conversion of ethanol into 1,3-butadiene. *Theor. Exp. Chem.* **2016**, *52*, 51–56. [CrossRef]
35. Han, Z.; Li, X.; Zhang, M.; Liu, Z.; Gao, M. Sol–gel synthesis of $ZrO_2–SiO_2$ catalysts for the transformation of bioethanol and acetaldehyde into 1,3-butadiene. *RSC Adv.* **2015**, *5*, 103982–103988. [CrossRef]
36. Cheong, J.L.; Shao, Y.; Tan, S.J. R.; Li, X.; Zhang, Y.; Lee, S.S. Highly active and selective Zr/MCF catalyst for production of 1,3-butadiene from ethanol in a dual fixed bed reactor system. *ACS Sustain. Chem. Eng.* **2016**, *4*, 4887–4894. [CrossRef]
37. De Baerdemaeker, T.; Feyen, M.; Müller, U.; Yilmaz, B.; Xiao, F.S.; Zhang, W.; Yokoi, T.; Bao, X.; Gies, H.; De Vos, D.E. Bimetallic Zn and Hf on silica catalysts for the conversion of ethanol to 1,3-butadiene. *ACS Catal.* **2015**, *5*, 3393–3397. [CrossRef]
38. Kyriienko, P.I.; Larina, O.V.; Soloviev, S.O.; Orlyk, S.M.; Dzwigaj, S. High selectivity of TaSiBEA zeolite catalysts in 1,3-butadiene production from ethanol and acetaldehyde mixture. *Catal. Commun.* **2016**, *77*, 123–126. [CrossRef]
39. Kyriienko, P.I.; Larina, O.V.; Popovych, N.O.; Soloviev, S.O.; Millot, Y.; Dzwigaj, S. Effect of the niobium state on the properties of NbSiBEA as bifunctional catalysts for gas- and liquid-phase tandem processes. *J. Mol. Catal. A* **2016**, *424*, 27–36. [CrossRef]
40. La-Salvia, N.; Lovón-Quintana, J.J.; Valença, G.P. Vapor-phase catalytic conversion of ethanol into 1,3-butadiene on Cr-Ba/MCM-41 catalysts. *Brazilian J. Chem. Eng.* **2015**, *32*, 489–500. [CrossRef]
41. Corson, B.; Jones, H.; Welling, C.; Hinckley, J.; Stahly, E. Butadiene from ethyl alcohol. Catalysis in the one-and two-stop processes. *Ind. Eng. Chem.* **1950**, *42*, 359–373. [CrossRef]
42. Ohnishi, R.; Akimoto, T.; Tanabe, K. Pronounced catalytic activity and selectivity of $MgO–SiO_2–Na_2O$ for synthesis of buta-1,3-diene from ethanol. *J. Chem. Soc., Chem. Commun.* **1985**, *70*, 1613–1614. [CrossRef]
43. Patel, A.D.; Meesters, K.; den Uil, H.; de Jong, E.; Blok, K.; Patel, M.K. Sustainability assessment of novel chemical processes at early stage: Application to biobased processes. *Energy Environ. Sci.* **2012**, *5*, 8430. [CrossRef]
44. Lewandowski, M.; Babu, G.S.; Vezzoli, M.; Jones, M.D.; Owen, R.E.; Mattia, D.; Plucinski, P.; Mikolajska, E.; Ochenduszko, A.; Apperley, D.C. Investigations into the conversion of ethanol to 1,3-butadiene using $MgO:SiO_2$ supported catalysts. *Catal. Commun.* **2014**, *49*, 25–28. [CrossRef]
45. Liu, P.; Hensen, E.J. M. Highly efficient and robust $Au/MgCuCr_2O_4$ catalyst for gas-phase oxidation of ethanol to acetaldehyde. *J. Am. Chem. Soc.* **2013**, *135*, 14032–14035. [CrossRef] [PubMed]
46. Bhattacharyya, S.K.; Avasthi, B.N. One-step catalytic conversion of ethanol to butadiene in a fluidized bed. *Ind. Eng. Chem. Process Des. Dev.* **1963**, *2*, 45–51. [CrossRef]
47. Kim, T.W.; Kim, J.W.; Kim, S.Y.; Chae, H.J.; Kim, J.R.; Jeong, S.Y.; Kim, C.U. Butadiene production from bioethanol and acetaldehyde over tantalum oxide-supported spherical silica catalysts for circulating fluidized bed. *Chem. Eng. J.* **2014**, *278*, 217–223. [CrossRef]

48. Quattlebaum, W.M.; Toussaint, W.J.; Dunn, J.T. Deoxygenation of certain aldehydes and ketones: preparation of butadiene and styrene. *J. Am. Chem. Soc.* **1947**, *1491*, 593–599. [CrossRef]
49. Sushkevich, V.L.; Palagin, D.; Ivanova, I.I. With open arms: Open sites of ZrBEA zeolite facilitate selective synthesis of butadiene from ethanol. *ACS Catal.* **2015**, *5*, 4833–4836. [CrossRef]
50. Angelici, C.; Meirer, F.; Van Der Eerden, A.M.J.; Schaink, H.L.; Goryachev, A.; Hofmann, J.P.; Hensen, E.J. M.; Weckhuysen, B.M.; Bruijnincx, P.C.A. Ex situ and operando studies on the role of copper in Cu-promoted SiO_2–MgO catalysts for the Lebedev ethanol-to-butadiene process. *ACS Catal.* **2015**, *5*, 6005–6015. [CrossRef]
51. Angelici, C.; Velthoen, M.E.Z.; Weckhuysen, B.M.; Bruijnincx, P.C.A. Influence of acid–base properties on the Lebedev ethanol-to-butadiene process catalyzed by SiO_2–MgO materials. *Catal. Sci. Technol.* **2015**, *5*, 2869–2879. [CrossRef]
52. Kvisle, S.; Aguero, A.; Sneeden, R.P.A. Transformation of ethanol into 1,3-butadiene over magnesium oxide/silica catalysts. *Appl. Catal.* **1988**, *43*, 117–131. [CrossRef]
53. Ordomskiy, V.V.; Sushkevich, V.L.; Ivanova, I.I. One-Step Method for Butadiene Production. U.S. Patent 8,921,635, 30 December 2014.
54. Ordomsky, V.V.; Sushkevich, V.L.; Ivanova, I.I. Study of acetaldehyde condensation chemistry over magnesia and zirconia supported on silica. *J. Mol. Catal. A* **2010**, *333*, 85–93. [CrossRef]
55. Sekiguchi, Y.; Akiyama, S.; Urakawa, W.; Koyama, T.R.; Miyaji, A.; Motokura, K.; Baba, T. One-step catalytic conversion of ethanol into 1,3-butadiene using zinc-containing talc. *Catal. Commun.* **2015**, *68*, 20–24. [CrossRef]
56. Simakova, O. A.; Davis, R.J.; Murzin, D.Y. *Biomass Processing over Gold Catalysts*; SpringerBriefs in Molecular Science; Springer International Publishing: Heidelberg, Germany, 2013.
57. Guan, Y.; Hensen, E.J.M. Ethanol dehydrogenation by gold catalysts: The effect of the gold particle size and the presence of oxygen. *Appl. Catal. A* **2009**, *361*, 49–56. [CrossRef]
58. Shimizu, K.I.; Sugino, K.; Sawabe, K.; Satsuma, A. Oxidant-free dehydrogenation of alcohols heterogeneously catalyzed by cooperation of silver clusters and acid-base sites on alumina. *Chem. -A Eur. J.* **2009**, *15*, 2341–2351. [CrossRef] [PubMed]
59. Sushkevich, V.L.; Ivanova, I.I.; Taarning, E. Mechanistic study of ethanol dehydrogenation over silica-supported silver. *ChemCatChem* **2013**, *5*, 2367–2373. [CrossRef]
60. Klein, A.; Keisers, K.; Palkovits, R. Formation of 1,3-butadiene from ethanol in a two-step process using modified zeolite-β catalysts. *Appl. Catal. A* **2015**, *1*, 192–202. [CrossRef]
61. Larina, O.V.; Kyriienko, P.I.; Soloviev, S.O. Effect of the addition of zirconium dioxide on the catalytic properties of $ZnO/MgO\text{-}SiO_2$ compositions in the production of 1,3-butadiene from ethanol. *Theor. Exp. Chem.* **2015**, *51*, 244–249. [CrossRef]
62. Kitayama, Y.; Michishita, A. Catalytic activity of fibrous clay mineral sepiolite for butadiene formation from ethanol. *J. Chem. Soc. Chem. Commun.* **1981**, *9*, 401–402. [CrossRef]
63. Kitayama, Y.; Satoh, M.; Kodama, T. Preparation of large surface area nickel magnesium silicate and its catalytic activity for conversion of ethanol into buta-1,3-diene. *Catal. Lett.* **1996**, *36*, 95–97. [CrossRef]
64. Kitayama, Y.; Shimizu, K.; Kodama, T.; Murai, S.; Mizusima, T.; Hayakawa, M.; Muraoka, M. Role of intracrystalline tunnels of sepiolite for catalytic activity. *Stud. Surf. Sci. Catal.* **2002**, *142*, 675–682.
65. Parr, R.G.; Pearson, R.G. Absolute hardness: Companion parameter to absolute electronegativity. *J. Am. Chem. Soc.* **1983**, *105*, 7512–7516. [CrossRef]
66. Yang, W.; Parr, R.G. Hardness, softness, and the fukui function in the electronic theory of metals and catalysis. *Proc. Natl. Acad. Sci.* **1985**, *82*, 6723–6726. [CrossRef] [PubMed]
67. Toussaint, W.J.; Dunn, J.T.; Jackson, D.R. Production of butadiene from alcohol. *Ind. Eng. Chem.* **1947**, *39*, 120–125. [CrossRef]
68. Sushkevich, V.L.; Ivanova, I.I.; Tolborg, S.; Taarning, E. Meerwein-Ponndorf-Verley-Oppenauer reaction of crotonaldehyde with ethanol over Zr-containing catalysts. *J. Catal.* **2014**, *316*, 121–129. [CrossRef]
69. Sushkevich, V.L.; Ivanova, I.I.; Taarning, E. Ethanol conversion into butadiene over Zr-containing molecular sieves doped with silver. *Green Chem.* **2015**, *17*, 2552–2559. [CrossRef]
70. Sushkevich, V.L.; Vimont, A.; Travert, A.; Ivanova, I.I. Spectroscopic evidence for open and closed Lewis acid sites in ZrBEA zeolites spectroscopic evidence for open and closed Lewis acid sites in ZrBEA zeolites. *J. Phys. Chem. C* **2015**, *119*, 17633–17639. [CrossRef]

71. Courtney, T.D.; Chang, C.; Gorte, R.J.; Lobo, R.F.; Fan, W.; Nikolakis, V. Microporous and mesoporous materials effect of water treatment on Sn-BEA zeolite: Origin of 960 cm^{-1} FTIR peak. *Microporous Mesoporous Mater.* **2015**, *210*, 69–76. [CrossRef]
72. Ratnasamy, P.; Srinivas, D.; Knözinger, H. Active sites and reactive intermediates in titanium silicate molecular sieves. *Adv. Catal.* **2004**, *48*, 1–169. [CrossRef]
73. Boronat, M.; Concepción, P.; Corma, A.; Renz, M.; Valencia, S. Determination of the catalytically active oxidation Lewis acid sites in Sn-beta zeolites, and their optimisation by the combination of theoretical and experimental studies. *J. Catal.* **2005**, *234*, 111–118. [CrossRef]
74. Boronat, M.; Concepción, P.; Corma, A.; Navarro, M.T.; Renz, M.; Valencia, S. Reactivity in the confined spaces of zeolites: The interplay between spectroscopy and theory to develop structure–activity relationships for catalysis. *Phys. Chem. Chem. Phys.* **2009**, *11*, 2876–2884. [CrossRef] [PubMed]
75. Harris, J.W.; Cordon, M.J.; Di Iorio, J.R.; Vega-vila, J.C.; Ribeiro, F.H.; Gounder, R. Titration and quantification of open and closed Lewis acid sites in Sn-Beta zeolites that catalyze glucose isomerization. *J. Catal.* **2016**, *335*, 141–154. [CrossRef]
76. Zhu, Y.; Chuah, G.; Jaenicke, S. Chemo- and regioselective Meerwein-Ponndorf-Verley and Oppenauer reactions catalyzed by Al-free Zr-zeolite beta. *J. Catal.* **2004**, *227*, 1–10. [CrossRef]
77. Sun, J.; Zhu, K.; Gao, F.; Wang, C.; Liu, J.; Peden, C.H.F.; Wang, Y. Direct conversion of bio-ethanol to isobutene on nanosized $Zn_xZr_yO_z$ mixed oxides with balanced acid-base sites. *J. Am. Chem. Soc.* **2011**, *133*, 11096–11099. [CrossRef] [PubMed]
78. Liu, J.Y.; Su, W.N.; Rick, J.; Yang, S.C.; Cheng, J.H.; Pan, C.J.; Lee, J.F.; Hwang, B.J. Hierarchical copper-decorated nickel nanocatalysts supported on La_2O_3 for low-temperature steam reforming of ethanol. *ChemSusChem* **2014**, *7*, 570–576. [CrossRef] [PubMed]
79. Frey, A.M.; Karmee, S.K.; de Jong, K.P.; Bitter, J.H.; Hanefeld, U. Supported La_2O_3 and MgO nanoparticles as solid base catalysts for aldol reactions while suppressing dehydration at room temperature. *ChemCatChem* **2013**, *5*, 594–600. [CrossRef]
80. Boukha, Z.; Fitian, L.; López-Haro, M.; Mora, M.; Ruiz, J.R.; Jiménez-Sanchidrián, C.; Blanco, G.; Calvino, J.J.; Cifredo, G.A.; Trasobares, S.; et al. Influence of the calcination temperature on the nano-structural properties, surface basicity, and catalytic behavior of alumina-supported lanthana samples. *J. Catal.* **2010**, *272*, 121–130. [CrossRef]
81. Kozlowski, J.T.; Davis, R.J. Sodium modification of zirconia catalysts for ethanol coupling to 1-butanol. *J. Energy Chem.* **2013**, *22*, 58–64. [CrossRef]
82. Han, Y.; Lee, S.S.; Ying, J.Y. Spherical siliceous mesocellular foam particles for high-speed size exclusion chromatography. *Chem. Mater.* **2007**, *19*, 2292–2298. [CrossRef]
83. Legendre, M.; Cornet, D. Catalytic oxidation of ethanol over tantalum oxide. *J. Catal.* **1972**, *25*, 194–203. [CrossRef]
84. Tanabe, K. Catalytic application of niobium compounds. *Catal. Today* **2003**, *78*, 65–77. [CrossRef]
85. Jehng, J.M.; Wachs, I.E. The molecular structures and reactivity of supported niobium oxide catalysts. *Catal. Today* **1990**, *8*, 37–55. [CrossRef]
86. Jehng, J.-M.; Wachs, I.E. Molecular structures of supported niobium oxide catalysts under ambient conditions. *J. Mol. Catal.* **1991**, *67*, 369–387. [CrossRef]
87. Kosslick, H.; Lischke, G.; Parlitz, B.; Storek, W.; Fricke, R. Acidity and active sites of Al-MCM-41. *Appl. Catal. A* **1999**, *184*, 49–60. [CrossRef]
88. Aimon, D.; Panier, E. La mise en pratique de l'économie circulaire chez Michelin. *Ann. des Mines-Responsab. Environ.* **2014**. [CrossRef]